Mechanisms of Cancer Cell Motility in vivo

Sophie Pinner

Tumour Cell Biology Laboratory
Cancer Research UK London Research Institute
44 Lincoln's Inn Fields
London
WC2A 3PX

Supervisor: Dr Erik Sahai

Thesis submitted for degree, Doctor of Philosophy
University College London 2008

ProQuest LLC
789 East Eisenhower Parkway
P.O. Box 1346
Ann Arbor, MI 48106-1346

Declaration

I Sophie Pinner declare that all the work contained within this thesis is my own and where work has been conducted in collaboration with other labs or individuals or obtained from other sources, this is stated clearly in the appropriate place.

Some of the work in this thesis although originally my own has been subsequently published in scientific journals before the date that this thesis is submitted. The published works are included in the appendices and it must be noted that the copyrights of anything contained within these publications now belongs to the publishing journal.

Abstract

This thesis describes investigations into mechanisms responsible for cancer cell motility in vivo. Chapters 1 and 2 provide a review of current literature in this field and also describe the techniques used to generate the following the results. Chapter 3 describes a candidate-based approach to investigate whether ROCK1 might be regulated by phosphorylation. Mutagenesis of ROCK1 was carried out at 3 chosen sites (T233 T380 T398) in the activation loop and the hydrophobic domain and the phenotypes of the mutants were analysed. Chapter 4 describes a parallel approach finding phosphorylation sites in ROCK1 by mass spectrometry. From these results T518 was chosen for further investigation and its possible function is investigated.

Chapter 5 describes an siRNA screen designed to identify novel regulators of the cortical acto-myosin cytoskeleton. The read-out for this was based on the disruption of rounded blebbing morphology of A375 cells cultured on 3D gel matrices. The rounded morphology is similar to that observed in amoeboid cancer cell motility in vivo, therefore we hypothesised that genes required for contracted, rounded morphology might also be required for motility. Results identified PDK1 amongst other genes as a potential regulator of contractile forces in A375 cells and the role of PDK1 was investigated further. It was found that PDK1 was required both in vitro and in vivo for amoeboid cell motility. Chapters 6,7 and 8 detail the investigations into the mechanism of how PDK1 regulates the cytoskeleton and amoeboid cell motility. It was shown that PDK1 was responsible for the localisation of ROCK1 but not ROCK2 at the plasma membrane. This regulation was achieved by the direct binding of ROCK1 to PDK1. It was further found that PDK1 was able to compete with and prevent RhoE, a negative regulator of ROCK1, from binding.

Chapter 9 investigates the relationship between cell morphology, motility and pigment production. It was found that it was possible to image melanin containing vesicles using multiphoton excitation, and using this technique, the motile behaviour of pigmented melanoma cells was observed in vivo. It was found that motile invasive cells tended to contain less melanin than non-motile cells suggesting that they were less well differentiated. This chapter details investigations into what differences in signalling could be responsible for a switch to a de-differentiated, more invasive/metastatic phenotype. The final chapter discusses the findings contained within this thesis and the possible implications.

Acknowledgements

Firstly thanks go to Erik, for giving me the privileged position of first lab member and first student of the Tumour Cell Biology Lab. Choosing Erik's lab for my PhD has been the best decision I ever made. He has always made time for me, however busy he has been, and has taught me everything from how to design and carry out useful experiments, and understand what I'm doing, to how to spell the word 'dependent'. I would also like to put into writing that I appreciate how good it has been that Erik pushed me (very hard), because I have achieved more than I would have thought possible when I started 4 years ago.

Thanks also to the rest of the Tumour Cell Biology Lab, especially Steve, who have made every day in the lab fun, and have tried to make sure I know my place and to think before I speak. Although I'm excited to be moving to a new lab and starting new things, it will be very tough for any new lab to live up to how brilliant TCB has been, and I'm am very sad to be leaving

Table of Contents

Abbreviations

a.a	amino acid
α-MSH	α-Melanocyte stimulating hormone
ACTH	adrenocorticotropic hormone
ADF	actin depolymerising factor
ASP	Agouti signalling protein
BMP	bone morphogenetic protein
CDK	cyclin-dependent kinase
CREB	cAMP response element-binding transcription factor
EGF	Epidermal growth factor
EMT	Epithelial to mesenchymal transition
ERM	Ezrin/radixin/meosin family
FAK	Focal adhesion kinase
F-actin	Filamentous actin
G-actin	Monomeric globular actin
GAP	GTPase activating proteins
GDI	GDP dissociation inhibitors
GEF	Guanine nucleotide exchange factors
GGTs	geranylgeranyltransferase
I.F.	Immunofluorescence
I.P.	Immunoprecipitation
KD	kinase dead
MC1R	melanocortin-1 receptor
MITF	microphthalmia-associated transcription factor
MLC	myosin-light chain
MLCK	myosin-light chain kinase
MLCP	myosin-light-chain phosphatase
PAK	p21-activated kinase
PDK1	Phosphoinsositiol dependent kinase 1
PH	pleckstrin homology
PIF	PDK1-interacting fragment
PKA	cAMP-dependent kinase
PTEN	phosphatase and tensin-homologue
RBD	Rho-binding domain
Rho	Ras-homologue family
RID	Rho-interacting domain
ROCK	Rho- kinase
SCC	squamous cell carcinoma
SMAD	Small Mothers Against Decapentaplegic
SRF	Serum response factor
TGF-β	Transforming growth factor-beta
WASP	Wiskott Aldrich syndrome protein
WAVE	WASP-family verprolin-homologous protein-1
WT	Wild-type
ZIPK	zipper-interacting protein kinase

List of Figures

The figure numbers highlighted in **bold** have an accompanying **supplementary movie.**

Supplementary Movies

Figure 5.3 – Actin Cytoskeleton

A375 cells transfected with either control non-targeting siRNA or PDK1 targeting siRNA were plated on deformable collagen/matrigel gels, then fixed and stained with TRITC phalloidin. The two movies shown are rotating 3D reconstructions of the acting cytoskeleton.

A- Control actin

B- PDK1 siRNA actin

Figure 5.7 A375 GFP CAAX

A375 cells expressing GFP-CAAX were plated on deformable collagen/matrigel gels and imaged using confocal microscopy at a rate of 1 frame every 3 seconds. 4 Movies are shown.

A. Control CAAX – cells treated with control non-targeting siRNA

B. PDK1 siRNA CAAX – cells transfected with PDK1 targeting oligos

C. Blebbistatin CAAX- cells treated with 2.5 μM Blebbistatin during imaging

D. Cytochalasin D CAAX – cells treated with 2 μM Cytochalasin D during imaging

Figure 6.2 A375 cell motility in vivo

Movies from in vivo intravital imaging of A375 GFP CAAX xenograft tumours. 4 movies are shown.

A- Whole tumour area and matrix – shows 3D reconstruction of tumour area imaged including the surrounding collagen fibres (in red)

B- Whole tumour area GFP only – Shows only the tumour cells in tumour area imaged. Note amoeboid movement at tumour margin, and elongated cell movement further away from the tumour margin.

C- Amoeboid crop – Shows time-lapse of the amoeboid movement shown in figure 6.2 top two panels

D- Elongated crop – Shows time-lapse of the elongated movement shown in figure 6.2 lower 2 panels.

Figure 6.10 A375 cell motility in vivo continued

Movies from in vivo intravital imaging of A375 GFP CAAX xenograft tumours. 2 movies are shown.

A- PDK1 knockdown – Shows protrusive type of cell motility that constitutes the majority of cell movement events in the PDK1 knockdown tumours

B- Chaotic blebbing switching to amoeboid – Shows an example of the plasticity in cell motility. The cell shown switches from blebbing chaotically in one position (similar to what is seen in vitro) to rapid directional amoeboid movement.

Figure 7.8 GFP ROCK time-lapse

A375 cells were transfected with either control non-targeting siRNA or PDK1 targeting siRNA oligos and also GFP-ROCK1 were plated on collagen/matrigel matrix and imaged at a rate of 1 frame every 3 seconds. 4 movies are shown.

A- Control GFP ROCK1 – shows the localisation of ROCK1 during blebbing cell movement

B- Control kymograph – movie of the control cell slice used for the kymograph in figure 7.8 panel ii.

C- PDK1 siRNA GFP ROCK1 a – shows the cytoplasmic localisation of ROCK1 in cells depleted of PDK1

D- PDK1 siRNA GFP ROCK1 b – Shows that even when ROCK1 is asymmetrically distributed in cells lacking PDK1, ROCK1 is unable to drive cell motility as in the control cells.

Figure 8.11 Double knockdown restored cell motility

MTLn3E cells transfected with control non-targeting siRNA, PDK1 targeting siRNA or both PDK1 and RhoE targeting siRNA were plated on deformable collagen/matrigel matrix and imaged by phase contrast at a rate of 1 frame every 5 minutes. 1 movie is shown that sequentially shows the motile behaviour of cells from each transfection

A- MTLn3E phase time-lapse – this movie first shows control cells, then elongated PDK1 depleted cells and finally the rescued cell motility when PDK1 and RhoE are knocked down together.

Figure 9.9 B16 cell motility in vivo

B16 F2 cells stably expressing GFP CAAX were injected subcutaneously into the flank of nude mice. Intravital multiphoton time-lapse imaging is shown.

A- Whole tumour area – Shows the whole imaged area. Tumour cells are in green, collagen fibres are in blue, and pigment containing speckles are shown in pink.

B- Crop collective and single cell – cropped area of the above movie showing and example of both single cell movement and also a group of cells moving collectively.

Figure 9.20 TGFβ1 and TGFβ2 increase cell motility of B16F2 cells in vitro.

B16F2 cells were plated on deformable collagen/matrigel matrix and treated with either MSH, TGFβ1 or TGFβ2 for 24 hours before imaging. Cells were then imaged by phase contrast for 16 hours.

A- untreated B16F2 cells

B- B16F2 cells treated with TGFβ2

B16F2 cells treated with TGFβ2 have less dendritic morphology and move much more rapidly.

1 Chapter 1 – Introduction

This thesis reports investigations into mechanisms of cancer cell motility with particular focus on the behaviour of cells in vivo, and in complex 3-dimensional in vitro environments. This introduction will cover current knowledge of cell motility and focus particularly on metastasis and modes of cancer cell motility. The main cell type that has been used as a model system for the experiments carried out is melanoma, so particular attention will be paid to the origins of melanoma and its invasive behaviour. The signalling pathways that have been found to play a role in the types of cell motility investigated here are focussed around the generation of contractile forces, so current knowledge of Rho and ROCK signalling is reviewed in detail. It was also found that PDK1 was required for regulation of ROCK, so the role of PI3K signalling and phospholipids in cell motility is discussed. Finally it was found that pigment production and invasive potential of melanoma cells was influenced by TGF-β signalling.

This introduction will cover a wide range of signalling pathways, which reflects the complexity of cell motility mechanisms in vivo. This thesis only begins to uncover some of the details as to how cancer cells really move and invade in vivo; more work is required to investigate this issue in detail.

1.1 Melanoma

The majority of the experiments in this thesis have utilised melanoma cell lines as a model system. Melanoma is a type of skin cancer arising from the aberrant proliferation of melanocytes. It is relatively easy to treat provided metastasis has not occurred, however metastatic melanoma is particularly aggressive and prognosis is very poor [1]. The highly invasive nature of this cancer type made it an interesting model in which to study cell motility.

1.1.1 Functions of melanocytes

Melanocytes reside in the lower levels of the epidermis and exist at an approximate ratio of 1:10 with keratinocytes. The melanocyte stretches out long dendritic process and the melanin

that the melanocyte produces is exported along the dendrites and is taken up by the keratinocytes (Figure 1.1)[2]. This is the process that gives skin its colour. Pigment production is largely determined by the expression of melanocortin-1 receptor (MC1R) which is a G-protein coupled receptor positively linked to adenylate cyclase by the G-protein subunit Gαs. MC1R is stimulated by agonists α-Melanocyte stimulating hormone (α-MSH) and adrenocorticotropic hormone (ACTH)[2]. Stimulation by both α-MSH and ACTH can up regulate the expression of MC1R forming a positive feed back loop. Agouti signalling protein (ASP) is an antagonist for MC1R [2].

MC1R driven increases in cAMP activate cAMP-dependent kinase (PKA), which in turn activate the cAMP response element-binding transcription factor (CREB). Activity of CREB leads to the transcription of microphthalmia-associated transcription factor (MITF). MITF has many target genes but among them are genes encoding the enzymes critical for melanin production, such as tyrosinase. In addition to regulating MITF, cAMP levels down-regulate PI3K activity as well as stimulate Rac activity and inhibit Rho activity which leads to the dendritic cell morphology [3, 4]. In fact it has even been reported that inhibition of RhoA is additionally required for melanogenesis as well as dendrite formation [5].

UV radiation is harmful to cells as it produces free radicals able to cause DNA damage. In response to UV light, melanocytes are stimulated to rapidly oxidise and polymerise existing melanin that is rapidly exported to keratinocytes migrating upwards, and skin gets darker in colour. The increase in pigment in the upper layers of the skin is thought to help protect the stem cells and melanocytes in the lower levels of the skin from DNA damage [6]. The expression of microphthalmia-associated transcription factor (MITF) is also up regulated rapidly following UV exposure. The up regulation of MITF is thought to be required for production of pigment and also play a role in effective repair of DNA damage.

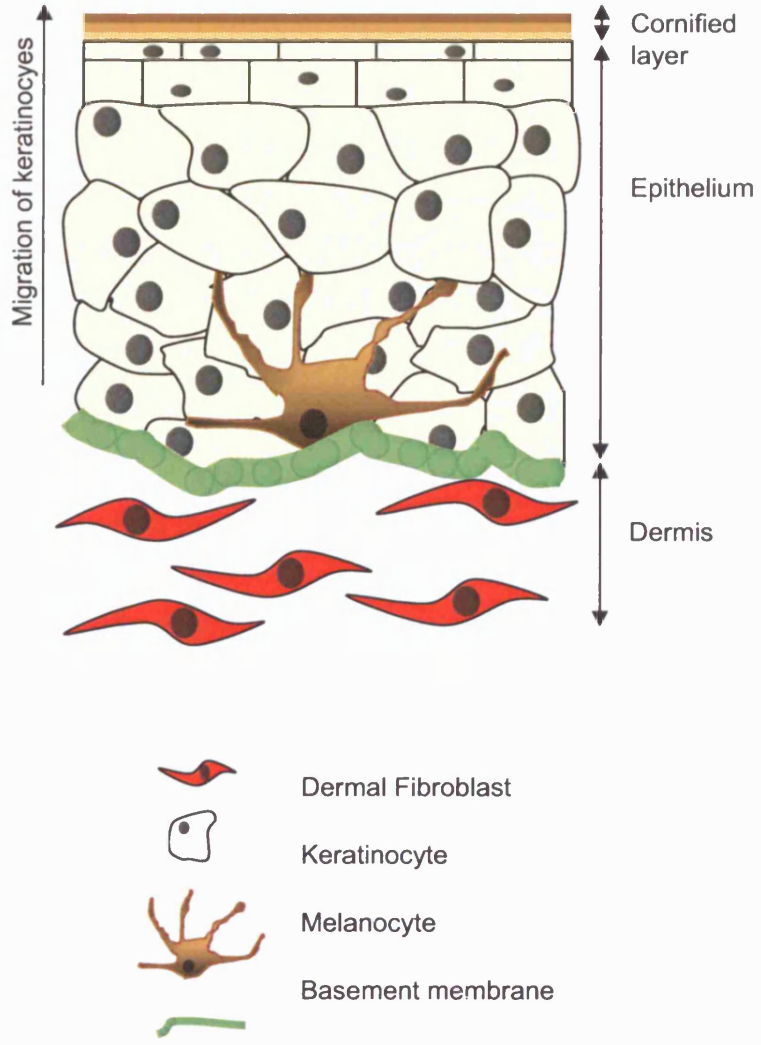

Figure 1.1 Schematic diagram showing the position of melanocytes in the skin. Melanocytes reside in the basal area of the epidermis. Melanin is produced and transported along dendrites then exported and taken up by surrounding keratinocytes. The keratinocytes migrate upwards to form the protective cornified layer of the epidermis that is in contact with the outside environment.

1.1.2 Melanin

Melanin is a pigment found in both plants and animals. In humans melanin is found in the skin, hair, iris and also in certain pigment containing neurones in the substantia nigra [2]. The chemical properties of melanin means that it acts to protect cells from harmful radiation. Melanin molecules absorb UV-light and convert the energy to heat. This keeps the production of free radicals at a minimum and reduces DNA damage [7]. There are several different forms of melanin. Eumelanin and Pheomelanin are found in human skin, Neuromelanin is present in specific neurones in the substantia nigra. Eumelanin is found in two forms, black and brown, and they are more abundant in people with dark skin. Blonde individuals tend to have less black eumelanin and a small amount of brown eumelanin. Pheomelanin is red in colour and is responsible for the colouring of red hair. The function of neuromelanin in the brain is as yet unclear, but loss of these pigmented neurones is correlated with degenerative diseases such as Parkinson's disease [8].

Melanin molecules are synthesised from tyrosine and the first and rate-limiting step of melanin production is the conversion of tyrosine to dopaquinone by the enzyme tyrosinase [2]. Individuals with dark skin contain similar numbers of melanocytes in their skin as fair-skinned individuals however the tyrosinase activity and the pigment production in black skin is much higher [2]. Melanocytes synthesise melanin molecules in melanosomes that are transported to the cell periphery using the microtubule network, which is dependent on kinesin. At the cell periphery, a Rab27A complex is required to allow melanosomes to be recruited onto the actin network. The melanosomes are then anchored to the plasma membrane through an interaction of Slp2, Rab27A and phosphatidyl serine in the membrane. The melanin can then be released from the melanocyte and taken up by the surrounding keratinocytes. Rab27A is transcriptionally up regulated by increases in cAMP levels and this can promote the interaction of melanosomes with cortical actin at the cell periphery, increasing the rate of export [9].

1.1.3 The origin and differentiation of melanocytes

Melanocytes are generally a very stable population in the lower level of the epidermis (Figure 1.1) or at the base of hair follicles and proliferate very slowly in contrast to the transit amplifying population of keratinocytes that proliferate relatively rapidly. Melanoblasts originate from the neural crest, a population of cells that develops from the neural tube. The

neural crest cells migrate and differentiate to form diverse tissues ranging from cranio-facial structures, neurones and melanocytes [10]. They must develop and migrate to the appropriate sites then survive and differentiate depending on signals for the local environment [10]. MITF plays a critical role in promoting the differentiation of melanocytes [11]. The mutation of MITF in mouse models results in reduced numbers of melanocyte precursor cells, whereas constitutive MITF expression in vitro is able to convert murine fibroblasts to melanocyte-like cells [11]. It is thought that MITF controls differentiation of melanocytes but is also required for the survival of cells in the neural crest lineage. A potential mechanism for this has been described by McGill et al, who found that MITF was able to transcriptionally regulate Bcl2 to protect cells from apoptosis [12].

1.1.4 Melanoma

Exposure to UV light is the major risk factor for developing melanoma. The initiation of melanoma is the aberrant proliferation of melanocytes which gives rise to nevi within the epidermis. The majority of these nevi do not progress to malignant disease, but it was thought a small sub-set can progress and begin to invade into the dermis (vertical growth phase) before becoming metastatic and spreading to distant sites. This has recently been challenged and it has been proposed that metastatic melanoma originates from new nevi which rapidly progress to malignant disease [1]. To understand malignant melanoma it is important to determine the genetic changes occurring between benign nevi and melanoma invading the dermis [1].

One major advance in the understanding of melanoma was the discovery that the serine threonine kinase B-RAF was mutated in 66 % of all malignant melanoma, and that V599E accounted for 80% of all B-RAF mutations and significantly increased B-RAF kinase activity [13]. B-RAF signals through the MAPK pathways to increase levels of phosphorylated ERK. ERK has many substrates, both nuclear and cytoplasmic, which can increase cell proliferation, apoptosis and survival [14]. Activating mutations in N-RAS, which is upstream of B-RAF are able to account for the majority of the melanomas that do not express mutant B-RAF. Mutation of both N-RAS and B-RAF is rare and these oncogenic mutations are generally exclusive of one another [14]. However the role of B-RAF in melanoma progression remains unclear, as many benign nevi also express mutant B-RAF, so expression of over active B-RAF is not necessarily sufficient for the progression to metastatic disease. Another

commonly mutated gene found in melanoma is phosphatase and tensin-homologue (PTEN) [15, 16]. Similarly to B-RAF, mutation of PTEN is generally found mutually exclusively of N-RAS mutations. However simultaneous mutation of both B-RAF and PTEN in the same tumour does occur [16]. PTEN is a phosphatase that converts $PI(3,4,5)P_3$ to $PI(4,5)P_2$. Mutations in PTEN result in elevated $PI(3,4,5)P_3$ and therefore increased Akt/PKB signalling, leading to increased proliferation and reduced cell death.

1.1.5 Invasive behaviour of melanoma

Developing melanoblasts are a non-pigmented, motile cell population. However differentiated melanocytes are fixed in their position in the skin and produce pigment. The idea that the motile behaviour of developing melanoblasts might predispose melanoma to being highly aggressive has been tested. Gupta et al. found that when cell lines of different origins were transformed with the same set of oncogenes, only melanocytes became metastatic whereas other cell lines could form tumours but were not invasive [17]. It was discovered that non-transformed melanocytes still expressed Slug, a transcription factor governing neural crest migration, and that expression of Slug co-operated with the oncogenic mutations to give rise to intrinsically invasive tumours [17]. This information has led researchers to hypothesise that the invasive behaviour of melanoma arises due to a failure of melanoma cells to differentiate, meaning that the mechanisms for cell motility which should have been shut down are still potentially active. For example, RhoA, which is inhibited during differentiation and needs to be active at only low levels to allow the formation of dendrites. In this case the failure to differentiate might allow high levels of Rho activity that could be responsible for increased cell motility. The role of RhoA in cell motility is discussed later.

There is some interesting evidence to support the hypothesis that invasive behaviour correlates with poorly differentiated tumours. MITF, the transcription factor critical for melanocyte differentiation and survival has been linked to invasive behaviour of melanoma. Firstly it has been found that MITF is able to regulate the gene DIAPH1 encoding Dia1 [18]. Low levels of MITF led to down-regulation of Dia1 which in turn resulted in higher levels of ROCK signalling which is linked to amoeboid cell invasion (see 1.8.2). MITF also plays a role in cell proliferation, and low levels of MITF can cause cell cycle arrest; but complete loss of MITF is detrimental to the survival of melanoma cells as they are unable to proliferate [18].

Put together, these results might suggest that motile melanoma cells are also less proliferative. Another study has shown that over-expression of MITF in melanoma cell lines rendered the cells less invasive. MITF over-expression caused the up regulation of melanocyte differentiation markers and xenograft tumours from these cells were smaller in size and failed to metastasise [19]. Both of these studies strongly suggest that less well-differentiated melanoma cells are also more invasive and have greater metastatic potential. There are also cases of amelanotic malignant melanomas [20]. Patients with these tumours have a particularly poor prognosis, which may suggest that the lack of pigmentation and presumably less well-differentiated status of these nevi mean that they are inherently more aggressive. However because of the lack of pigment production, it is also true that amelanotic melanoma is usually harder to diagnose and is usually identified at a later stage than pigmented lesions which could also explain why the prognosis is very poor [20].

It has been suggested that the microenvironment is also important for the aggressive phenotype of melanoma. Normal differentiated melanocytes can be transiently converted to an aggressive melanoma-type cell by placing them in contact with melanoma cells. However the converse is not true and the normal melanocyte microenvironment is not able to convert aggressive melanoma cells to less invasive differentiated cells [21]. However, an embryonic environment is able to re-programme metastatic melanoma cells. Firstly it has been shown that metastatic melanoma cells injected into a chick embryo would migrate and follow the path of normal neural crest cells rather than forming tumours [22]. It has also been found that metastatic melanoma cells express nodal, a member of the Transforming growth factor-β (TGF-β) super-family, which is normally expressed during embryonic development. Over-expression of nodal in melanoma inhibits differentiation [23, 24]. These findings suggest that invasive melanoma is less differentiated and that aggressive cells could be controlled with the correct cues from the microenvironment. If it would be possible to treat aggressive melanoma by mimicking signalling from an embryonic environment it may be possible to induce the melanoma cells to differentiate causing them to stop invading and proliferating. The aggressive cells of a melanoma tumour could be less differentiated because they have lost the differentiation signalling required, but another hypothesis is that the aggressive cells were never properly differentiated and are a type of cancer stem cell. Highly aggressive melanoma cell subsets have been reported to have a molecular signature similar to pluripotent stem cells [25]. This hypothesis is as yet unproven but several markers such as

ABCB5 have been found and can be used to isolate populations of cells that contain a higher proportion of stem cells as measured by tumourigenic potential [26]. The relationship between pigment production, invasive behaviour and cell morphology is investigated in chapter 9.

1.2 TGF-β signalling

Transforming-growth factor β ligands are a family of cytokines and in humans there are 42 isoforms which are split between 2 sub-families; TGFβ/Activin/Nodal family and the bone morphogenetic protein (BMP)/growth and differentiation factor (GDF) family. TGF ligands interact with membrane serine/threonine kinase receptors[27] (Figure 1.2). Ligands are thought to exist as dimers and interact with hetero-tetrameric receptors made up of 2 type II receptors and 2 type I receptors. Upon ligand binding the type II receptor phosphorylates and activates the type I receptor. The activated type I receptor then phosphorylates the receptor SMADs (Small Mothers Against Decapentaplegic) (Figure 1.2). In the case of the canonical TGFβ signalling, the receptor SMADs are SMAD2 or SMAD3. Once phosphorylated, SMAD2 or SMAD3 interact with SMAD4 to form a complex, and translocate to the nucleus. In the nucleus, the SMAD complex combines with other transcription factors to regulate gene transcription (Figure 1.2)[28]. Different cell types express different combinations of SMAD co-factors so the transcriptional profile is cell type dependent. SMAD7 is an inhibitory SMAD and acts to inhibit the activation of receptor SMADs and compete for binding to SMAD4. SMAD7 can also disrupt receptor SMAD complexes from binding to DNA [29].

TGFβ signalling controls many aspects of cell behaviour. TGFβ has been characterised as a growth inhibitory chemokine but it has also become clear that the growth inhibitory effects of TGFβ are dependent on the cell type and also the differentiation status of the stimulated cell, and that in some contexts TGFβ can have the opposite effect. During embryogenesis, TGFβ signalling does not act as a growth inhibitor, but as cells mature they gain the ability to respond to TGFβ in a different way and either stop growing or undergo apoptosis. TGFβ in cancer is a much-discussed topic, as tumour cells can also overcome the growth arrest signals downstream of TGFβ and instead TGFβ can stimulate cells to become more invasive and increase their metastatic potential.

In tumour cells increased TGFβ production is correlated with increased severity and higher tumour grades [30]. TGFβ signalling can inhibit the growth and proliferation of leukocytes such as T-lymphocytes, and this can increase the ability of tumour cells to evade detection by the immune system [31]. TGFβ can also signal to other cells in the tumour microenvironment, such as endothelial cells, to stimulate angiogenesis through the induction of VEGF [32]. TGFβ can also act on the stromal fibroblasts causing them to up regulate proteases such as MMP9 and changing their behaviour, making them more invasive and more prone to promote tumour cell invasion [33]. When TGFβ acts on the tumour cells themselves, it can stimulate an epithelial to mesenchymal transition (EMT) as discussed above. TGFβ induces transcription of SNAIL, which can repress transcription of E-cadherin, causing cells to become less epithelial [34, 35]. For cells to invade, they must also acquire motile behaviour, which requires re-organisation of the actin cytoskeleton. The role of TGFβ in melanoma may be at least in part SMAD-independent as it has been reported that there is significant cross talk between TGFβ and ERK signalling. It has been shown that TGFβ is able to signal through RhoA and RhoB to induce stress fibre formation and actin polymerisation [36]. It is still unclear how TGFβ is able to signal to Rho, but it has been seen that the activation of Rho is extremely rapid following TGFβ stimulation [36]. A recent paper has gone further and suggested that TGFβ signalling over long periods of time not only induces EMT but switches the profile of cancer cells to cells with more stem cell-like properties [37].

The skin is one organ that is very sensitive to TGFβ signalling. If TGFβ is expressed in differentiated suprabasal layers of the epidermis then this causes an increase in the rate of cell division [38, 39], whereas expression of TGFβ in the proliferating cells in the basal level caused growth arrest [40]. TGFβ has also been reported to play a role in melanoma progression. Increased expression of TGFβ isoforms in melanoma has been reported [41]. TGFβ2 and TGFβ3 are not expressed in normal melanocytes but are up regulated in melanoma and seem to increase as tumours progress [42].

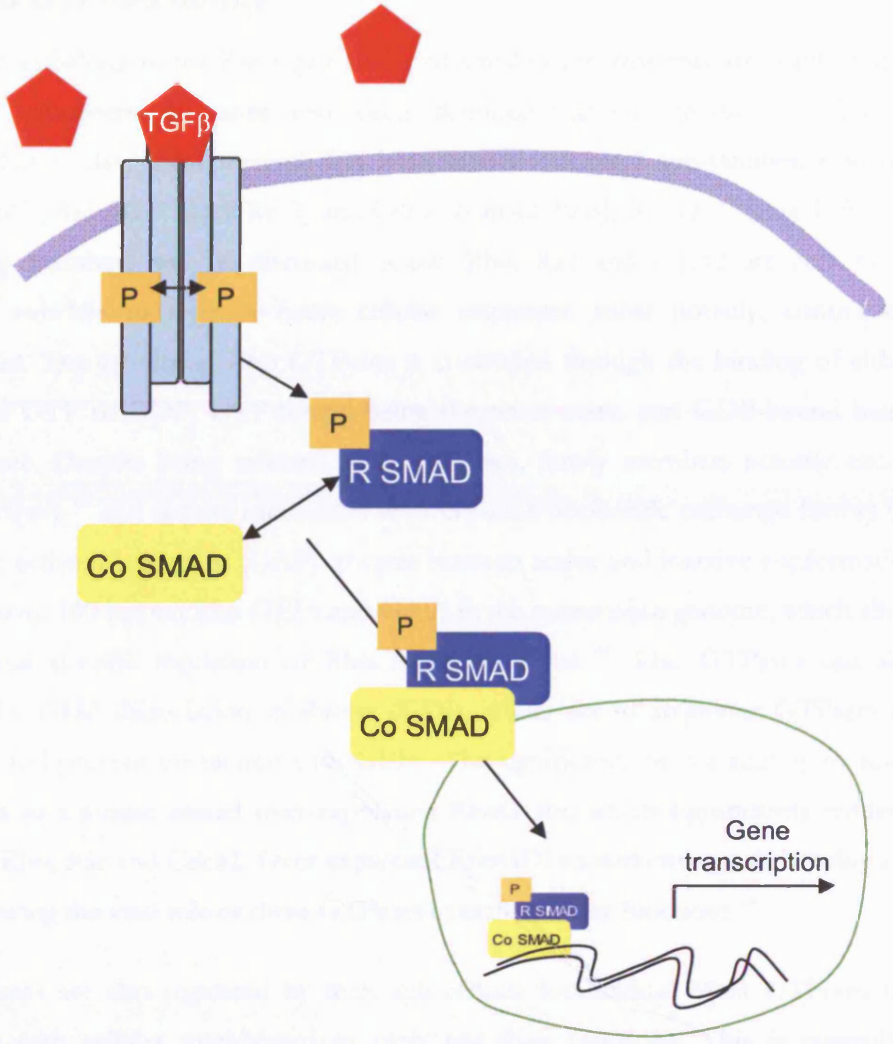

Figure 1.2 Schematic diagram of TGF-β signalling. TGFβ ligand binds to heteromeric transmembrane serine/threonine kinase receptors. Activation and transphosphorylation of the receptors leads to the phosphorylation of receptor SMAD, SMAD2 or SMAD3 (R-SMAD). Receptor SMADs can then form a complex with the Co SMAD, SMAD4, and these complexes translocate to the nucleus. In the nucleus the SMAD complex binds to DNA and initiates gene transcription.

1.3 Rho GTPase family

Rho GTPases belong to the Ras super family of small G-proteins that are highly conserved among all eukaryotes. 20 genes have been identified that encode different Rho family members but to date most research has been carried out on 3 sub-families; Rho (RhoA, RhoB, RhoC), Rac (Rac1 Rac2 Rac3) and Cdc42 (Cdc42, RhoJ, RhoQ) (Figure 1.3). Atypical Rho family members will be discussed below. Rho, Rac and Cdc42 are able to act as molecular switches to regulate many cellular responses, most notably, control of the cytoskeleton. The activity of Rho GTPases is controlled through the binding of either the nucleotides GTP or GDP, GTP-bound being the active state, and GDP-bound being the inactive state. Despite being referred to as GTPases, family members actually elicit little GTPase activity [43] and require interaction with Guanine nucleotide exchange factors (GEF) or GTPase activating proteins (GAP) to cycle between active and inactive conformations [44]. There are over 100 known Rho GEFs and GAPs in the mammalian genome, which allow for complex and specific regulation of Rho family GTPases [44]. Rho GTPases can also be regulated by GDP dissociation inhibitors (GDI), which act to sequester GTPases in the cytoplasm and prevent interaction with GEFs. The significance of the activity of RhoGDI was shown in a mouse model over-expressing RhoGDIα, which significantly reduced the activity of Rho, Rac and Cdc42. Over-expressed RhoGDI caused embryonic lethality at early stages, showing the vital role of these GTPases in many cellular functions [45].

Rho GTPases are also regulated by their sub cellular localisation. Most GTPases require interaction with cellular membranes to carry out their functions. This is controlled by modification of a C-terminal CAAX sequence (A= aliphatic residue). Firstly the CAAX cysteine is modified and linked to either farnesyl or geranylgeranyl lipid by either farnesyl transferases or geranylgeranyltransferases (GGTs). Substrate specificity is determined by the amino acid in the 'X' position, although most Rho family members are geranylgeranylated. The C-terminus is then cleaved to remove 'AAX'. The final step to the modification is the methylation of the exposed cysteine residue [46]. The result of the modifications is to leave a hydrophobic C-terminal domain when the rest of the molecule is relatively hydrophilic. This hydrophobic domain, in conjunction with basic amino acids immediately upstream then allows the GTPase to be inserted in the plasma membrane [46]. Immediately upstream of the CAAX motif is a hypervariable region that is also implicated in the regulation and localisation of Rho family members. Rac1 and RhoA both contain polybasic residues in their

hypervariable region similar to K-Ras and are required in some cases (K-Ras, Rac1) for plasma membrane localisation [47].

Over a decade ago it was found that RhoA regulated the formation of actin stress fibres, Rac induced actin polymerisation for lamellipodia and membrane ruffling, and Cdc42 promoted actin assembly into filopodia [48, 49]. Since this initial finding it has been shown in many different systems that these Rho GTPases act as master regulators to control the actin cytoskeleton in many different cell contexts. Control of the actin cytoskeleton can also lead to regulation of gene transcription. Serum response factor (SRF) is a transcription factor that controls transcription of many genes activated by mitogenic stimuli such as serum addition. SRF is activated downstream of a mechanism which is able to sense the levels of unpolymerised G-actin in the cytoplasm. This regulatory mechanism is able to sense the depletion of the G-actin pool and up regulate mRNA production. The activity of Rho, Rac and Cdc42 can stimulate the polymerisation of actin and therefore indirectly activate SRF, altering the transcriptional profile of the cells [50]. Rac and Cdc42 can also alter transcription by activating JNK and p38 MAPK pathways though this is thought to be independent of their activities affecting the cytoskeleton [51, 52]. The activity of the transcription factor NFκB can also be regulated by PAK1, which is an effector of Rac1 and Cdc42 [53].

Rho, Rac and Cdc42 are also able to control cell cycle progression [54]. This was first observed when cells were treated with Clostridium botulinum C3 transferase[54 55], or microinjected with dominant negative forms of Rac and Cdc42, which caused a G1-S-phase cell cycle arrest. RhoA is able to inhibit the transcription of p21, a potent cyclin-dependent kinase (CDK) inhibitor [56]. Additionally, over-expression of Rac1 or Cdc42 that are deficient in GTPase activity has been found to be sufficient to induce cyclin-D1 expression[57]. Although it has been seen that Rho, Rac and Cdc42 families of GTPases have distinct effects on the cytoskeleton, it is also true that these pathways are intimately linked and over-lapping, as downstream effector proteins are able to interact with more than one Rho GTPase. For example p21-activated kinase (PAK) family members interact with Rac1, Rac2, Rac3, Cdc42, as well as some other less well studied family members [58].

1.3.1 RhoA sub-family

Rho stands for Ras homologue gene family. RhoA, RhoB, and RhoC are highly homologous in sequence (~85% identity based amino acid sequence) (Figure 1.3) but seem to have

distinct non-redundant functions despite all three isoforms being ubiquitously expressed in all tested tissues[59]. The C-terminal CAAX sequence of the 3 Rho proteins is the most variable and could dictate their specificity by controlling their different sub-cellular localisation. RhoB localises mainly to late endosomes, whereas activated RhoA and RhoC are found at the plasma membrane or in the cytoplasm[59].

Rho isoforms interact with their regulator GEFs and GAPs and also to their downstream effectors through regions named switch1 and switch2. The switch1 region clamps GTP or GDP between itself and the rest of the molecule, and interaction with a magnesium ion is essential for binding to GDP [60]. This magnesium ion is removed by interaction with GEFs and promotes nucleotide release.

The control of filamentous actin is achieved by the binding of active Rho GTPases to their effectors. RhoA is able to directly stimulate actin polymerisation through activation of diaphanous-related formins (Dia proteins)[61] [62]. The activation of ROCK by RhoA can also contribute to an increase in actin filaments through the phosphorylation and inhibition of cofilin. ROCK and mDia are also able to work together in the generation of stress fibres. Rho proteins are also implicated in the regulation of cell adhesions. The turnover of adhesions is required for effective cell motility, and Rho has been shown to be required for the release of cell adhesions in the rear [63]. RhoA and RhoC are also able to regulate adherens junctions and tight junctions through the activation of ROCK. Regulation of ROCK is the focus of chapters 3 and 4 so will be discussed in greater detail below.

RhoA and RhoB are able to promote transformation of cultured fibroblasts and RhoA has been shown to be over-expressed in several cancer cell lines. The transformation induced by RhoA requires the activity of ROCK effectors [64]. In contrast, RhoC does not seem to be able to induce transformation but RhoC has been found to be up regulated in tumours that have increased metastatic potential [65, 66]. RhoC has also been reported to interact more strongly with the effectors ROCK1 and ROCK2 than RhoA, so RhoC could be up regulated in metastatic tumours, to initiate ROCK-driven cell motility [65].

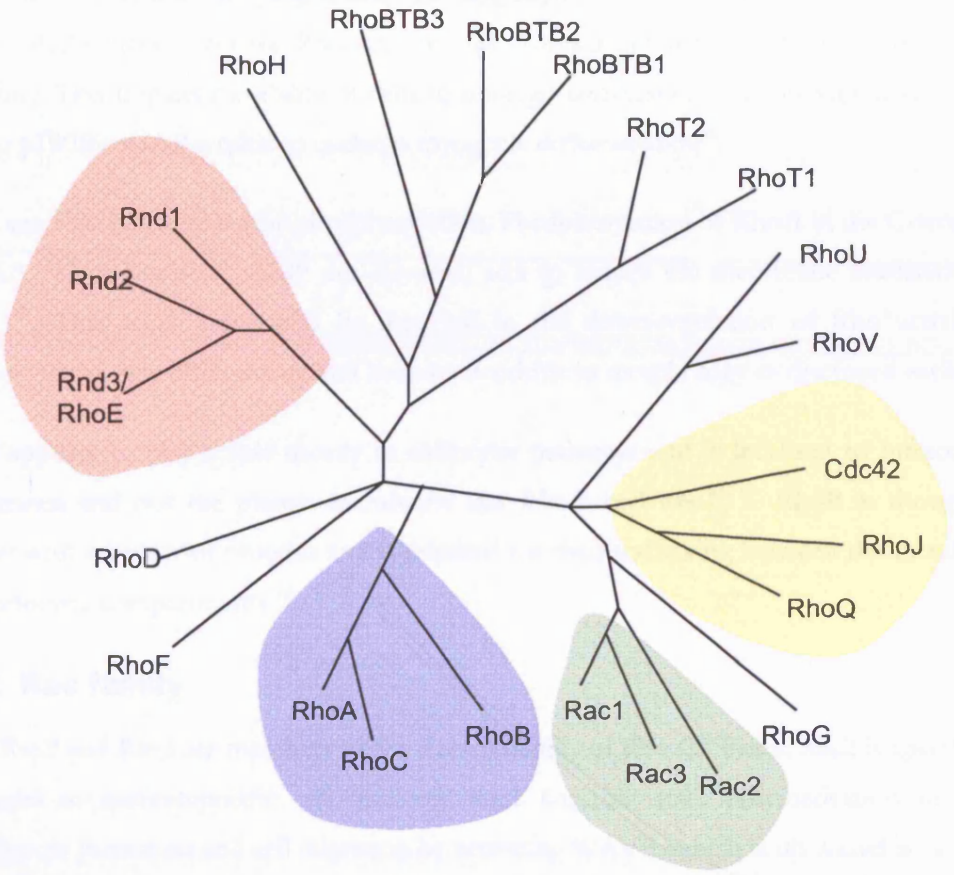

Figure 1.3 Rho family of GTPases. The 23 members of the Rho family of GTPases are shown grouped together by their homology to each other. Highlighted are the RhoA sub-family, the Rac family, the Cdc42 family and also the Rnd family of atypical Rho family GTPases.

Rho activity has also been implicated in differentiation in numerous systems [67]. As mentioned above, inhibition of Rho activity seems to be required for differentiation of melanocytes and formation of dendrites, but adjusting Rho activity has also been shown to alter the differentiation programme of adipocytes and myocytes [68]. Mice lacking p190RhoGAP have excessive Rho activity; this causes a down-modulation of insulin/IGF signalling. This impairs the ability of cells to undergo conversion to adipocytes, instead cells lacking p190RhoGAP tended to undergo myogenic differentiation[68].

RhoA can also be regulated by phosphorylation. Phosphorylation of RhoA in the C-terminus by PKA, when levels of cAMP are elevated, acts to reduce the membrane localisation of RhoA [69]. This could potentially be involved in the down-regulation of Rho activity in melanocytes as they differentiate and become dendritic in morphology as discussed earlier.

RhoB appears to play a role mostly in endocytic pathways and is localised to intracellular membranes and not the plasma membrane like RhoA and RhoC [59]. RhoB is thought to interact with a variety of proteins and is required for their trafficking between the membrane and endocytic compartments [70].

1.3.2 Rac family

Rac1, Rac2 and Rac3 are members of the Rac subfamily of Rho GTPases. Rac2 is specifically expressed in haematopoietic cell lineages. Rac1 controls actin polymerisation to drive lamellipodia formation and cell migration by activating WAVE, which is discussed later. Rac3 is not required for lamellipodium formation but depletion of Rac3 still strongly inhibited cell invasion through 3D matrix, even though cell migration in 2D was not affected. [71, 72].

Rac and Rho have been shown to be antagonistic in a variety of contexts, and this exclusivity in signalling would act to spatially separate Rho and Rac activity in cell. One way in which Rac is able to antagonise Rho activity is through p190RhoGAP. Rac activity is able to induce the translocation of p190RhoGAP to adherens junctions where it locally inhibits Rho activity [73]. There is also an opposite mechanism by which Rho activity leads to the activation of a Rac GAP, FilGAP to inactivate Rac [74].

1.3.3 Cdc42 family

Cdc42 and related family members RhoJ and RhoQ are able to activate actin polymerisation [75-77]. When GTP-bound Cdc42 binds to PI(4,5)P_2 in the cell membrane, this recruits Wiskott Aldrich syndrome protein (WASP) and changes conformation that allows the activation of N-WASP[76]. The subsequent recruitment of the ARP2/3 complex then drives actin polymerisation at the cell periphery[78]. MRCK is another effector of Cdc42, able to co-ordinate the actin cytoskeleton. Signalling through this pathway has been shown to be required for the collective migration of squamous carcinoma cells in 3D environments [79]. Another group of Cdc42 effectors are the p21-activated kinases (PAKs). Activity of PAKs can lead to the dissolution of actin stress fibres, and also the activation of the MAPK pathway activating JNK[80]. Cdc42 is also involved in a cell polarity complex through binding to Par3, Par6 and atypical PKCs[81], and can act to control apical/basolateral polarity and the maintenance of cell junctions[81].

1.3.4 Atypical Rho family GTPases

The atypical Rho GTPases include Rnd1/RhoE, Rnd2, Rnd3, RhoBTB1, RhoBTB2, RhoH, RhoT1, RhoT2, RhoU, and RhoV (Figure 1.3). These Rho family members are not regulated in the same way as the family members described above. Although they contain a GTPase domain, this domain is frequently different in sequence form the classical Rho GTPases in residues critical for hydrolysis of the bound nucleotide, meaning that they are GTPase defective. Therefore instead of their activity being regulated by GEFs/GAPs and the exchange of GTP for GDP, regulation is generally via their expression level, their degradation or their protein-protein interactions [82].

Rnd1, Rnd2, and Rnd3 (RhoE) are one branch of the atypical Rho family. Rnd proteins bind only very weakly to GDP and have very low GTPase activity, so they exist predominantly in GTP-bound state [82]. RhoE is interesting, as many of RhoE's functions appear to be the opposite to the functions of RhoA [83]. Over-expression of RhoE leads to a loss of actin stress fibres and the induction of many branching protrusions. RhoE is able to bind to p190RhoGAP causing increased GAP activity towards RhoA and causing a reduction in the levels of active GTP-bound RhoA [83 84]. RhoE can also inhibit Rho activity by directly binding to the Rho effector ROCK1. Although RhoE and RhoA have relatively similar structures they bind to different parts of the ROCK1 sequence [85]. It is also interesting that RhoE

specifically interacts with ROCK1 and not the closely related ROCK2. RhoE binds to ROCK1 around the kinase domain, and requires the amino acid sequences 375-420, and also a region in the extreme N-terminus.

RhoE is phosphorylated by ROCK1 at several residues, this phosphorylation causes RhoE to localise to the cytoplasm in a similar way to the phosphorylation of RhoA by PKA [69]. In addition to altering RhoE localisation, phosphorylation of RhoE by ROCK1 also increases the protein stability of RhoE [86]. The phosphorylation of RhoE by ROCK does not affect the binding of ROCK1 to RhoE so it is possible that ROCK1 and RhoE interact at cell membranes, then move into the cytoplasm together, meaning that ROCK1 could inhibit its own activity by phosphorylating RhoE to increase RhoE stability causing ROCK1 to be sequestered and inhibited in the cytosol.

RhoE has been shown to be regulated by p53. p53 is able to induce RhoE expression in response to DNA damage, and the increased levels of RhoE act to inhibit ROCK1-mediated apoptosis [87, 88]. A recent paper has also implicated p53 in cell motility driven by Rho and ROCK. It is possible that the role of p53 in this context is also through the up regulation of RhoE and the subsequent inhibition of ROCK1 signalling [89].

1.4 Activity and function of Rho-kinases

ROCK1 and ROCK2 are effectors of RhoA-GTP RhoB-GTP and RhoC-GTP. They are also termed ROKβ and ROKα/Rho-kinase, respectively. The term 'ROCK' is used to mean ROCK1 and ROCK2 collectively. ROCK1 and ROCK2 are members of the AGC family of serine threonine kinases based on sequence homology of their catalytic subunits (Figure 1.4). Both ROCK1 and ROCK2 contain an N-terminal kinase domain, a coiled coil region and a Rho-binding domain, and a PH domain in the C-terminus (Figure 1.5). They are largely similar in sequence so it was assumed that they would carry out similar functions and act largely redundantly. This has since been shown not to be the case. The differences in their functions are discussed below.

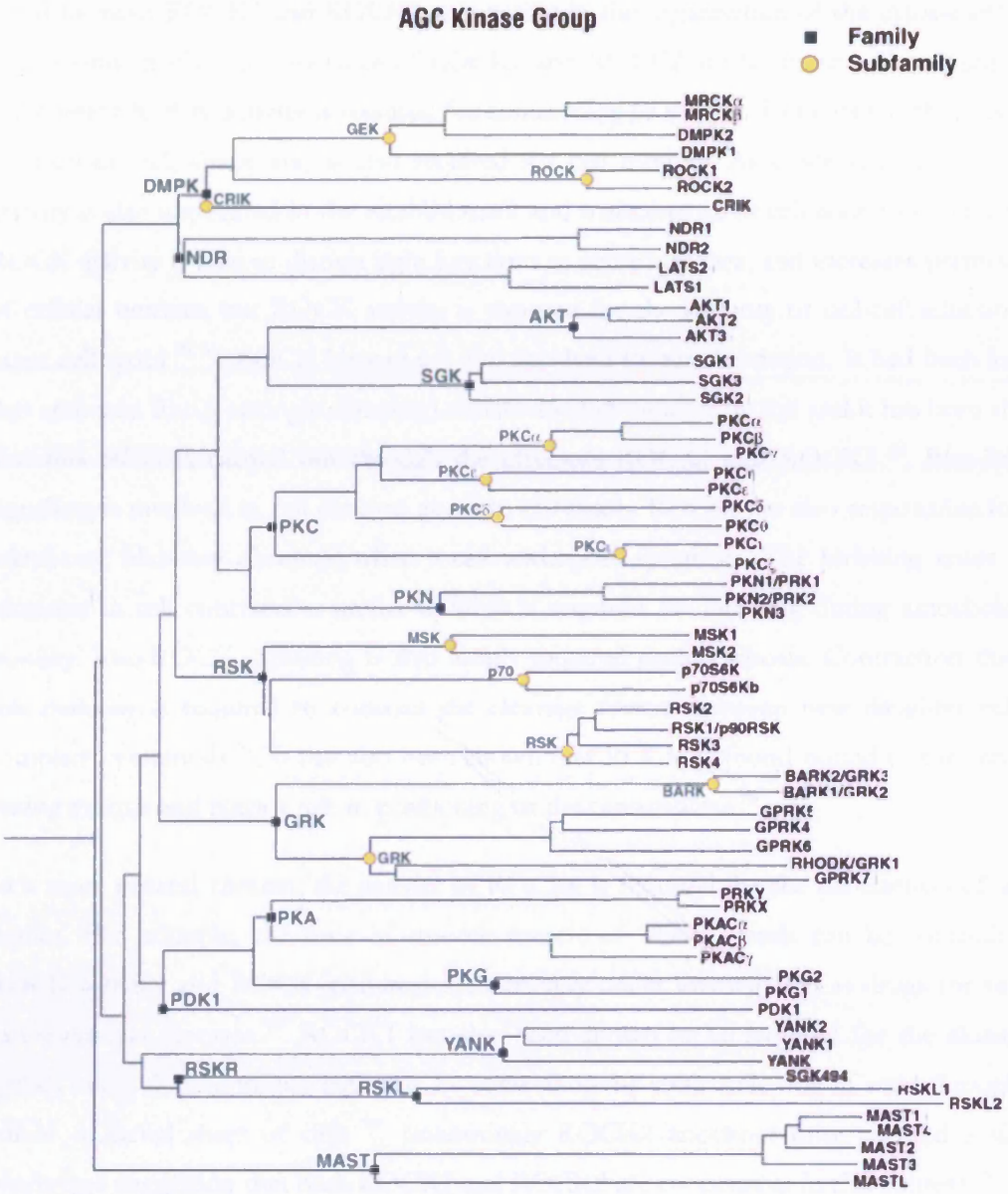

Figure 1.4 Diagram showing members of the AGC family of protein kinases. This diagram is adapted from http://www.cellsignal.com/reference/kinase/agc.html. Family members are grouped together based on homology to one another.

Although the focus of the experiments in this thesis is to investigate the regulation of ROCK (used to mean ROCK1 and ROCK2 generically) in the organisation of the cytoskeleton for cell motility in vivo, the activities of ROCK1 and ROCK2 are far more wide ranging. In a cell context ROCK activity is required for contractility of F-actin filaments which is required to maintain cell shape and is also required for cell motility. As described above, ROCK activity is also implicated in the establishment and maintenance of cell adhesions. Too much ROCK activity is able to disrupt tight junctions in some contexts, and increases permeability of cellular barriers, but ROCK activity is required for the integrity of cell-cell adhesions in other cell types [90, 91]. ROCK kinases are also involved in transformation. It had been known that activated RhoA strongly enhanced transformation induced by Raf and it has been shown that this effect is carried out through the effectors ROCK1 and ROCK2 [64]. Rho-ROCK signalling is involved in cell division and also cell-death. ROCKs are also responsible for the membrane blebbing observed when a cell undergoes apoptosis. The blebbing arises from increases in cell contraction similar to what is required for blebbing during amoeboid cell motility. Rho-ROCK signalling is also locally required during mitosis. Contraction through this pathway is required to contract the cleavage furrow between new daughter cells to complete cytokinesis [92]. It has also been shown that ROCK is found bound to the centriole during mitosis and plays a role in positioning of the centrosomes [93].

In a more general context, the activity of ROCKs is required for the contraction of whole tissues. For example, the tone of smooth muscle of blood vessels can be controlled by ROCK activity, and ROCK inhibitors are currently under investigation as drugs for various cardiovascular diseases [94]. ROCK1 has also been shown to be required for the closure of eyelids in developing mouse embryos, by controlling the contractile ring of actin through the whole epithelial sheet of cells [95]. Interestingly ROCK2 knockout mice showed a similar phenotype suggesting that both ROCK1 and ROCK2 are cooperating in this context [96].

1.4.1 ROCK substrates

The consensus site for phosphorylation by ROCKs is generally agreed to be R/KXS/T or R/KXXS/T [97]. ROCKs can also be autophosphorylated although these sites have not yet been identified to know if and how they affect ROCK function [98]. The kinase domains of ROCK1 and ROCK2 are 92 % similar in sequence so it is likely that both kinases would be able to phosphorylate the same substrates at least in vitro. Potential substrates have not

always been tested against both ROCK1 and ROCK2 but it is difficult to determine whether what is tested in vitro is truly physiological. As discussed below, it is possible that ROCK1 and ROCK2 have different functions due to different localisation. Localisation would also impact the substrates that each kinase is in contact with.

ROCKs phosphorylate myosin-light chain (MLC) in vitro on S19. This is the same residue that is phosphorylated by myosin-light chain kinase (MLCK). MLCK usually requires the presence of Ca^{2+}, but it appears that ROCK may not [99]. ROCK also increases levels of phosphorylated MLC by phosphorylating and inhibiting myosin-light-chain phosphatase (MLCP) (also known as MYPT1) [97]. It is difficult to measure in vivo whether the increase in pMLC following ROCK activity is directly due to phosphorylation of MLC by ROCK or mostly through the inhibition of MLCP, so it is still questionable whether MLC is a genuine ROCK substrate in vivo. ROCK is also able to phosphorylate zipper-interacting protein (ZIPK) kinase. ZIP kinase is able to phosphorylate MLC directly and also inhibit MLCP in a similar way to ROCK. One other recently described target of ROCK is the Rac GAP FilGAP (FilaminA-binding Rho GTPase activating protein). ROCK activity downstream of RhoA is able to activate the activity if FilGAP and therefore inactivate Rac.

Other targets of ROCK are the LIM kinases. Phosphorylation activates LIMK and leads to the phosphorylation of the LIMK target cofilin, which inactivates cofilin. Cofilin normally functions to bind actin filaments and causes depolymerisation and together with ARP2/3 causes more branching [100]. Therefore ROCK activity promotes the generation of thick F-actin filaments and inhibits branching. ROCK activity can also affect the cross linking of actin to the plasma membrane by the phosphorylation of Ezrin/radixin/meosin (ERM) family members [101]. Phosphorylation by ROCK interferes with their intramolecular interactions that are required for their cross linking functions and promotes their interaction with the plasma membrane [101].

The major role of ROCK1 and ROCK2 is to coordinate contraction of actin filaments but it is also becoming clear that these kinases are involved in many processes governing the organisation of the cell shape and therefore also cell motility [102].

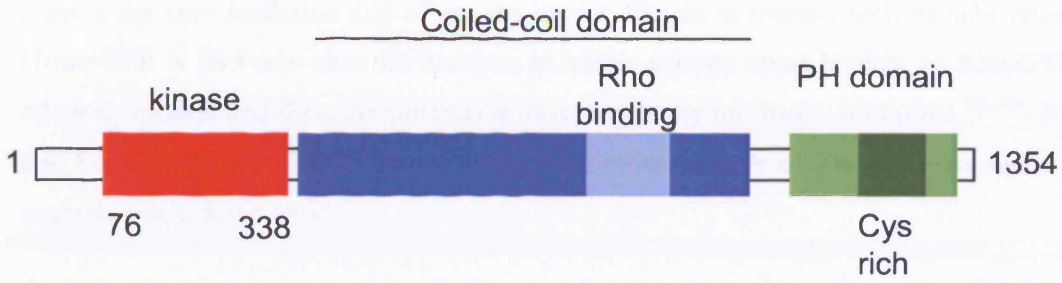

Figure 1.5 Diagram of the domain structure of ROCK1. ROCK 1 and ROCK2 are highly homologous members of the AGC family of kinases. The kinase domain is located in the N-terminus. The central part of the sequence encodes a coiled coil structure implicated in the dimerisation of ROCK molecules and also contains a Rho-binding domain. In the C-terminus there is a pleckstrin homology (PH) domain which is split by a cysteine rich sequence, numbering indicates ROCK1 aminio acid sequence.

1.4.2 Mechanism of activation

ROCK1 and ROCK2 (collectively termed ROCK) are thought to exist in an auto-inhibited conformation with the C-terminus binding to the N-terminus and obscuring the kinase domain. The mechanism for activation has been thought to be that RhoA-GTP or RhoC-GTP binds to the Rho-binding domain in the C-terminus (Figure 1.5). This interaction then relieves the auto inhibition and allows the kinase domain to interact with its substrates [103]. However it is also true that this increase in kinase activity upon binding to Rho-GTP is relatively modest and there are potentially more regulatory mechanisms in place [104, 105]. It has also been shown that ROCK2 can be activated independently of Rho by some lipids, for example arachadonic acid [106].

Analysis of crystal structures have further revealed that the coiled coil domain of ROCK is likely to exist in a parallel dimer even when not bound to RhoGTP, it is also likely that dimers could interact to form tetramers [103]. This is in contrast to a similar kinase PKN that also interacts with RhoA, but does so as an anti-parallel coiled coil dimer [107]. ROCK binds to Rho-GTP through contacts with between 10/13 residues in the extreme C-terminal end of the parallel-coiled coil region [108]. The hypothesis that Rho-binding activates ROCK activity has been supported by experiments using region specific antibodies, and it was found that an antibody targeting the Rho-Binding domain of ROCK2 was able activate kinase activity independently of Rho [103]. ROCK1 and ROCK2 can also be activated independently of Rho during apoptosis; in this context ROCK1 is activated by caspase 3 cleaving off the inhibitory C-terminus, ROCK2 is cleaved by a different mechanism by granzyme B, resulting in similar consequences as caspase cleavage of ROCK1.

The Rho-binding domain (RBD) in the C-terminus has been well characterised but there have also been other regions of the ROCK molecule implicated in Rho-binding. Firstly another Rho-interacting domain (RID) directly adjacent to the Rho-binding domain has been identified and appears to co-operate with the RBD to bind Rho in a GTP-dependent manner [109]. Secondly an HR1-like domain was identified in the coiled coil region between 420-550 a.a. which had structural similarity to the equivalent domain in PKN that is involved in Rho-binding. However the binding of this HR1 domain to Rho appeared to be independent of GTP-loading of Rho. The HR1 domain may bind to RhoA at sites outside the switch regions and perhaps contributes to conformational changes required for kinase activity [109].

As discussed above, Rho GTPases are able to localise to cell membranes through the modification of their C-terminus. The binding of Rho to ROCK could also permit the localisation of ROCK at the plasma membrane. This could mean that Rho-binding activates ROCK in two ways; conformational change to activate kinase activity, and membrane localisation to bring ROCK to interact with substrates.

Other members of the AGC family of kinases are regulated by phosphorylation in either the activation loop or the hydrophobic extension of the kinase domain [110, 111]. To this point this has not been shown to be true for ROCK1 or ROCK2 and investigation into whether ROCK is also regulated by phosphorylation is carried out by mutational analysis and by mass spectrometry and is described in chapters 3 and 4.

The pleckstrin homology (PH) domains of ROCK1 and ROCK2 have not been extensively studied. The PH domains of ROCK1 and ROCK2 share only 65-70 % sequence identity suggesting that this region could be responsible for functional differences between the two kinases [112]. The PH domain is unusual in that the PH domain is split by a cysteine rich sequence (Figure 1.5)[108]. This may impact the role of the PH domain in the regulation of ROCK. Investigation into the PH domain of ROCK2 found that antibodies against the PH domain inhibited stress fibre formation and caused ROCK2 to mislocalise suggesting a functional for for the PH domain [103]. Analysis of the importance of the C-terminus has also been carried out in ROCK1. Ishizaki and colleagues cloned sequential truncations of ROCK1 and examined the phenotypes induced. It was found that Δ1 mutant (lacking PH domain) and Δ2 mutant (lacking PH domain and also Rho-binding domain) were both able to induce stress fibres to the same degree, meaning that neither the PH domain or Rho was required for this phenotype, however the pattern of stress fibres was altered, and were in a star-like pattern rather than parallel. Cells expressing Δ5 mutant (1-375) were not able to induce the changes in actin morphology and this mutant had reduced kinase activity in vitro [98]. It has since been shown that the hydrophobic motif of ROCK1 is required for dimerisation of the kinase, which is able to explain the lack of activity in this mutant [113]. The different sensitivity of ROCK1 and ROCK2 to phospholipids has been shown to result in ROCK1 and ROCK2 regulating different cellular pools of myosin [114], it may also explain the different roles of ROCK1 and ROCK2 in the regulation of fibronectin matrix assembly [115].

1.4.3 Negative regulators of ROCK activity

The best characterised inhibitor of ROCK signalling is RhoE [85]. RhoE binds specifically to ROCK1 and not to ROCK2 to inhibit stress fibre formation. Other small GTPases from the Ras super family have also been shown to inhibit ROCK activity. Gem was discovered through a yeast 2-hybrid screen to interact with ROCK1 in a region adjacent to the Rho-binding domain (RBD), and over-expression of Gem was able to inhibit ROCK activity cause cells to lose actin stress fibres and become dendritic or collapsed [116]. Interestingly Gem only caused a decrease in MLC phosphorylation and not cofilin phosphorylation potentially implicating this interaction in the substrate specificity of ROCK1. The region bound by Gem overlaps with a less well characterised Rho-interacting domain of ROCK1 that is discussed below. It could be hypothesised that Gem competes with Rho for binding to this region of ROCK1.

1.4.4 Distinct functions of ROCK1 and ROCK2

The different mechanisms of regulation of ROCK1 and ROCK2 are discussed above. ROCK1 and ROCK2 have also been shown to play non-redundant roles in a variety of cellular processes. Firstly selective knockdown of either ROCK1 or ROCK2 by siRNA results in alterations to the actin cytoskeleton, suggesting they are not able to compensate for one another [114]. Furthermore double knockdown of both ROCK1 and ROCK2 has a more striking phenotype than either depleted alone (this is confirmed in the siRNA screen in chapter 5). ROCK2 has been genetically deleted in mice and it was found to cause embryonic lethality at around E13.5, probably due to placental dysfunction. This is further evidence that ROCK1 is not able to compensate for loss of ROCK2 [117]. The two ROCK proteins also interact with different binding partners; for example, RhoE binds and inhibited only ROCK1, whereas Raf1 only binds to ROCK2 [85, 118].

Both ROCK1 and ROCK2 are able to regulate the actin cytoskeleton, yet even in this role they appear to control different aspects. It was found that ROCK1 was largely responsible for the generation of stress fibres and that ROCK2 was required for phagocytosis and was sensitive to the presence of PI(3,4,5)P3 whereas ROCK1 was not [114]. This sensitivity to membrane lipids meant that ROCK2 was mostly located to ruffling membranes, presumably where PI3K activity is high, whereas ROCK1 was seen to have a more general membrane distribution [114]. It has also been shown that ROCK1 and ROCK2 might have different

substrates, for example myosin light chain phosphorylation on S19 was sensitive to ROCK1 levels but not ROCK2 [114].

1.5 PDK1 functions

PDK1 is a 63kDa serine/threonine kinase that is ubiquitously expressed in human tissues. PDK1, like ROCK1 and ROCK2 also belongs to the AGC family of protein kinases (Figure 1.4). PDK1 has been termed a 'master kinase' due to the fact that it is responsible for interacting with and activating so many downstream signalling pathways (Figure 1.6). One major signalling pathway downstream of PDK1 is Akt/PKB. Akt/PKB in turn signals to many different downstream targets. PKB signalling promotes cell survival, through inhibition of caspase 9 activity, and inhibition of Bcl-2 family member Bad to give cells a resistance to apoptosis [119]. Akt/PKB is also required for insulin signalling pathways and can signal through proteins such as GSK3 and mTOR to stimulate cell growth and increase cell metabolism. Independently of Akt/PKB, PDK1 can also signal to S6K, a ribosomal protein that is also a regulator of cell metabolism and cell size through the regulation of translation [119]. PDK1 has also been implicated in cell motility. It has been shown that PDK1 is required for endothelial cell migration [120], and also that PDK1 is able to regulate the organisation of cortical actin through interaction with the Rho effector PKN [121].

PDK1 contains a C-terminal PH domain that binds to $PI(3,4,5)P_3$ and $PI(3,4)P_2$ in the plasma membrane (Figure 1.6). Both of these lipids are products of PI3K activity, and when PI3K activity is high, PDK1 is localised to plasma membranes through its PH domain. When $PI(3,4,5)P_3$ levels are low PDK1 is mostly cytoplasmic [122]. PDK1 is likely to have just as important a role in the cytoplasm, as at the cell membrane, because in organisms such as fission yeast and plants, the PDK1 homologues do not contain a PH domain [119].

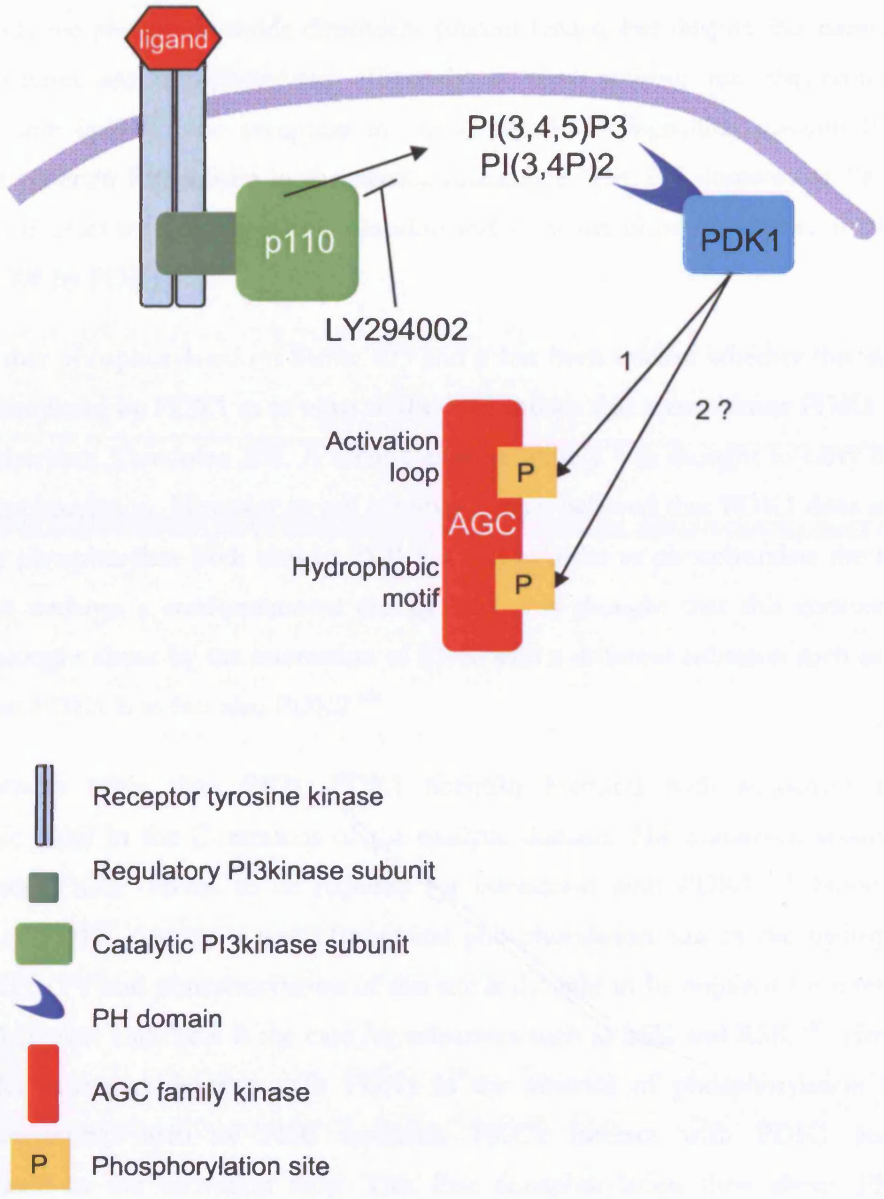

Figure 1.6 Schematic diagram of PI3K signalling and PDK1 activity. PI3K activity can be stimulated by receptor tyrosine kinases such as PDGF receptor. PI3K phosphorylates inositol lipids in the plasma membrane. PDK1 interacts with $PI(3,4)P_2$ and $PI(3,4,5)P_3$ via its PH domain. PDK1 interacts with other AGC kinases such as PKB and can activate their activity by phosphorylating their activation loop (1) and/or their hydrophobic motif (2).

PDK1 stands for phosphoinositide-dependent protein kinase, but despite this name, most PDK1 substrates are phosphorylated efficiently in vitro without the requirement for interaction with lipid [119]; the exception to this is Akt/PKB. Signalling through PI3K is required to generate PI(3,4,5)P3 in the plasma membrane. The PH domains of PKB and PDK1 then interact with this lipid to co-localise and allow the phosphorylation of PKB on Threonine 308 by PDK1 [123].

PKB is further phosphorylated on Serine 473 and it has been unclear whether this site was also phosphorylated by PDK1 as in vitro studies had shown that recombinant PDK1 would only phosphorylate Threonine 308. A second enzyme, PDK2 was thought to carry out the second phosphorylation. However in cell contexts is now believed that PDK1 does actually sequentially phosphorylate both sites in PKB but that in order to phosphorylate the second site it must undergo a conformational change, and it is thought that this conformation change is brought about by the interaction of PDK with a different substrate such as PRK; meaning that PDK1 is in fact also PDK2 [124].

With substrates other than PKB, PDK1 normally interacts with sequences in the hydrophobic motif in the C-terminus of the catalytic domain. The conserved sequence in AGC kinases 'FXXF' seems to be required for interaction with PDK1 [111]. Some AGC substrates of PDK1 contain a serine/threonine phosphorylation site in the hydrophobic motif; FXXFS/TY and phosphorylation of this site is thought to be required for interaction with PDK1 (Figure 1.6). This is the case for substrates such as S6K and RSK [125]. However, other PDK1 substrates interact with PDK1 in the absence of phosphorylation in the hydrophobic motif, such as PKC isoforms. PKC's interact with PDK1 and are phosphorylated in the activation loop. This first phosphorylation then allows PKC to autophosphorylate itself at other sites including the hydrophobic motif that confers its full active conformation [110, 126]. The phosphorylated hydrophobic motif is sometimes known to form an intramolecular interaction with phosphate binding pocket, and it is this interaction and conformational change that is thought to stabilise the proteins [111].

PDK1 itself, despite being an AGC family kinase does not contain a hydrophobic motif at the C-terminus of its kinase domain. However PDK1 does still contain the hydrophobic pocket capable of interacting with a hydrophobic motif of other AGC kinases. This pocket has been termed the PDK1-interacting fragment (PIF) pocket [127]. The PIF pocket is essential

for interaction of PDK1 with hydrophobic motifs of AGC kinases such as S6K and RSK but not for interaction with Akt/PKB. This has been elegantly shown in a genetic mouse model where both copies of PDK1 were replaced with a 'knock in' gene that had full catalytic activity but had a disrupted PIF pocket [128]. This model was able to prove conclusively that PDK1 has two distinct ways of interacting and activating its downstream targets; one involving the PIF pocket and one that does not. Targeting the PIF pocket of PDK1 may potentially allow the generation of drugs that specifically block only part of PDK1 function and do not block signalling through Akt/PKB.

1.6 Cell motility

Cell motility is a vital process in organisms ranging from single celled amoebae to complex mammals. Although the aim of the experiments in this thesis have focused on aberrant acquisition of cell motility in tumour cells, it is important to highlight the numerous normal and essential functions that require cell motility. On the simplest level, cell motility allows single celled organisms to change location and search for nutrients and suitable conditions to survive in. Even microbes such as vaccinia and shigella are able to hijack cell motility machinery of the cells they infect in order to spread and infect neighbouring cells [129] [130].

There are many different ways in which cells can move within an organism. They move in collective cohorts and also as single cells. During development, cells must migrate in order to organise themselves into tissues, for example during the formation of human facial structures. The layers of mesoderm must migrate towards each other and fuse, if migration is insufficient a cleft palette can result [131]. Collective migration is common in multicellular organisms during development as organs and other structures being to form. However collective migration is not restricted to development. For example, groups of endothelial cells are able to migrate together to sprout new blood vessels, a process that allows the vasculature to remodel itself. This process can also be stimulated by tumour cells and initiates the formation of new blood vessels to provide oxygen and nutrients to a growing tumour [132]. Collective cell migration is also continuously occurring in the tissues that require high rates of turnover, such as the skin and the lining of the gut. Cells in these tissues undergo a large amount of stress and are physically sloughed off the surface regularly. To replace these old cells, new cells are produced by proliferating stem cells in the lower parts of the tissue. In the case of the gut, the new cells must collectively migrate up from the base of the crypts

continuously to keep the gut lining functional [133]. Collective migration is also required during wound healing in order to close a wound as quickly as possible to limit the chance of infection [134].

Single cell migration is also vital. Perhaps the best example of this is the migration of immune cells. Populations of immune cells continuously survey the tissues of the body searching for foreign antigens, prepared to initiate an immune response if necessary [135]. During their trafficking, leukocytes are able to move into and out of lymph nodes responding to cues that guide them in the correct direction [135]. Recent research has also suggested that there are specific populations of immune cells primed to survey specific tissues [136]. This is potentially very significant as is could mean that to treat autoimmune diseases, it may not be necessary to inhibit the whole immune system, but instead target a specific population of leukocytes leaving the remaining surveillance system intact. In the case of infection or injury immune cells, such as neutrophils are able to respond and infiltrate the affected tissue extremely quickly [137]. The speed of the response implies that they are able to traverse endothelial barriers extremely easily; the question of whether tumour cells are able to mimic this in order to metastasise will be addressed later.

1.7 Mechanisms of cell motility

In order for a cell or a group of cells to be able to move they can organise polarity so as to have a defined front and back, then make a protrusion in the right direction. Having done this, the cell must then make contacts with the surrounding matrix and/or other cells to tether itself to its new position. Finally contractile forces are also required to maintain cell integrity, to pull the rear of the cell along with the front (Figure 1.7). Optimal migration and cell speed requires a delicate balance between adhesion and contraction[138]. The timing and coordination of these processes is critical, as in many cases these process are occurring simultaneously but in different areas of the cell. Cell adhesion is very important, but too much adhesion and a cell could tether itself too tightly to the substrate to move. Cell contraction is able to detach weaker adhesions at the back of the cell which is important to move forwards, but uncontrolled cell contraction could overcome too many of the cell adhesions and can also be detrimental..

Most investigation into cell motility has been carried out by studying the behaviour of cells, such as fibroblasts, migrating across rigid surfaces. By culturing cells in a collagen matrix, it is now possible to monitor cell motility in vitro in deformable 3D-environments that more closely mimic the environment that cells might encounter in vivo. It is clear that cells behave differently in these two different in vitro environments and it is now important to bridge the gap and discover how current knowledge of cell motility applies to cell moving in 3D and in vivo.

1.7.1 Cell protrusions

The first step to initiate cell motility is usually to generate a cell protrusion. Many different types of cell protrusions have been identified, such as lamellipodia, filopodia, podosomes and membrane blebs. Most cell protrusions require actin polymerisation to provide the propulsion to drive the cell membrane forwards [139]. Monomeric globular actin (G-actin) molecules assemble asymmetrically; the plus-end or barbed end is the site at which new actin monomers are added and the minus-end or pointed end is less dynamic. The structure of actin filaments is controlled by proteins that directly bind to actin and control processes such as: nucleating, capping, severing, depolymerising, cross linking and bundling of filaments [139].

The activation of Rho family GTPases Cdc42 and Rac can stimulate actin polymerisation by initiating the nucleation of new actin filaments. Cdc42 bound to GTP interacts with Wiskott-Aldrich syndrome protein (WASP), relieving WASP auto-inhibition and promoting the interaction of WASP with actin filaments and also with the ARP2/3 complex [77, 140]. WASP was initially identified as the protein involved in the immunosuppressive condition Wiskott-Aldrich Syndrome, and its expression is restricted to haematopoietic cell lineages. It is N-WASP that is found in most other cell types, and performs an analogous function to WASP [77]. The interaction of N-WASP and ARP2/3 with actin filaments causes branching the existing filament at a 70° angle. It is thought that this occurs because the ARP2/3 complex mimics the shape of an actin dimer allowing new actin monomers to bind [141]. Another nucleation promoting factor is WAVE (WASP-family verprolin-homologous protein-1). The binding of GTP-bound Rac can activate WAVE; the interaction with Rac recruits WAVE and ARP2/3 to the membrane causing localised actin polymerisation [141]. Actin filaments can also be lengthened by the activity of formins. Formins bind to the barbed ends of actin

filaments and promote the lengthening but not the branching of filaments. Unlike ARP2/3, formins remain at the tips of the actin filaments as they lengthen.

Actin polymerisation is also a self-organising process and can be reconstituted in vitro with the right combination of proteins; actin depolymerising factor (ADF)/cofilin, profilin, capping proteins, and nucleating factor ARP2/3 [142]. Newly synthesised filaments are initially weakly coupled to the rest of the actin cytoskeleton but subsequently the actin polymerisation is coupled with new cell adhesions and can then anchor the cell as contractile forces are applied [143].

Filopodia are long, thin, unipolar, actin-driven cell projections that can act as scouts for the cell, sensing the nearby environment [144]. Developing blood vessels include a leading tip cell that is able to sense direction of VEGF gradients [145]. The tip cell of the endothelial sprout produces multiple filopodia to sense direction and also to make contacts with other new vessels to make branches. Filopodia can be driven by the activity of the small GTPase Cdc42 driving actin bundling at the leading edge [44]. The straight actin filaments are thought to be induced mostly through the activity of formins, or through the activity of Ena/VASP proteins which attach to the barbed ends to drive the formation of long unbranched actin filaments [144]. Filopodia do not appear to require the activity of N-WASP, as they are still present in N-WASP deficient cells [146]. Lamellipodia are broad protrusions at the front of cells migrating across 2D substrates. Lamellipodia are typically driven by actin polymerisation downstream of Rac activation [48]. Lamellipodia require the nucleation activity of ARP2/3 to promote the progression of a broad, branching actin network.

Another cell protrusion, thought to be used by cells to invade matrices is the podosome. These are actin-rich structures associated with protease activity and driven by activation of the tyrosine kinase Src. Podosomes force their way into underlying matrix and are able to induce proteolytic degradation of matrix in their path through the localised activity of secreted matrix-metallo-proteases [147]. Podosomes have been observed in monocyte-derived cells, fibroblasts and also some carcinoma cells, where they are termed invadopodia [148]. Podosomes are one possible mechanism to explain how invasive cancer cells are able to cross basement membranes.

Another type of cell protrusion that is not directly driven by actin polymerisation is membrane blebbing. Blebs are thought to be generated by contractile forces squeezing the cell contents and increases in hydrostatic pressure forcing parts of the membrane to detach from the under lying actin cytoskeleton and protrude as a bleb [149]. Contractile forces driven by alterations on acto-myosin downstream of Rho-ROCK signalling are described below. The membrane bleb is formed at weaker points in the actin cortex, and as expansion of the bleb ceases, the actin cortex reassembles [150]. Blebbing has been observed in Dictyostelium in response to the chemoattractant cAMP [151]. Bleb-like protrusions have also been observed in primordial germ cells in zebrafish [152]. Blebbing in this context is driven by contraction of myosin, stimulated in regions of the cell with higher intracellular calcium levels [152]. This mechanism of cell protrusion is not well studied at present but it is becoming clear that blebbing can be utilised by cancer cells moving in an amoeboid manner and may be very relevant to the motility of invasive tumour cells in vivo [153-155]. Membrane blebbing can also be associated with apoptosis. However in this type of blebbing ROCK is activated by caspase cleavage, so the activation of Rho is not required [156].

1.7.2 Cell adhesions

A new protrusion must form attachments to the surrounding matrix to tether the moving cell to its new position. Contractile forces applied to the new adhesions will then be able to cause the translocation of the cell body. Cell adhesions also generate intracellular signals to control cell behaviour. For example, if a cell loses attachment to the matrix or to surrounding cells apoptosis can be induced, and is termed anoikis [157]. Interestingly it is also true that transformed cancer cells are less reliant on signals from cell adhesions and a common measure of transformation is to suspend cells in soft agar. In this assay transformed cells are able to survive and proliferate in the absence of adhesion to a substrate, so called anchourage-independent growth [26].

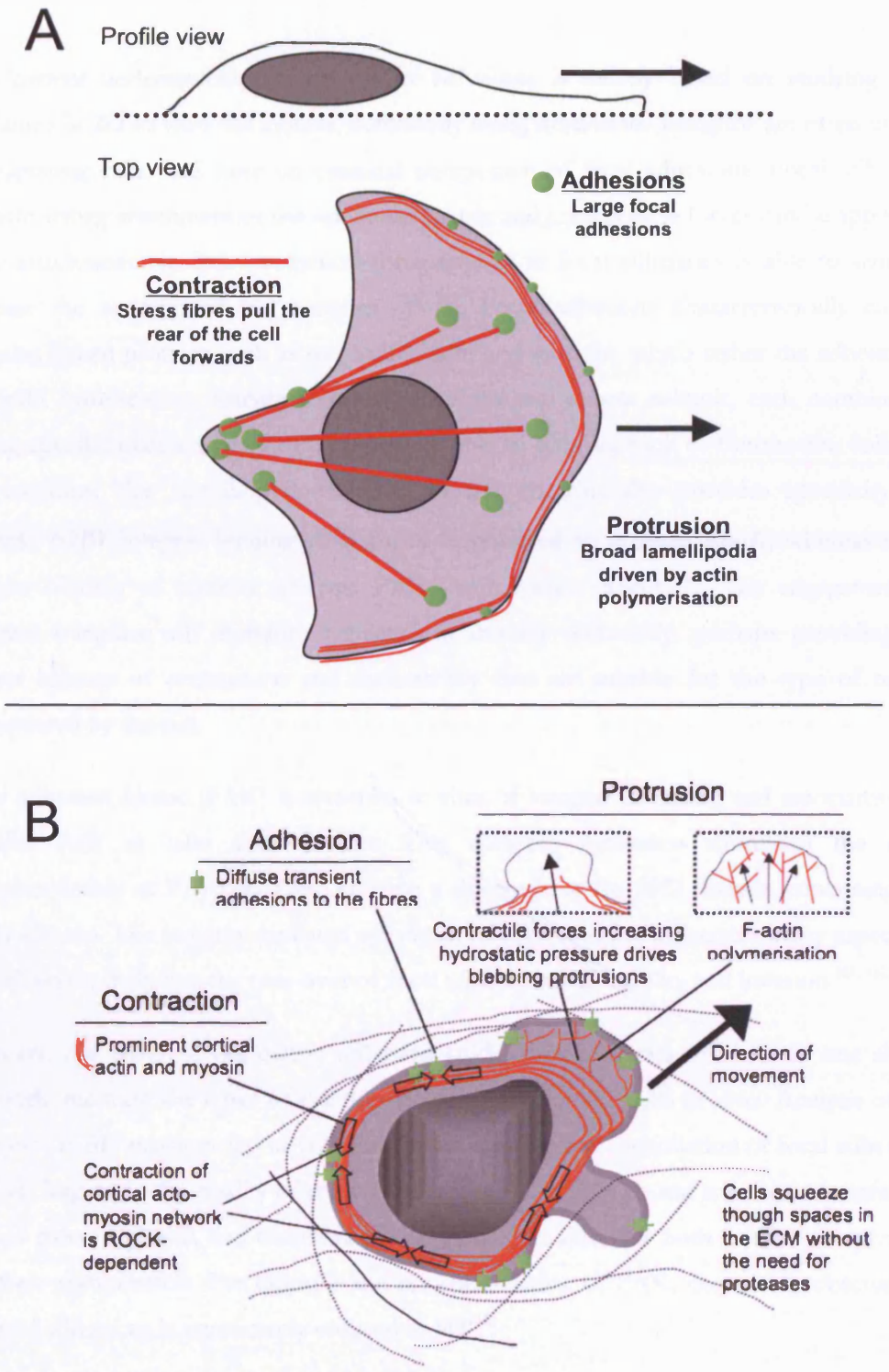

Figure 1.7 Schematic diagram of cell motility mechanisms in 2D and in 3D systems. A) diagram showing cell motility across 2D substrates, cells are spread with broad lamelipodia and F-actin stress fibres. B) diagram showing mechanisms of amoeboid cell motility in 3D environments. Cells are contracted and show membrane blebs. F-actin is organised around the cell cortex. In both diagrams the large arrows indicate the direction of movement.

Our current understanding of cell-matrix adhesions is mostly based on studying focal adhesions in 2D in vitro cell culture, commonly using fibroblasts. Integrins are often utilised by migrating cells, and form an essential component of focal adhesions. Focal adhesions mediate strong attachment of the cell to the matrix and considerable forces can be applied to these attachments, in fact mechanical force applied to focal adhesions is able to signal to increase the strength of the complex [158, 159]. Focal adhesions characteristically contain integrins linked proteins such as to paxillin, talin and vinculin, which tether the adhesion to the actin cytoskeleton. Integrins contain an alpha and a beta subunit, each combination having specific matrix substrates that they are able to bind to, such as fibronectin, collagen, and laminins. The signalling downstream of the integrins also provides specificity, for example $\alpha 2\beta 1$ integrin binding to collagen is reported to activate RhoA, whereas $\alpha 3\beta 1$ integrin binding to laminin activates PAK1 and inhibits RhoA [160]. The engagement of different integrins will therefore regulate cell motility differently, perhaps providing the correct balance of protrusions and contractility that are suitable for the type of matrix encountered by the cell.

Focal adhesion kinase (FAK) is recruited to sites of integrin clustering and associates with proteins such as talin and vinculin. This complex formation stimulates the auto-phosphorylation of FAK on Y397 creating a docking site for SH2 domain containing Src family kinases. The integrin-mediated activation of FAK and Src influences many aspects of cell behaviour including the turn-over of focal adhesions, cell motility and invasion [161, 162]

However, the types of cell-matrix adhesion studies in fibroblasts in vitro do not always accurately replicate the types of cell adhesions used by motile cells in vivo. Analysis of cell adhesions in 3D matrices and in vivo has shown that size and organisation of focal adhesions depends largely on the rigidity of the substrate [163]. In vivo cells do not encounter a surface as rigid as glass or plastic, and therefore the adhesions are different both in their morphology and their composition. For example the phosphorylation of FAK, commonly observed in 2D focal adhesions is significantly reduced in 3D[163].

It has recently been reported that immune cells are able to migrate in vivo without the requirement for integrins [164]. This work showed that dendritic cells were able to migrate between peripheral tissues and draining lymph nodes even when all expressed integrins had been genetically deleted. They conclude that 2D and not 3D cell migration is dependent on

integrin-type adhesions. Instead it is hypothesised that the dendritic cells are motile due to 'squeezing', which is dependent on myosin II [164]. It is possible that cancer cells moving in an amoeboid manner use similar integrin-independent mechanisms, and we have observed that carcinoma cells are motile in vivo when integrin β1 is depleted (Sahai lab-unpublished data). It is thought that some cancer cells moving in an amoeboid manner use an alternative type of adhesion complex, but the molecules that could be used have not yet been identified.

1.7.3 Generating contractile force

The component of cell motility required move the cell body and to detach adhesions is the generation of contractile force. Without contraction the front of the cell would move forwards but the result would be only stretching of the cell unless the back of the cell was retracted. Cell moving across 2D surfaces often exhibit actin stress fibres. A stress fibre contains between 10-30 actin filaments that are held together by cross linking proteins such as α-actinin, or fascin which interact with the actin bundles at specific points periodically spaced along the fibre [165]. Myosin is also combined with actin, and contraction is able to occur when the phosphorylated light chain of myosin binds to the actin filament allowing an increase in the myosin ATPase activity; the binding of myosin to the actin fibres is controlled by another class of actin interactor, tropomyosin [166]. Myosin light chain (MLC) can be phosphorylated on two residues, T18 and S19, and the regulation of the levels of phosphorylated myosin light chain is critical to the regulation of contractile forces within a cell [167]. Cell motility requires both the assembly of filamentous actin and also generation of contractile forces. Inhibition of either actin polymerisation (e.g. cytochalasinD treatment) or myosin ATPase activity (e.g. Blebbistatin treatment) impedes cell motility.

Stress fibres were found to be regulated by the activity of RhoA through its effectors ROCK1 and ROCK2 (collectively termed ROCK). ROCK1 and ROCK2 are serine threonine kinases that are able to increase the availability if phosphorylated myosin-light-chain in several ways. Firstly by phosphorylating and inhibited myosin-light-chain phosphatase, secondly by phosphorylating zipper-interacting protein kinase (ZIPK) which in turn phosphorylates MLC on both T18 and S19 [168], and finally perhaps by phosphorylating MLC directly at S19 [165].

Another RhoA effector mDia is also required for the correct organisation of stress fibres. ROCK activation alone tends to typically form a star-like pattern of stress fibres in the centre

of the cell. mDia acts to extend the polymerisation of actin filaments from cell membranes. It is thought that to produce thick parallel stress fibres downstream of RhoA, mDia is required. However activation of mDia alone does not induce thickly bundled actin filaments. The activities of both ROCK and mDia are required in concert for the proper organisation of actin [169].

Stress fibres are the predominant form of contractile actin structure seen in 2D cell culture. In 3-dimensional culture and in vivo actin can still be bundled and it is likely that the mechanisms controlling contractility are similar. However the actin bundles tend to be located around the cell periphery creating a thick actin cortex and are not always seen as stress fibres [154]. Contractility in 3-dimensions can help to keep cells rounded, and as discussed above, is able to generate hydrostatic pressure to force out bleb-like protrusions.

Myosin light chain phosphorylation can also be regulated by MRCK down stream of Cdc42 [170]. It has been found that Rho-ROCK signalling drives rounded amoeboid cell motility, but in the absence of ROCK signalling, cells are still able to invade in an elongated/mesenchymal manner. Elongated cell invasion still required contractility as it is inhibited by blebbistatin, but this was regulated by Cdc42 and MRCK instead of Rho and ROCK [170]. Additionally signalling through Cdc42 and MRCK has been shown to control contractility in groups of cells moving collectively, and acts to maintain cohesion within the groups of cells by regulating bundles of contractile myosin that are continuous around the edges of the group rather than within each individual cell [79].

It is clear that contractility is required for different types of cell motility, whether this is in 2-dimensions or in vivo, in single cells or collective groups. The organisation of contractile machinery however varies between different modes of motility. Depending on the mechanism of cell motility used, cells are able to activate different signalling pathways in different spatial locations, enabling cell migration.

1.7.4 Cell polarity during motility

Polarity is required for the normal functioning of many cells in healthy tissues. Polarity allows the cell to maintain its correct position between other cells and allows cells to function together as a tissue. Apical basolateral polarity is essential for the functioning of epithelial cell layers. The polarisation leads to the transport of specific proteins to the surface at which they

are required, and cell-cell junctions function to maintain the separation of the apical and basolateral surfaces. The loss of cell polarity in epithelial layers is associated with disruption of epithelial barrier function. Loss of polarity also occurs in carcinomas undergoing and epithelial to mesenchymal transition and is associated with higher invasive potential [171].

Cell polarity can also occur within single cells to define the front and the back during cell migration. This is very clearly seen when adherent cells such as fibroblasts migrate across a 2D substrate. The front of the cell is normally characterised by the presence of a cell protrusion such as a lamellipodia driven by actin polymerisation. Actin polymerisation does not occur at the rear of the cell, instead thick filamentous actin cables are contracted to pull the 'tail' forwards as the front pushes forwards. RhoA activity, which controls contractility of cells is high at the back and is involved in retraction of the rear. Levels of RhoA were thought to be reduced at the front of the cell and instead active Rac and Cdc42 are recruited drive actin polymerisation [172]. One mechanism that restricts RhoA activation at the front is the degradation of RhoA following ubiquitination by the HECT domain E3 ubiquitin ligase Smurf1 [173, 174]. However, in cells moving in 3-dimensional environments, it has also been shown that Rho signalling and contractility of myosin is also required at the front of cells [154, 175, 176].

Sub-cellular organelles are also re-positioned within cells as polarity is established. This organisation has been extensively studied utilising confluent layers of adherent cells and scratching a 'wound' across the cells. Cells will then polarise and start to migrate into the space created. It has been shown that structures such as the MTOC and Golgi apparatus will be organised to the front of the nucleus as a cell polarises [172]. The positioning of the MTOC requires microtubule dynamics and the positioning of the Golgi is actin-dependent[177].

The polarisation of motile cells can help to maintain direction to migration. In cells moving across a 2D substrate it is clear to see that polarisation is stably maintained and signalling events at the front and back of the cells can be easily monitored, as there is a reasonable degree of spatial separation. When cells move in a 3-dimensional environment polarisation is less clear. Immune cells and some tumour cells moving in an amoeboid manner are rounded and contracted meaning there is less spatial separation between the front and the back. Cells

are also able to change direction very quickly, so it would seem that cell polarity can also be less stable and more transient, but still functional to allow cells to sense direction.

1.7.5 Directional migration

In many cells the direction of motility is influenced by local environmental cues. Chemotaxis is the ability of cells to organise their movements based on the direction of a specific molecule present in their environment. Chemotaxis is required for sperm to find and fertilise an egg, it is also required for the migration of neurons as the brain develops. Cells can respond to gradients of a variety of molecules and migrate towards them. For example Dictyostelium will migrate towards higher concentrations of cAMP and arachadonic acid [178]. These chemoattractants cause release of intracellular calcium that is required for motile behaviour [179]. Cells are also able to follow gradients of adhesion molecules and matrix such as fibronectin; this directional motility is termed haptotaxis, and is important for migrating cells in developing embryos but is also used by some cancer cells during the metastatic process [180, 181]. One important question is how cells polarise and move directionally across very shallow gradients over large distances in vivo. For example, immune cells homing to lymph nodes from peripheral tissues. This would require an amplification of signalling to reinforce and exaggerate the differences in the gradient from front to back.

Signalling pathways such as PI3K signalling have been documented to be specifically activated at the front of migrating cells in response to chemotactic stimuli. This signalling is able to promote actin polymerisation in the direction of the stimulus. It has been seen that $PI(3,4,5)P_3$ is selectively accumulated at the front of migrating cells [182, 183] and is removed from the sides and rear of the cell by the localised action of phosphatase and tensin homologue (PTEN) [184]. However this model that PI3K is activated by higher concentrations of chemoattractant at the front of cells to drive protrusions has been challenged by a new theory suggesting that protrusive activity generates cell extensions at random, and that direction is determined by selecting the protrusion which is in the most accurate direction [185]. This suggests that PI3K activity controls the generation of protrusions but does not control their directionality.

Neutrophils respond to gradients of chemokines such as IL-8 but also to bacterial peptides such as fMLP. Interestingly, the requirement for PI3K signalling to sense these two gradients

is different and it is suggested that neutrophils responding to fMLP do not require PI3K signalling [186]. There is also evidence that metastasising tumour cells are able to respond to chemokines and that this directional migration leads to the presence of secondary tumours in particular target organs; this is addressed in more detail in a later section [187]. Chemokines bind to specific G-protein coupled receptors in the cell membranes to trigger signalling events to control immune cells activation in addition to cell migration. Much research is underway to determine whether specifically blocking chemokine signalling could be beneficial to patients suffering autoimmune diseases, inflammation and also cancer [187, 188].

In vitro, chemotaxis is modelled using soluble chemoattractants presented to cells either by separation of two chambers, between which the migrating cells may preferentially migrate towards a chemokine, for example the Dunn Chamber, or the chemoattractant is contained within a pipette which can be moved and the cells follow [189]. This has been useful to show the principles of chemotaxis. How chemotaxis occurs in vivo is now being investigated. Firstly gradients in vivo are set up over very large distances between tissues; furthermore the gradient must remain stable for long periods of time. The presence of matrix components may act as a hindrance to diffusing chemoattractant molecules, or conversely the chemoattractant molecules could be bound to matrix components and presented to passing cells. One recent paper has suggested that interstitial flow within tissues can act to guide cells. It was found that chemokine secreted by the migrating cell was drawn in the direction of interstitial flow, meaning that the cell can provide their own chemotaxis gradient and may explain how tumour cells are able to migrate to draining lymph nodes [190]. It is also possible that migrating cells do not require the chemokine to be presented as a gradient. Work into how the lateral-line primordium migrates during zebrafish development has shown that cells at the leading edge of the cohort require the presence of SDF-1 [191]. However, if the SDF-1 is absent at any point along their route, the cohort of cells is able to turn around and follow the SDF-1, still present from the direction they have just traveled from, in the opposite direction, meaning that the SDF-1 is unlikely to be presented as a gradient [192].

1.8 Metastasis

Metastasis is the process by which malignant cancer cells are able to leave the primary tumour and arrive in secondary sites to form secondary tumours (Figure 1.8). If a primary tumour is identified early and surgery to remove it is successful then the outcome for the

patient is generally good, however if cancer cells are found to have spread the prognosis for the patient is much worsened. Most of cancer deaths are due to the onset of metastatic disease, which makes this an important area of cancer research with potentially huge benefits to patients.

Until recently, the process of metastatic spread of tumours has been difficult to study in detail. Most studies relied on the development of macroscopic secondary tumours as a measure of the metastatic capability of tumour cells. Clinically, metastatic disease is studied through the use of tissue sections taken from patients by biopsy. This approach has been useful to determine the organisation of secondary tumours and to analyse protein expression, but it lacks the dynamic information to explain what happens to cells between leaving the primary tumour and arriving and proliferating and forming the secondary tumour. Important studies conducted in the 1950's and 60's, directly observed cancer dissemination by implanting tumours into rabbit ears [193]. These studies pre-dated our genetic understanding of cancer, and the discovery of fluorescent proteins, so used very simple imaging technologies. The development of intravital confocal microscopy technology has allowed researchers to visualise the motile behaviour of tumour cells in the primary tumour with high resolution, and start to put together a picture of how cancer cells move in vivo.

Our estimates indicate that between 1-5% of cells in the primary tumour are motile (Giampieri *et al.* – unpublished data). This suggests that even though metastatic disease is associated with higher-grade tumours and is thought to be a late stage of tumour progression, tumour cells are able to invade, at least locally, from a much earlier stage than originally thought [194]. Despite large numbers of cells acquiring motile behaviour and leaving the primary tumour, the number of metastatic secondary tumours is relatively low. This implies that the whole process of metastasis is inefficient and that only a minority of cells manage to complete every step required.

For a cancer cell to metastasise, it must first release itself from the rest of the primary tumour cells. In carcinomas, cell-cell contacts are generally maintained and can be seen by the presence of E-cadherin at cell junctions [195]. Loss of E-cadherin is thought to correlate with increased invasive potential, and is sometimes indicative of epithelial to mesenchymal transition (EMT), which is discussed later [171, 195].

Of these motile cells, some may invade blood vessels to enter the blood stream, and others may migrate to draining lymph nodes (Figure 1.8). It has been shown that tumour cells are able to orientate themselves towards blood vessels meaning that there may be some chemotactic response to an unknown factor produced by the blood vessels [196]. It has also been shown that macrophages infiltrating the tumour are able to aid cancer cells entering the circulation [197]. Entering blood and the lymphatic circulations are the ways in which cancer cell are able to travel large distances from the primary site and arrive in new organs, but it is still unclear whether movement through the lymphatic vessels or the blood is the primary mode of transit from the primary tumour [198].

The method used by tumour cells to enter blood vessels is also unclear. It is thought that tumour cells would need to use proteases to degrade basement membrane surrounding the endothelial cells before entering the vessels (Figure 1.8). However this may not always be the case as recent research has shown that tumour cells are able to up regulate endothelial specific genes and incorporate themselves into the walls of blood vessels [199] [200]. This process has been termed vascular mimicry and potentially explains how tumour cells would be able to enter the vasculature without requiring proteases. Another potential mechanism of entry to the vasculature is for the cancer cell to mimic the transendothelial migration mechanisms of leukocytes such as neutrophils. Neutrophils are able to cross endothelial barriers in matters of minutes and recent research has shown that this is due to the generation of high levels of mechanical force that disrupts endothelial cell junctions [201].

Once in the blood stream, tumour cells must be able to survive transit in the circulation. The shear forces exerted are considerable and the majority of cells entering the blood are likely to undergo apoptosis even if they reach a secondary site. It has been shown that metastatic and non-metastatic cells are able to interact with blood vessels in primary tumours but that the metastatic cells are better able to survive the sheer stresses [202]. It also seems that rounded, contractile cell morphology is more suitable for entry into the blood vessels and survival in the blood stream [173]. Perhaps contractile forces enable cells to maintain greater cortical rigidity, which protect the cancer cell from damage and enable cells to withstand greater mechanical stresses.

If an invasive cancer cell survives transit in the blood stream, it will probably come to rest in a capillary bed where it will slow down and get lodged, for example in the lungs (Figure 1.8).

It has been shown that tumour cells can lodge in small vessels in association with platelets in a small clot [203]. Following arrest in a blood vessel, the clot is dissolved and the tumour cells interact with the endothelium by attaching and spreading [203]. This process may be important for subsequent extravasation. It is also possible that tumour cells do not need to extravasate, but proliferate within the capillary and invade into the lung tissue subsequently when the metastatic secondary tumour reaches a larger volume.

The final location of tumour cells travelling in the blood can be determined by the next capillary bed they reach and get lodged in. However there are also specific examples of certain tumour types preferentially metastasising to certain sites. For example breast cancer cells often metastasize to bones [204]. This tissue specificity could either be due to the cancer cells specifically migrating to these organs, but it could also be because the cancer cells are only able to survive and proliferate in certain locations. This question was first addressed over 100 years ago, when Paget hypothesised that sites of metastasis were defined by both the cancer cell (the seed) and also the microenvironment of the secondary site (soil)[205]. This hypothesis still holds true and research has shown many examples of tumour cells expressing receptors to enable them to home to tissues specifically expressing certain cytokines [206]. For example the expression of CXCR4 is highly up regulated in some breast tumours and may be responsible for the metastases seen in bone where expression of the CXCR4 ligand SDF-1 is highly expressed.

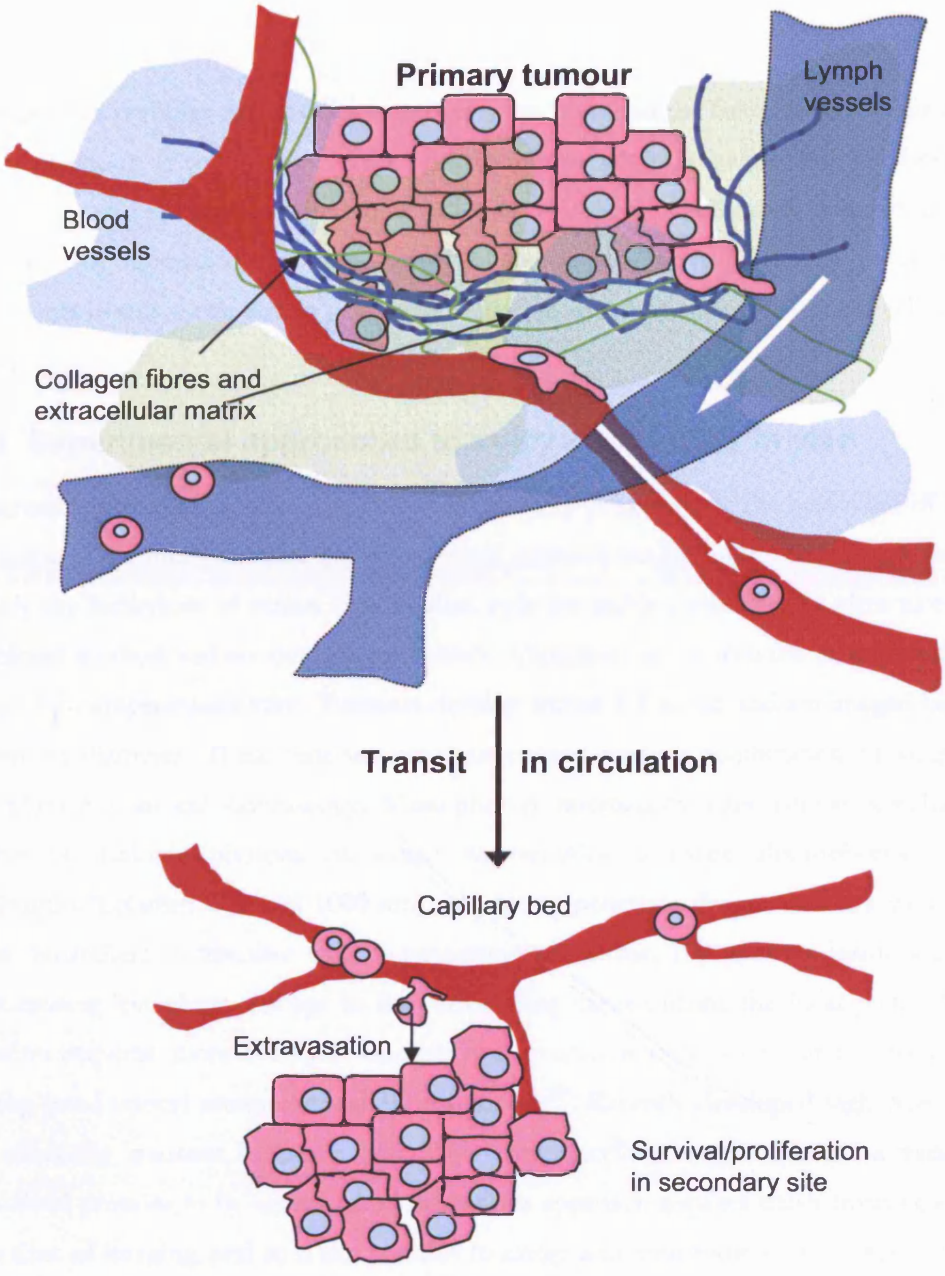

Figure 1.8 The metastatic process. For tumour cells to spread to distant site and form secondary tumours, they must escape from the primary tumour and invade the surrounding matrix. Having done this some cells will enter the blood or lymphatic vessels and be carried to other organs. On reaching a capillary bed they may become lodged. To form a secondary tumour the cells must also extravasate and be able to survive and proliferate in their new environment.

Metastasis is a complex and inefficient process, but one essential factor is the acquisition of motile behaviour. If cell motility in the primary tumour could be successfully inhibited, and the numbers of cells entering the blood and lymph could be significantly reduced, then the occurrence of metastatic secondary tumours should also be substantially reduced. The experiments in this thesis aim to gain more insight in the mechanisms of cancer cell motility in vivo.

1.8.1 Experimental approaches to study cell motility in vivo

Numerous approaches are now available to researchers to investigate the behaviour of cancer cells in vivo. The method utilised in this thesis is intravital multiphoton microscopy. In order to study the behaviour of cancer cells in vivo, cells are stably transfected in vitro to express fluorescent markers and are then injected either subcutaneously or into the mammary fat pad of immune-compromised mice. Tumours develop within 2-4 weeks and are imaged between 4-6 mm in diameter. These tumours are then imaged using a combination of single and multi-photon confocal microscopy. Multi-photon microscopy uses almost simultaneous delivery of multiple photons of longer wavelengths to excite fluorophores. Longer wavelengths (between 600 and 1000 nm) are able to penetrate deeper into tissues and this allows researchers to visualise what is happening more than 100 microns inside a tumour whilst causing less photo-damage to the surrounding tissue outside the focal point. Also as excitation requires more than just one photon, excitation only occurs at the focal point allowing good optical sectioning and 3D resolution [207]. Recently developed high N.A. lenses that efficiently transmit infra-red light allow the subcellular localisation of a variety of cytoskeletal proteins to be visualised. However this approach requires either invasive surgery at the time of imaging, and so is not possible to image a tumour more than once, or window chambers can be implanted which allow multiple imaging sessions of one site but have the disadvantage of creating a rather artificial environment. Other non-invasive imaging techniques have lower resolution but nonetheless have many applications and are a useful adjunct to multi-photon microscopy.

Much of the tissue architecture can be seen using reflectance imaging, including some circulating immune cells. The collagen fibres, by virtue of their protein structure can also be seen using second harmonic signals (a complex physical process which generates light exactly half the wavelength that they are illuminated with) [208]. Blood vessels can be seen either as

areas containing less dense matrix when imaged by reflectance, or a fluorescently labelled marker can be injected intravenously. The fluorescently labelled cell lines can then be imaged against the background of the tissue microenvironment. Fluorescent proteins can be used to observe the localisation of cell structures including the plasma membrane, the nucleus or proteins of interest during cell movement events [198].

To model the tumour environment and amoeboid motility in vitro 3D matrices comprising mostly collagen (2-4 mg/ml) can be used [209]. This creates an environment with similar elastic properties to tumour tissue [210]. Cells mixed within this matrix, or plated on top behave similarly to what we observe in vivo. Cells displaying amoeboid motility in vivo appear rounded when plated on a 3D matrix and have prominent cortical actin.

1.8.2 Cancer cell motility in vivo

Cancer cells are able to move and invade in a variety of ways. It is also possible for tumour cells to switch modes of motility when one mechanism is inhibited [211]. This plasticity in cancer cell motility presents a huge challenge when designing potential future treatments and it is likely that successful anti-metastatic treatments will need to block different modes of cell motility simultaneously.

In vivo, cancer cells are able to move with a range of morphologies. Cells can invade as individual cells in either an amoeboid or an elongated manner, and they are also able to move as collective cohorts [212]. These categories of cell motility are not completely distinct, and tumour cells are often able to switch between modes, this is discussed below. The mesenchymal type of cell motility is characterised by elongated fibroblast-like cell morphology. Elongated cells utilise integrin-based adhesions and up-regulate cell surface proteases to degrade extracellular matrix in their path [213]. This type of cell migration requires active Rac and Cdc42 but is less dependent on Rho signalling [153, 170, 214]. Due to the time required to degrade the matrix and to turnover integrin adhesions, this type of cell motility is relatively slow.

Epithelial to mesenchymal transition (EMT) is a well-documented phenomenon that occurs during morphogenesis during embryonic development [171]. EMT in adult tissues contributes to the pathology of fibrotic conditions for example in the kidney. EMT in this context prevents the proper functioning of the epithelial tissue[215]. EMT is also thought to occur in

carcinomas as they begin to become invasive, in cases where tumours of epithelial origin are observed to move in an elongated manner. EMT is characterised by the loss of epithelial markers such as E-cadherin, and the simultaneous up regulation of mesenchymal markers such as vimentin. EMT can be induced and maintained by TGF-β signalling which was discussed earlier. Prolonged TGF-β signalling causes changes in the transcriptional profile of cells through the activation of transcription factors such as twist, slug and snail [216, 217]. These changes in protein expression cause cells to lose cell-cell adhesion and start to become motile. Analysis of tumour tissue has shown that cells at the tumour periphery are less epithelial in morphology, and in some cases, look more similar to fibroblasts, and have started to express mesenchymal markers [218]. The cells that are more mesenchymal in nature are thought to be able to lead cell invasion by degrading and deforming surrounding matrix.

It has also been shown that EMT is not always required for cell invasion. For example squamous cell carcinoma cells (SCC) are able to collectively invade whilst retaining epithelial characteristics. Their invasion is possible because the stromal fibroblasts are able to lead the invading strands of SCCs. The mesenchymal properties of the fibroblasts allow them to remodel the matrix and lay down components such as fibronectin. They also deform the matrix, leaving holes for SCCs to move through and thick tracks of collagen to guide them [79]. This is an example of epithelial-like cells hijacking the mesenchymal properties of resident host cells to invade, and shows clearly that although remodelling of the matrix is required, it is not necessary for the carcinoma cells to carry out this function themselves by undergoing EMT.

Recent advances in microscopy techniques has allowed the visualisation of the behaviour of live tumour cells, and it has been seen that tumour cells of different origins (carcinoma, and melanoma) commonly move very rapidly in an amoeboid manner. In contrast to mesenchymal migration, amoeboid cell migration is extremely rapid (up to 15 microns/min). Amoeboid cell migration of tumour cells resembles the dynamic movement of the amoeba Dictyostelium [219]. Amoeboid cell migration is driven by dynamic changes in cell shape downstream of strong contractile forces. Amoeboid cell motility requires signalling through RhoA and ROCK but does not require integrins or stable focal adhesions with the matrix [220]. The dynamic changes in cell shape are sufficient to physically deform the matrix and/or allow cells to squeeze through small spaces without requiring degradation of the matrix by proteases [154]. This type of cell motility is also used by migrating leukocytes [164]. Amoeboid

cells are generally rounded in morphology and can exhibit membrane blebs due to high contractile forces driven by Rho and ROCK signalling (see above). Perhaps a full conversion from epithelial to mesenchymal characteristics is not always occurring, as it seems clear that cancer cells are able to be individually motile in vivo without the need to activate mesenchymal gene expression [221].

The ability of cancer cells to switch between mesenchymal and amoeboid motility has also been documented [222]. Blockade of protease function inhibited mesenchymal cell motility but amoeboid blebbing motility still allowed cells to invade. Blocking Rho-ROCK signalling inhibited amoeboid cell invasion but cells were still able to invade in a mesenchymal manner. A combined blockade of both mechanisms was required to completely inhibit cell invasion [153]. These results can help to explain why clinical trials of Matrix-metallo-proteases have been relatively unsuccessful [223 224, 225].

Switching between modes of invasion may also be required by cancer cells to complete the metastatic process, as both mesenchymal and amoeboid cell motility have distinct characteristics. Amoeboid cell motility is fast and it is also likely that rounded contractile morphology is advantageous when travelling through the blood and colonising a secondary site. However when a cell is faced with a very dense matrix that does not permit amoeboid cells to squeeze through, protease activity might be required. Protease activity may also be required for cells to degrade and pass through a basement membrane to enter blood vessels. It will be interesting to find out whether the inter-conversion of cell motility mechanisms occurs in vivo.

One very interesting observation from the in vivo studies of cancer cell motility was that some areas of tumour show no cell motility whilst other areas of the same tumour contain many motile cells (Figure 6.1). Although the ability of a cell to become motile may be in part determined by intrinsic factors, it seems that the microenvironment also plays an important role. As discussed above it has been shown that host stromal fibroblasts are able to induce the collective invasion of SCC. Other examples of host cell/tumour cell interactions have also been documented. For example, it has been reported that tumour associated macrophages produce Epidermal growth factor (EGF) which stimulates motility in mammary carcinoma cells. In turn the carcinoma cells produce CSF-1, which stimulates the

macrophages to produce more EGF [226]. This paracrine loop is likely to be just one of many signalling interactions between tumour cells and host cells.

In conclusion, the study of cancer cell motility in vivo is still at an early stage. Despite the range of modes of motility so far observed, it is also clear that tumours show a huge degree of heterogeneity, which has not been modelled previously in 2D assays. The signalling pathways that determine why one cell or group of cells should be motile and its neighbours not are likely to be complex and will require much more investigation. Also the mechanisms allowing cells to switch between collective and single cell invasion, and also between elongated/mesenchymal and amoeboid motility are still poorly understood. The interplay between tumour cells and surrounding host cells will also be important to explore further. The work documented in this thesis aims to uncover some of the mechanisms controlling cancer cell motility in vivo with particular focus on amoeboid cell motility.

2 Materials and Methods

2.1 Reagents and chemicals

Below is a list of commonly used reagents; other reagents will be specified in the section for the assay in which it was used.

Sodium Chloride (NaCl), Potassium Chloride (KCl), TRIZMA base, TRIZMA HCl, Potassium phosphate (KH_2PO_4), Sodium phosphate (Na_2HPO_4), ethylene diamine tetraacetic acid (EDTA), glycine, Dithiothreitol (DTT), β-mercaptoethanol, Sodium Pyrophosphate, Sodium Orthovanadate ($NaVO_4$), Sodium deoxycholate, Tetramethylethylenediamine (TEMED), Ethanol (EtOH), aprotinin, leupeptin, hydrochloric acid (HCl), Dimethyl sulphoxide (DMSO), TWEEN-20, TRITON X100, nonyl phenoxylpolyethoxylethanol, (NP-40), Brij35, bromophenol blue, Brilliant blue, ponceau S, Bovine serum albumin (BSA), Adenosine triphosphate (ATP), Feotal Calf Serum (FCS), were all purchased from SIGMA.

Methanol (MeOH), acetic acid, glycerol, Boric acid, sodium dodecylsulphate (SDS), magnesium chloride ($MgCl_2$) were purchased from Fisher Scientific.

Matrigel and Rat-tail collagen type I were purchased from BD biosciences, α-MEM was purchased from GIBCO.

2.1.1 Enzymes

Restriction enzymes were purchased from NEB and were supplied with the appropriate buffers. PCR reactions were carried out using Phusion also from NEB, and was supplied with two different reaction buffers, HF buffer was used in all cases for site directed mutagenesis. Ligation reactions were carried out using T4 DNA ligase also from NEB. Details of reaction conditions are given in later sections.

2.1.2 Buffers and solutions

Some of the buffers and solutions used repeatedly throughout these experiments are listed below. Alterations to these are specified in the sections below in the appropriate places.

Phosphate buffered saline (PBS):

1.5 mM KH_2PO_4, 8 mM Na_2HPO_4, 2.7 mM KCl, 137 mM NaCl, pH 7.4

Tris buffered saline (TBS)

137 mM NaCl, 2.7 mM KCl, 20 mM TRIZMA HCl, pH 7.4

TE Buffer

10mM Tris HCl pH 7.5, 1mM EDTA

10X Protein Buffer

1.92M glycine, 0.25M Tris base

SDS running buffer

100 ml 10X protein buffer, 890 ml dH_2O, 10 ml 10% SDS

Transfer Buffer 1 litre

200 ml Methanol, 100 ml 10X protein buffer, 1ml 10% SDS

10X TBE Buffer

108 g Tris base, 55 g Boric acid, 9.3 g Na4EDTA, dH_2O to 1 Litre

(pH is 8.3 and does not need to be adjusted use 0.5X for running agarose gels)

2x SDS gel loading buffer

100mM Tris HCl pH 6.8, 4% SDS, 20% glycerol, 200mM β-mercaptoethanol, 0.2 % bromophenol blue

Lysis buffer

50 mM Tris pH 7.5, 1 % triton x100, 10 mM $MgCl_2$, 150 mM NaCl, 1 mM DTT, 40 mM Na pyrophosphate, 1 mM $NaVO_4$, 2 mM PMSF, 50 ng/ul, 0.025 % NP 40, 0.05 % deoxycholate, 10 μg/ml aprotinin, 10 μg/ml leupeptin, dH_2O

Kinase assay buffer

50 mM Tris pH 7.5, 1 mM EDTA pH8.0, 10 mM $MgCl_2$, 50 mM NaCl, 0.03% Brij35, 1 mM DTT, 40 mM Na pyrophosphate, 1 mM $NaVO_4$, 2 mM PMSF, 50 ng/ul, 0.025 % NP 40, 0.05 % deoxycholate, 10 µg/ml aprotinin, 10 µg/ml leupeptin, 10 µM ATP, dH_2O

2.2 Mammalian Cell culture manipulations

2.2.1 Cell lines

A375 cells are amelanotic human melanoma cells. A375 cells were cultured in DMEM + 10% FCS in 10% CO_2. Polyclonal cell lines stably expressing GFP-MLC and monoclonal cell lines with stable knockdown of PDK-1were also cultured in these conditions after they had been selected in antibiotic containing media (see later). Two types of A375 cells are used in these experiments, A375P and A375M2. A375P are used as a model system for looking for increases in ROCK activity, A375M2 cells are used as a model to look for the disruption of rounded cell morphology e.g. the siRNA screen and the in vivo experiments. MTLn3E cells were originally isolated from a rat mammary carcinoma. MTLn3E cells were cultured in α-MEM + 5% FCS in 5% CO_2. B16 F2 cells are a mouse, pigment-producing melanoma cell line. B16 F2 cells were cultured in DMEM + 10% FCS in 10% CO_2.

2.2.2 Cell culture

DMEM was made to the following protocol in house by media production services.

E4 - Formulation (Dulbecco's MEM)	mg/litre
Inorganic Salts	
CaCl2.2H2O	265.00
Fe(NO3)3	0.1
KCl CaCl2.2H2O	400.00
Mg Fe(NO3)3	200.00
Na(KCl	6400.00
NaH MgSO4. 7H2O	140.00
Amir NaCl	
L- A NaH2PO4.2H2O	84.00
L-C Amino Acids	48.00
L-H L- Arginine mono.HCl	42.00
L-G L-Cystine	584.00
Gly L-Histidine mono.HCl	30.00
L-Is L-Glutamine	104.80
L-L Glycine	104.80
L-Isoleucine	
L-Leucine	

L-Lysine mono.HCl	146.20
L-Methionine	30.00
L-Phenylalanine	66.00
L-Serine	42.00
L-Threonine	95.20
L-Tryptophan	16.00
L-Tyrosine	72.40
L-Valine	93.60
Inositol	7.00
Vitamins	
Choline Chloride	4.00
Folic acid	4.00
Nicotinamide	4.00
DL-pantothenic acid, Ca salt	4.00
Pyridoxal HCl	4.00
Riboflavin	0.40
Thiamine HCl (aneurine)	4.00
Other Compounds	
D-Glucose	4500.00
Phenol red	15.00
$NaHCO_3$	3700.00
Penicillin	100,000 units
Streptomycin Sulphate	100.00
Sodium pyruvate	110.00
Antimycotic (Butyl-p-hydroxybenzoate)	0.2

α-MEM was purchased in powdered form from GIBCO (11900-073) and was made up with sodium bicarbonate according to the manufacturer's instructions.

Cells were removed from cell culture dishes with 0.1% trypsin and 0.02% versene after washing the cells with PBS. Trypsin was neutralised by adding 10 ml media containing 10% FCS.

2.2.3 Generation of 3D collagen/matrigel matrix

The gel-mix used throughout the 3D in vitro assays are previously described [209]. The components are as follows.

20% Matrigel (BD biosciences)

3.2 mg/ml Collagen type 1 (BD biosciences),

10% FCS

Collagen type 1 was mixed with 5X αMEM with sodium bicarbonate to neutralise the acidic pH. Matrigel and FCS were added to the concentrations above. The volume was made up with 1X media +10% FCS that was suitable for the cell line used in the subsequent assay.
The gel mix was then spread into glass-bottomed cell culture dishes from MatTek using the tip of a sealed glass pipette. 45 µl was used to cover a coverslip 1.3 mm in diameter. The gels were left for 15 min at 37 °C to set before they were covered with media and cells.

2.2.4 Transient DNA transfections

Cells were plated in 6 well plates 24 hours before transfection. A375 cells and MTLn3E cells were transfected with effectene (Qiagen). 1 µg DNA was mixed with 100 µl EC buffer + 3 µl enhancer solution. After 20 minutes, 10 µl of effectene was added to the mix. After a further 20 minutes, 900 µl of complete media was added and the total mix (1 ml) was added to the cells. The cells were washed with PBS after 2 ½ hours and left in the appropriate media + 10 % FCS to recover over-night before any further manipulation. In cases where cells are co-transfected with more than one DNA construct, the two plasmids were mixed in equal concentrations in the transfection mix, using a total of 1.5 µg DNA.
On occasions where cells where subsequently analysed by immune fluorescence, cells were trypsinised 24 hours after transfection and plated on glass-bottomed MatTek dishes or collagen/matrigel gels for imaging. Cells could also be treated with inhibitors after transfection before fixation.

2.2.5 Transfection of siRNA oligos

siRNA oligos were ordered from Dharmacon and stock concentrations made up at 20 µM. For the siRNA screen, Dharmacon provided a 96 well plate, each well containing a smart pool of 4 siRNA oligos for each gene. The oligos in the plate was also made up at 20 µM. siRNA oligos were used in the transfections at a final concentration of 100 nM. The transfection reagent used was oligofectamine (Invitrogen).

Transfection mix:

Per well for a 48 well plate

1) 1 µl siRNA oligo (stock concentration 20 µM) mixed with 11.5 µl opti-MEM

2) 1 µl oligofectamine reagent + 11.5 µl opti-MEM

After 5 minutes mix both 1) and 2) together and incubate for a further 20 minutes for complexes to form. Wash cells and add 175 µl opti-MEM to each well. Add the 25 µl of siRNA and oligofectamine reagent mix and leave on cells for 8 hours. Transfection is stopped by adding opti-MEM containing 30 % FCS, so that the final concentration of FCS was 10 %.

For the siRNA screen, 20,000 A375 cells were plated into each well of 2 x 48 well plates and allowed to adhere over-night. 200 µl of transfection mix (see above) was added to each well for 8 hours. After this time 100 µl of opti-MEM + 30 % FCS was added to each well. 24 hours later the cells were washed and media replaced with DMEM + 10 % FCS.

For transfection of siRNA oligos for use in other assays the siRNA oligos were used at a final concentration of 100 nM. The transfections were scaled up to 6 well plates containing 150,000 A375 cells according to the instructions supplied with the oligofectamine reagent.

Briefly, for a 6 well plate:
1) 5 µl siRNA oligo (stock concentration 20 µM)
Mixed with 75 µl opti-MEM
2) 5 µl oligofectamine reagent + 15 µl opti-MEM

After 10 minutes mix 1) and 2) and leave for 20 minutes. Then add 900 µl opti-MEM and ass the total mix (1 ml) to the 6 well plate.

2.2.6 siRNA oligos used in transient knockdown experiments

Target	Oligo name	Dharmacon number	Sequence
RhoA	RHOA#2	D-003860-02	GAACUAUGUGGCAGAUAUCUU
PDK1	PDK1#1	D-003017-05	CAAGAGACCUCGUGGAGAAUU
PDK1	PDK1#2	D-003017-06	GACCAGAGGCCAAGAAUUUUU
RHOE	RHOE#1	D-007794-02	GAACGUGAAAUGCAAGAUAUU
RHOE	RHOE#2	D-007794-03	GAAAUUAUCCAGCAAAUCUUU

In cases when cells were transfected with siRNA oligos and also DNA constructs, the siRNA transfection was carried out first, as above, and 24 hours later, after the cells had been

recovered in DMEM + 10 % FCS, the DNA transfection was carried out as detailed above. Two separate transfections was the preferred method to obtain optimal knockdown and also optimal expression of the DNA construct. In cases when cells were depleted of both PDK1 and RhoE, siRNA oligos were mixed in equal concentration in the reaction mix and the total final concentration of oligo was 150 nM.

2.2.7 siRNA screening in A375 cells

As detailed above, a 96-well plate containing smart-pools of 4 siRNA oligos targeted against each gene was acquired from Dharmacon. The genes included had been selected in collaboration with other group leaders at the LRI and included genes known to be involved in cell motility, cell adhesion, actin dynamics and also some other major signalling pathways. The gene symbols and Dharmacon catalogue numbers are listed below. The plate also contained several non-targeting siRNA controls and also empty wells also as controls.

CTTN M-010508-00,
WASL M-006444-01,
PXN M-005163-00,
VCL M-009288-00,
TLN1 M-012949-00,
RAC1 M-003560-02,
RAC2 M-007741-00,
RAC3 M-008836-01,
CDC42 M-005057-00,
RHOA M-003860-00,
RHOB M-008395-01,
RHOC M-008555-00,
RHOD M-008940-00,
ARHE M-007794-01,
RND1 M-008929-00,
ARHN M-009727-00,
RHOF M-008316-00,
RHOG M-008995-00,
RHOH M-008804-00,
RHOJ M-010367-00,
RHOQ M-009943-00,
RHOU M-009882-00,
RHOV M-006374-00,
RHOBTB1 M-009389-00,
RHOBTB2 M-009252-00,
RHOBTB3 M-020480-01,
RHOT1 M-010365-00,
RHOT2 M-008340-00,
DIAPH1 M-010347-01,
DIAPH2 M-012029-00, ,
WASF1 M-011557-00,
WASF2 M-012141-00,
CFL1 M-012707-00,
PTK2B M-003165-03,
ITGA1 M-008516-00,
ITGA2 M-004566-01,
ITGA3 M-004571-01,
ITGAV M-004565-03,
ITGA5 M-00803-01,
ITGA6 M-007214-00,
ITGB1 M-004506-00,
ITGB3, M-004124-02,
ITGB4 M-008011-01,
CIT M-004613-01,
AKT1 M-003000-02,
AKT2 M-003001-01,
AKT3.M-003002-02.
PDK1 D-003017-05

For ROCK1, ROCK2, MRCKα MRCKβ specific sequences were used as previously published[170] [114]. A375 cells transfected with the siRNA oligos as detailed above. 36 hours after transfection, the cells were trypsinised and plated onto collagen/matrigel gels in glass-bottomed 8-well chambers (Lab-Tek) in a total volume of 250 µl (see above for details of gel mix). Cells were allowed to adhere for 24 hours and then were fixed with 4 % PFA for 10

minutes. Cells were then permiabilised with 0.25 % TRITON X100 in PBS for 10 minutes before blocking in 3 % BSA in PBS for 1 hour. Cells were then stained with TRITC phalloidin and propidium iodide. (see immune fluorescence section for more details). Each well was then imaged using confocal microscopy. 7 z-sections taken at 2-micron intervals were captured for each field, and subsequently these images were projected onto a single plain to allow a more 3D representation of each field to be compared. These pictures were taken by both Erik Sahai and myself.

2.2.8 Screen of small molecule inhibitors in A375 cells

In a parallel analysis to the siRNA screening, A375 cells were also treated with a range of small molecule inhibitors to see what affect they had on cell morphology. A375 cells were plated onto collagen/matrigel gels in glass-bottomed 8-well chambers similarly to above and allowed to adhere over-night. The cells were then treated for 18 hours with the inhibitors below at the concentrations listed. Following this the cells were fixed and stained with TRITC phalloidin and propidium iodide as above. The inhibitors and their targets are listed below:

DMSO 0.05%,
Blebbistatin 5 μM (non-muscle myosin),
TAT-C3 500 nM [55] (Rho),
Y2763210 μM (ROCK),
HA1077 10 μM (ROCK,PKA),
H1152 5 μM (ROCK),
U0126 10 μM (MEK1/2),
SB203580 10 μM (p38 MAPK's),
SP600125 10 μM (JNK's),
AG1478 10 μM (EGFR's),
SB431542 10 μM (TGFbetaRI, Alk4,5,7),
LY294002 20 μM (PI-3K's),
BIM 0.5 μM (PKC's),
ML-7 25 μM (MLCK),
PP2 10 μM (Src family kinases),
Go6983 10 μM (PKC's).

2.2.9 Generation of stably transfected cell lines

A375 cells stably expressing GFP-MLC were generated by transiently transfecting cells with eGFP-MLC. Cells were then cultured in selection media, DMEM + 10 % FCS + 1 mg/ml G418 for 2 weeks. Subsequent sorting of the cells for GFP expression by FACS then ensured high expression.

A375 cells stably depleted of PDK1 were generated by infecting the cells with retrovirus and subsequent selection of infected cells with puromycin (2.5 mg/ml). Retrovirus was made by

transfecting the amphotropic cell line phoenix-AMPHO with effectene with the DNA construct pSuperRetro manipulated include shRNA sequences targeted against PDK1 (see below for details). The media from the phoenix-AMPHO cells was removed and mixed with polybrene (SIGMA) (0.4 mg/ml final concentration), and incubated for 15 minutes, before it was added to A375 cells, which had been plated in 6-well cell culture plates. 48 hours after infection the A375 cells were washed with fresh media and trypsinised before plating them at low density in 15 cm cell culture dishes. They were then selected in media containing 2.5 mg/ml puromycin (SIGMA). Individual clones were selected and tested for their expression of PDK1 by western blotting.

B16 F2 cells were infected with retrovirus to stably express either mRFP CAAX, or GFP CAAX. As above, phoenix-AMPHO cells were transfected with Effectene with the pBABE puro vector modified to include sequences encoding mRFP CAAX, or GFP CAAX (see below for details). As above the media containing the virus was used to infect B16 F2 cells plated in 6-well cell culture plates. The B16F2 cells stably expressing the constructs were selected with puromycin. The B16F2 GFP CAAX and B16F2 mRFP CAAX were cultured as polyclonal cell lines.

2.2.10 FACS analysis and cell sorting

Fluorescent stably labelled cells lines were sorted by flow cytometry to ensure a high proportion of brightly labelled cells were used for injections for the generation of xenograft tumours. To prepare cells for FACS analysis, cells were trypsinised, then centrifuged at 1200 rpm for 5 min. The cell pellet was then washed with sterile PBS and centrifuged again at 1200 rpm. Then the cell pellet was resuspended in PBS and filtered through a 70 micron sterile cell filter (BD Falcon). The filtered cells were then transferred to a polypropylene FACS tube (BD Falcon). Sorted cells were collected in the same type of tube containing media + 10 % FCS. After sorting cells were re-plated and cultured as normal.

Tumour cells isolated from B16F2 GFP-CAAX xenograft tumours were also analysed by FACS. Mice were culled when tumours reached 1 cm in diameter. The tumours were dissected and cut into small pieces. The tumour pieces were incubated in collagenase/dispase (Roche) in PBS (1 mg/ml) for 2 hours at 37 °C, at which point the majority of cells had dissociated and were in solution. The cell suspension was filtered 2-3 times through 70 micron filters. The cells were then centrifuged at 1200 rpm for 5 min and the cell pellet was

resuspended in PBS. The tumours cells were identified by their emission in the range of 500-530 nm (GFP). The tumour cells were then sorted into high and low melanin expression by their emission in the violet range. As a control a B16F2 tumour that did not express GFP was analysed along side. The two populations of B16F2 cells expressing either high or low melanin levels were then collected and RNA was extracted for analysis by microarray.

2.2.11 Extraction of RNA from FACS sorted B16F2 tumour cells

The cell populations expressing either high or low levels of melanin separated by FACS sorting were centrifuged at 1200 rpm for 10 minutes. Typically around 100,000 cells could be collected in each gate from 3 dissected tumours. RNA was then extracted using the RNeasy kit (Qiagen). Briefly, the pelleted cells were resuspended in 350 µl RLT buffer and disrupted by passing the lysate through a 20-guage needle 20 times. 350 µl 70 % EtOH was added and the sample was loaded onto a spin column and centrifuged for 15 s at 10,000 rpm. DNA digestion was carried out on the column and then the column was washed with RW1 buffer. 500 µl RPE buffer was then washed through the column and when the column was completely dry, the RNA was eluted in 20 µl RNAase free water.

The quality of the RNA samples was checked by running 1 µl of each on a Aglient Bioanalyser using an RNA pico chip. Profiles obtained from the chip are shown in chapter 9. Microarray analysis was carried out in collaboration with the Paterson institute. Affymetrix chips (MOE430 2.0) were used which included probes of the whole mouse genome.

2.3 Nucleic acid manipulations

2.3.1 Preparation of DNA

E.coli transformed with the DNA construct of interest were grown in 100 ml LB broth over-night with the appropriate antibiotic included (ampicillin 50 µg/ml, kanamycin 50 µg/ml). DNA was then extracted from the E.coli using the Qiagen midi kit according to the manufacturers instructions. Briefly: Spin down culture at 4,000 rpm, remove all broth. Resupsend pellet in 10mls buffer P1 containing RNAase. Add 10 ml buffer P2 – mixture turns viscous. Incubate at room temp for 5 min. Add 10 ml chilled P3 – mix gently white precipitate forms containing all cell debris. Incubate on ice for 15-20 mins. Centrifuge on full speed at 4C for 30 mins. Collect supernatant and spin again to remove all precipitate.

Equilibrate column with QBT buffer, add cleared supernatant to column. Wash x2 with 30 mls buffer QC. Elute DNA in 5mls buffer QF. Precipitate by adding 3.5mls propan-2-ol to 5ml eluted DNA. Centrifuge mix at 10,000 rpm at 4 °C and wash pellet in 70 % EtOH. Dry pellet and resuspend in TE buffer.
An in house research service laboratory carried out Minipreps, using a robot for high through put.

2.3.2 Nucleic acid quantification

The concentration of nucleic acid from minipreps or maxi preps was determined using 'nanodrop' equipment (Thermo Scientific) that reads the absorbance of 1 µl sample at a wavelength of 230 nm.

2.3.3 PCR mutagenesis

Mutagenesis was carried out by PCR in 2 steps. Firstly studying the nucleotide sequence and choosing appropriate restriction sites determined a fragment of DNA that was easily cloned in and out of the vector/gene of interest. In the case of myc-ROCK1 pCAGGS, this fragment was cut using Xba-I sites, one site that was within the gene another which was in the vector prior to the myc-tag. Mutagenesis primers were then designed to change the nucleotides so as to cause a different amino acid to be coded at the position of interest.

The first step of the PCR was to amplify the front half of the fragment using a forward primer including the restriction site (e.g. Xba-I) and the reverse mutagenesis primer. The same was done for the 2nd half of the fragment (using a reverse primer including the restriction site and the forward mutagenesis primer). These two PCR products were purified to be used in the second step of the PCR. The second step used the two mutant PCR products and the two primers, forward and reverse, that contain the restriction sites in order to clone the PCR product back into the vector. The two PCR products from the first step will bind to each other and prime each other, as the area covered by the mutagenesis primers is over-lapping and complementary. The product from the 2^{nd} round of PCR is purified and then digested with the appropriate restriction enzymes e.g. Xba-I. The vector undergoes the same digest and is also treated with calf intestinal phophatase (CIP). Ligations were then carried out as below.

The mutation in the Rho binding domain was carried out using Xho-1 sites, T518A mutation was made using a fragment cut with Nsi-1 and Sph-1. Mutations of PDK1 were made using the whole gene cut from the vector with EcoRI.

PCR reactions

1 µl DNA template (10 ng)

10 µl 5X HF buffer (supplied with Phusion polymerase)

1 µl forward primer (10 pmol)

1 µl reverse primer (10 pmol)

2 µl dNTPs (1 mM)

1 µl Phusion polymerase

1 µl DMSO

dH_2O to 50 µl

Temperature cycles

95 °C 5 min

96 °C 1 min - denaturing

52 °C 1 min - annealing

72 °C 1 -3 min - extension return to denaturing x 18 - 25 cycles

4 °C hold

2.3.4 DNA sequencing

All cloning of DNA constructs was checked by sequencing the maxiprep before they were used in a cell-based assay. Big Dye terminator (BDT) kit (Applied Biosystems) was used according to manufacturers instructions. Each sequencing reaction contained:

8 µl BDT reaction mix

1 µl DNA (100 ng)

1 µl primer (3.2 pmol)

10 µl dH_2O

The temperature cycles were as follows:

95 °C 1 min

96 °C 10 sec - denaturing

61 °C 5 sec - annealing

60 °C 4 min - extension return to denaturing x 25 cycles

4 °C hold

Annealing temperature was calculated for each primer. Approximately 5 °C below melting temperature was routinely used.

Sequencing reactions were precipitated by adding 2 µl of 125 mM EDTA, and 2 µl of 3M sodium acetate (pH 5.2). after mixing, 50 µl 100 % EtOH was added and the mixes were left at room temperature for 10-15 min. Mixes were then centrifuged at 2000 rpm for 30 min. the supernatant was removed and the pellets washed with 100 µl 70 % EtOH. Tubes were centrifuged again at 3000 rpm for 30 mins. The supernatant was removed and pellets allowed to dry at room temperature. The purified DNA was then analysed by an in house research services laboratory.

2.3.5 Purification of DNA fragments from agarose gels

DNA bands cut from agarose gels were purified using an Illustra™ DNA and gel band purification kit (GE Healthcare) according to the manufacturers instructions. Briefly, the agarose band containing DNA is dissolved in 300 µl extraction buffer heated to 65 °C for 5-10 min. The dissolved band is then added to a column and centrifuged at 13,000 rpm for 1 min. The column is then washed with 500 µl wash buffer. When column is dry, the DNA is eluted with 20-50 µl dH_2O.

2.3.6 Ligation of DNA fragments

A small amount of both the vector and insert fragments were run out on an agarose gel to determine ratios. Ligation reactions were set up using a range of ratios (vector:insert) between 1:1 to 1:5. Each 20 µl ligation reaction contained: 2 µl T4 ligase buffer, 1 ul ATP (10 µM stock concentration), 1 µl vector DNA, 1-3 µl insert fragment DNA, 1 µl T4 ligase,

dH2O. The reaction was left at room temperature for at least 4 hours. The ligation reaction was then used to transform competent E.coli.

2.4 Plasmids and oligonucleotides

2.4.1 Mammalian expression constructs

Myc-ROCK1 constructs:

The full-length wild-type ROCK1 used throughout these experiments was previously described [98]. The cDNA sequence matches that of the human gene (NM_005406). ROCK1 is cloned into the pCAGGS vector with an N-terminal myc-tag under the control of a CMV promoter.

Truncated myc-ROCK1

The truncated ROCK1 used in these experiments is previously described [98] and is termed Δ3 ROCK1 in that publication. This truncation was made by Xho-1 digestion of the full-length myc-ROCK1 pCAGGS construct described above. This results in the removal of the C-terminus of ROCK1 leaving the sequence coding amino acids 1-727 remaining. The shortened plasmid was re-ligated using T4 ligase as described above.

Truncated myc-ROCK1 CAAX

This construct was clone from the truncated myc-ROCK1 detailed above. The CAAX sequences of K-Ras and RhoA were cloned onto the C-terminus. Complimentary oligo primers were ordered from SIGMA to create sticky ends complimentary to Xho-I restrictions sites.

Forward K-Ras CAAX primer:

T CGA AAA AAG ATG AGC AAG GAC GGC AAG AAG AAG AAG AAG AAG AGC AAG ACA AAG TGT GTA ATT ATG TAA GC

Reverse K-Ras CAAX primer:

TCG AGC TTA CAT AAT TAC ACA CTT TGT CTT GCT CTT CTT CTT CTT CTT CTT GCC GTC CTT GCT CAT CTT TTT

Forward RhoA CAAX primer:

T CGA ATG GCT ACG AGA GCT GCT CTG CAA GCT AGA CGT GGG AAG AAA AAA TCT GGG TGC CTT GTC TTG TAA GC

Reverse RhoA CAAX primer:

TCG AGC TTA CAA GAC AAG GCA CCC AGA TTT TTT CTT CCC ACG TCT AGC TTG CAG AGC AGC TCT CGT AGC CAT

The oligos were annealed by mixing equal amounts of each oligo primer (100 pg) together in 50 µl annealing buffer (50 mM HEPES, 100 mM NaCl, pH 7.4) The annealing mixture was heated to 95 °C for 10 min. Then the annealing mix was transferred to a glass beaker containing water heated to boiling point. The mix was allowed to cool to room temperature.

The annealed oligos were then phosphorylated by adding 1 µl polynucleotide kinase (PNK) to the annealing reaction and incubating for 30 minutes at 37 °C. The kinase was denatured by heating the reaction to 65 °C for 5 min. The annealed and phosphorylated oligos were then run out on a 2.5 % agarose gel. The band was cut out and extracted using the GFX kit according to the manufacturers instructions (see above) and eluted in 50 µl deionised water. The concentration of DNA was measured using the Nanodrop spectrometer. Meanwhile the truncated pCAGGS myc-ROCK1 was digested with Xho-I to linearise it by opening the vector at the C-terminal end of ROCK1, and dephosphorylated with Calf intestinal phosphatase (CIP). The vector was also run out on an agarose gel and the band was cut out and purified using the GFX kit as described above. Ligations were set up so as to ensure that in each reaction there were 2X as many 'ends' of the annealed primers as the free ends of the vector. This was calculated from the measured DNA concentrations and the known sizes of each fragment. Ligations were carried out and transformed in E.coli as described below.

Myc-ROCK1 I1009A

This mutation of ROCK1 is in the Rho-binding domain in the C-terminus of ROCK1 and has previously been reported to disrupt the binding of ROCK1 to RhoA [98]. This mutation was introduced by 2-step PCR that is described above. The C-terminus of ROCK1 that is contained within 2 Xho-I restriction sites was the fragment used for the PCR mutagenesis. The mutagenic primers were as follows:

Original sequence:	ACAAATTGGCAGAAATAATGAATCG
Mutagenesis primer forward:	ACAAATTGGCAGAAGCAATGAATCG
Mutagenesis primer reverse:	CGATTCATTGCTTCTGCCAATTTGT

Myc-ROCK1 T-A mutations in the activation loop and hydrophobic motif.

All the mutations of ROCK1 in the activation loop or the hydrophobic motif were carried out by 2-step PCR utilising an 1597 bp Xba-I digested fragment which cuts within ROCK1 and also in the pCAGGS vector prior to the N-terminal myc-tag.

T233A original sequence:	CATGGTACGATGTGATACAGCGGTTGGAACACC
Mutagenesis primer forward:	CATGGTACGATGTGATGCAGCGGTTGGAACACC
Mutagenesis primer reverse:	GGTGTTCCAACCGCTGCATCACATCGTACCATG
D232A original sequence:	CATGGTACGATGTGATACAGCGGTTGGAACACC
Mutagenesis primer forward:	CATGGTACGATGTGCTACAGCGGTTGGAACACC
Mutagenesis primer reverse:	GGTGTTCCAACCGCTGTAGCACATCGTACCATG

The double mutant D232A T233A was cloned using T233A myc-ROCK1 as a template.

D232A T233A original sequence:	CATGGTACGATGTGAT***GCA***GCGGTTGGAACACC
Mutagenesis primer forward:	CATGGTACGATGTGCT***GCA***GCGGTTGGAACACC

Mutagenesis primer reverse: GGTGTTCCAACCGC***TGC***AGCACATCGTACCATG

T380A original sequence: GATAAAGGAGAGGAAGAAACATTCCCTATTCCTAAAGCT

Mutagenesis primer forward: GATAAAGGAGAGGAAGAAGCATTCCCTATTCCTAAAGCT

Mutagenesis primer reverse: AGCTTTAGGAATAGGGAATGCTTCTTCCTCTCCTTTATC

T398A original sequence: TCAACTACCTTTTGTAGGATTTACATATTATAGCAATCG

Mutagenesis primer forward: TCAACTACCTTTTGTAGGATTTGCATATTATAGCAATCG

Mutagenesis primer reverse: CGATTGCTATAATATGCAAATCCTACAAAAGGTAGTTGA

T380D original sequence: GATAAAGGAGAGGAAGAAACATTCCCTATTCCTAAAGCT

Mutagenesis primer forward: GATAAAGGAGAGGAAGAAGACTTCCCTATTCCTAAAGCT

Mutagenesis primer reverse: AGCTTTAGGAATAGGGAAGTCTTCTTCCTCTCCTTTATC

T398E original sequence: TCAACTACCTTTTGTAGGATTTACATATTATAGCAATCG

Mutagenesis primer forward: TCAACTACCTTTTGTAGGATTTGAATATTATAGCAATCG

Mutagenesis primer reverse: CGATTGCTATAATATTCAAATCCTACAAAAGGTAGTTGA

T398D original sequence: TCAACTACCTTTTGTAGGATTTACATATTATAGCAATCG

Mutagenesis primer forward: TCAACTACCTTTTGTAGGATTTGACTATTATAGCAATCG

Mutagenesis primer reverse: CGATTGCTATAATAGTCAAATCCTACAAAAGGTAGTTGA

Truncations of the T-A mutants were cloned as above, by digest with Xho-I and re-ligation of the shorter vector.

Myc-ROCK1 T518A

This mutation of ROCK1 was cloned by 2-step PCR using a fragment of pCAGGS ROCK1 (2415 bp) cut out by digestion with Nsi-I and Sph-I.

T518A original sequence: GTAGAAAATGAAGTTTCTACATTAAAGGATCAGTTGGAA

Mutagenesis primer forward: GTAGAAAATGAAGTTTCTGCATTAAAGGATCAGTTGGAA

Mutagenesis primer reverse: TTCCAACTGATCCTTTAATGCAGAAACTTCATTTTCTAC

pCAGGS Myc-ROCK2

This construct is was a gift from M. Olson and contains the ROCK2 sequence from *Bos Taurus.*

eGFP C1/C3

These constructs were purchased from Clontech (6084-1).

GFP RhoE

The human RhoE was cloned from pGEX 2T into eGFP C3 by digestion with EcoRI.

GFP MLC

MLC2 was cloned by PCR from the image clone into eGFP C1 by Erik Sahai.

GFP ROCK1

ROCK1 was cloned by PCR from pCAGGs myc-ROCK1 into eGFP by PCR by Cristina Hidalgo.

Flag-PDK1 siRNA resistant

The human PDK1 sequence was cloned by PCR from a vector, which was a gift David Stoke at UCSF into pRK5.1 Flag. pRK5.1 (Genentech, Inc.) was previously modified by Steven Hooper to include an N-terminal Flag tag sequence. The PCR primers were designed to include EcoRI sequences at both the N-terminus and the C-terminus. The PCR product and the vector were digested with EcoRI. The vector was also treated with CIP. Once the PDK1 sequence had been cloned into the appropriate backbone vector, the sequence was then modified by mutagenesis to allow expression of the construct in the presence of siRNA targeted against PDK1 by changing *ttt tcg aca aga tcc cta* to *ttc tcc acg agg tct ctt*.

Flag-PDK1 siRNA resistant KD

Further mutation of pRK5.1 Flag PDK1 was undertaken to introduce a mutation on the kinase domain to inhibit kinase activity.

K111A original sequence:	CCTCCAGAGAATATGCGATTAAAATTCTGGAGAAGC
Mutagenesis primer forward:	CCTCCAGAGAATATGCGATTGCAATTCTGGAGAAGC
Mutagenesis primer reverse:	GCTTCTCCAGAATTGCAATCGCATATTCTCTGGAGG

Flag-PDK1 siRNA resistant PH deleted

The C-terminus of siRNA resistant PDK1 was deleted by PCR so that the last amino acid now encoded was S408. The PCR primers were designed to include EcoRI sequences at both the N-terminus and the C-terminus. The PCR product and the vector were digested with EcoRI. The vector was also treated with CIP.

2.4.2 Bacterial expression constructs

pGEX KG MLC

MLC2 was cloned by PCR from the image clone into pGEX KG using the restriction sites Xba-I and HindIII.

pGEX KG Rhotekin

This construct is previously described [227].

pGEX 2T RhoE

This construct was a gift from Michael Way.

pGEX 6P3 ROCK sequences

All of the following constructs were cloned by PCR into pGEX 6P3 using EcoRI and NotI restriction sites.

pGEX 6P3 ROCK2 (358-421 a.a.)

pGEX 6P3 ROCK1 (338-415 a.a.)

pGEX 6P3 ROCK1 (338-378 a.a.)

pGEX 6P3 ROCK1 (375-415 a.a.)

similar constructs of ROCK1 were cloned from the T-A mutants to include the mutations in the hydrophobic motif.

2.4.3 Viral expression constructs

pBabe puro GFP CAAX

The CAAX sequence of K-Ras was cloned onto the C-terminus of the GFP sequence in the vector eGFP C1 (Clontech) using the annealed oligos described above. (Steven Hooper carried out this step of the cloning). GFP CAAX was first linearised by digestion with Nco-1 and this digested end was blunted by incubation with the DNA polymerase 1, Large (Klenow) fragment (NEB) for 30 mins at 25 °C. The blunted product was then digested with EcoRI to release the GFP sequence with its C-terminal CAAX sequence. The vector pBabe puro was digested with SnaBI and EcoRI and treated with CIP. The ligation was carried out in the standard way described above.

pBabe puro mRFP CAAX

Using eGFP C1 CAAX (CAAX sequence from K-Ras as above) vector as a starting point, this vector had been modified to remove the GFP and replace this with the sequence encoding mRFP (this cloning had been carried out by Cristina Hidalgo). mRFP CAAX was cloned from this by PCR using primers incorporating a SnaB1 restriction site at the N-terminal end and an EcoRI restriction site at the C-terminal end. Both the PCR product and pBabe puro vector were digested with SnaB1 and EcoRI. The vector was also treated with CIP.

pSuperRetro shRNA PDK1#1

Double stranded oligos were annealed and cloned into pSuper Retro using BglII and HindIII restriction sites, below is the template for the shRNA oligos. Underlined are the gene targeting sequences.

GATCCCXXXXXXXXXXXXXXXXXXTTCAAGAGAXXXXXXXXXXXXXXXXXXTTTTTGGAAA

AGCTTTTCCAAAAAXXXXXXXXXXXXXXXXXXTCTCTTGAAXXXXXXXXXXXXXXXXXXGG

GATCCCCAAGAGACCTCGTGGAGAATTCAAGAGATTCTCCACGAGGTCTCTTGTTTTTGGAAA

AGCTTTTCCAAAAACAAGAGACCTCGTGGAGAATCTCTTGAATTCTCCACGAGGTCTCTTGGG

pLentilox4.4 CAG-Gap-Cherry

This construct that labels membranes with Cherry was a gift from Frank Gertler

pLentilox4.4 CAG-Gap-eGFP

This construct that labels membranes with GFP was a gift from Frank Gertler.

2.5 Bacterial techniques

2.5.1 Bacterial media and plates

Competent E.coli were grown in suspension in LB broth containing the appropriate antibiotic to select for the construct they were expressing. Transformations were plated onto 10 cm dishes containing Agar also containing the appropriate antibiotic. either ampicillin (50 ug/ml) or kanamycin (50 ug/ml).

2.5.2 Bacterial strains

Competent Novablue, originally purchased from Novagen were used for transformations of all plasmids for minipreps and maxipreps. BL21(DE3)pLysS were used for the expression of GST fusion proteins.

Competent E.coli were generated as follows.

Firstly the E.coli taken from glycerol stock were grown over night in 20 ml LB broth at 37 °C with shaking. The following morning 5 ml of the 20 ml culture was added to 500 ml of fresh LB broth and the culture was grown at 37 °C with shaking until the optical density (measured at a wavelength of 600 nm) of the culture reached 0.6, indicating that the culture was in an exponential growth phase. At this point the flasks containing the cultures were chilled on ice. The bacteria were then spun down at 4,000 rpm at 4 °C for 20 minutes. The supernatant was removed and the pelleted bacteria resuspended in 3 ml sterile Transformation buffer 1 (TFB1). Make up to 100 ml with TFB1. Pellet bacterial by

centrifuging at 4,000 rpm at 4 °C for 15 minutes. Remove supernatant and resuspend pellet in 20 ml sterile chilled Transformation Buffer 2 (TFB2). Keep bacterial suspension on ice for 10-15 minutes, before aliquoting the bacteria into 1.5 ml eppendorf tubes and snap freezing the in dry ice.

Transformation Buffer 1 (TFB1)

Potassium Acetate, CH3COOK	30 mM
Manganese Chloride, MnCl2	50 mM
Potassium Chloride, KCl	100 mM
Calcium Chloride, CaCl2	10 mM
Glycerol	15 %

Transformation Buffer 2 (TFB2)

MOPS	10 mM
Calcium chloride, CaCl2	76 mM
Potassium Chloride, KCl	10 mM
Glycerol	15 %
Adjust to pH 7 with HCl	

2.5.3 Transformation of E. coli

Competant Nova blue or BL21(DE3)pLysS were thawed on ice for 15 minutes. 100 ul of bacterial suspension was mixed with 10 ng of plasmid DNA or ligated DNA fragments and incubated on ice for a further 15 minutes. The bacteria and DNA were then heated to 42 °C in a water bath for precisely 1 min. Then returned to ice for 2 minutes. 1 ml LB broth was added to the eppendorf tube and the bacteria were incubated for 45 min at 37 °C with shaking. The bacteria were then pelleted by centrifugation at 4,000 rpm for 5 minutes and resuspended in 200 ul LB. The 200 ul of bacteria was then added to an agar plate containing the appropriate antibiotic resistance and spread over the surface. The plate was incubated over night at 37 °C and colony formation was then observed.

2.5.4 Production of GST fusion proteins

BL21(DE3)pLysS E.coli were transformed with pGEX vectors containing the cDNA sequences for the protein of interest. One of the resulting colonies was then added to 20 ml LB broth containing both ampicillin (50 mg/ml) and chloramphenicol (34 mg/ml), and grown over night. The following morning 5 ml of this culture was added to 500 ml fresh LB

broth containing ampicillin (50 mg/ml) and chloramphenicol (34 mg/ml), and grown until the OD 600 of the culture reached 0.6. At this point IPTG was added to a final concentration of 0.3 mM and the culture was incubated for a further 4 hours at 37 °C. The bacteria were then pelleted by centrifugation at 4000 rpm for 20 minutes at 4 °C. The bacterial pellet was resuspended in 30 ml TBS containing 1 mM DTT, 5 mM $MgCl_2$, and protease inhibitors, then frozen at -80 °C. Bacteria were lysed by thawing in cold water followed by sonication on ice. Bacterial lysates were then further centrifuged to remove insoluble cellular debris. The cleared bacterial lysate was then aliquoted and stored at -80 °C. When the protein was required for an assay, one aliquot was defrosted on ice and glutathione agarose beads were added. Binding was carried out at 4 °C for 1 hour rotating the tube constantly. After binding the beads were washed 3 times with TBS containing 1 mM DTT, 5 mM MgCl2 and protease inhibitors. A final wash was carried out in whichever buffer was being used for the subsequent experiment.

2.5.5 Cleavage and purification of recombinant MLC protein from bacterial lysates

GST-MLC was synthesised in E.coli transformed with the plasmid pGEX KG MLC. Protein expression was induced as above. The bacterial lysate containing GST-MLC was first incubated with glutathione agarose beads for 2 hours. The supernatant was removed and the beads washed 3 times with TBS containing 1 mM DTT, 5 mM $MgCl_2$ and protease inhibitors. The beads were then resuspended in 5 ml TBS + 1 mM DTT + 1 mM $MgCl_2$ + 1 mM $CaCl_2$ + 30 units thrombin over-night at 4 °C to cleave the MLC from the GST. The supernatant was removed and incubated with p-aminobenzamidine beads for one hour. The supernatant containing MLC was then aliquoted and snap frozen.

2.6 Protein manipulations

2.6.1 Preparation of cell lysates for biochemical assays or western blotting

Plates containing cells for lysis were washed with cold PBS. Lysis buffer (see 2.1.2) was added to the plate and cells were scraped and collected in a 1.5 ml eppendorf tube. For 10 cm dishes 300 µl of lysis buffer was used. Lysates were incubated on ice for 10 minutes then

centrifuged at 2000 rpm for 5 minutes to remove nuclear debris. The supernatant was then used for the biochemical assay. To make lysates for western blotting directly, 2X SDS sample buffer was added to the cell lysate and the sample was boiled at 95 °C for 5 -10 min.
Tumour samples were prepared for western blotting by taking frozen tumour tissue and adding lysis buffer. The tissue was dissociated by maceration. The concentration of the resulting lysates was tested by Bradford assay in order to load equal amounts on the SDS-page gels.

2.6.2 Immune precipitation and kinase assays

Myc-tagged ROCK1 constructs were immune precipitated from A375 cells plated in 10 cm cell culture dishes at 80 % confluence 48 hours after they had been transfected using effectene (see 2.2.4). Cell lysates were prepared as above (2.6.1). To each cell lysate (300 µl) 20 µl protein G agarose beads and 10 µg 9E10 monoclonal antibody were added. The lysate, beads and antibody were incubated for 2 hours at 4 °C whilst being rotated constantly. After this time the beads were washed 3 times with 500 µl lysis buffer.

For kinase assays an extra wash in kinase assay buffer was included at the end. The beads bound to myc-ROCK1 were then used to phosphorylate recombinant MLC. 50 µl kinase assay buffer containing 1 µg MLC was added to each tube of beads and the reaction was incubated at 30 °C for 30 minutes. Reactions were stopped by adding 50 µl of 2X SDS sample buffer to each reaction and boiling at 95 °C for 5 minutes. The kinase assay were then analysed by SDS-PAGE followed by western blotting for p-MLC (Cell signalling 3671). Total kinase was measured by blotting with 9E10.

2.6.3 Radioactive kinase assays

Recombinant kinases ROCK1 (Upstate, 14-601) and PDK1 (Calbiochem, 521270) were used to phosphorylate recombinant substrates Akt1 (gift from Peter Parker), GST-RhoE (see 2.5.4), and MLC2 (see 2.5.5). Each reaction was carried out in 50 µl kinase assay buffer containing 0.1 µl ^{32}P ATP in addition to the normal concentration of 'cold' ATP. Reactions were incubated for 30 mins at 30 °C, 2X SDS sample buffer was added to stop the reactions. Samples were analysed by SDS-PAGE and the gel was stained as detailed below. The gel was

then dried by placing it onto a sheet of 3MM paper in a gel dryer at 70 °C for 6 hours. The dried gel was then placed in a cassette and was used to expose X-ray film.

2.6.4 Protein quantification using Bradford reagent

Bradford reagent was obtained from BioRad, and was diluted 1:5 with H_2O diluted protein samples. A standard curve was made using bovine serum albumin (BSA) with concentrations of 0, 50, 100, 200, 500, 1000 μg/ml. Cell lysates to be tested were diluted so as to fall within the range of the standard curve. Assays were carried out in 96-well plates, each well contained 200 μl of BSA solution or diluted cell lysate + 50 μl of Bradford reagent. The absorbance of each well was read on a spectrophotometer at a wavelength of 595 nm. Concentrations of samples were calculated relative to the standard curve. The volumes of the cell lysates were then adjusted so as to load equal quantities of each onto the SDS-PAGE gel for analysis by western blotting.

2.6.5 SDS-PAGE

Polyacrylamide gels were poured into mini-gel systems manufactured by BioRad. Generally 1.5 mm gels with 10 wells loaded with up to 50 μl of sample were used. Gels were made to the following protocol: 0.1 % SDS, 375 mM TRIS HCl pH 8.8, 8-15 % poly acrylamide, 0.1 % APS, 0.001 % TEMED. Once poured the gel was over-laid with dH_20 to ensure it was flat and allowed to set for 10 min. When set, the dH_20 was removed and stacking gel was overlaid: 0.1 % SDS, 125 mM TRIS HCl pH 6.8, 5 % acrylamide, 0.1 % APS, 0.001 % TEMED. The comb was inserted. When the stacking gel was set the gel was set up in a running tank (BioRad). The comb was removed and the wells washed with SDS running buffer. The cassette was then filled with SDS running buffer and enough buffer was added to the outer compartment to cover the bottom of the gels. Up to 50 μl of sample was loaded into each well. One well was used to run a prestained ladder (Benchmark, Invitrogen). The gel was run at 70 mA for 2 hours.

2.6.6 Staining of proteins in SDS PAGE gels

After running, the gel was removed from the glass plates and washed in dH_2O. The gel was then stained using, 45 % Methanol, 10 % acetic acid containing 0.25 g/l Brilliant Blue R (SIGMA) for 30 minutes at room temperature. The gel was then washed in dH_2O, and then

destained over-night using, 33 % Methanol, 10 % acetic acid. The bands of separated proteins were then visible. The gel could then be photographed or dried.

2.6.7 Western Blotting procedure

After running, the proteins in the gel were transferred to Polyvinylidene Fluoride membrane (PVDF). The gel was placed on top of 2 sheets of 3MM chromatography paper (Whatmann), the PVDF membrane, which had been pre-wet in methanol, was then laid on top if the gel, followed by 2 more sheets of 3MM paper. This 'sandwich' was then loaded into the transfer cassette (BioRad). The tank was filled with transfer buffer and the gel was transferred for 3 hours at 150 mA. After transfer the membrane was washed with dH_2O then blocked by incubated the membrane with blocking buffer (TBS + 5 % milk (Marvel), + 2 % BSA) for 2 hours. Primary antibodies were generally incubated with the membrane overnight at 4 °C at a dilution of 1:1000 in TBS + 1 % milk). Primary antibodies were washed off with 3X 5 min washes in TBS + 1 % milk + 0.01 % TWEEN-20. HRP-labelled secondary antibodies (PIERCE) were used at a dilution of 1:50,000 in TBS + 1 % milk and incubated with the membrane for 1 hour. Secondary antibodies were washed off the membrane in 3X 5 min washes with TBS. The blot was then developed by rinsing the blot for 1 min in 2 ml of 'west dura' ECL (PIERCE). The blot was then used to expose chemoluminescent film (GE Healthcare).

2.6.8 Antibodies for western blotting

Target	Antibody	Source		Dilution
Myc-tag	9E10	in house monoclonal		1:1000
FLAG-tag	anti-FLAG M2	SIGMA	(F1804)	1:3000
PDK1	anti-PDK1	Cell Signalling	(3062)	1:1000
ROCK1	anti-ROCK1	Chemicon	(AB3885)	1:1000
MLC2	Myosin Light Chain 2	Cell Signalling	(3672)	1:1000
pMLC2	Phospho-pMLC (ser19)	Cell Signalling	(3671)	1:1000
RhoE	monoclonal anti-RhoE	SIGMA	(R6153)	1:1000
Tubulin	anti-β-Tubulin 1	SIGMA	(T7816)	1:10000
GFP	anti-GFP	Roche	(11814460001)	1:1000
pSMAD2	phospho-Smad2	Cell signalling	(3101)	1:1000
RhoA	RhoA (26C4)	Santa Cruz	(sc-418)	1:500

2.6.9 Preparation of protein samples for mass spectrometry analysis

For mass spectrometry analysis, pre-cast gels (Nupage Bis-Tris 4-12 %, Invitrogen) were used to run the samples. Each lane contained 2 μg recombinant ROCK1 (Upstate, 14-601) which had been incubated in kinase assay buffer +/- Y27632 for 30 minutes at 30 °C then mixed with SDS sample buffer as described above. The precast gels were run in tanks also from Invitrogen using Nupage MOPS SDS running buffer (Invitrogen). After running gels were taken out of the casing and stained as detailed above. The mass spectrometry laboratory then cut the protein out of the gel and digested it with trypsin ready for analysis.

2.6.10 RhoGTP pull down assays

A375 cells transfected with either control siRNA oligos or oligos targeted against PDK-1, were serum starved for 6 hours then stimulated with 20% FCS for 5 minutes before cells were lysed in lysis buffer. The Rho-binding domain of Rhotekin was tagged with GST and expressed in E.coli Expression was induced as above. The bacterial lysate containing GST-RBD Rhoteckin was incubated with Glutathione agarose beads for 2 hours at 4 C. Beads were extensively washed with cell lysis buffer before incubation with cell lysates from A375 serum stimulated cells for 2 hours at 4 °C. Beads were then extensively washed with lysis buffer and bound proteins were eluted with 2X SDS sample buffer. RhoGTP levels were determined by western blotting these samples for RhoA, and comparing the results with the levels of RhoA in the total cell lysate.

2.6.11 GST pull down assays

Bacterial lysates containing GST RhoE were incubated with glutathione agarose beads at 4 °C for 2 hours. Beads were washed extensively with lysis buffer, before incubation with A375 cell lysates expressing myc-ROCK1 or myc-ROCK1 and siRNA resistant PDK1 for 3 hours 4 C (cell lysates were also modified by the addition of recombinant PDK1 (Calbiochem, 521270). Beads were washed extensively with lysis buffer. Bound protein was eluted using 2X SDS sample buffer, then binding was analysed by western blotting using 9E10.

For analysis of the binding between ROCK1 fragments and PDK1, bacterial lysates containing GST ROCK fragments or GST alone as a control, were incubated with glutathione agarose beads as above followed by extensive washing. Beads were incubated with 100 ng purified PDK-1 (521270 Calbiochem) diluted in kinase assay buffer for 2 hours at 4 °C. beads were then washed 3X with kinase assay buffer. Proteins were eluted with 2X SDS sample buffer, and binding was determined by western blot using PDK1 antibody (3062, Cell Signalling Technology)

2.6.12 Competition binding assays

Bacterial lysates containing GST-RhoE were incubated with glutathione agarose beads as above and washed 3X in kinase assay buffer. The beads were then incubated with recombinant ROCK1 (Upstate, 14-601) either alone or in combination with recombinant PDK1 (Calbiochem, 521270), in kinase assay buffer for 3 hours at 4 °C. the solutions containing recombinant ROCK1 and PDK1 were incubated for 20 minutes on ice before adding the mixture to the beads bound to GST-RhoE. After the binding, the beads were washed 3 times with kinase assay buffer and 2X SDS sample buffer was added. The samples were boiled for 5 minutes and then analysed by western blotting.

2.6.13 Co-immunoprecipitation of ROCK1 and RhoE

A375 cells expressing either the empty pSuper Retro vector or stably depleted of PDK1 were plated in 15 cm dishes. When 80 % confluent, Cells were lysed in 20mM HEPES pH7.5, 2mM EDTA, 150mM NaCl, 1mM DTT + protease inhibitors and passed through a 19G

needle repeatedly before centrifugation at 1000G for 5 minutes at 4°C. NP40 was added to 0.05% before addition of 2ug ROCK1 antibody (Santa Cruz sc-6056) and protein G agarose beads. This mixture was then rotated for 3 hours at 4°C before 3 washes with the same lysis buffer above + 0.05%NP40. 2X SDS sample buffer was added to the beads and the samples were analysed by western blotting for endogenous ROCK1, PDK1 and RhoE (see antibodies for western blotting for details).

2.7 In vivo techniques

All the following procedures were carried out under the project licence 70/6164 held by Dr Erik Sahai.

2.7.1 Generation of xenograft tumours

In order to grow xenograft tumours for in vivo imaging, A375 cells or B16F2 cells were engineered in vitro to stably express fluorescent markers GFP-MLC or GFP-CAAX. 1 X 10^6 fluorescent cancer cells were then injected subcutaneously into the flank of nude mice, in 100 µl PBS. A375 tumours grew to 5 mm in diameter in approximately 4 weeks, B16F2 tumours grew to 5 mm in diameter in approximately 10 days.

2.7.2 Labelling cell lines with cell tracker dyes

A375 cells expressing GFP-MLC and either the empty pSuper Retro vector or stably depleted of PDK1 were used for lung colonisation assays (see below). To distinguish the two different cell populations either the controls or the PDK1 depleted cells were labelled with the red cell tracker dye SNARF (Molecular Probes). The cells to be labelled were washed with PBS and then incubated with PBS containing SNARF (1:500 dilution) for 15 minutes at 37 °C. After this time the cells were washed with PBS, and trypsinised. The successful labelling of the cells was determined by checking a small amount on a glass cover slip under the fluorescence microscope.

2.7.3 Lung colonisation assays

These lung colonisation experiments were carried out in 3 different ways.

1) 500,000 A375 cells expressing the empty pSuper Retro construct or stably depleted of PDK1 as well as expressing GFP-MLC were injected into the tail

vein of nude mice. After 4 weeks, the mice were culled and the lungs were dissected. The lungs were imaged using confocal microscopy. The total numbers of metastases were counted for each cell line injected. 3 mice were used for each cell line.

2) In this internally controlled experiment, control A375 GFP-MLC cells were labelled with cell tracker dye SNARF (see above) and mixed in equal numbers with PDK1 depleted A375 GFP-MLC cells. A total of 500,000 cells were injected into the tail vein of nude mice. As controls, labelled control cells were mixed with unlabelled control cells and also the staining of the cells was carried out in the reverse to ensure there was no effect of the cell tracker dye on the ability of the cells to colonise the lungs. 24 hours after injection the mice were culled and the lungs were dissected. In each field of view the ratio of the number of control cells to PDK1 depleted cells was calculated. 2 different PDK1 depleted cell lines were used and 2 mice were used for each combination of cell lines injected.

3) MTLn3E cells expressing with CAG-gap Cherry or CAG-gap eGFP were transfected in vitro with either control siRNA or siRNA oligos against PDK1 (oligo 2). Differently coloured control and PDK1 depleted cells were then mixed in equal numbers and injected into the tail vein of nude mice (total 250,000 cells). Mice were culled at either 2 hours or 24 hours post injection and the lungs were dissected and imaged as above. In each field of cells the numbers of control cells and PDK1 depleted cells were compared.

2.8 Microscopy techniques

2.8.1 Immunofluorescence

Cells were fixed using 4% paraformaldehyde, and permiabilised using 0.25 % Triton X100. Samples were blocked for 1 hour with 3% BSA, 0.1% Triton, in PBS before incubation with primary antibody in PBS + 1 % BSA + 0.1 % TWEEN. Primary antibody was incubated on samples over-night at 4 °C then washed off in 3 washes of 10 minutes with PBS containing 0.1 % Tween-20 and 1 % BSA. Fluorescent Alexa secondary antibodies (Molecular probes) were used diluted 1:200 in PBS + 3 % BSA + 0.1 % Tween-20 for 2 hours, then washed off

using 3 washes of PBS containing 0.1 % TWEEN-20. Immune fluorescence of cells on glass cover-slips and on matrigel/collagen gels was carried out in the same way.

Myc- ROCK1 and myc-ROCK2 were visualised using monoclonal antibodies 9E10 (mouse) or Jak6 (rat). Endogenous ROCK1 was stained using Rock1(C-19): sc-6055 (Santa Cruz Biotechnology) (rabbit). Phospho-MLC was stained using phospho-myosin light chain 2 (Thr18/Ser19) antibody (Cell Signalling Technology 3674)(rabbit). FLAG-PDK1 was stained for using monoclonal ANTI-FLAG M2 antibody (SIGMA F-1804)(mouse). F-actin was visualised using FITC or TRITC labelled phalloidin (SIGMA). Images were taken using confocal microscopy.

2.8.2 Phase contrast time lapse microscopy

Cells were plated on top of a deformable matrigel/collagen gels on glass bottomed cell culture plates (MatTek) 24 hours before imaging. Cells were incubated at 37°C with 10% CO_2 in DMEM media contain 10% FCS during imaging. Imaging was carried out on a Nikon microscope with a motorised stage for multiple positions (controlled by Metamorph software) using a 20X phase 1 objective.

2.8.3 Confocal time-lapse microscopy

A375 cells transiently transfected with ROCK-GFP or GFP-CAAX were plated on top of deformable collagen gels as detailed above, and imaged using a Zeiss LSM510 confocal microscope. In assays in which inhibitors were added, for example cytochalasinD or blebbistatin, these drugs were mixed at 3X concentration in media and added by syringe with care during the imaging process. The final concentration of each of these inhibitors was 5 μM. Images were taken at 2 sec intervals.

2.8.4 Multiphoton in vivo imaging of primary tumours

The xenograft tumours (described above) were imaged when they reached between 4-6 mm in diameter. The mice were anesthetised using isofluorane carried on oxygen, and anaesthetic was maintained during imaging using a mouthpiece, which the head of the mouse was laid inside. Our licence permits imaging in this way for a period of 3 hours, during this time, 4-5 time-lapse movies were captured, each covering a depth of approximately 50 microns with 7

z-sections. Images were captured every 90 s for A375 tumours and every 30 s for B16F2 tumours, as B16F2 cells moved at faster speeds. The tumour was partially separated from the flank in order to lay the tumour on a cover slip and image it from underneath. The blood vessels remained intact and blood flow could be monitored by intravenous injection of fluorescently labelled dextran. After imaging the mouse was culled by dislocation of the neck (one of the allowed schedule 1 methods). The tumour material was dissected and snap frozen to be used to make tumour cell lysates or for sectioning.

The in vivo imaging was carried out using a femto-second-pulsed Ti-Sapphire laser from Chameleon using wavelengths between 820 and 900 nm. Collagen fibres were imaged by second harmonic signals that are collected at half the multi-photon excitation wavelength. Other matrix components and some host cells could be imaged by reflectance using a single photon laser. A375 GFP-MLC tumours and A375 GFP-MLC PDK1-depleted tumours were imaged by Erik Sahai. A375 GFP-MLC tumours treated either with or without ROCK inhibitor Y27632 were imaged partly by Erik Sahai and partly by myself. B16F2 tumours were imaged by myself.
A375 GFP-MLC tumours treated with Y27632 were analysed by in vivo multi-photon imaging 48 hours after the initial dose of the inhibitor. Inhibitor was administered in 3 intra-peritoneal doses of 40 mg/kg in 100 µl sterile PBS (48, 24 and 1 hour before imaging).

2.8.5 Spectral analysis of melanin pigment in B16 cells

The emission on the pigment containing vesicles was analysed using a META detector attached to a Zeiss510 confocal microscope following excitation using 800 nm wavelengths. Speckles with different spectra are coloured either red, green or blue based on the pattern of their emission. The excitation spectra were obtained by scanning through wavelengths between 690 and 1050 nm. The emission was collected in each of the different emission channels and this was not found to alter the excitation max.

Lifetime imaging was also carried out using a FLIM detector on the same microscope. Emitted photons were collected for 30 seconds following continuous excitation with a femto-second-pulsed Ti-Sapphire laser. The photon count is shown as a scatter graph against time. Assistance with these experiments was provided by Peter Jordon of the light microscopy facility.

2.9 Data analysis

2.9.1 Quantification of cell morphology

Phase contrast images of A375 or MTLn3E cells plated on collagen/matrigel gels were used for this analysis. Using Volocity software, the cell shape was drawn around by hand and the measurements of perimeter and area were calculated. Over 100 cells were analysed for each different cell population. These measurements were then used to calculated the ratio of $(\text{perimeter})^2/4\pi(\text{area})$. Box and whisker plots showing the range of these values were drawn using Prism (Graphpad). The box and whisker plots show the following values: min, 25th percentile, median, 75th percentile, max.

The same analysis was carried out on still images taken from the in vivo multiphoton movies. A375 cells within the tumour were drawn around manually as above when the cell shape could be distinguished clearly. Over 400 cells from either control or PDK1 depleted tumours from 4 different mice were analysed. Data was presented in box plots as above.

2.9.2 Cell tracking

Tracking of A375 or MTLn3E cells plated on collagen/matrigel cells was carried out using data from phase contrast time-lapse movies captured using MetaMorph software. Images were taken of each position chosen every 2-5 minutes. These time-lapse stacks then underwent automatic cell tracking, again using MetaMorph software. Briefly, in the first frame the cells are selected with the mouse and an area around the cell is identified. Through each frame the software determines the new position of each cell. If the software fails to identify the cell in the next frame, for example when a cell undergoes a division, or if the cell moves out of the frame, the user is able to pause the analysis and instruct the program as to the accurate position of the cell, or to terminate that track. The tracking data is stored as a log file. The calculation of cell speed was carried out using Mathmatica (Wolfram research). The data from the tracking, stored in log files was inputted to a template designed by Daniel Zicha. The cell speed is presented by Mathematica as box and whisker plots. The box and whisker plots show the following values: min, 25th percentile, median, 75th percentile, max.

2.9.3 Co-localisation

A375 cells expressing both myc-ROCK1 and FLAG-PDK1 and stained with both JAK6 and anti-FLAG, and followed by Alexa fluorescent secondary antibodies, were imaged by confocal microscopy. The images were then analysed using LSM image examiner (Zeiss). Using the threshold tool, pixels with high signal (above 100 units (max 250)) of both myc and FLAG staining were selected and highlighted. The images showing the highlighted pixels revealed the degree of co-localisation, and where in the cells this colocalisation occurred.

B16F2 cells plated on glass cover slips were imaged using a combination of fluorescence, reflectance and transmitted light using a confocal microscope. The transmitted light images showed the melanin containing vesicles as black dots. This greyscale transmitted light images were inverted and pseudocoloured. This new image was then overlaid with the reflectance image and the degree of colocalisation was determined in the same manner as above.

2.9.4 Kymographs

Confocal time-lapse movies of A375 cells expressing GFP-ROCK1 were analysed using LSM image examiner. A narrow rectangle, which traversed the cell cortex was drawn using the overlay tool. This region was extracted using the overlay tool and individual images of the selected section were saved, each one 2 seconds later in real time than the previous one. These narrow images were then lined up in sequence to show the change in GFP-ROCK localisation over time in that region.

2.9.5 Quantification of spread area

Confocal images of A375 cells expressing myc-ROCK1 or myc-ROCK mutant constructs and stained with 9E10 and alexa fluorescent secondary antibodies, were analysed using ImageJ. The area covered by the transfected cells was calculated by drawing round the cell shape and then using the measure tool. This area was then compared to the area of the untransfected cells in the same field. The ratio of the area compared to the untransfected cells was used to compare the contractile ability of the different ROCK1 constructs expressed. Between 20 and 30 cells were quantified from 2 independent experiments. The data is presented as a histogram plotting the mean and the standard deviation.

2.9.6 Quantification of relative melanin expression

In vivo movies of B16F2 cells stably expressing GFP-CAAX were analysed using LSM image examiner. Using the region of interest tool, firstly the background level of signal intensity of the melanin expression was quantified in a region containing no tumour cells. Next the same tool was used to quantify the mean melanin expression in the area containing tumour cells. The background measurement was subtracted from this value. Motile cells within the movie were identified and the intensity of the melanin expression was measured by drawing around the cell shape in the first frame the cell was seen to be moving. The relative melanin expression was calculated by subtracting the background measurement and determining the ratio between the expression of melanin in the cell and the average of the tumour field. The same analysis was carried out for non-motile cells where the cell shape could be determined clearly. This analysis was carried out for over 150 motile cells and over 300 non motile cells from 16 movies from 5 different mice. Data is presented as a frequency distribution showing relative values on the Y-axis.

2.9.7 Statistical Analysis

To analyse the statistical significance of changes in cell morphology the non-parametric Mann Whitney-U test was used. Phenotypic category data was analysed by chi-squared tests. The microarray results were analysed by the bioinformatics department by Phil East. The ranges of values for each chip were normalised to each other and then points with very low intensity were excluded from the analysis. The results show genes that were consistently up or down regulated in all three of the replicates. Results are presented as average fold change.

3 Chapter 3 - Analysis of potential phospho-acceptor sites in ROCK1

3.1 Chapter summary

ROCK activity in a cell has drastic consequences on cell morphology, cell motility and many other processes such as the completion of cytokinesis and regulation of the cell cycle [102]. Considering the significant consequences of aberrant ROCK activity, it is logical that ROCK activity would be tightly controlled. The activation of ROCK downstream of the Rho family GTPases is well confirmed, however this may not be enough to finely tune ROCK activity [98, 104]. It could be conceived that RhoGTP binding to ROCK is only an initiating step in the regulation of these kinases. Other members of the AGC family of kinases are regulated by phosphorylation. To check whether ROCK1 is also regulated in this way sequence alignments with other AGC family members were conducted and candidate potential phospho-acceptor sites were identified (T233, T380, T398). These amino acids were mutated to alanine residues and the resulting mutants were analysed. Changes in localisation and/or kinase activity were determined. It was found that mutation of T233 in the activation loop did not affect the function of ROCK1 and there was no evidence that phosphorylation of the activation loop was required to activate ROCK1. Mutation of T380 caused ROCK1 to mislocalise and was less able than wild-type ROCK1 to induce membrane blebbing, however the kinase activity of T380A ROCK1 was not altered. Mutation of T398 caused ROCK1 to become mislocalised similarly to T380A ROCK1 however the phenotype was more severe and kinase activity was also compromised. It was further found that T380A ROCK1 bound better to RhoE, a negative regulator of ROCK1, which provides a potential mechanism as to why this site is able to regulate ROCK function. Acidic substitutions of T380 and T398 were also cloned to examine whether these mutations could render ROCK1 constitutively active. This chapter details these findings.

3.2 ROCK kinase activity does not require binding to RhoGTP

WT ROCK1 when over-expressed causes A375 cells to round up and exhibit membrane blebs, as a result of increased contractile forces. The requirement for RhoA binding for ROCK1 to cause this phenotype was examined, as published research to date had focused mainly on the interaction of Rho with ROCK1 as the mechanism for activation of the kinase.

The binding of RhoA to ROCK was blocked in 3 different ways, and the resulting phenotypes of over-expressed proteins were compared to wild type (WT) ROCK1 (Figure 3.1A). WT ROCK1 when over-expressed causes A375 cells to round up and exhibit membrane blebs, as a result of increased contractile forces. Firstly the phenotype of the truncated ROCK1 (1-727 a.a.) was examined (Figure 3.1B). This truncation removes the Rho-binding domain and the PH domain in the C-terminus. Over-expression of myc-ROCK1 (1-727 a.a.) in A375 cells caused a concentration of thickened stress fibres in the cytoplasm but transfected cells did not become contracted and exhibit membrane blebs. Secondly a mutation was made in the Rho-binding domain of ROCK1 (I1009A) that has been previously reported to inhibit the interaction of ROCK1 and RhoA [98]. Over-expression of myc-ROCK1 (I1009A) in A375 cells resulted in cells that contained thickened stress fibres but remained spread, and did not exhibit membrane blebs (Figure 3.1C). Thirdly, wild-type ROCK1 was over-expressed in A375 cells that had been transfected with siRNA oligos targeted against RhoA. The efficiency of siRNA transfection is shown by the western blot in Figure 3.1E. The depletion of RhoA also resulted in cells expressing ROCK1 exhibiting thickened stress fibres but not membrane blebbing as seen when wild-type ROCK1 is expressed alone (Figure 3.1D). The combination of these experiments suggests that the interaction of ROCK1 with RhoA is critical for ROCK1 to cause cell contraction and membrane blebbing. It was also observed that the membrane localisation of wild-type ROCK1 was lost when binding to RhoA was inhibited (see arrow). Interestingly, although cell blebbing was inhibited, the over-expression of ROCK1 still caused thickening of stress fibres suggesting that RhoA binding was not absolutely required for ROCK1 kinase activity.

To confirm this, immunoprecipitaion kinase assays were performed with wild type ROCK1 and ROCK1 (I1009A). The ability of ROCK1 to phosphorylate recombinant MLC in vitro did not appear to be significantly altered by this mutation (Figure 3.2). There may perhaps be a slight change in activity but having repeated this experiment several times, no consistent increased or decrease was observed. This confirmed that RhoA-binding is not required for ROCK1 kinase activity, but instead controls the sub-cellular localisation of ROCK1.

3.2.1 Localisation of truncated ROCK1 to the plasma membrane is not sufficient for full functionality

Initial results had identified that localisation in addition to kinase activity was important for full function of ROCK1. We speculated that restoring membrane localisation should restore

full function. This was achieved by cloning the C-terminal CAAX sequence of K-Ras or RhoA onto the C-terminus of truncated ROCK1 (1-727 a.a.). This tag caused ROCK to be localised diffusely over the plasma membrane in contrast to myc-tagged truncated ROCK1 that was localised diffusely in the cytoplasm (Figure 3.3). When the active truncated ROCK was at the plasma membrane it was able to induce some membrane blebbing. However this blebbing was not the same as the blebbing that is induced by full-length wild type ROCK1. Wild type ROCK 1 causes blebbing by causing contraction of the whole cell. The cells over-expressing ROCK1 become rounded, as some of the cell adhesions holding the cell spread flat are overcome by excess contractile forces. The blebbing induced by membrane tagged truncated ROCK1 was restricted to some areas of cell membrane and the cells generally remained well spread suggesting that the level of contractile force induced in those cells was less than in cells expressing wild type ROCK1, or that the contractile force generated was less well coupled to the membrane and was not able to induce such dramatic blebbing. Considering that the deletion of the C-terminus of ROCK1 results in a more active kinase in vitro [98], it was surprising that localisation of this construct to the membrane was not enough to induce strong cell contraction and cell rounding. This experiment was strong evidence that localisation to the membrane was not enough for contraction and blebbing activity of ROCK1, and that additional signals may be required.

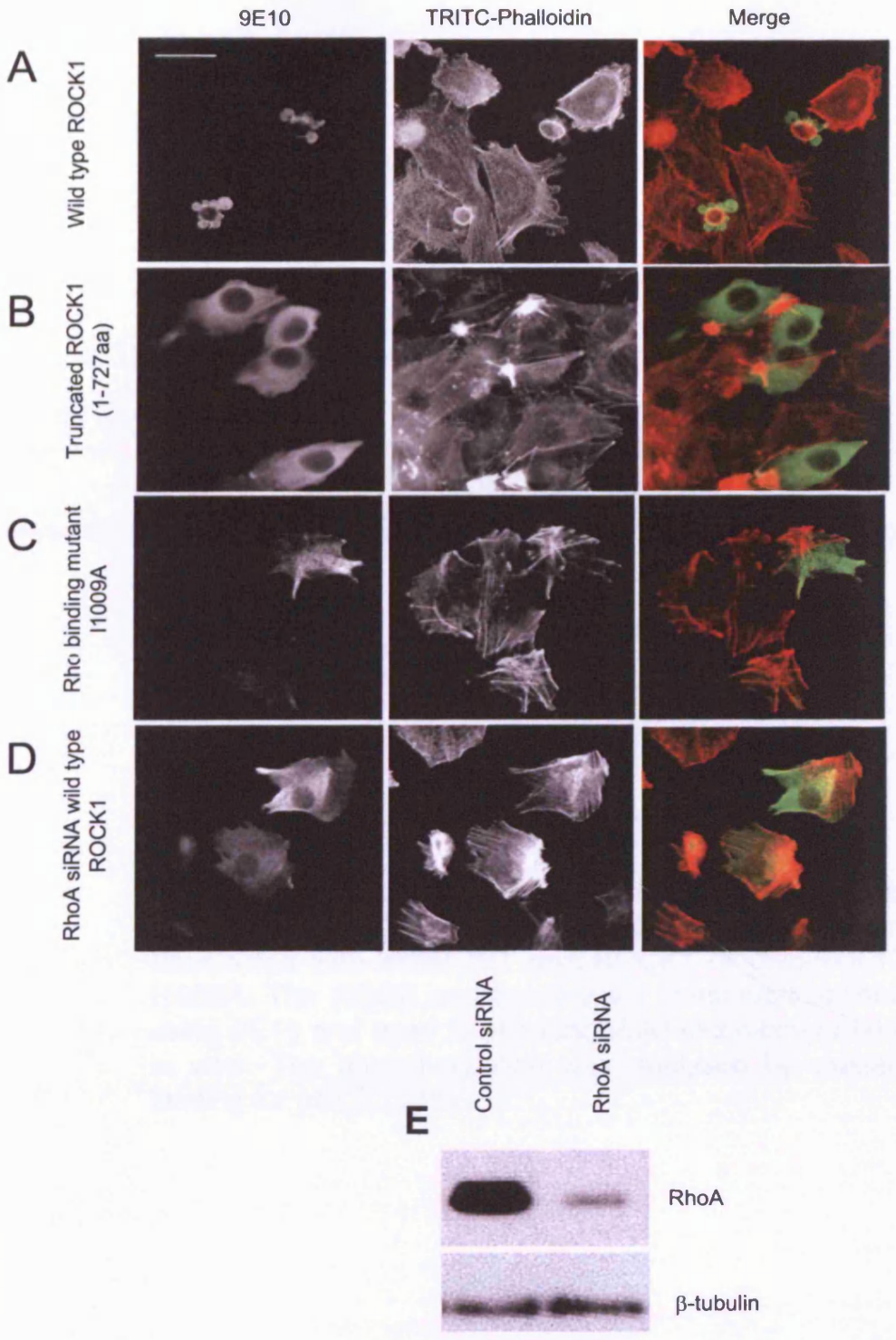

Figure 3.1 ROCK kinase activity is independent of binding to RhoGTP. Myc-tagged ROCK 1 constructs over-expressed in A375P cells plated on glass coverslips. Cells were fixed and stained with 9E10 and TRITC phalloidin. A) Arrow shows membrane localisation of wild type ROCK1. B)C) ROCK1 mutants were expressed in A375 cells D) RhoA was depleted by siRNA transfection, siRNA oligos were transfected using oligofectamine 24 hours before DNA transfection. (scale bar indicates 50 μm) E) Western blot showing knockdown of RhoA by siRNA transfection.

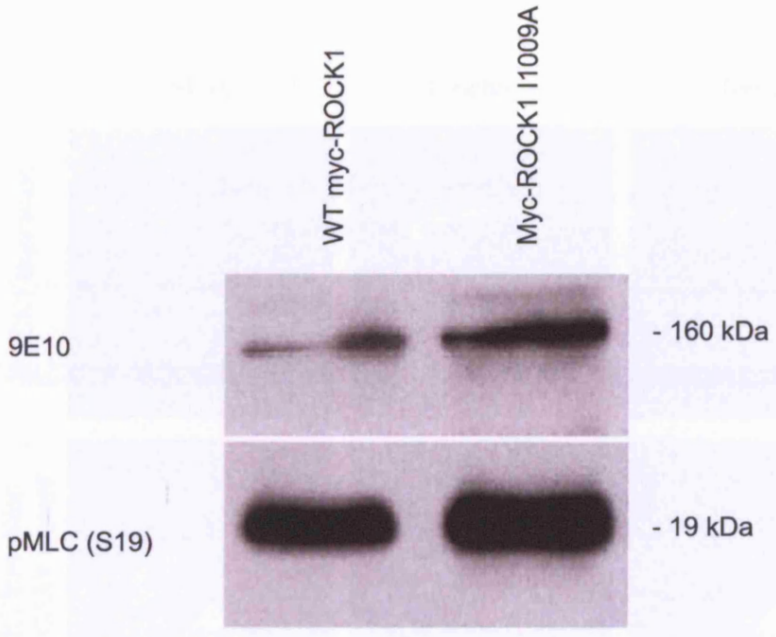

Figure 3.2 Mutation of the Rho-binding domain does not inhibit ROCK1 kinase activity. A375 cells were transfected with either WT myc-ROCK1 or myc-ROCK1 I1009A. The ROCK constructs were immunoprecipitated using 9E10 and used to phosphorylate recombinant MLC in vitro. The phosphorylation was analysed by western blotting for pMLC (S19).

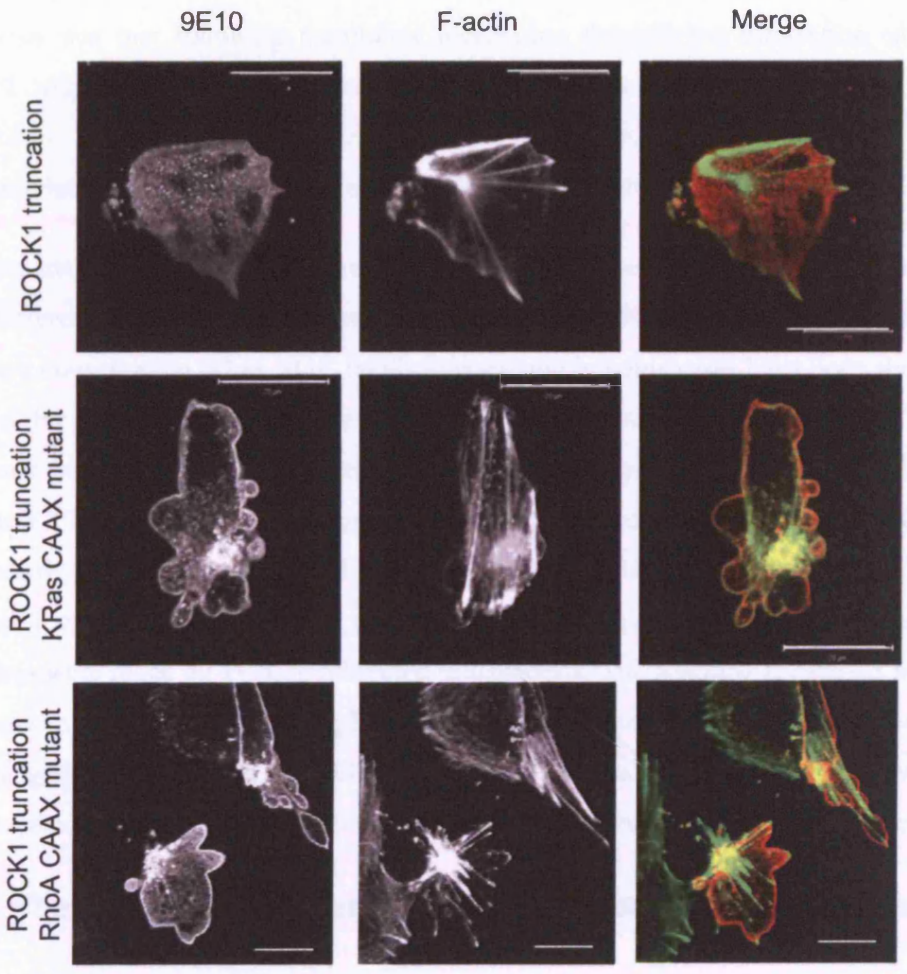

Figure 3.3 The phenotype of truncated ROCK1 when localised to the plasma membrane. Truncated ROCK1 (1-727 a.a.) is unable to reach the plasma membrane because it is missing the Rho-binding domain. The CAAX sequence of KRas or RhoA was tagged to the C-terminus of this construct and it was expressed in A375 cells plated on glass cover slips. Cells were fixed and stained with 9E10 and FITC phalloidin. Scale bar indicates 20 μm.

3.3 Analysis of potential phospho-acceptor sites in ROCK1

3.3.1 Identification of candidate sites

An investigation into other mechanisms of ROCK1 regulation was begun. The next hypothesis was that following membrane localisation through the interaction with RhoA, ROCK1 might be further modified to enhance its kinase activity. The most common mechanism of regulation of kinase activity is through phosphorylation. Possible phosphorylation sites on ROCK1 were investigated to test this hypothesis.

Scan-site analysis of ROCK1 was performed (http://scansite.mit.edu/). Threonine residues in the activation loop and the hydrophobic motif of the kinase domain were identified as they were conserved in other AGC family kinases, and in some cases have been shown to be required for kinase activity (Figure 3.4) [123, 228]. ROCK1 shows a high level of sequence homology with Akt/PKB in the activation loop and the hydrophobic domain. T233, T237, T380 and T398 were chosen as potential phospho-acceptor sites to investigate further by mutagenesis (Figure 3.4). T233 and T237 are situated in the activation loop and T380 and T398 are found in the hydrophobic extension of the kinase domain. T-A mutations of these 4 residues were made by PCR site-directed mutagenesis. The resulting constructs were over-expressed in A375 cells and the phenotypes of transfected cells were compared to cells expressing Wild-type ROCK1 and GFP only as a control transfection. However, mutation of T237 resulted in a construct that would not express, so this was not followed further.

3.3.2 Phenotypic categories used to classification of ROCK mutants

Cells expressing myc-ROCK1 constructs were fixed and stained with 9E10 antibody and TRITC labelled phalloidin. The phenotypes of transfected cells were categorised based on their actin organisation and on the localisation of the transfected myc-ROCK1 construct (Figure 3.5).

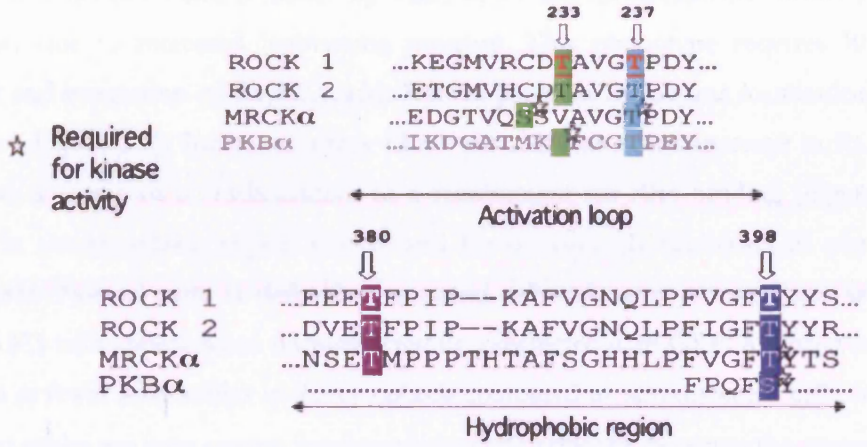

Figure 3.4 Sequence analysis shows that ROCK1 contains residues conserved in other AGC family members which have been shown to be required for kinase activity. Sequences were aligned using ClustalW software. Conserved residues were noted and 4 candidate phospho-acceptor sites were targeted for analysis by mutagenesis.

Actin organisation was defined as: 1. Blebbing, 2. Increased stress fibres, 3. Normal, 4. Reduced stress fibres, 5. Collapsed; blebbing being the strongest ROCK-driven phenotype, and collapsed being the result of reduced ROCK activity (Figure 3.5). Blebbing is the result of strong contractile forces in the acto-myosin cell cortex, which over-comes some of the cell adhesions and causes cells to round up. Parts of the cell membrane are forced out into blebs probably due to increased hydrostatic pressure. This phenotype requires ROCK kinase activity and interaction of ROCK1 with Rho to promote membrane localisation of ROCK1 (see also Figure 3.1). Increased stress fibres are also due to an increase in ROCK activity however it seems to be independent of a requirement for Rho binding (Figure 3.1). Actin cables in the cytoplasm appear thicker and are occasionally clustering in one part of the cytoplasm. Normal actin is defined as a spread cell with some stress fibres as this is how most A375 cells appear when untransfected or transfected with GFP. Reduced stress fibres is defined as fewer actin cables in the cytoplasm compared to untransfected cells, in some cases no actin cables are seen except for around the cell periphery, however the spread area of the cell remains similar to untransfected cells. 'Collapsed' cells are defined as cells that contain little filamentous actin and appear elongated or stretched so that their spread area is reduced compared to control cells. Cells can become elongated because they are unable to co-ordinate contraction to release the rear of the cell as they migrate. This phenotype is caused by a lack of ROCK activity and cells treated with a ROCK inhibitor Y27632 can also exhibit this collapsed phenotype.

The localisation of myc-ROCK1 constructs was categorised as: 1.Membrane diffuse, 2. Membrane punctate, 3. mixed, 4. Cytoplasmic. Blebbing cells generally also showed membrane diffuse localisation of over-expressed ROCK1, meaning that the majority of the expressed protein was localised uniformly over the plasma membrane. Membrane punctate localisation was defined as patches of intense ROCK1 staining which was at the plasma membrane. Mixed localisation was when the ROCK construct was partially at the cell membrane but a significant portion of the staining was also cytoplasmic

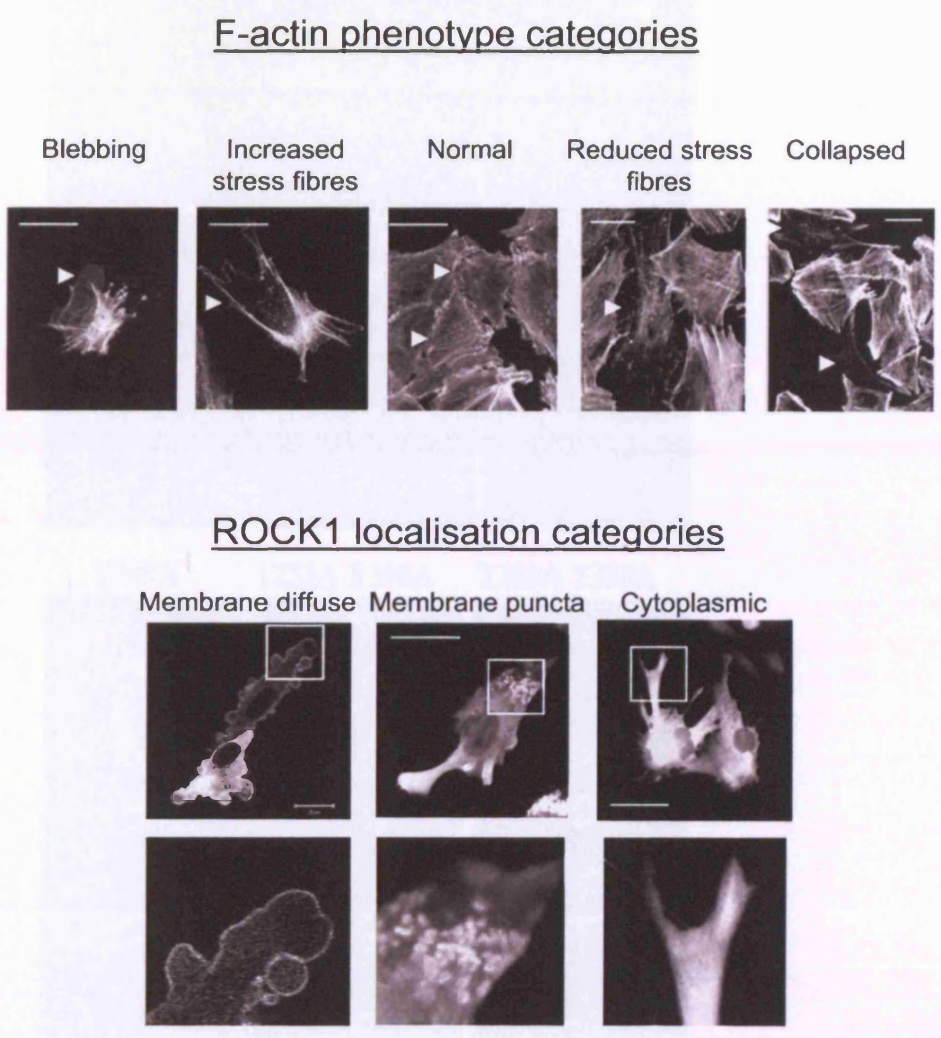

Figure 3.5 Examples of myc-ROCK1 over-expression in A375 cells. The phenotype of over-expressed myc-ROCK1 in A375 cells was categorised based on the effect on the actin cytoskeleton and the localisation of the ROCK construct based on immunofluorescence of cells stained with 9E10 antibody followed by anti mouse alexa 488 secondary antibody and TRITC phalloidin. Arrowheads indicate the transfected cells in the upper panel. Highlighted squares in the lower panel indicate regions which are shown at higher magnification below. Scale bar indicates 20 μm.

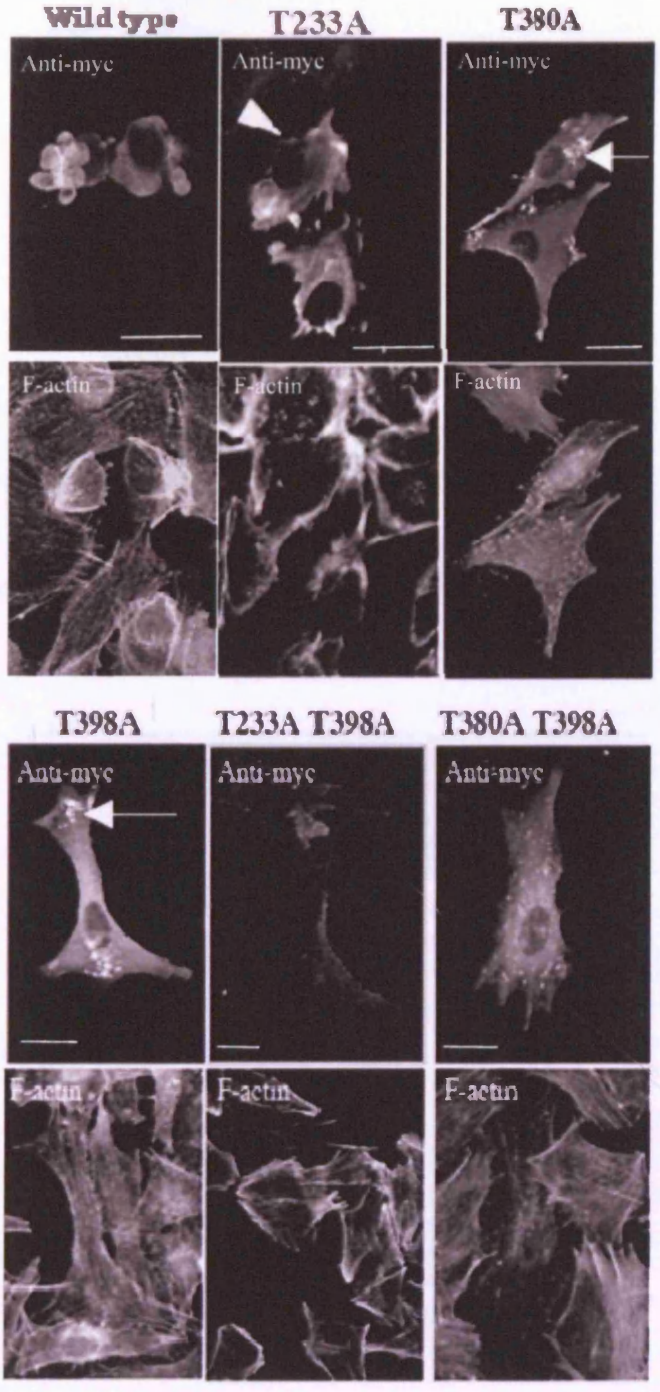

Figure 3.6 Examples of phenotypes seen when myc-ROCK1 mutants are over-expressed in A375 cells. Immune fluorescence showing localisation and f-actin organisation of A375 cells expressing myc-ROCK1 constructs. Cells were fixed and stained with 9E10 and TRITC phalloidin. Representative images of the predominant phenotype are shown. Arrows indicate difference in myc-ROCK1 localisation. Scale bar indicates 20 μm.

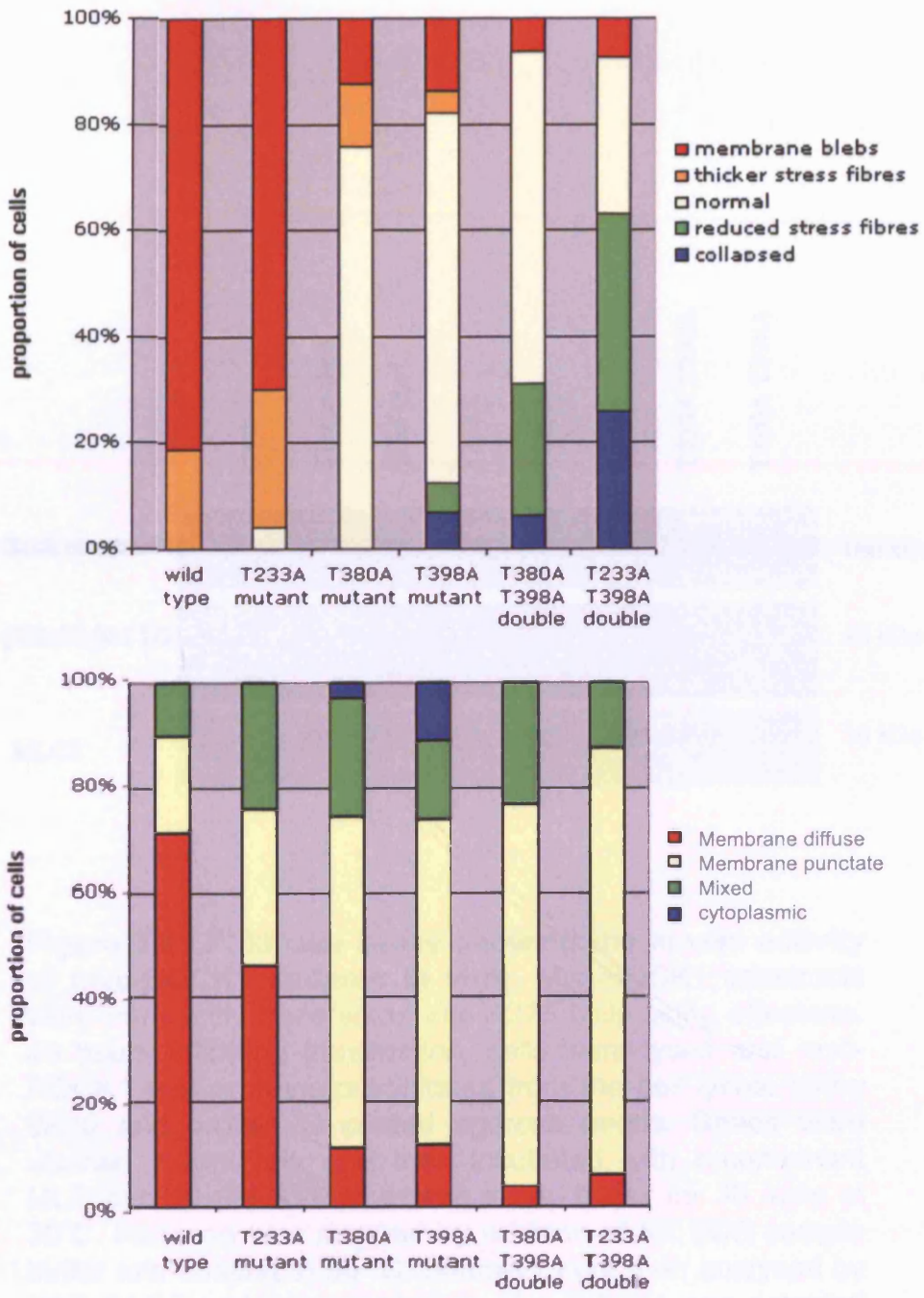

Figure 3.7 Analysis of phenotypes of myc-ROCK1 mutants. Constructs were over-expressed in A375 cells. 48 hours later cells were fixed and stained with 9E10 and TRITC phalloidin. Cells expressing myc-ROCK1 mutants were counted and separated into categories as shown in figure 3.5. A) quantification of actin phenotypes, B) quantification of myc-ROCK1 localisation. Graphs show pooled results from 3 independent experiments, each experiment includes >75 cells per mutant analysed.

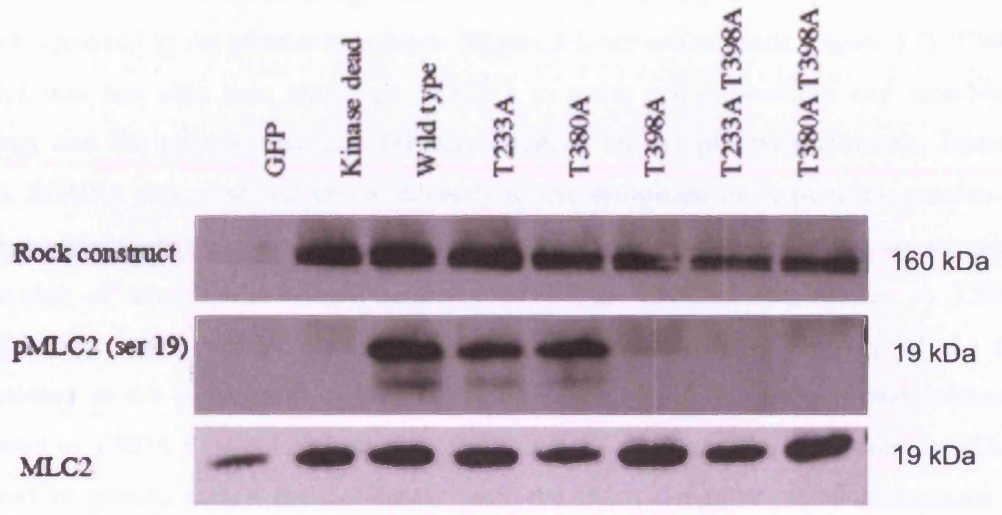

Figure 3.8 I.P. kinase assay showing the kinase activity of myc-ROCK1 mutants in vitro. Myc-ROCK1 constructs were transiently transfected into A375 cells using effectene. 48 hours following transfection, cells were lysed and myc-ROCK1 was immune-precipitated from the cell lysate using 9E10 and protein G coated agarose beads. Beads were washed extensively and then incubated with recombinant MLC and 10 μM ATP in kinase assay buffer for 30 mins at 30˚C. Reaction was stopped by addition of 5X SDS sample buffer and heating to 95 ˚C. Samples were then analysed by SDS PAGE and western blotting. Myc-ROCK1 was detected with 9E10 antibody.

3.3.3 Phenotypes of T233A, T380A, T398A myc-ROCK1 mutants

The myc-tagged ROCK1 mutant constructs were over-expressed in A375 melanoma cells. The phenotypes of the transfected cells were compared the phenotype of over-expressed wild-type myc-ROCK1 (Figure 3.6, Figure 3.7). T233A ROCK1 was able to cause cell contraction and membrane blebbing, similar to over-expression of wild-type ROCK1. It also diffusely localised to the plasma membrane (Figure 3.6, see arrow heads, Figure 3.7). T380A ROCK1 was less able than wild type ROCK1 to cause cell contraction and membrane blebbing, and the protein was not diffusely localised on the plasma membrane. Instead, T380A ROCK1 was observed either diffusely in the cytoplasm or in punctate patches. It therefore seems that T380A ROCK1 is both mislocalised and less able to stimulate contractility of acto-myosin. The phenotype of T398A ROCK1 was similar to T380A ROCK1, but over-expression was slightly more detrimental to the integrity of the cell cytoskeleton as the proportion of cells classified in the 'collapsed' category was increased compared to T380A ROCK1 expressing cells. T398A ROCK1was also mislocalised and was observed in puncta rather than diffusely over the plasma membrane. Combinations of mutations T233A T398A and T380A T398A tended to have a more severe phenotype than the single mutations. This suggested that perhaps T233 did have some function although there was no obvious phenotype when `T233 was mutated alone.

3.3.4 Kinase activity of T233A, T380A, T398A myc-ROCK1 mutants

T233A ROCK1 in addition to showing a wild-type phenotype when over expressed also showed kinase activity against MLC in vitro in an I.P. kinase assay that was similar to that of WT (Figure 3.8). In repeats of this experiment there was occasionally a marginal decrease in kinase activity but this was not completely consistent and if there is a small change in activity then this method of measuring activity is not sensitive enough to conclude whether there is a real difference. Therefore there is little evidence to suggest that mutation of T233 in the activation loop affects either ROCK1 localisation or kinase activity, and therefore T233 is unlikely to be a regulatory phosphorylation site. T380A although showing altered localisation and reduced cell blebbing in A375 cells had full kinase activity in an I.P. kinase assay against MLC. T398A showed reduced kinase activity in vitro against MLC, which is consistent with the phenotype of reduced stress fibres and collapsed cytoskeleton seen in some A375 cells. T398A therefore has potential to be a regulatory phosphorylation site in ROCK1.

3.3.5 Phenotype of D232AT233A ROCK1

It is possible that there was no phenotype seen with T233A ROCK1 because there is a charged residue, D232, adjacent to this threonine, which might be able to act as a substitute for the positive charge of a phosphorylated threonine in the T233 position. D232 is perhaps able to confer an active conformation of the kinase domain even when T233 is not phosphorylated. To check this possibility, a further mutation of ROCK1 was cloned: D232AT233A ROCK1. However this ROCK1 mutant did not show reduced membrane blebbing either, when expressed in A375 cells. Arrows indicate blebbing cells (Figure 3.9).

3.3.6 Inhibition of PI3K causes mislocalisation of over-expressed ROCK1

Results to this point had shown that both localisation and kinase activity were required for the function of ROCK1. We had already seen that inhibiting the interaction with RhoA caused ROCK to be located in the cytoplasm rather than at the plasma membrane (Figure 3.1). Mislocalisation was also observed when T380 and T398 were mutated to alanine. However, these mutations did not prevent ROCK1 from reaching the plasma membrane so presumably these mutants were still able to interact with RhoA adequately. However, at the plasma membrane, these mutant ROCK1 constructs were not able to spread diffusely over the membrane and were sometimes observed in puncta instead.

ROCK1 and ROCK2 also contain a PH domain in the C-terminus and in the case of ROCK2 it had been reported that the PH domain was able to bind to PI(3,4,5)P3[103]. Additionally phosphorylation of the residue analogous to T398 in ROCK1 in Akt/PKB is dependent on PI(3,4,5)P3 [229]. To test what cell signalling events might be required for the diffuse membrane localisation of ROCK1, and whether phospho-inositol lipids were involved, full length wild-type ROCK1 was transfected into A375 cells and the cells were subsequently treated with an inhibitor of PI3K (Figure 3.10). Interestingly when PI3K was inhibited, full-length wild type ROCK1 sometimes became localised in puncta similar to what had been seen when T380A or T398A had been over-expressed. The cells treated with LY294002 were less contracted and did not exhibit membrane blebs (Figure 3.10). This suggested that PI3K signalling was permitting the diffuse membrane localisation of ROCK1.

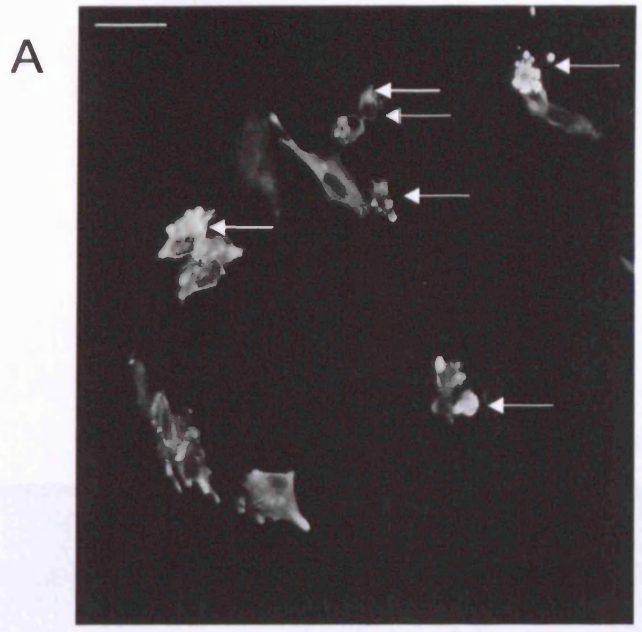

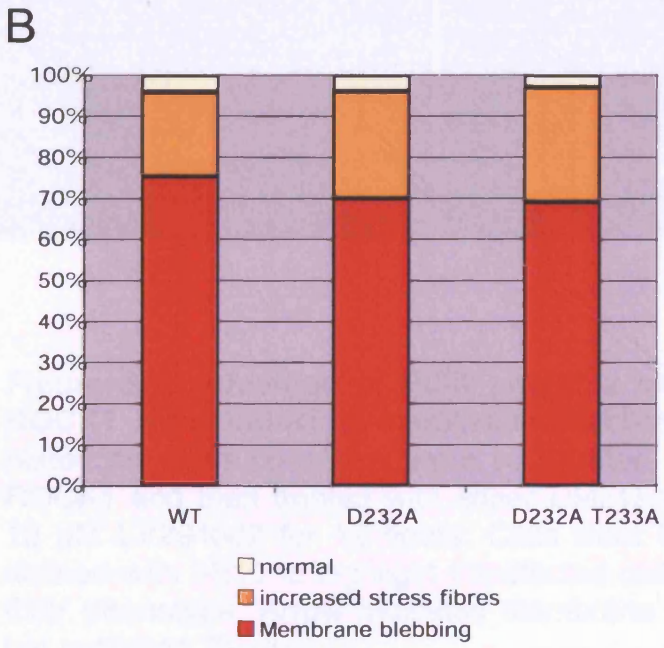

Figure 3.9 D232A T233A ROCK1 is still able to induce membrane blebbing. A) A375 cells were transfected with myc-ROCK1 D232A T233A then fixed and stained with 9E10. Transfected cells were observed. Arrows indicate cells still able to contract and exhibit membrane blebs. Scale bar indicates 50 µm. **B)** Graph showing quantification of actin phenotypes of A375 cells over-expressing D232A and D232A T233A myc-ROCK1 mutants, from 3 independent experiments, each experiment include >50 cells for each condition.

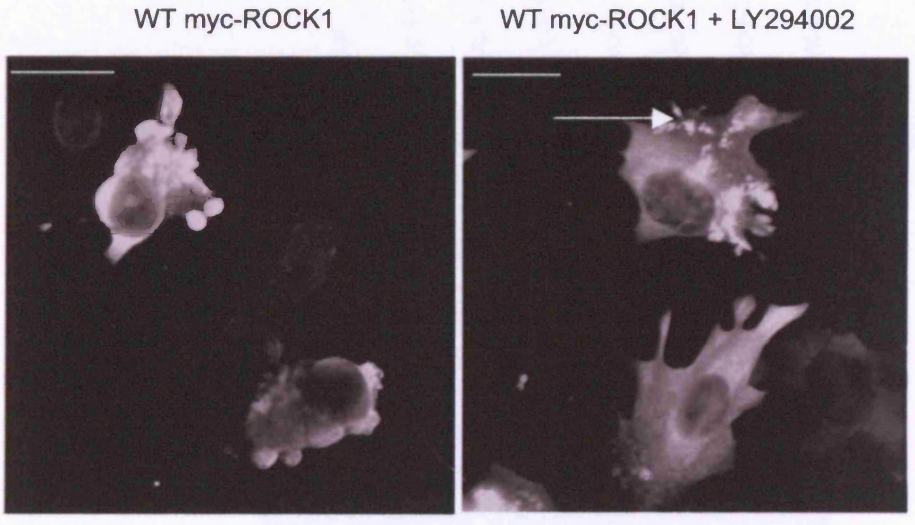

Figure 3.10 Inhibition of PI3K prevents over-expressed ROCK1 from inducing membrane blebbing. A375 cells plated on glass coverslips were transfected with WT myc-ROCK1 and then treated with either DMSO as a control or 10 μM LY294002 for 12 hours. Cells were then fixed and stained with 9E10 to highlight transfected cells and analyse their phenotype. Arrow indicates membrane puncta. Scale bar indicates 20 μm.

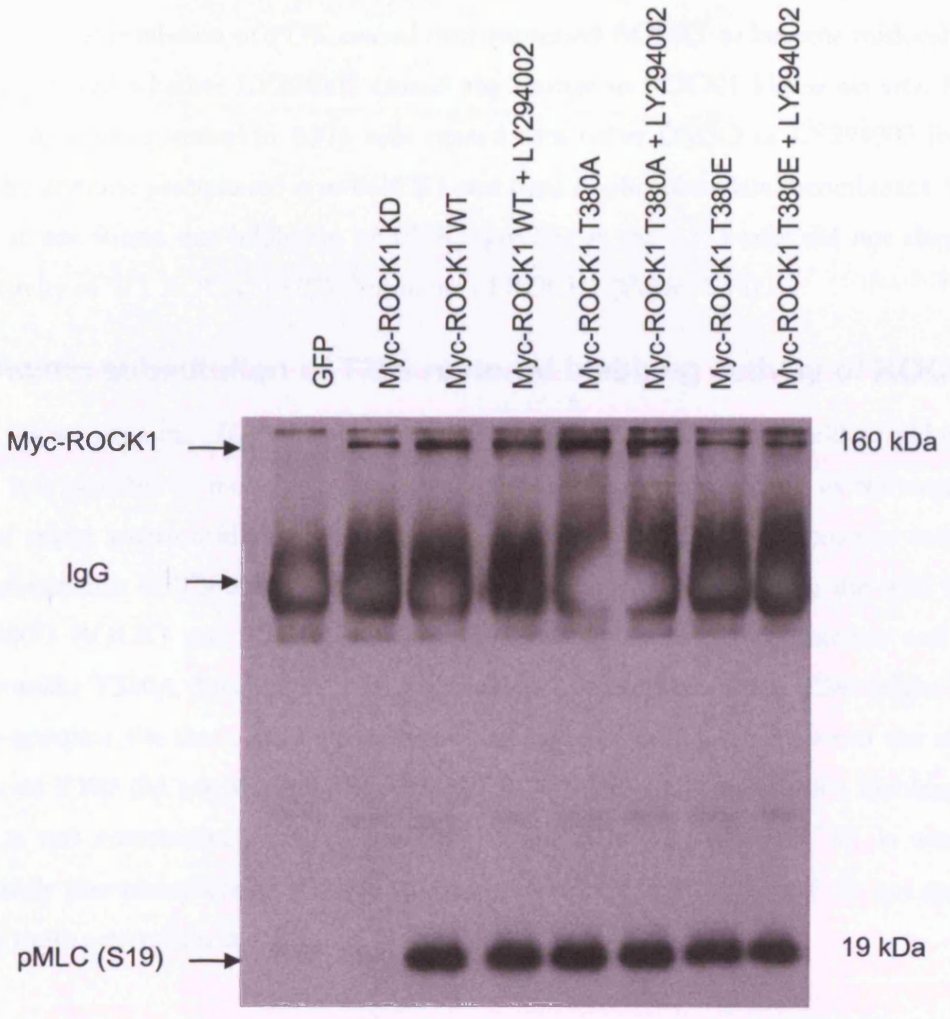

Figure 3.11 Inhibition of PI3K does not inhibit kinase activity of ROCK1. A375 cells were transfected with Myc-ROCK1 constructs or GFP as a control. Myc-ROCK1 constructs were immune precipitated with 9E10 and used to phosphorylate recombinant MLC in vitro. Phosphorylation was determined by western blotting for pMLC (S19). Level of kinase was determined by western blotting with 9E10.

3.3.7 Inhibition of PI3K does not inhibit kinase activity of ROCK1.

Having seen that inhibition of PI3K caused over-expressed ROCK1 to become mislocalised, it was next tested whether LY294002 caused any change to ROCK1 kinase activity. Myc-ROCK1 was over-expressed in A375 cells treated with either DMSO or LY294002 for 12 hours. The immune precipitated myc-ROCK1 was used to phosphorylate recombinant MLC in vitro. It was found that inhibition of PI3K signalling in the A375 cells did not alter the kinase activity of WT ROCK1 or T380 mutants of ROCK1 (Figure 3.11).

3.3.8 Acidic substitution of T380 restored blebbing activity of ROCK1

We next investigated the effect of substituting the threonine residue for an acidic residue. In this way it is possible to model a constitutively phosphorylated amino acid as the negative charge of acidic amino acid can mimic the charge of a phosphorylated threonine residue. Acidic substitution of T380 was able to restore the phenotype to resemble the wild type. Both T380D ROCK1 and T380E ROCK1 were able to cause cell contraction and cell blebbing unlike T380A (Figure 3.12). This phenotypic data suggested that T380 might be a phospho-acceptor site that played a role in the regulation of ROCK1. However the acidic mutation of T380 did not increase the ability if ROCK1 to cause membrane blebbing so perhaps is not constitutively active. Another possibility is that WT ROCK1 is actually constitutively phosphorylated at T380 in vivo and therefore T380D or T380E do not appear to be any more active than the WT.

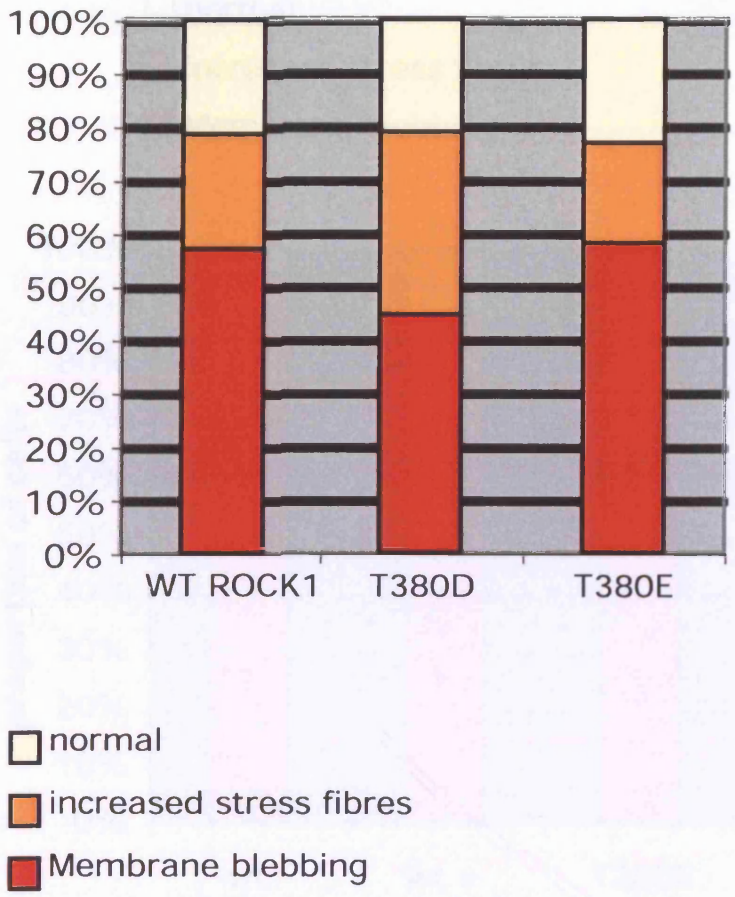

Figure 3.12 Mutation of T380 to acidic residues does not inhibit membrane blebbing. A375 cells plated on glass coverslips were transfected with either WT myc-ROCK1 or T380D or T380E mutant myc-ROCK1 constructs. Cells were fixed and stained with 9E10 40 hours after transfection and the phenotypes of the transfected cells was analysed. Graph contains data from 3 independent experiments, each experiment includes >50 cells for each condition.

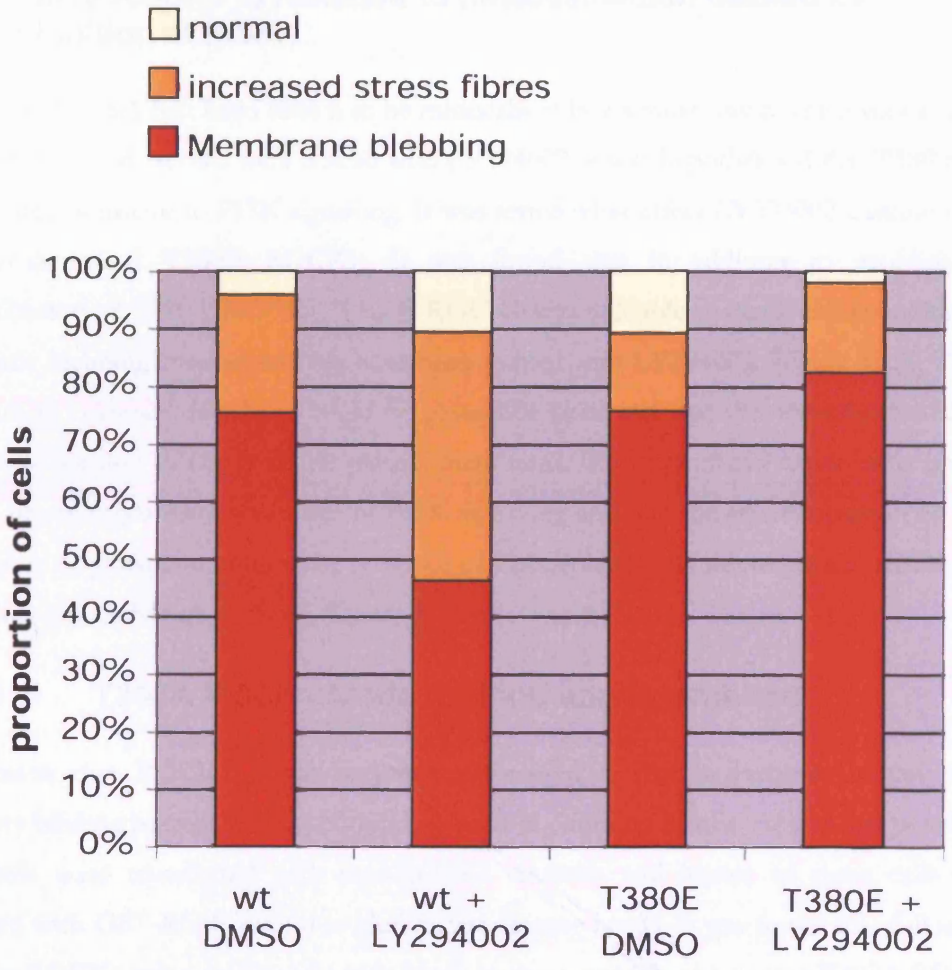

Figure 3.13 T380E myc-ROCK1 is able to cause membrane blebbing in the presence of LY294002. A375 cells plated on glass coverslips were transfected with either WT myc-ROCK1 or T380E myc-ROCK1. Cells were treated with either DMSO or 10 μM LY294002 for 12 hours then fixed and stained with 9E10. The phenotype of the transfected cells was analysed. Graph contains data from 2 independent experiments, each experiment contains > 50 cells for each condition.

3.3.9 T380E ROCK1 is resistant to mislocalisation caused by inhibition of PI3K.

As T380A ROCK1 had been shown to be mislocalised in a similar way to the mislocalisation of WT ROCK1 when cells were treated with LY294002, it was hypothesised that T380 might be regulated/sensitive to PI3K signalling. It was tested what effect LY294002 treatment had on over-expressed T380E ROCK1. It was found that in addition to avoiding the mislocalisation of T380A ROCK1, T380E ROCK1 was still able to cause cell rounding and membrane blebbing even when cells have been treated with LY294002 (Figure 3.13). This is again strong evidence that T380 might be phosphorylated and that this modification allows ROCK1 to localise diffusely at the plasma membrane. The hypothesis would now be that T380 is phosphorylated downstream of PI3K signalling and that the acidic mutation of T380 to aspartate or glutamate mimics the presence of a phosphorylated threonine and therefore is resistant to the inhibition of PI3K (Figure 3.13).

3.3.10 T380A ROCK1 binds to RhoE and is inhibited

One reason that ROCK1 could become mislocalised is that it becomes bound to an inhibitory binding partner. One such binding partner could be RhoE. To test this possibility A375 cells were transfected with myc-ROCK1 mutants and lysates of these cells were incubated with GST-RhoE bound to glutathione agarose beads. It was found that full length wild type ROCK1 interacted poorly with RhoE in these conditions however T380A ROCK1 bound to RhoE much more strongly (Figure 3.14). This suggests that if T380 is a phosphorylation site in ROCK1 then its function could be to inhibit the interaction with the negative regulator RhoE.

As T380E ROCK1 had been able to rescue the phenotypic defects of T380A ROCK1 and was also resistant to mislocalisation caused by inhibition of PI3K, the binding of T380E to RhoE was also tested in the same assay. However in contrast to other assays, T380E behaved similarly to T380A and bound more strongly to RhoE than wild type ROCK1 (Figure 3.14). This was surprising as in other tests T380E had behaved similarly to the WT myc-ROCK1 in over-expression assays and also the T380E myc-ROCK1 construct had been shown to be resistant to inhibitory effects of PI3K.

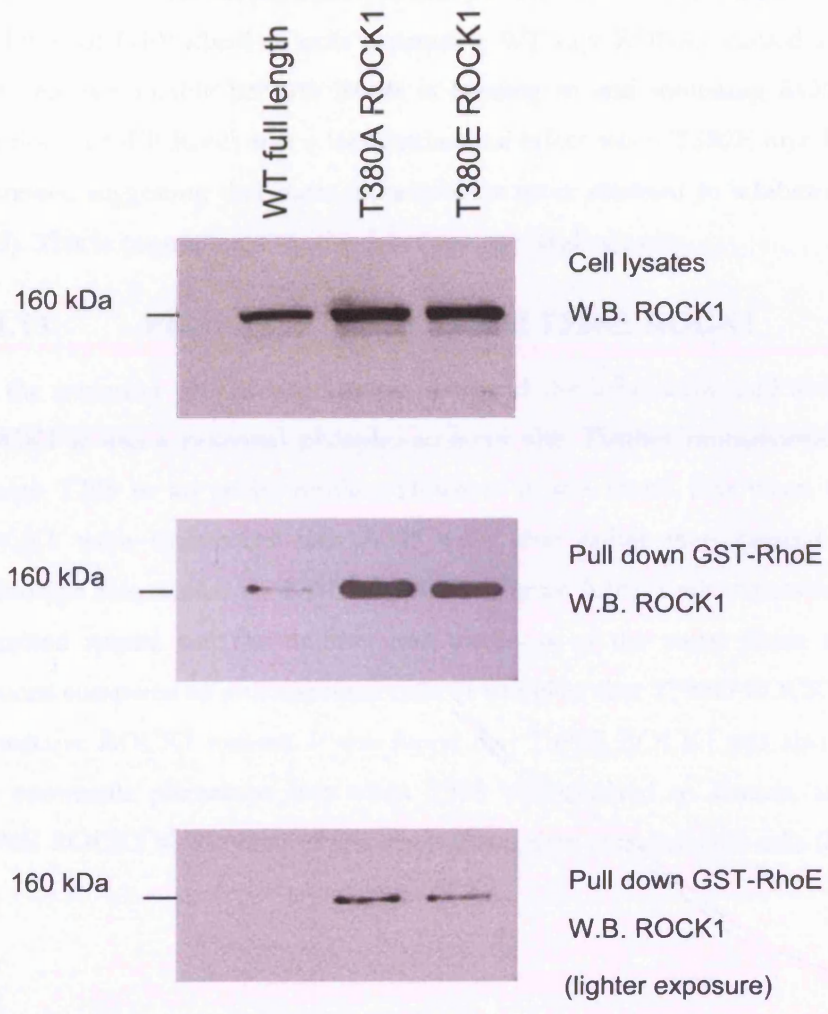

Figure 3.14 T380A ROCK1 binds to RhoE better than WT ROCK1. A375 cells were transfected with myc-ROCK1 constructs. Cell lysates were then incubated with GST-RhoE. The amount of each ROCK construct bound to RhoE was determined by western blotting.

The interaction of T380 ROCK1 mutants with RhoE was also tested in a cellular context by over-expressing the myc-ROCK1 constructs with GFP-RhoE in A375 cells (Figure 3.15). Addition of GFP-RhoE to cells expressing WT myc-ROCK1 caused an inhibition of cell blebbing presumably because RhoE is binding to and inhibiting ROCK1. However the addition of GFP-RhoE had a less detrimental effect when T380E myc-ROCK1 were over-expressed suggesting that these mutants were more resistant to inhibition by RhoE (Figure 3.15). This is contradictory to the data from the binding assay.

3.3.11 Phenotype of T398D and T398E ROCK1

As the mutation of T398 to alanine disrupted the localisation and also kinase activity of ROCK1 it was a potential phospho-acceptor site. Further mutagenesis was conducted to change T398 to an acidic residue. However it was found that when T398D or T398E ROCK1 were transfected into A375 cells, that rather than causing cell blebbing, the phenotype was similar to T398A ROCK1 (Figure 3.16). Cells expressing T398D ROCK1 remained spread and the number and thickness of the stress fibres they contained was reduced compared to untransfected cells. It was clear that T398D ROCK1 was also acting as an inactive ROCK1 mutant. It was found that T398E ROCK1 was also not able to restore the contractile phenotype lost when T398 was mutated to alanine, and cells expressing T398E ROCK1 also contained less stress fibres than untransfected cells (Figure 3.16).

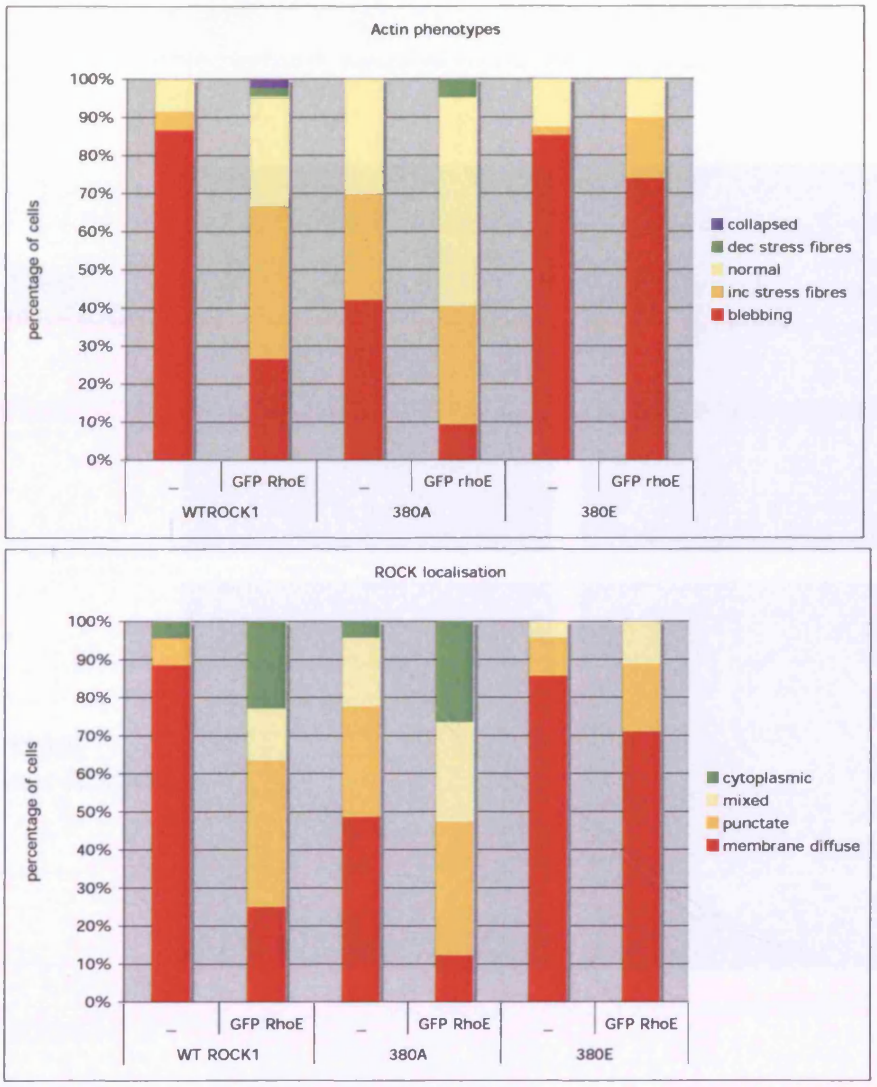

Figure 3.15 Quantification of myc-ROCK1 over-expressed phenotypes with co-expressed GFP RhoE. The first graph shows the actin phenotype of the cells expressing myc-ROCK1 constructs and cells expressing myc-ROCK1 constructs and GFP-RhoE. The lower graph categorises the localisation of the myc-ROCK1 construct. Graphs contain data pooled from 2 independent experiments, each experiment contains data from >50 cells for each condition.

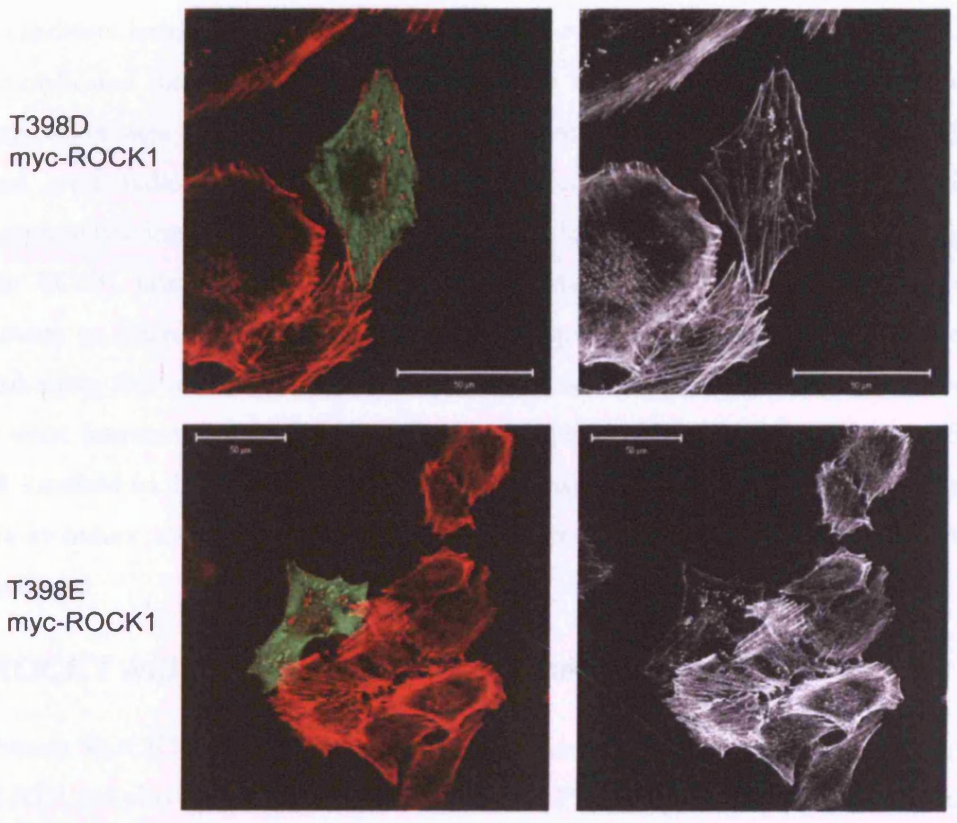

Figure 3.16 Acidic mutation of T398 does not restore a wild-type-like ROCK1 phenotype. A375 cells were transfected with T398D or T398E myc-ROCK1 plated on glass cover slips and stained with 9E10 and TRITC phalloidin. Scale bar indicates 50 µm.

4 Chapter 4 - Mass Spectrometry analysis of ROCK1

4.1 Chapter summary

As the candidate based approach to finding phosphorylation sites in ROCK1 was proving more complicated than first thought, an alternative approach for investigating potential phosphorylation sites on ROCK1 was undertaken. Recombinant ROCK1 (17-535 a.a.) was incubated with radio-labelled ATP and it was found that ROCK1 would robustly autophosphorylate itself and that this autophosphorylation could be blocked by treatment with the ROCK inhibitor Y27632. The phosphorylated protein was analysed by mass spectrometry to determine on which sites these phosphorylation events occurred. One site identified using this method was T518. This amino acid was then mutated to alanine to analyse what function phosphorylation at this site might have. It was found that T518A ROCK1 localised to the plasma membrane and also had full kinase activity in vitro but was less able to induce membrane blebbing that WT myc-ROCK1. This chapter details these initial findings.

4.2 ROCK1 will autophosphorylate itself in vitro

Recombinant ROCK1 (17-537 a.a.) was incubated in kinase assay buffer containing ^{32}P-labelled ATP and also 10 μM Y27632 or recombinant PDK1. PDK1 was included because it has been previously shown that PDK1 will phosphorylate other members of the AGC family of kinases [119]. Samples were separated by SDS-PAGE and the gel was then dried and used to expose X-ray film. As the recombinant ROCK1 used only included the first part of the protein, ROCK1 migrated at a size of approximately 60 kDa and the recombinant PDK1 ran just above ROCK1 at approximately 62 kDa. Results showed that ROCK1 will robustly autophosphorylate itself and that this autophosphorylation can be almost completely inhibited by the addition of Y27632 to the reaction (Figure 4.1). The third lane of the gel shows two bands, as both ROCK1 and PDK1 will autophosphorylate themselves. However, the intensity of the ROCK1 phosphorylation is not altered suggesting that ROCK1 (17-537 a.a.) is not a PDK1 substrate.

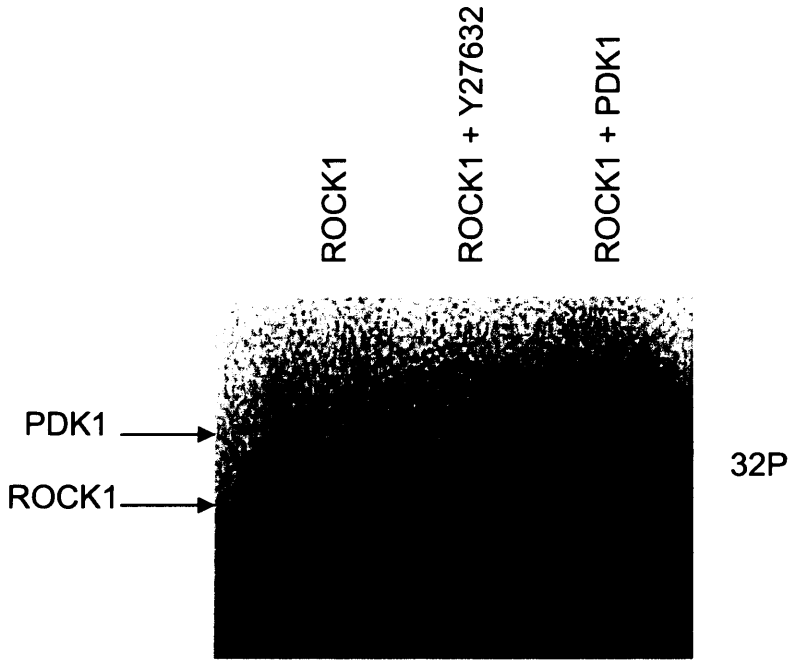

Figure 4.1 Recombinant ROCK1 will autophosphorylate itself in vitro. Recombinant ROCK1 was incubated in kinase assay buffer with ^{32}P ATP with either 10 μM Y27632 or recombinant PDK1. Samples were run on SDS-PAGE, gel was used to expose x-ray film.

4.3 Autophosphorylation sites in ROCK1

To investigate which sites were auto-phosphorylated in recombinant ROCK1, the kinase reaction was repeated this time without ^{32}P labelled ATP. The samples were separated by SDS-PAGE and the gel was stained as above. The bands were cut out of the gel and digested with trypsin. The resulting peptide fragments were fractionated by HPLC and then analysed by mass spectrometry (Protein analysis laboratory, Nick Totty). Results showed that the following peptides were found to be phosphorylated at serine/threonine residues. The results were then compared to a ROCK1 sample incubated with Y27632 to identify sites that were present only in the sample without inhibitor treatment. Several phosphorylation sites were also found in the Y27632 treated sample, which indicated that these sites are already phosphorylated on the kinase before the in vitro assay. This phosphorylation most probably occurs during protein production in the insect cell system used.

Y27632 treated sample	Control sample	SITES
YL**SS**ANPNDNR	YL**SS**ANPNDNR	**S398, S399**
T**SS**NADKSLQESLQK	T**SS**NADKSLQESLQK	**S417, S418**
	NLE**S**TVSQIEK	**S479,**
	NVENEVS**T**LKDQLEDLKK	**T518,**

Table 4.1

Table showing the phosphorylated peptides identified by mass spectrometry in the control sample and the sample treated with Y27632. Residues highlighted in red show the phosphorylated sites in that peptide.

Other phosphorylation sites were also identified but at this point have not been identified more than once. The peptides above have been seen several times in 3 independent runs and therefore the data for these sites are fully convincing and we are confident that these sites are real.

The data in Figures 4.2-4.5 shows the spectra of the fragmented peptides. The first three peptides listed in table 4.1 flew well in the 6510 Agilent QTOF machine and so we were able to get a good spread of both 'b' and 'y' fragmentation ions to confirm these results. For some unknown reason, the last peptide above although easily identified, did not fragment and fly on this machine. The pattern of fragmentation ions was therefore shown by analysing fractionated peptide on the Applied Biosystems 4000 Q trap machine, in a process called

precursor ion scanning. For all of the above peptides we were able to identify a fragment whose mass was 98 kDa smaller than the parent peptide. This mass corresponds to the loss of phosphoric acid (H_3PO_4) and means that the parent peptide did contain a phosphate group. The fragment seen that is 80 kDa smaller than the parent corresponds to the loss of the phosphate group alone. A broad range of 'b' and 'y' ions were also identified for all peptides. The b series corresponds to fragmentation starting at the N-terminus of the peptide, and the y series of ions corresponds to fragmentation starting at the C-terminus of the peptide. Having a large range of these ions provides further strong evidence that the identity of the peptide is really the phosphorylated peptide that matches the mass of the parent ion.

T518 was initially chosen to investigate further as it was one of the two sites clearly phosphorylated by ROCK1 itself and could potentially be a regulatory autophosphorylation site.

MS/MS Fragmentation of TSSNADKSLQESLQK
Found in gi|111111|, his-tagged ROCK 17-535aa [human]

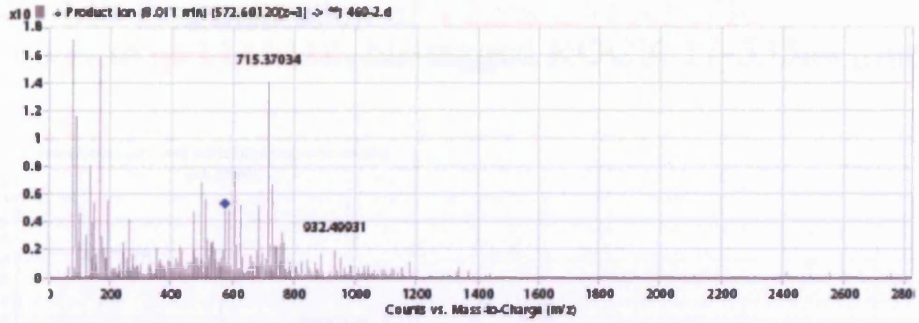

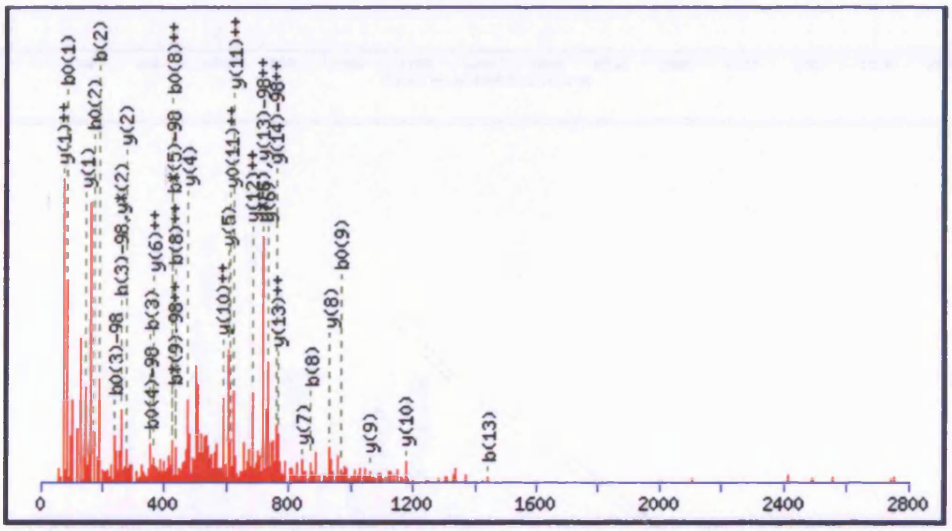

#	b	b++	b*	b*++	b0	b0++	Seq.	y	y++	y*	y*++	y0	y0++	#
1	102.0550	51.5311			84.0444	42.5258	T							15
2	189.0870	95.0471			171.0764	86.0418	S	1516.7602	758.8837	1499.7336	750.3704	1498.7496	749.8784	14
3	258.1084	129.5579			240.0979	120.5526	S	1429.7281	715.3677	1412.7016	706.8544	1411.7176	706.3624	13
4	372.1514	186.5793	355.1248	178.0660	354.1408	177.5740	N	1360.7067	680.8570	1343.6801	672.3437	1342.6961	671.8517	12
5	443.1885	222.0979	426.1619	213.5846	425.1779	213.0926	A	1246.6638	623.8355	1229.6372	615.3222	1228.6532	614.8302	11
6	558.2154	279.6113	541.1889	271.0981	540.2049	270.6061	D	1175.6266	588.3170	1158.6001	579.8037	1157.6161	579.3117	10
7	686.3104	343.6588	669.2838	335.1456	668.2998	334.6535	K	1060.5997	530.8035	1043.5732	522.2902	1042.5891	521.7982	9
8	773.3424	387.1748	756.3159	378.6616	755.3318	378.1696	S	932.5047	466.7560	915.4782	458.2427	914.4942	457.7507	8
9	886.4265	443.7169	869.3999	435.2036	868.4159	434.7116	L	845.4727	423.2400	828.4462	414.7267	827.4621	414.2347	7
10	1014.4851	507.7462	997.4585	499.2329	996.4745	498.7409	Q	732.3886	366.6980	715.3621	358.1847	714.3781	357.6927	6
11	1143.5276	572.2675	1126.5011	563.7542	1125.5171	563.2622	E	604.3301	302.6687	587.3035	294.1554	586.3195	293.6634	5
12	1230.5597	615.7835	1213.5331	607.2702	1212.5491	606.7782	S	475.2875	238.1474	458.2609	229.6341	457.2769	229.1421	4
13	1343.6437	672.3255	1326.6172	663.8122	1325.6332	663.3202	L	388.2554	194.6314	371.2289	186.1181			3
14	1471.7023	736.3548	1454.6758	727.8415	1453.6918	727.3495	Q	275.1714	138.0893	258.1448	129.5761			2
15							K	147.1128	74.0600	130.0863	65.5468			1

Figure 4.2 Mass spectrometry analysis of ROCK1.

TSSNADKSLQESLQK. A) the parent ion is shown with the blue diamond. These masses were measured using 6510 Agilent QTOF with integrated chip cube. B)shows the ions of the peptide when fragmented. C) table of the fragmented ions of the peptide.

MS/MS Fragmentation of YLSSANPNDNR
Found in gil1111111l, his-tagged ROCK 17-535aa [human]

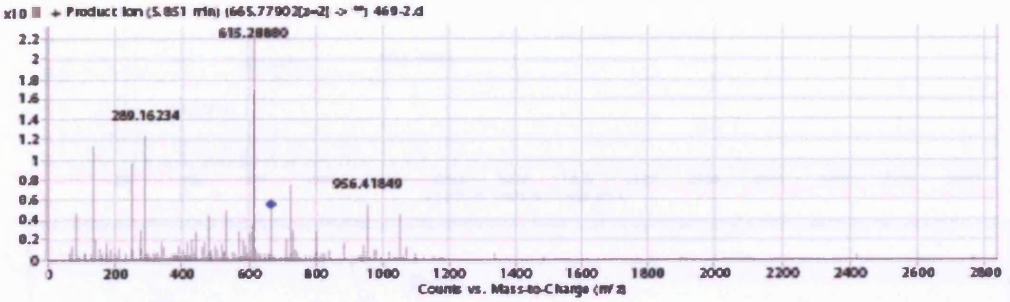

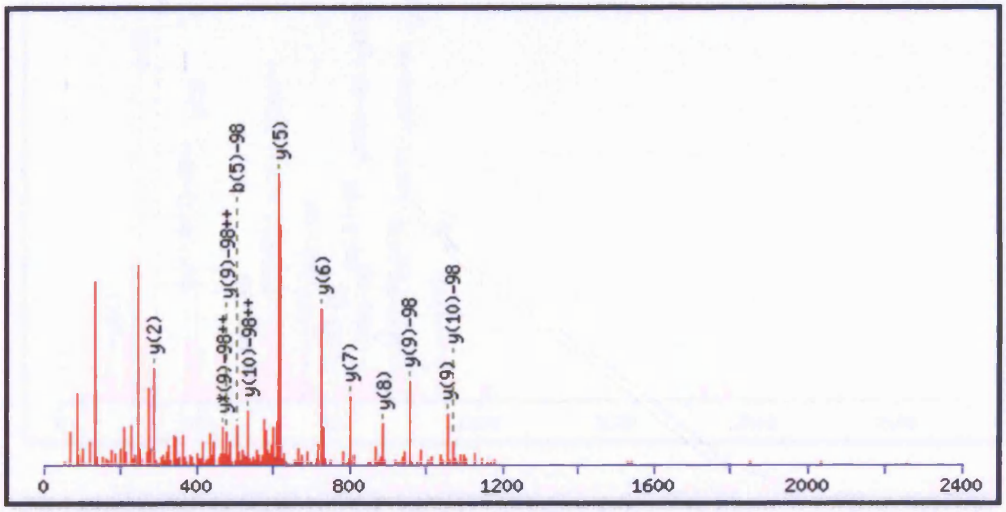

#	b	b^{++}	b*	b*$^{++}$	b^{0}	b^{0++}	Seq.	y	y^{++}	y*	y*$^{++}$	y^{0}	y^{0++}	#
1	164.0706	82.5389					Y							11
2	277.1547	139.0810					L	1069.5021	535.2547	1052.4756	526.7414	1051.4915	526.2494	10
3	346.1761	173.5917			328.1656	164.5864	S	956.4180	478.7127	939.3915	470.1994	938.4075	469.7074	9
4	433.2082	217.1077			415.1976	208.1024	S	887.3966	444.2019	870.3700	435.6887	869.3860	435.1966	8
5	504.2453	252.6263			486.2347	243.6210	A	800.3646	400.6859	783.3380	392.1726	782.3540	391.6806	7
6	618.2882	309.6477	601.2616	301.1345	600.2776	300.6425	N	729.3274	365.1674	712.3009	356.6541	711.3169	356.1621	6
7	715.3410	358.1741	698.3144	349.6608	697.3304	349.1688	P	615.2845	308.1459	598.2580	299.6326	597.2739	299.1406	5
8	829.3839	415.1956	812.3573	406.6823	811.3733	406.1903	N	518.2317	259.6195	501.2052	251.1062	500.2212	250.6142	4
9	944.4108	472.7091	927.3843	464.1958	926.4003	463.7038	D	404.1888	202.5980	387.1623	194.0848	386.1783	193.5928	3
10	1058.4538	529.7305	1041.4272	521.2172	1040.4432	520.7252	N	289.1619	145.0846	272.1353	136.5713			2
11							R	175.1190	88.0631	158.0924	79.5498			1

Figure 4.3 Mass spectrometry analysis of ROCK1.

YLSSANPDNDNR. A) the parent ion is shown with the blue diamond. These masses were measured using 6510 Agilent QTOF with integrated chip cube. B)shows the ions of the peptide when fragmented. C) table of the fragmented ions of the peptide.

MS/MS Fragmentation of NLESTVSQIEK
Found in gil111111ll, his-tagged ROCK 17-535aa [human]

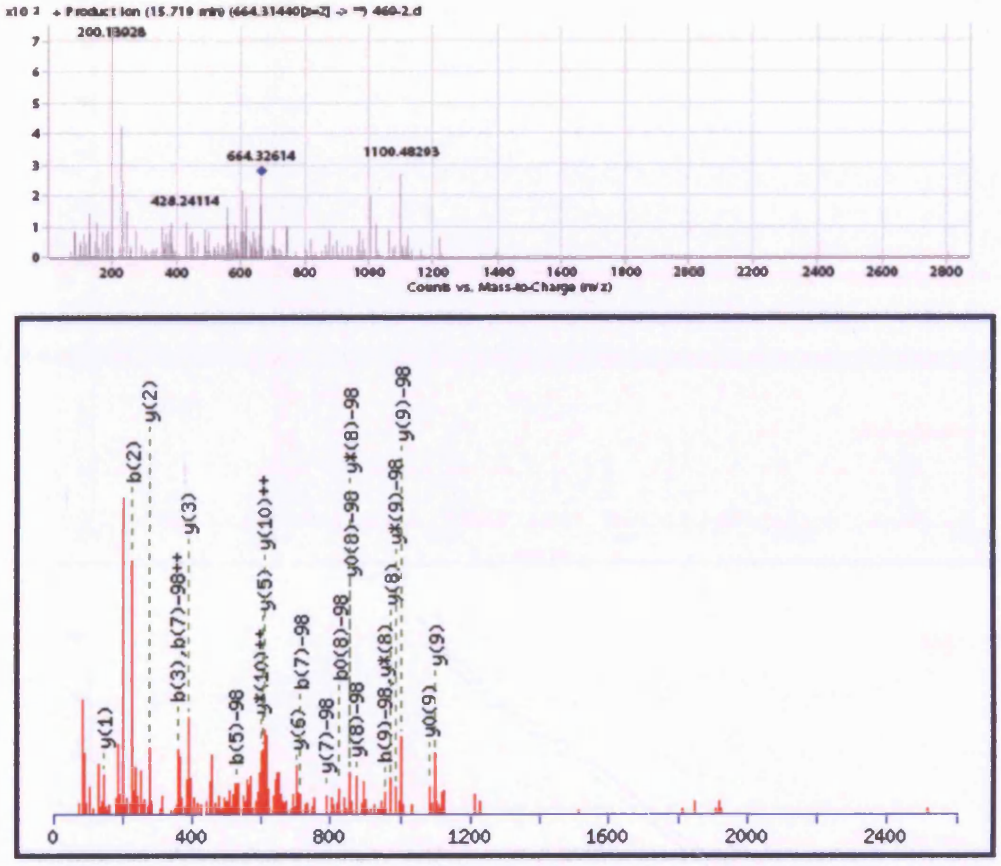

#	b	b++	b*	b*++	b0	b0++	Seq.	y	y++	y*	y*++	y0	y0++	#
1	115.0502	58.0287	98.0237	49.5155			N							11
2	228.1343	114.5708	211.1077	106.0575			L	1115.5943	558.3008	1098.5677	549.7875	1097.5837	549.2955	10
3	357.1769	179.0921	340.1503	170.5788	339.1663	170.0868	E	1002.5102	501.7587	985.4837	493.2455	984.4996	492.7535	9
4	444.2089	222.6081	427.1823	214.0948	426.1983	213.6028	S	873.4676	437.2374	856.4411	428.7242	855.4571	428.2322	8
5	527.2460	264.1266	510.2194	255.6134	509.2354	255.1214	T	786.4356	393.7214	769.4090	385.2082	768.4250	384.7161	7
6	626.3144	313.6608	609.2879	305.1476	608.3038	304.6556	V	703.3985	352.2029	686.3719	343.6896	685.3879	343.1976	6
7	713.3464	357.1769	696.3199	348.6636	695.3359	348.1716	S	604.3301	302.6687	587.3035	294.1554	586.3195	293.6634	5
8	841.4050	421.2061	824.3785	412.6929	823.3944	412.2009	Q	517.2980	259.1527	500.2715	250.6394	499.2875	250.1474	4
9	954.4891	477.7482	937.4625	469.2349	936.4785	468.7429	I	389.2395	195.1234	372.2129	186.6101	371.2289	186.1181	3
10	1083.5317	542.2695	1066.5051	533.7562	1065.5211	533.2642	E	276.1554	138.5813	259.1288	130.0681	258.1448	129.5761	2
11							K	147.1128	74.0600	130.0863	65.5468			1

Figure 4.4 Mass spectrometry analysis of ROCK1.

NLESTVSQIEK. A) the parent ion is shown with the blue diamond. These masses were measured using 6510 Agilent QTOF with integrated chip cube. B)shows the ions of the peptide when fragmented. C) table of the fragmented ions of the peptide.

MS and precursor ion scanning of NVENEVSTLKDQLEDLKK

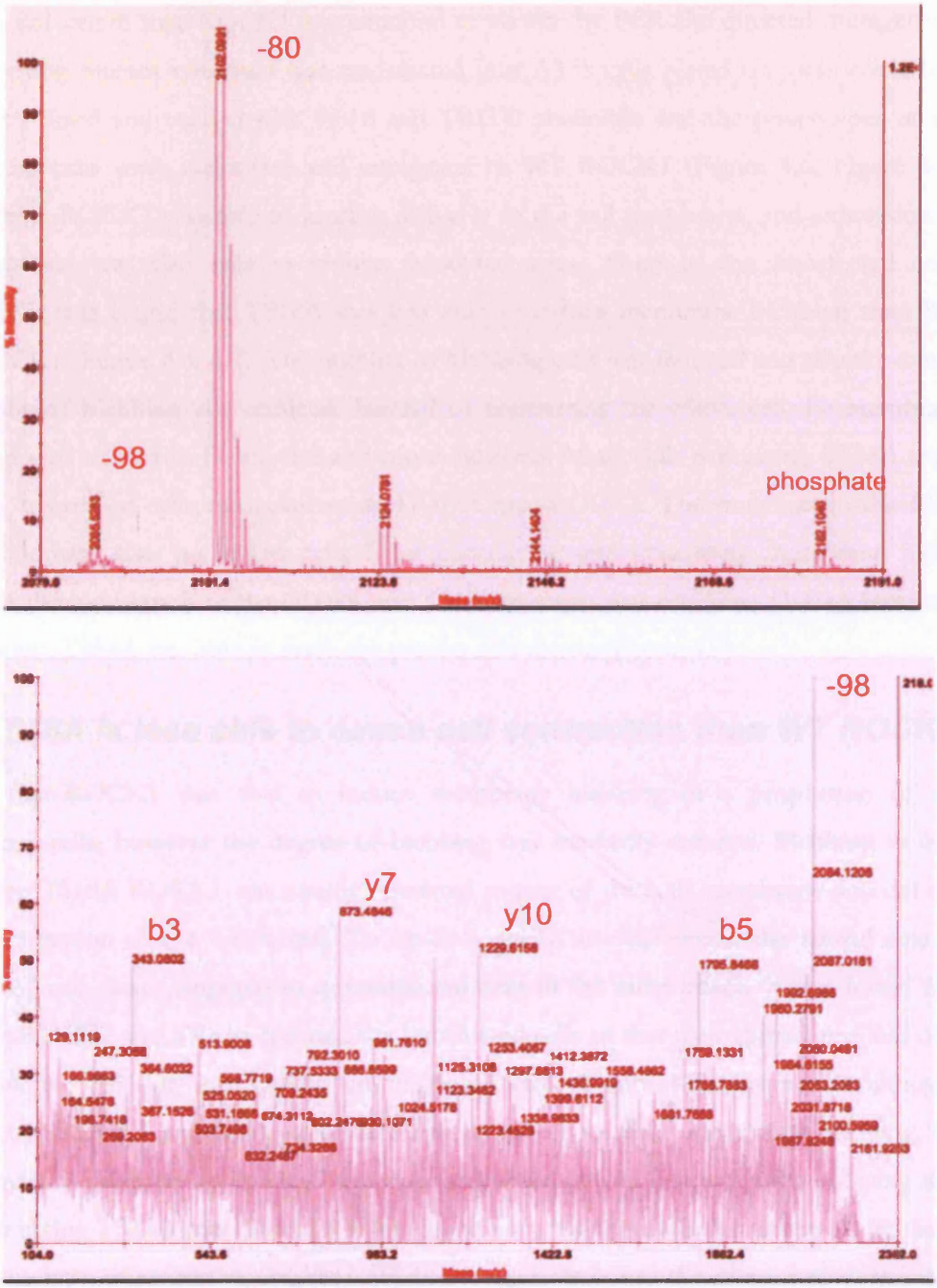

Figure 4.5 Mass spectrometry analysis of ROCK1.

NVENEVSTLKDQLEDLKK. This peptide was pound using radiolabelled ROCK1. The digested protein was fractionated the Edman sequences and the hot fractions analysed. A) the parent ion was found by running the fraction on Applied Biosystems 4700 proteomics analyser B)shows the ions of the peptide when fragmented. This analysis was carried out on the Applied biosystems 400 Q trap.

4.4 Analysis of T518A ROCK1

T518 in full length myc-ROCK1 was mutated to alanine by PCR site directed mutagenesis. The resulting mutant construct was transfected into A375 cells plated on glass coverslips. Cells were fixed and stained with 9E10 and TRITC phalloidin and the phenotypes of the transfected cells were quantified and compared to WT ROCK1 (Figure 4.6, Figure 4.7). T518A myc-ROCK1 was able to localise diffusely to the cell membrane, and expression of this construct was also able to induce thickened stress fibres in the transfected cells. However it was found that T518A was less able to induce membrane blebbing than WT myc-ROCK1 (Figure 4.6, 4.7). The number of blebbing cells was reduced and also the extent of membrane blebbing was reduced. Instead of contracting the whole cell the membrane blebs induced tended to be smaller and more localised. Many cells expressing T518A myc-ROCK1 resembled cells over-expressing I1009A myc-ROCK1. The mutation in the Rho-binding domain also prevented cells from contracting and generating membrane blebs. However the localisation of the I1009A and T518A mutants was different, I1009A remained cytoplasmic; T518A was able to reach the plasma membrane (Figure 4.7).

4.5 T518A is less able to cause cell contraction than WT ROCK1

T518A myc-ROCK1 was able to induce membrane blebbing in a proportion of the transfected cells, however the degree of blebbing was markedly reduced. Blebbing in cells expressing T518A ROCK1 was usually restricted to part of the cells membrane and did not cause contraction of the whole cell. To try to quantify this difference, the spread area of transfected cells was compared to untransfected cells in the same image. It was found that WT myc-ROCK1 was able to contract the transfected cells so that their spread area was only approximately 20% of surrounding untransfected cells (Figure 4.8). Meanwhile although T518A myc-ROCK1 expressing cells were able to induce localised membrane blebbing, the cells remained generally spread and this was confirmed by the quantification showing that cells expressing T518A myc-ROCK1 were spread over the same area as untransfected cells. This phenotype of restricted, localised cell blebbing is similar to the phenotype seen when truncated ROCK1 is localised to the plasma membrane by the addition of the K-Ras CAAX sequence (Figure 3.3).

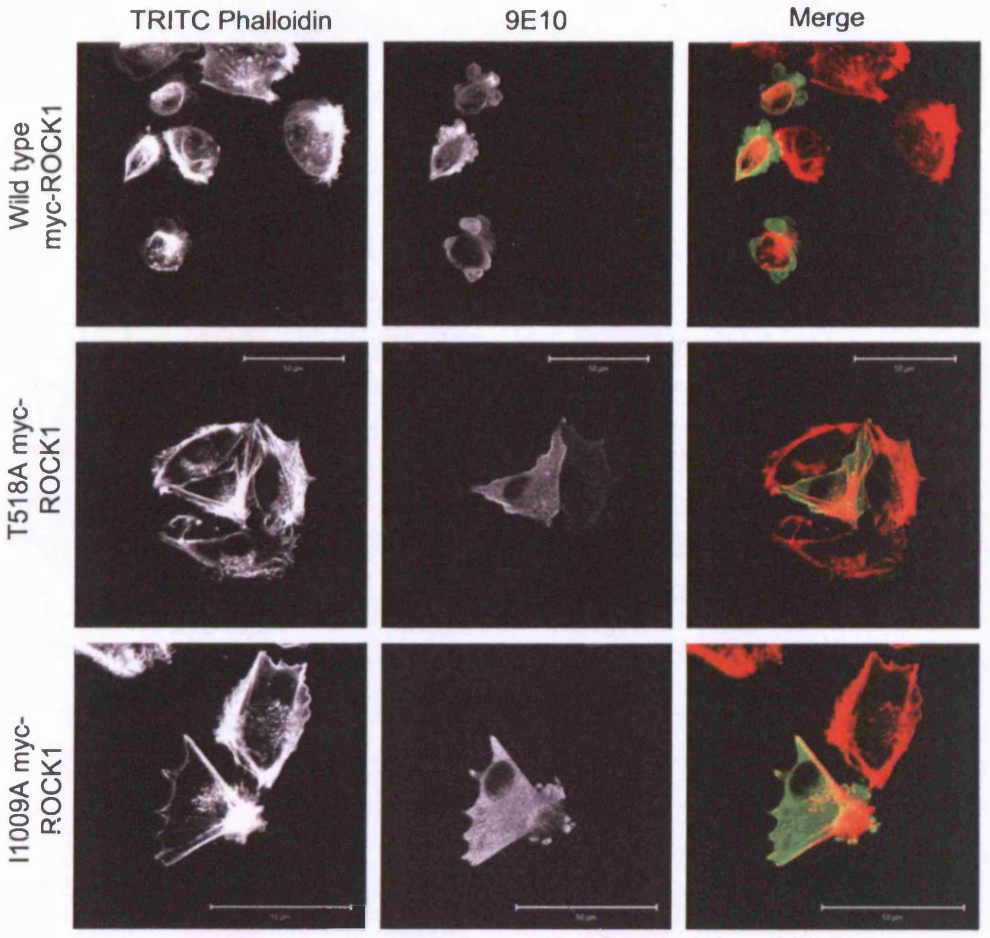

Figure 4.6 Phenotype of T518A ROCK1. A375 cells were transfected with either wild type myc-ROCK1, the Rho-binding mutant I1009A ROCK1 or T518A ROCK1. cells were fixed and stained with 9E10 and TRITC phalloidin. Scale bar indicates 50 µm.

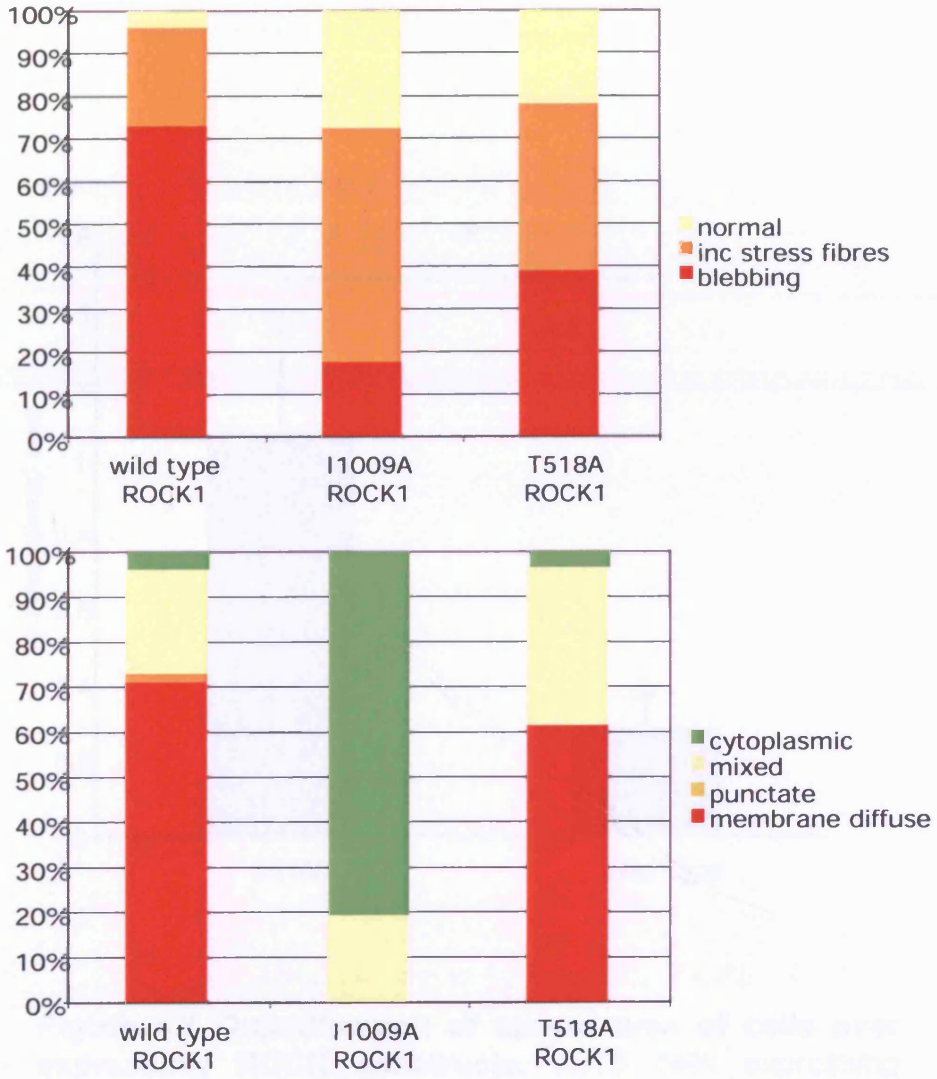

Figure 4.7 Analysis of the phenotype of T518A myc-ROCK1. A375 cells were transfected with either WT myc-ROCK1 or the Rho-binding mutant of ROCK1 (I1009A) and also T518A ROCK1. Cells were fixed and stained 48 hours after transfection and the transfected cells were analysed and placed into categories based on their morphology and F-actin staining, and the localisation of the ROCK construct. Graphs show data pooled from 3 independent experiments, each experiment contains >50 quantified cells.

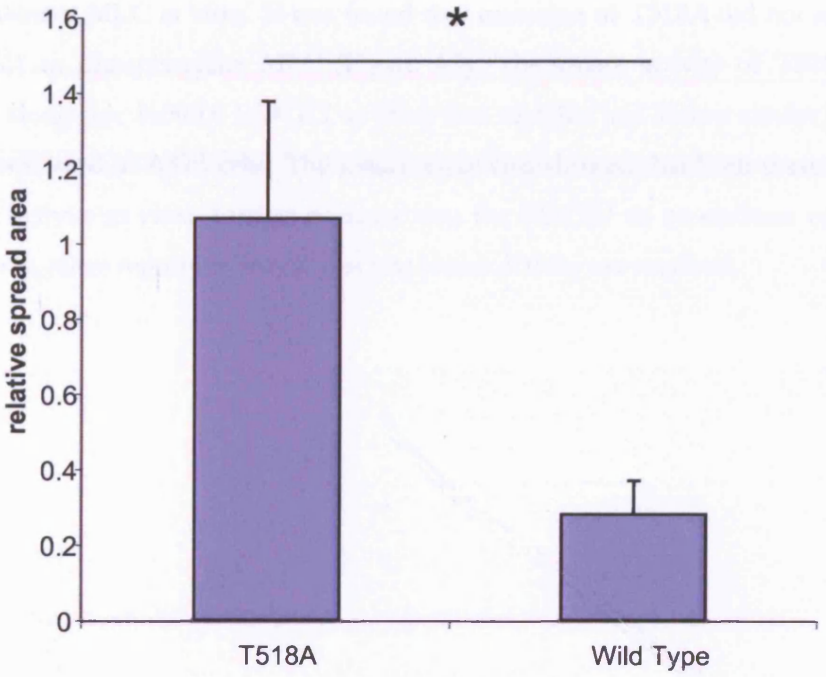

Figure 4.8 Quantification of spread area of cells over expressing ROCK constructs. A375 cells expressing either WT ROCK1 or T518A ROCK1 were fixed and stained with 9E10. Using ImageJ software the area covered by each transfected cell was measured against the area of untransfected cells in the same field. The histogram shows the mean of these ratios and standard deviation. A ratio of 1 indicates no difference in area from the untransfected cells. * indicates $p<0.001$ T-test.

4.6 T518A mutation does not inhibit kinase activity of ROCK1

So far the mutation of T518A had been shown to reduce the ability of over-expressed ROCK1 to cause cell contraction. However T518A myc-ROCK1 was localised correctly to the plasma membrane and was also able to induce thick stress fibres in transfected cells. It was next tested whether mutation of T518 affected kinase activity of ROCK1 in vitro (Figure 4.9). Myc-ROCK1 was immunoprecipitated from A375 cells and used to phosphorylate recombinant MLC in vitro. It was found that mutation of T518A did not alter the ability of ROCK1 to phosphorylate MLC (Figure 4.9). The kinase activity of T518A ROCK1 was tested along side I1009A ROCK1 as these two mutants had shown similar phenotype when over expressed in A375 cells. The kinase assay also showed that both these mutants had full kinase activity in vitro, further evidence that for ROCK1 to co-ordinate contraction of the cell body, more regulatory steps than just kinase activity are required.

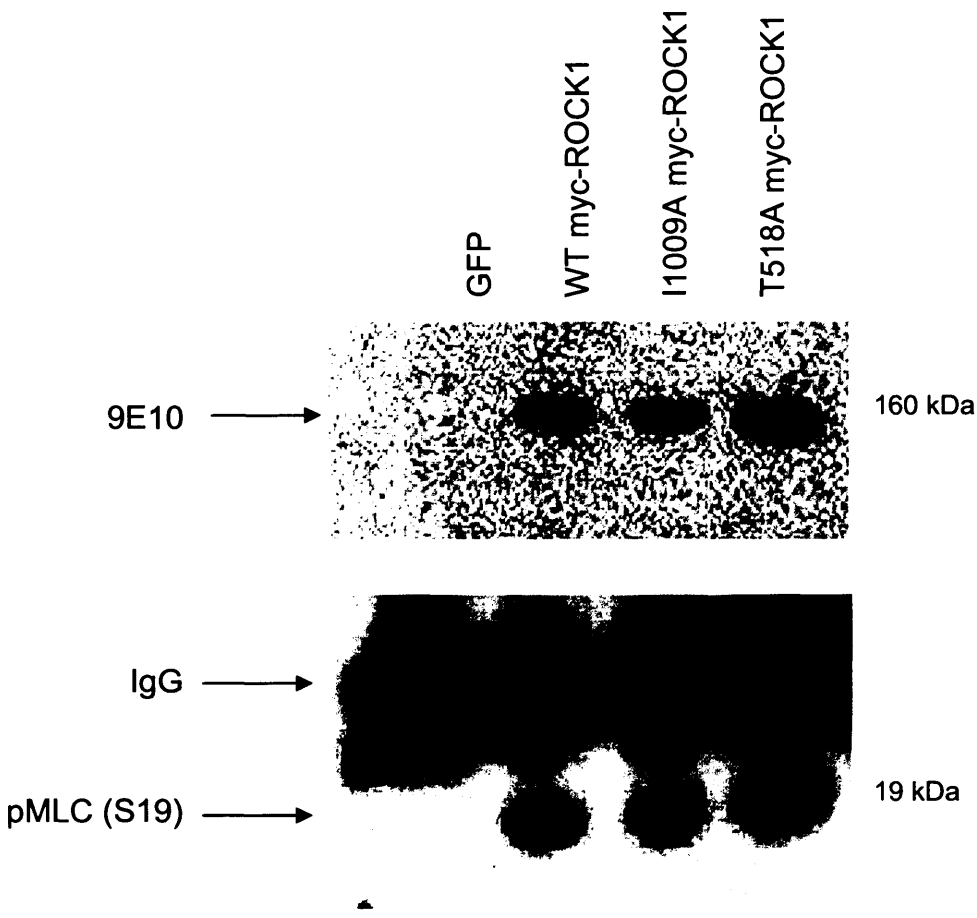

Figure 4.9 I.P. kinase assay of myc-ROCK1 mutants. A375 cells were transfected with either WT myc-ROCK1 or the rho-binding mutant I1009A myc-ROCK1 or T518A myc-ROCK1. The ROCK protein was immune precipitated using 9E10 and used to phosphorylate recombinant MLC in vitro.Samples were analysed by western blotting for pMLC (S19) and 9E10.

5 Chapter 5 - siRNA screen of potential regulators of ROCK-driven cortical actin contractility and amoeboid motility in A375 cells

5.1 Chapter summary

This chapter summarises the identification of PDK1 as a novel regulator of ROCK-driven acto-myosin contractility. To try to elucidate the signalling pathways which regulate ROCK-driven contractility and potentially also cell motility, an siRNA screen of proteins involved in cytoskeletal dynamics, cell adhesion, cell motility and other signalling pathways was carried out in A375 cells. In conjunction with this A375 cells were also treated with a range of pharmacological inhibitors. A375 cells were used for this screen, as it has been previously shown that they utilise amoeboid cell motility in vivo and are dependent on Rho and ROCK signalling for their rounded cell morphology [153]. Cells were plated on a deformable matrix of collagen and matrigel to model a 3D environment more similar to the in vivo situation. In this environment, A375 cells are, in the majority, rounded and exhibit membrane blebs. Treatments that disrupted this rounded cell morphology were listed as 'hits' as potential novel regulators of ROCK-driven cell contractility.

Several proteins with roles in cell motility and/or actin dynamics were identified in this screen, however it was chosen to investigate PDK1 further as it had not previously been linked with amoeboid cell motility or the regulation of Rho/ROCK signalling. It was found that PDK1 was required for ROCK to co-ordinate contraction of the cortical acto-myosin network and membrane blebbing. Furthermore PDK1 was required for cell motility in two cell lines utilising amoeboid morphology (A375 and MTLn3E).

5.2 siRNA screen for regulators of ROCK-driven cortical acto-myosin contractility

A selection of genes were hand-picked to be included in the siRNA screen for analysing changes in cell morphology. The whole of the Rho family of GTPases was included as these proteins have been shown to play a critical role in controlling the actin cytoskeleton and therefore also cell morphology. Other actin regulators such as cortactin, cofilin, WAVE and

N-WASP were included for the same reasons. The screen also included genes involved in cell adhesions such as integrin subunits, and their associated proteins such as paxillin. Kinases known to be involved in regulation of myosin were included such as MRCK and because of the interesting data in chapter 3 implicating PI3K signalling in the regulation of ROCK1, PDK1 and Akt isoforms were also included. This group of gene targets would hopefully reveal some of the regulatory mechanisms involved in rounded cell morphology and potentially amoeboid cell motility.

A375 cells transfected with either siRNA smart pools from Dharmacon, or treated with inhibitors and were plated onto collagen/matrigel gels. Cells were fixed 48 hours after transfection or after 18 hours of treatment with inhibitor. Cells were then stained with TRITC phalloidin and propidium iodide to show organisation of actin and also overall cell morphology (Figure 5.1, Figure 5.2).

Control, non-targeting siRNA transfected cells were mostly rounded with membrane blebs when plated on collagen/matrigel (see the first 2 panels in Figure 5.1, Figure 5.3). Reassuringly, siRNA knockdown of RhoA, ROCK1 or ROCK2 caused cells to become elongated and so served as positive controls (Figure 5.1, second panel on page 1 and right hand panels in the middle row on page 2). This was also the case when Rho and ROCK were inhibited with TAT-C3, Y27632, H1152, or HA1077 (Figure 5.2).

Knockdown of RhoC caused a phenotype similar to that of RhoA depletion but the phenotype was not as obvious. This was not unexpected because RhoA and RhoC have been previously shown to interact with the same downstream effectors [59]. RhoC has also been previously reported to be over-expressed in some metastatic tumour cells [66]. The difference in the severity of the phenotype may be due to the efficiency of knockdown. The only other Rho family member to cause a change in morphology in this screen was RhoU, which caused the cells to become flatter and in some cases slightly elongated. RhoU has been reported to play a role in the regulation of cell adhesions [230, 231]. No elongation was noted with knockdown of Rnd1, Rnd2 or RhoE, cells remained rounded and contracted. Likewise no dramatic change was seen when Rac1 Rac2, Rac3, or Cdc42 were knocked down (see middle panels on page 1 of Figure 5.1), although in the case of the Rac family it is possible that knockdown caused cells to become more rounded, though this is difficult to quantify judging only by eye.

Knockdown of Dia1 or Dia2 caused A375 cells to become flattened and more spread and in some cases elongated. These proteins can also signal downstream of RhoA [62, 232]. A strong disruption of rounded cell morphology was seen when paxillin or vinculin were depleted. They may perhaps play a role in the attachment of the actin cytoskeleton the cell membrane and the cell adhesions to the extracellular matrix.

It was interesting to see that knockdown of any of the integrins tested did not disrupt rounded cell morphology. Other groups have reported that amoeboid moving cells do not require integrin for their invasion [164, 221]. It seems that A375 cells do not require integrins for rounded morphology in 3D culture conditions. The unexpected hit from this analysis was PDK1. Knockdown of PDK1 caused A375 cells to become elongated with multiple protrusions similar to knock down of RhoA or inhibition of ROCK signalling. Interestingly knockdown of Akt1, Akt2 or Akt3 did not phenocopy the knockdown of PDK1. The role of PDK1 in amoeboid cell morphology is investigated in detail below.

Knockdown of MRCK isoforms also had no obvious effect on rounded cell morphology. MRCK is able to regulate myosin light chain and so also cell contractility in some circumstances [170] but it seems that in A375 cells MLC is regulated through pathways other than by MRCK. Results from the inhibitor treated cells show that contraction in A375 cells is mostly regulated through RhoA and ROCK as these were the only inhibitors to cause elongated cell morphology (see Figure 5.2).

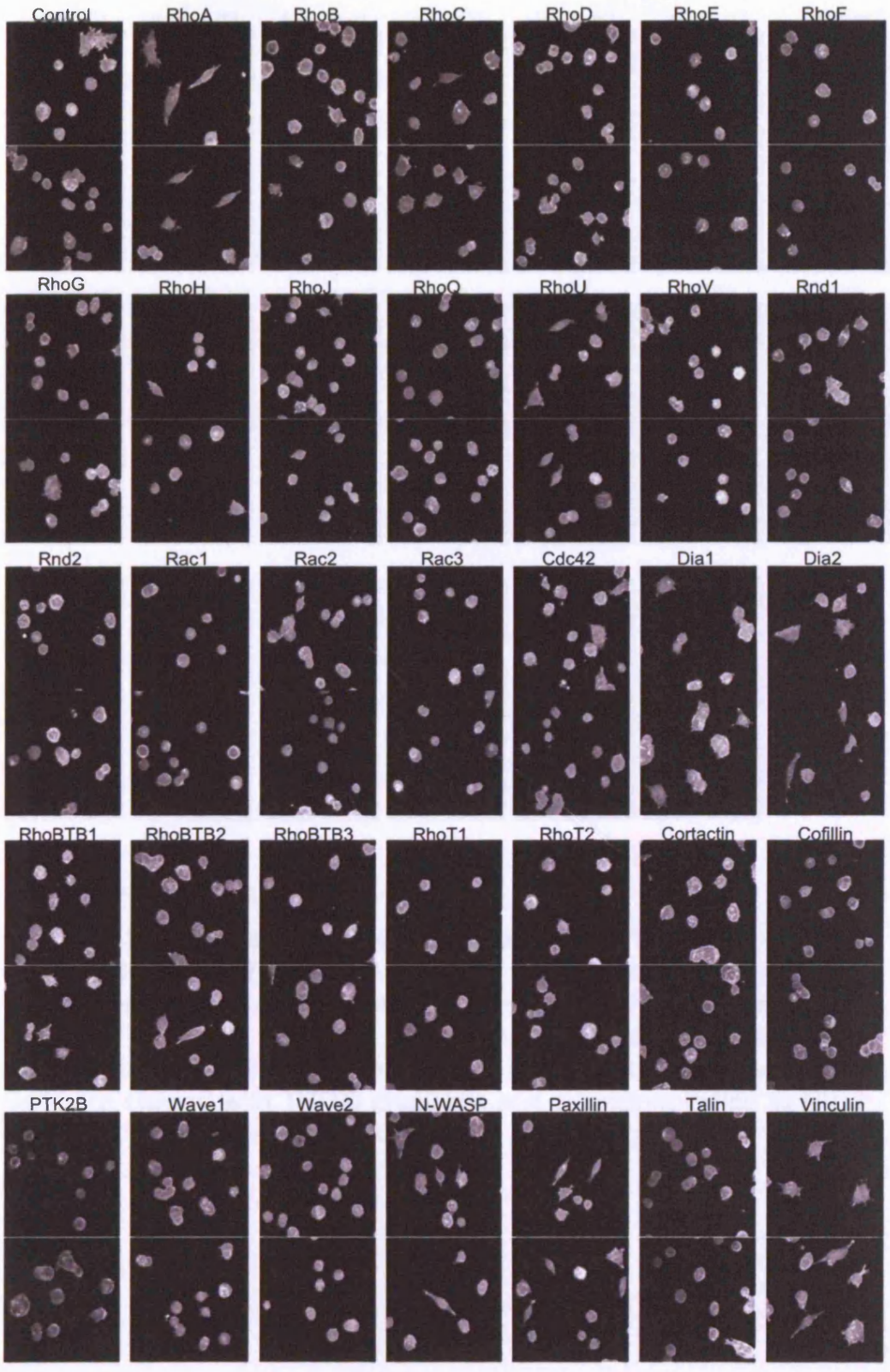

Figure 5.1 continued overleaf...

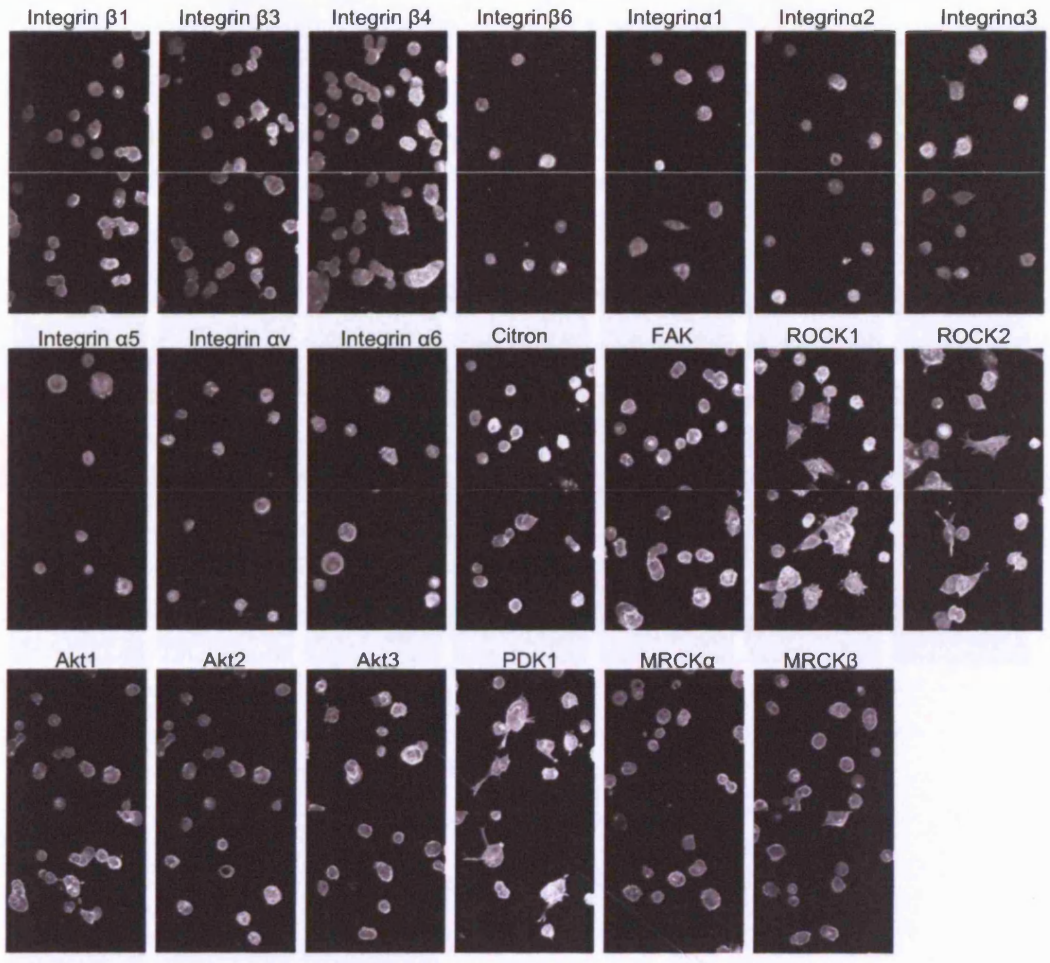

Figure 5.1 siRNA screen for regulators of cortical acto-myosin contractility in A375 cells. A375 cells were transfected with siRNA smartpools targeted against a variety of cytoskeletal proteins and other signalling pathways and then plated on top of 3d collagen/matrigel gels. 2 panels are shown for each gene knocked down in the screen. Cells are stained with TRITC phalloidin and propidium iodide to show the actin cytoskeleton and the overall cell morphology.

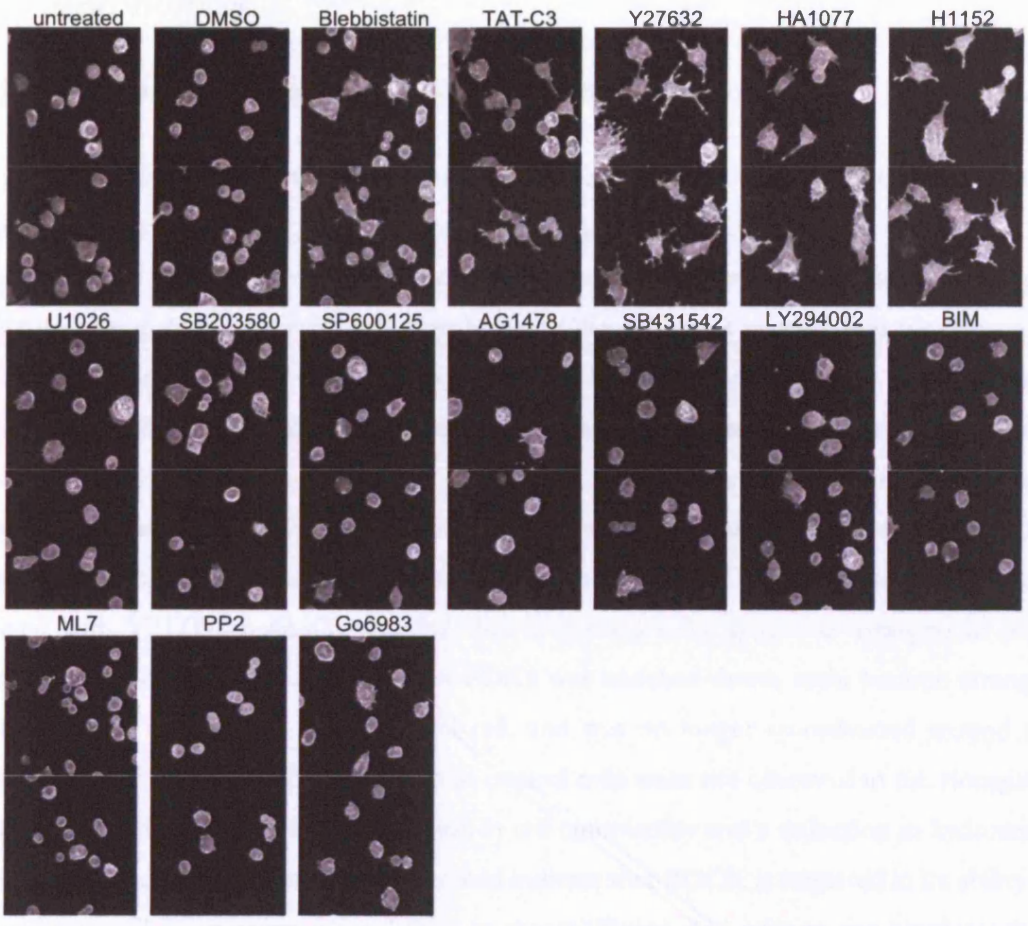

Figure 5.2 Small molecule inhibitor screen for regulators of cortical acto-myosin contractility in A375 cells. A375 cells were plated on top of 3d collagen/matrigel gels and treated with various inhibitors for 18 hours. 2 panels are shown for each treatment. Cells are stained with TRITC phalloidin and propidium iodide to show the actin cytoskeleton and the overall cell morphology.

5.3 PDK1 depletion causes disruption of rounded blebbing morphology

5.3.1 Analysis of changes in actin organisation

In order to continue the investigation into the role of PDK1 in the control of rounded cell morphology further, firstly the 4 oligos used to deplete PDK1 in the screen were tried separately. The deconvulution of the smartpool showed that 3 out for the 4 oligos caused the same disruption of the rounded cell morphology. Oligos 1 and 2 were chosen for remainder of the experiments as they were able to knock down PDK1 most efficiently. The depletion of PDK1 in A375 cells plated on deformable collagen/matrigel matrix caused a disruption of rounded blebbing morphology. Cells depleted of PDK1 became elongated with long, filopodia-like protrusions (Figure 5.3 please also see supplementary movies for more detailed images of the actin organisation). 3D reconstruction of multiple confocal z-sections of cells stained with TRITC phalloidin revealed that in control cells, actin was arranged in thick bundles all around the cell cortex. When PDK1 was knocked down, actin became arranged in long cables running the length of the cell, and was no longer co-ordinated around the whole cortex. The membrane blebs seen in control cells were not observed in the elongated, PDK1 depleted cells indicating a reduction in cell contractility and a reduction in hydrostatic pressure. These changes in morphology could indicate that ROCK is impaired in its ability to co-ordinate cell contractility when PDK1 is absent. Please also refer to the supplementary movies that accompany Figure 5.3 for more detail of the actin cytoskeleton.

5.3.2 Quantification of changes in morphology caused by siRNA depletion of PDK1

The changes in morphology were quantified in order to statistically compare the effect of PDK1 depletion to control morphology of A375 cells and also to the morphology of A375 cells treated with an inhibitor of ROCK (Y27632). To compare cell morphology, low magnification phase images of A375 cells on collagen/matrigel gels were analysed (Figure 5.4). The area and perimeter of cells was calculated by manually drawing around the cell shape using Volocity software. The ratio of $(\text{perimeter}^2)/(4\pi\text{area})$ was then compared. For a circle this ratio = 1. The higher the number, the more elongated the cell is and/or the more protrusions the cell has. The ratio of control transfected cells is around 1.2 indicating that

they are mostly rounded (Figure 5.4). Cells transfected with two different siRNA oligos against PDK1 were more elongated and had more protrusions. The median ratios of cells depleted of PDK1 were around 2.5, significantly higher than the controls ($p<0.001$ Mann Whitney U test). Although the median values of PDK1 depleted cells and Y27623 cells are fairly similar the spread of the values is different. Both cause cells to become more elongated and/or protrusive, but treatment with the inhibitor Y27632 has a more uniform effect on the whole population of cells. Western blots of A375 cell lysates transfected with siRNA against PDK1 showed an overall level of knockdown in the cell population of approximately 80%, (Figure 5.8), however siRNA transfection to deplete PDK1 had a much more variable effect on cell morphology than treatment with ROCK inhibitor. This might be an indication that transfection with siRNA does not effectively knockdown PDK1 in all cells.

Similar morphological changes were also observed in MTLn3E cells (Figure 5.5). The changes in morphology were less pronounced as cells depleted of PDK1 had a ratio of around 1.5, compared to 2.5 in A375 cells, however this was still statistically significantly higher than controls ($p<0.001$) (Figure 5.5).

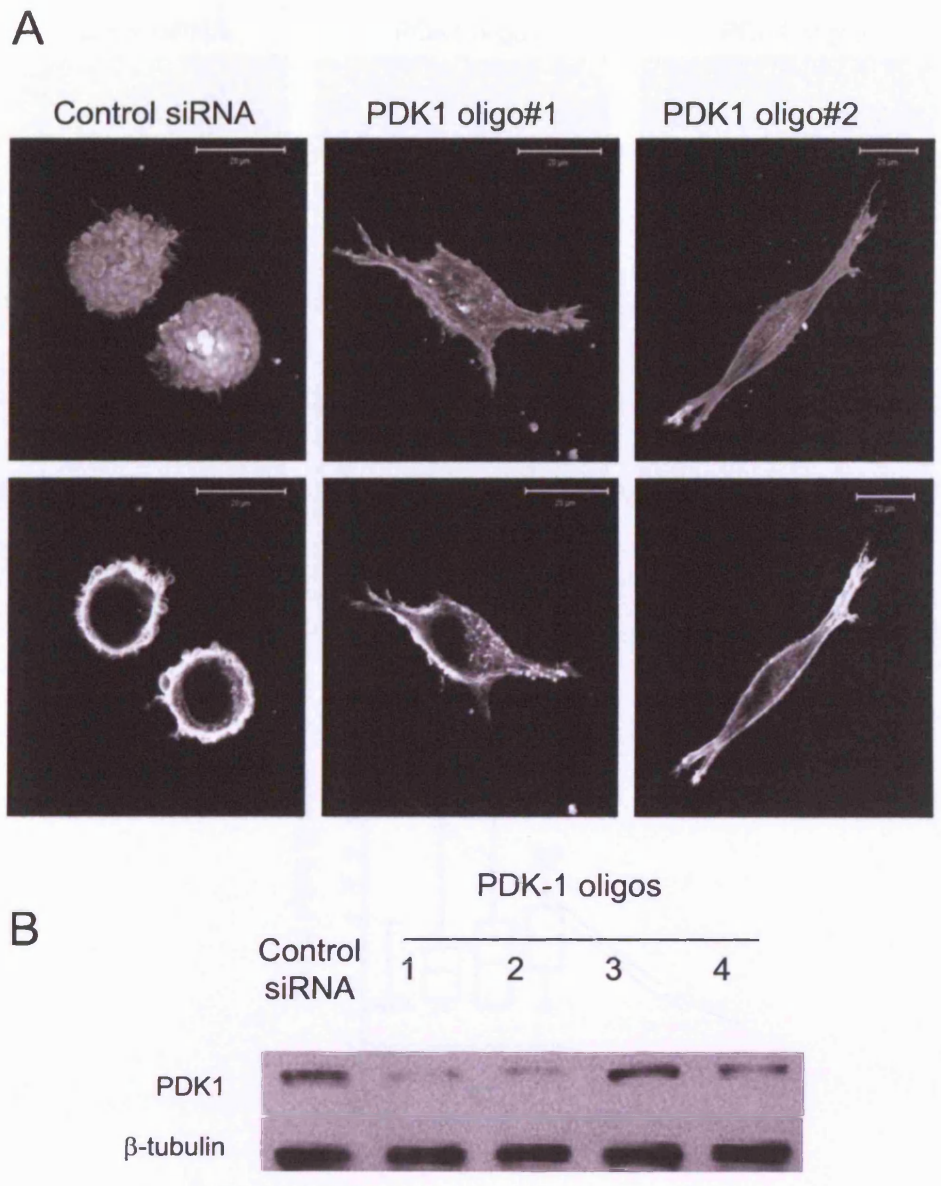

Figure 5.3 Actin phenotypes of A375 cells plated on deformable 3D matrix. A)A375 cells were transfected with either control siRNA or oligos targeted against PDK1. 24 hours after transfection cells were plated on a 3D collagen matrigel gel. 24 hours later cells were fixed and stained with TRITC phalloidin. Upper panel shows 3D reconstruction of cells and lower panels show one slice through the cell. Scale bar indicates 20 μm. Also see supplementary movies. B) Western blot showing the knockdown of PDK1 with 4 difference siRNA oligos.

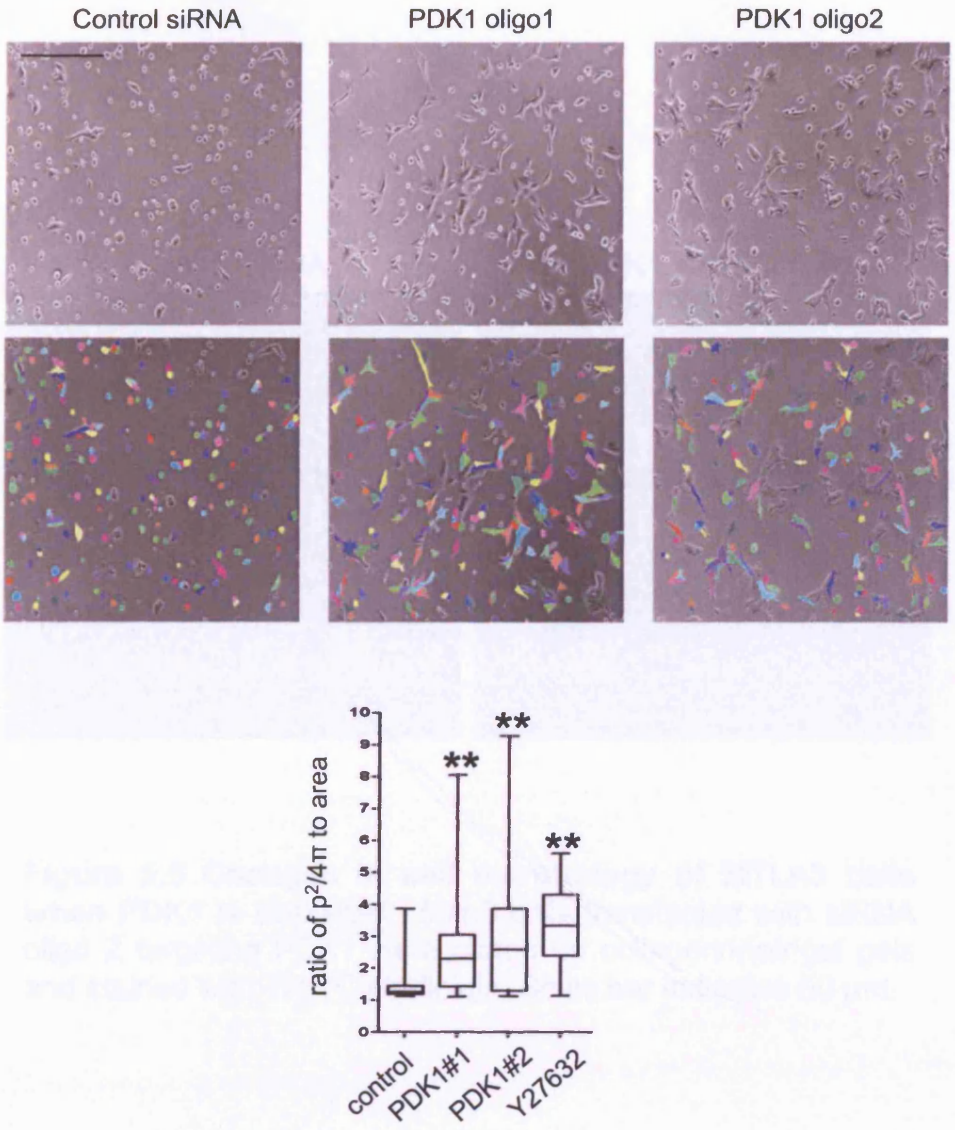

Figure 5.4 Quantification of changes in overall cell morphology of A375 cells plated on 3D matrix. Low power phase images of A375 cells transfected with either control or PDK1 targeting siRNA and plated on 3D matrix were used to analyse cell shape. Using Volocity software, cells were drawn around manually and measurements of the cell perimeter and cell area were collected. Ratios were calculated as $(\text{perimeter})^2/(2\pi\text{area})$. For circular objects this ratio=1. As cells become more elongated this ratio increases. Scale bar indicates 100 µm.

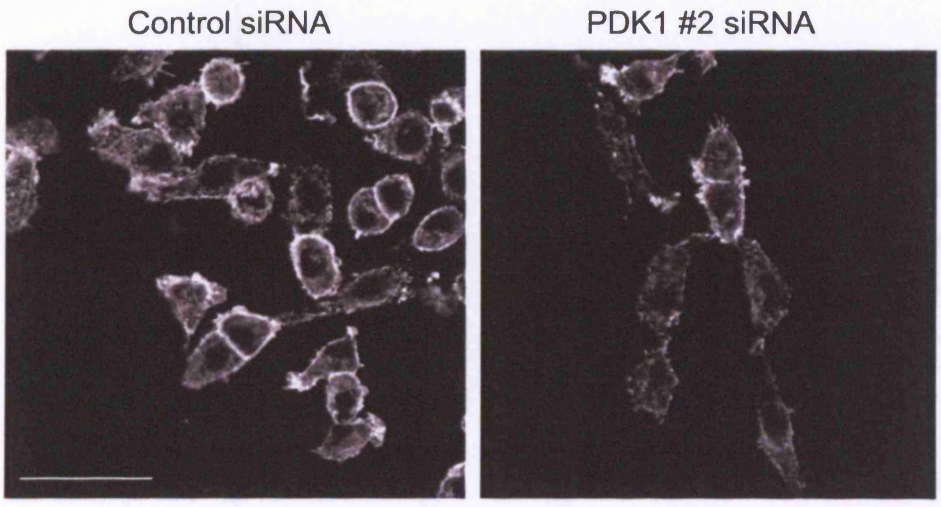

Figure 5.5 Changes in cell morphology of MTLn3 cells when PDK1 is depleted. Mtln3 cells transfected with siRNA oligo 2 targeting PDK1 were plated on collagen/matrigel gels and stained with TRITC phalloidin. Scale bar indicates 50 μm.

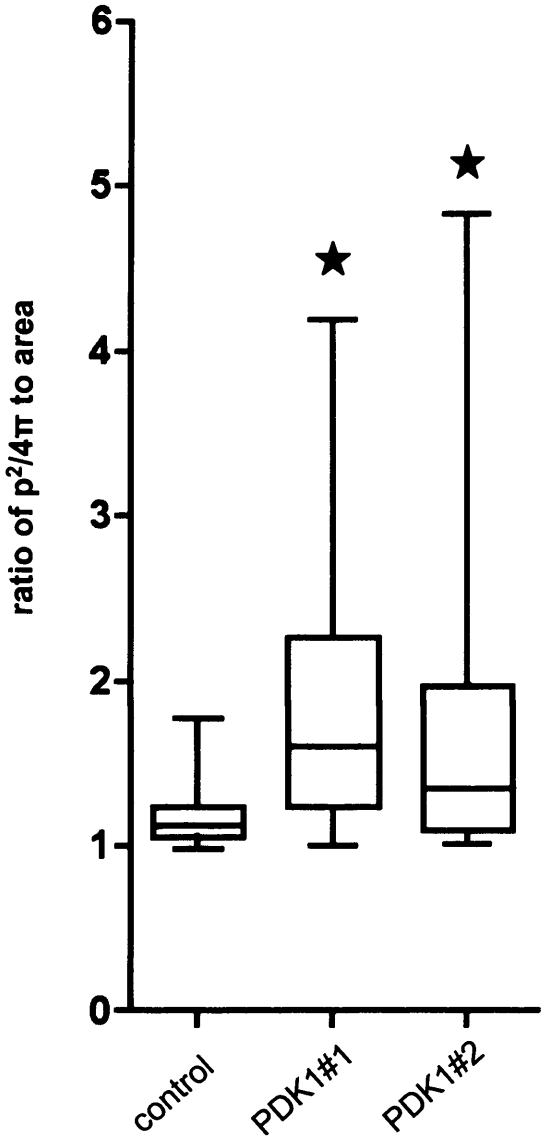

Figure 5.6 Quantification of changes in morphology of Mtln3 cells depleted of PDK1. Low power phase images of Mtln3 cells transfected with either control or PDK1 targeting oligos plated on collagen/matrigel matrix were used to calculate morphology using the ratio described previously. Star indicates $p<0.05$ Mann Whitney U test.

5.4 PDK1 is required for cell motility in deformable 3D environments

5.4.1 PDK1 is required for rapid acto-myosin driven blebbing motility in 3D environments

A375 cells plated on collagen/matrigel gels form large membrane blebs that are able to drive cell motility. This type of cell motility is extremely rapid but fairly inefficient and chaotic. To examine this type of cell motility in detail, individual cells expressing GFP-CAAX were imaged at high resolution using confocal microscopy at a rate of 1 frame every 2 seconds. Translocation of the cell centroid was measured to determine cell speed (Figure 5.7 and supplementary movies).

Control cells are able to move at rates up to 10 μm per minute. This rapid chaotic cell blebbing requires both actin organisation and myosin ATPase activity as treatment of blebbing cells with either 2 μM cytochalasin D or 2 μM Blebbistatin halted cell blebbing and motility (Figure 5.7 and supplementary movies). A375 cells depleted of PDK1 were elongated as had been previously seen. The rapid translocation of the cell centroid seen in control cells was completely lost and instead small filopodia protrusions were extended and retracted. The cell body was not moved at all in the same time period. This indicated that PDK1 depleted cells were defective in their ability to co-ordinate contractile forces through the actin cell cortex, and drive blebbing cell motility.

5.4.2 PDK1 is required for persistent cell motility

A375 cells move very inefficiently on deformable matrices, and only rarely were able to move any significant distance in any one direction. To determine whether PDK1 was required for more persistent cell motility as well as chaotic blebbing motility, A375 cells were plated on collagen/matrigel gels and tracked over 10 hours. Tracking was carried out using MetaMorph software, analysing the phase contrast movies. Taking images at 5-minute intervals is under sampling so much that the rapid blebbing is missed. Despite this, there was still a significant decrease in cell motility when PDK1 was knocked down with two different siRNA oligos (Figure 5.8).

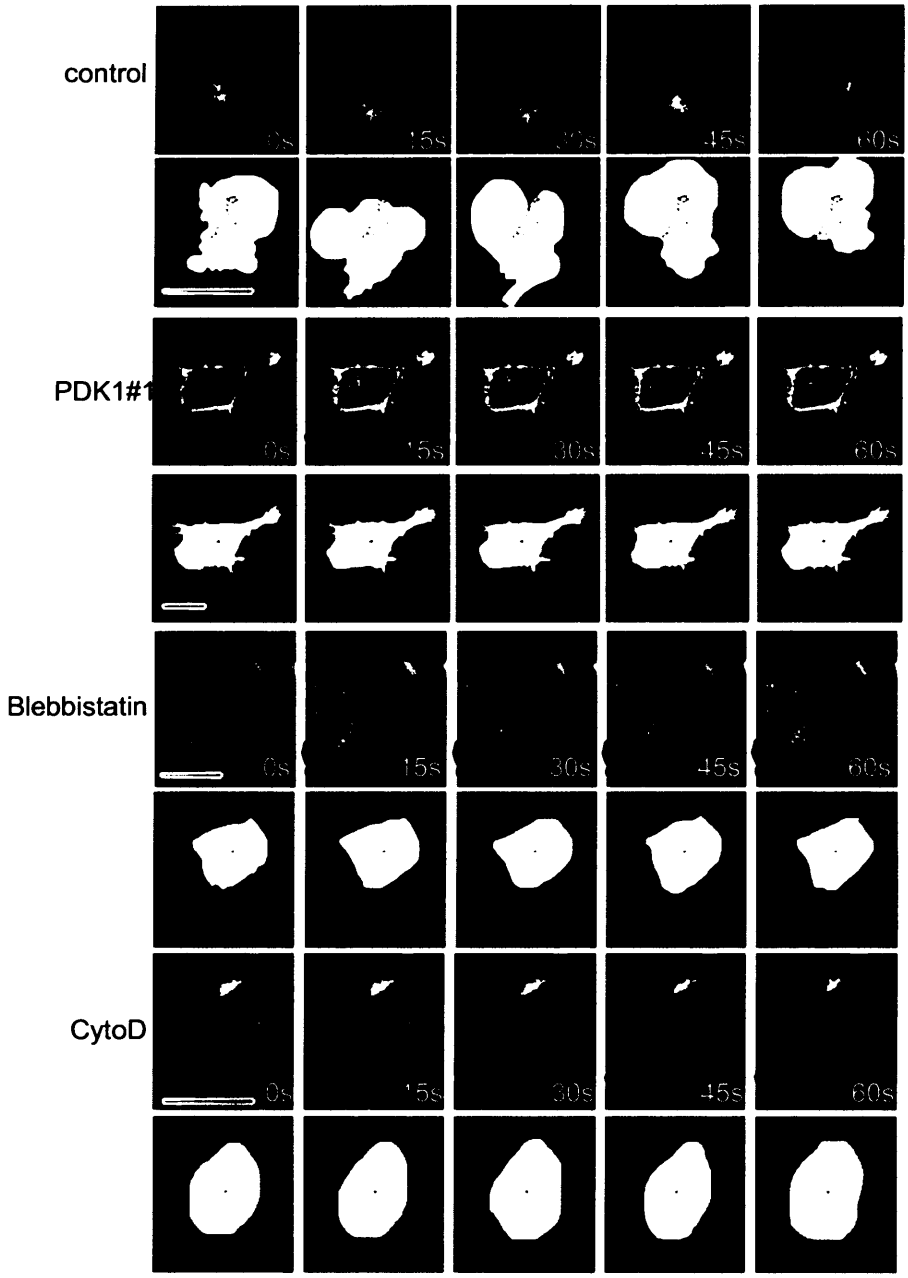

Figure 5.7 High resolution of amoeboid movement of A375 cells in vitro A375 cells stably expressing the membrane marker GFP-CAAX, were transfected with either control or PDK1 targeting siRNA were plated on 3D matrix. Cells were imaged at a rate of 1 frame every 3 seconds in order to visualise rapid blebbing motility. Treatment of these cells with either 2.5 μM blebbistatin or 2 μM cytochalasin D, or knockdown of PDK1, inhibited this form of motility.The upper panels for each treatment show the GFP signal, the lower panels show the tracking of the cell centroid. Please also see accompanying supplementary movies. Scale bar indicates 10 μm.

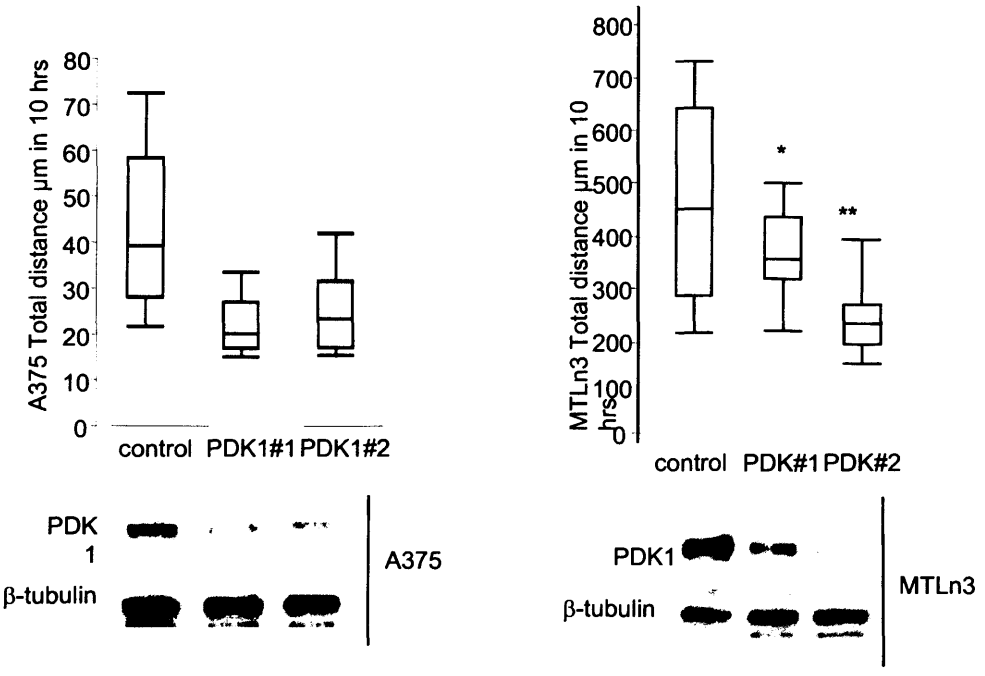

Figure 5.8 Low resolution analysis of cell movement. Low resolution phase contrast time-lapse sequences were analysed to determine the effect of PDK1 depletion on cell motility. Compared here are two different cell lines A375 and Mtln3. Below are the western blots analyses showing the level of PDK1 knockdown in the cell lysates. ** indicates $p<0.001$, * indicates $p<0.01$ (Mann Whitney U test).

To examine the effect of PDK1 depletion on cell motility in more detail, a different cell line was analysed, that exhibits more efficient, directed cell motility. MTLn3E are rat breast carcinoma cells and have also been previously shown to require ROCK-driven contractility for their motility and invasion in vivo [154]. The organisation of cortical actin in MTLn3E cells is also sensitive to depletion of PDK1 (Figure 5.6). When plated on collagen/matrigel gels, MTLn3E cells are rounded and have prominent cortical actin. They exhibit membrane blebs, but not as often or as prominently as A375 cells. They move in vivo and in deformable matrices in vitro, by extending a small pseudopod whilst keeping the rest of the cell round and contracted [154]. MTLn3E cells were plated on collagen/matrigel gels, and similar to A375 cells were imaged over 10 hours at 5 minute intervals.

MTLn3E cells move more directionally than A375 cells. The cells speeds measurable under these conditions are much higher in MTLn3E cells than A375 cells meaning that the differences in cell motility seen when PDK1 is depleted are more easily determined (Figure 5.8). Oligo 2 had a more significant effect than oligo 1 in MTLn3E cells. MTLn3E are rat cells and oligo1 has one mismatched base, and so depletes PDK1 less efficiently (Figure 5.8). Oligo 2 is perfectly matched against both rat and human PDK1 (Figure 5.8). This was determined by western blotting to check the efficiency of knockdown in MTLn3E cells. It seems that the effects on cell motility are directly related to the total levels of PDK1 in a dose-dependant manner. It is also clear that at least 2 different cell lines, capable of moving in a ROCK-dependent amoeboid manner require PDK1.

5.4.3 PDK1 is not required for cell motility on 2D substrates

Considering that PDK1 is involved in many much studied signalling pathways yet a role for cell motility had not previously been described, at the time these experiments were conducted. It was perhaps possible that PDK1 was only required for amoeboid cell motility which is only seen in 3D environments or in vivo. To check this hypothesis the role of PDK1 depletion on the morphology and motility of cells on 2D surfaces was examined. A375 cells were transfected with either control or PDK1 targeting siRNA oligos and plated onto glass-bottomed cell culture dishes. Time-lapse microscopy was carried out and cells were tracked automatically using MetaMorph software, as above. On glass A375 cells have broad lamellipodia and are able to move more persistently than in 3D environments. The most striking finding in 2D in vitro assays was that knockdown of PDK1 did not cause any measurable change in cell morphology (Figure 5.9). Also knockdown of PDK did not reduce

this type of 2D cell motility, if anything cells moved slightly faster but this was not statistically significant (Figure 5.10).

Control siRNA

PDK-1 oligo1

PDK-1 oligo2

Figure 5.9 Depletion of PDK1 does not alter cell morphology on 2D substrates. A375 cells were transfected withh siRNA oligos and plated onto glass cover-slips. 36 hours after transfected cells were fixed and stained with TRITC phalloidin and imaged were taken using confocal microscopy. Scale bar indicates 50 μm.

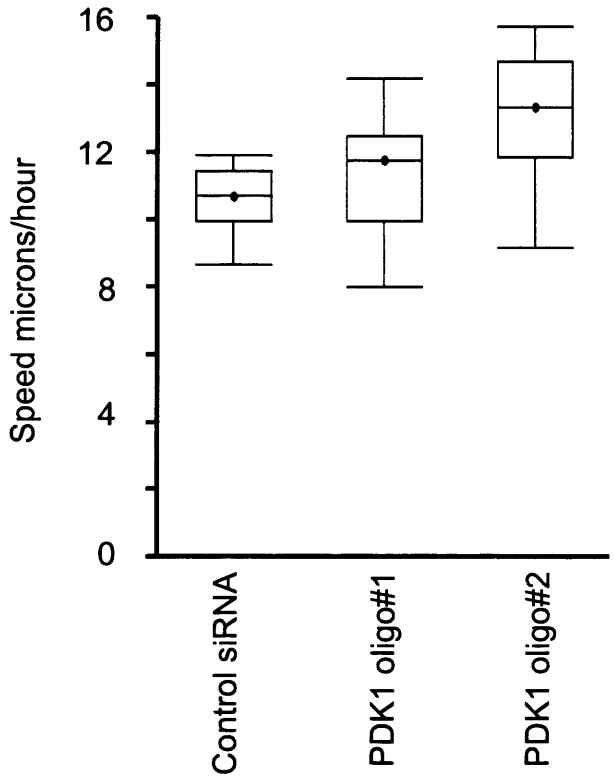

Figure 5.10 Analysis of cell motility in 2D environments. A375 cells were transfected with either control or PDK1 targeting oligos and plated onto glass-bottomed cell culture dishes. Low power phase contrast time-lapse sequences were analysed to determine cell speed.

6 Chapter 6 - PDK1 is required for A375 cell invasion in vivo

6.1 Chapter summary

This chapter describes the investigations into the possible roles of PDK1 and ROCK in amoeboid cell motility of cancer cells in vivo. Cell motility was monitored in primary xenograft tumours using multi-photon intravital imaging of anaesthetised mice. Firstly the role of ROCK1 and ROCK2 signalling in cancer cell motility in vivo was examined by treating mice with the inhibitor Y27632. A375 cells were injected subcutaneously in nude mice and the resulting tumours were imaged after 48 hours treatment with 3 doses of Y27632. It was found that Y27632 treated tumours showed a reduction in cell motility of approximately 50 % compared to control tumours treated with PBS. In more detailed analysis it was found that the reduction in motility was mostly caused by an inhibition of amoeboid cell motility.

The results from the siRNA screen had highlighted PDK1 as a potential regulator of cortical actin and rounded cell morphology. Further investigation confirmed this result and also found that PDK1 was required for cell motility, specifically on 3-dimensional, deformable environments. To confirm the relevance of these findings, the effect of PDK1 knockdown on cancer cell motility and invasion was examined in vivo. A375 cell lines stably depleted of PDK1 and also stably expressing GFP-MLC were generated and injected subcutaneously into the flank of nude mice. It was found that PDK1 caused elongated morphology and reduced cell motility in vivo as had been predicted by the in vitro studies. The ability of cells to colonise the lungs was also examined and it was also found that knockdown of PDK1 reduced the ability of cells to persist in the lung parenchyma. The results in this chapter reveal that PDK1 is required for cancer cell motility in vivo and potentially indicate that PDK1 may also play a role in other stages of metastasis.

6.2 Inhibition of ROCK signalling reduces cancer cell motility in vivo.

A375 cells within the xenograft tumours were visualised by their stable expression of GFP-MLC. The A375 cells within the tumour were generally densely packed and surrounded by a capsule of dense collagen fibres, which were imaged using 2nd harmonic signals following 2-

photon excitation. Control mice were treated with 3 intraperitoneal doses of PBS during the 48 hours prior to imaging. The A375 xenograft tumours imaged in mice treated with ROCK inhibitor, were injected with 3 doses of Y27632 (40 mg/kg) (note that this compound also inhibits PRKs) in PBS in the 48 hours prior to imaging, the last dose was given just before imaging was begun. Analysis of the resulting time-lapse movies was undertaken manually and the number of cells moving in each frame were counted and categorised as below. The number of movement events was then standardised to movements/mm^2/hour. The categories used for cell movement events were:

1. Rapid amoeboid movement
2. Elongated/ protrusions
3. Chaotic/ blebbing motility

Rapid amoeboid movement was defined as cells moving in a reasonably directed manner at speeds of between 1-5 μ/min. Elongated/ protrusions, was defined as cells making a significant protrusion, but it was not always followed by translocation of the whole cell body within the time period of the imaging. Chaotic/ blebbing motility was defined as cells moving with membrane blebs, but not in a directed manner. Cells of this type would exhibit membrane blebs similar to what we had seen when A375 cells were plated on a 3D deformable matrix in vitro. We were also able to observe switching between chaotic blebbing and rapid amoeboid movement, indicating that these categories are an over simplification of the cell motility phenotypes in vivo. Examples of amoeboid and elongated cell motility are shown in Figure 6.2 and in the supplementary movies that accompany Figure 6.2. The speed at which cells moved in vivo was calculated from the in vivo movies and it was found that cells moving in an amoeboid manner moved much faster than those moving in an elongated manner (median speed 3.5 μ/min compared to 1.3 μ/min (Figure 6.4)).

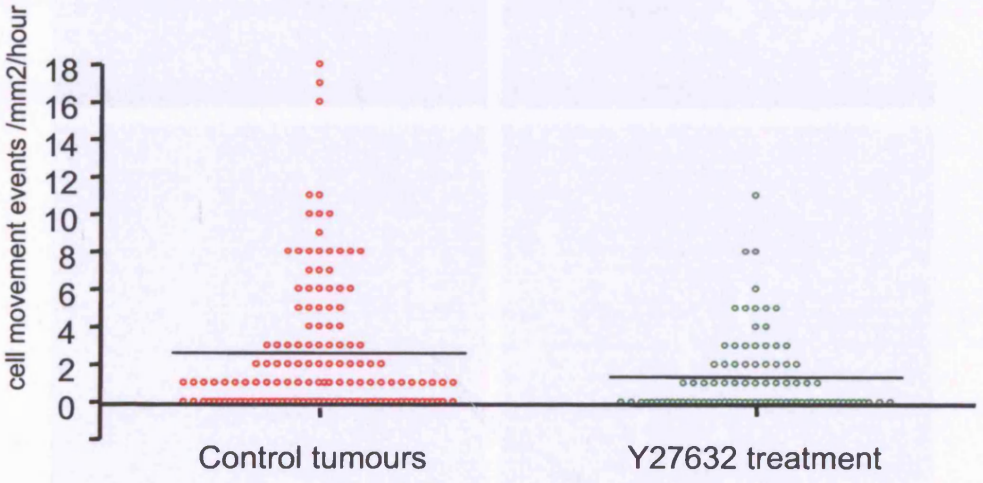

Figure 6.1 Inhibition of ROCK signalling in vivo reduced cancer cell motility. A375 GFP-MLC xenograft tumours were grown subcutaneously in nude mice. Y27632 was dosed I.P. in 3 doses in the 48 hours prior to imaging. Timelapse movies were analysed and cell movement events in each z-section were counted. Results are shown in a scatter plot, bars indicate mean number of movement events per imaged z-section.

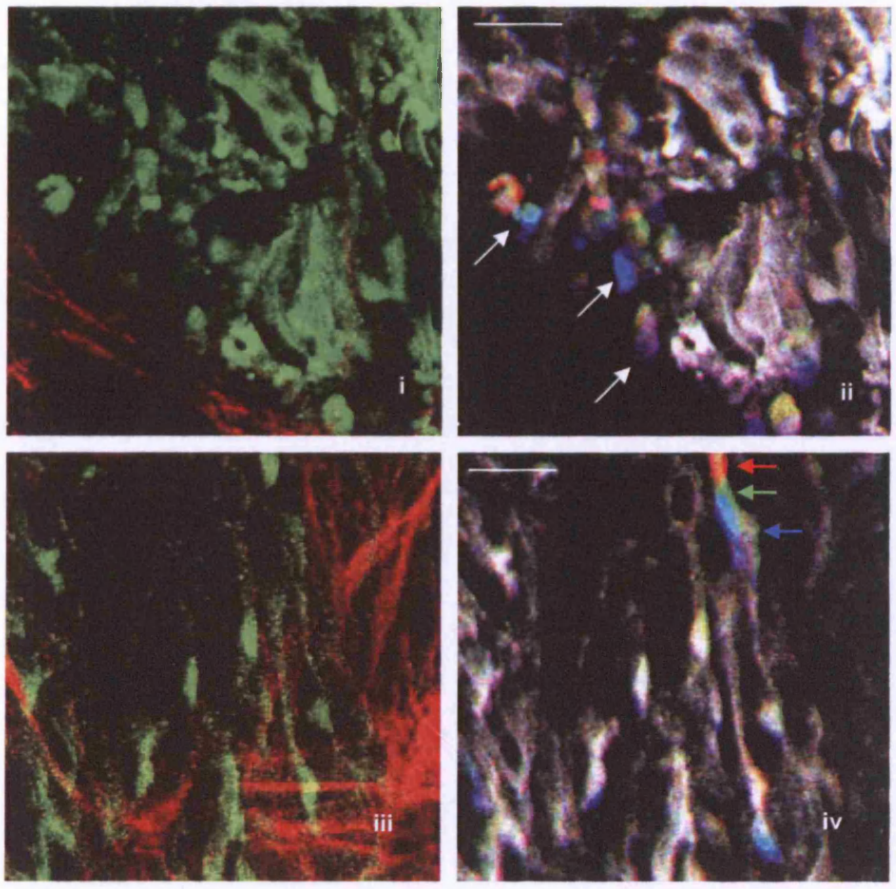

Figure 6.2 Images from in vivo multi-photon intravital microscopy of A375 subcutaneous tumour. Both areas shown are from the same tumour area. Panels i) and ii) show fast moving amoeboid motility. Panels iii) and iv) show elongated cell motility (please see accompanying supplementary movies). Panels ii) and iv) show overlaid images of 3 consecutive time points in red, green and blue. White pixels indicate stationary objects. The spatial separation of the coloured layers highlights the motile cells (arrows). Scale bar indicates 25 μm.

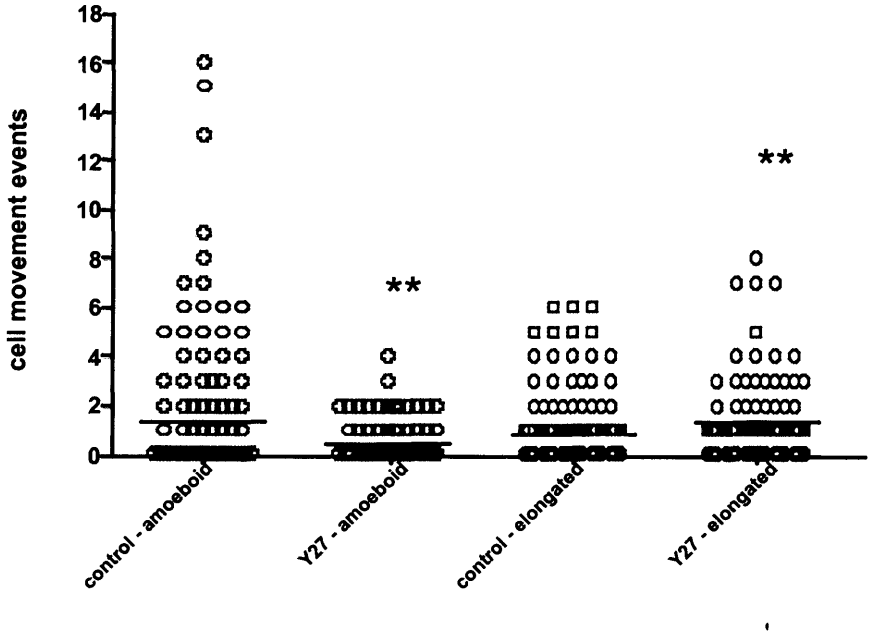

Figure 6.3 Inhibition of ROCK activity in vivo causes a reduction in amoeboid cell motility. A375 cells expressing GFP-MLC were injected subcutaneously into the flank of nude mice. When tumours reached 4-6 mm in diameter mice were given 3 doses of Y27632 in PBS (40 mg/kg) I.P. in the 36 hours prior to imaging. Control mice were doses with PBS alone. Time lapse movies were analysed and cell movement events were classified into amoeboid or elongated categories. Data is presented as movement events per z-section imaged. Black bars indicate mean values. ** indicated $p<0.01$ by Mann Whitney U test.

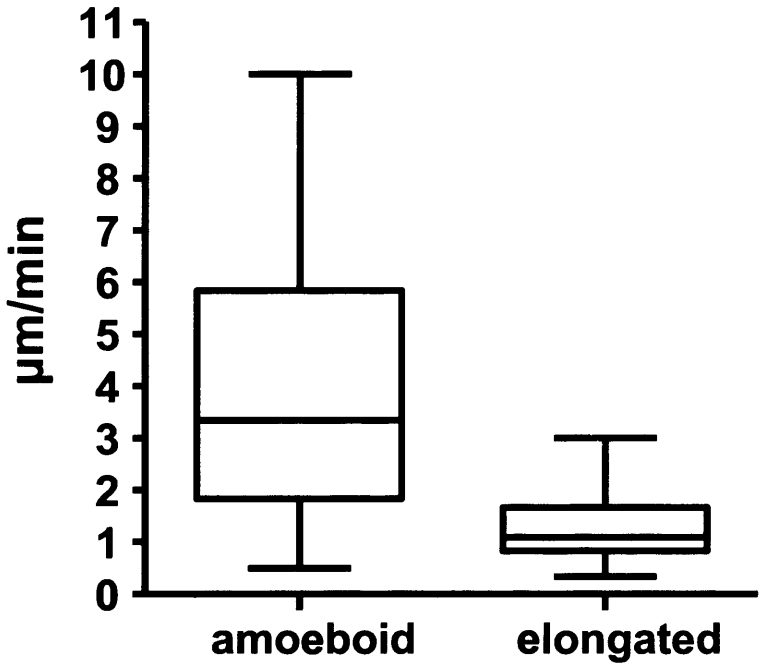

Figure 6.4 Comparison of cell speeds between different forms of cell motility in vivo. The above box plots show the quantification of cell speed in microns/minute. In vivo movies were analysed using LSM510 image examiner and the distance moved by motile cells was measured and divided by the time in minutes to give cell speed.

Control tumours cells moved in a mostly amoeboid manner with a smaller proportion of cells moving with an 'elongated' morphology. Y27632 treated tumours generally showed less cell movement events than control tumours (Figure 6.1). The reduction was around 50%, measured by the average number of movement events per z-section imaged. In both the control and Y27632 treated tumours, there were many areas of the tumour which showed no cell motility (note the many points plotted at zero), and overall it was estimated that only around 1 % of cells imaged were motile.

It was observed that the reduction in cell motility caused by Y27632 was mostly due to an inhibition of amoeboid cell motility and that cells moving in an elongated manner were not affected. It seems that ROCK/PRK signalling is required for amoeboid cell motility but dispensable for more elongated forms of cell motility (Figure 6.3).
It was next tested what role PDK1 had in cancer cell motility in vivo.

6.3 PDK1 depletion causes elongated cell morphology in primary tumours

6.3.1 Generation of stably PDK1 depleted A375 clones

A375 cells stably expressing GFP-MLC were also engineered to stably express an shRNA sequence targeted against PDK1. The Vector pSuper Retro containing a PDK1 targeting cassette was transfected into the amphotropic packaging cell line phoenixAMPHO to generate virus that was then used to infect the A375 GFP-MLC expressing cells. Infected cells were selected with puromycin and plated at low density. Colonies that formed were expanded and the level of PDK1 in each monoclonal cell line was determined by western blotting (Figure 6.5). Two different PDK knockdown clones (clone 3 and 8 (Figure 6.5)) were selected for the in vivo experiments along with a control monoclonal cell line that had been infected with an empty cassette pSuper Retro and a non infected polyclonal cell line expressing GFP-MLC alone. These cell lines were then used for generation of xenograft tumours in nude mice and imaged using intravital multi-photon microscopy to analyse their morphology and motile behaviour.

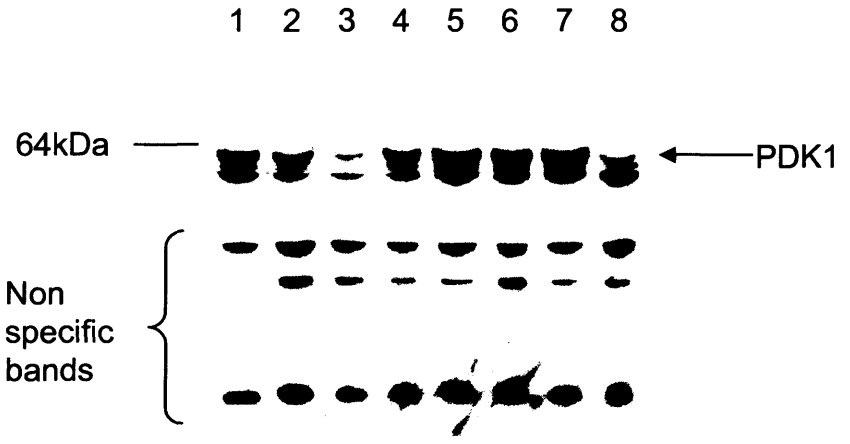

Figure 6.5 Testing monoclonal shRNA A375 cell lines for depletion of PDK1. Once colonies had formed following selection with G418, single cells clones were picked and grown in 6 well plates. Their expression of PDK1 was subsequently tested by western blotting. Clone 3 and clone 8 were chosen for subsequent experiments.

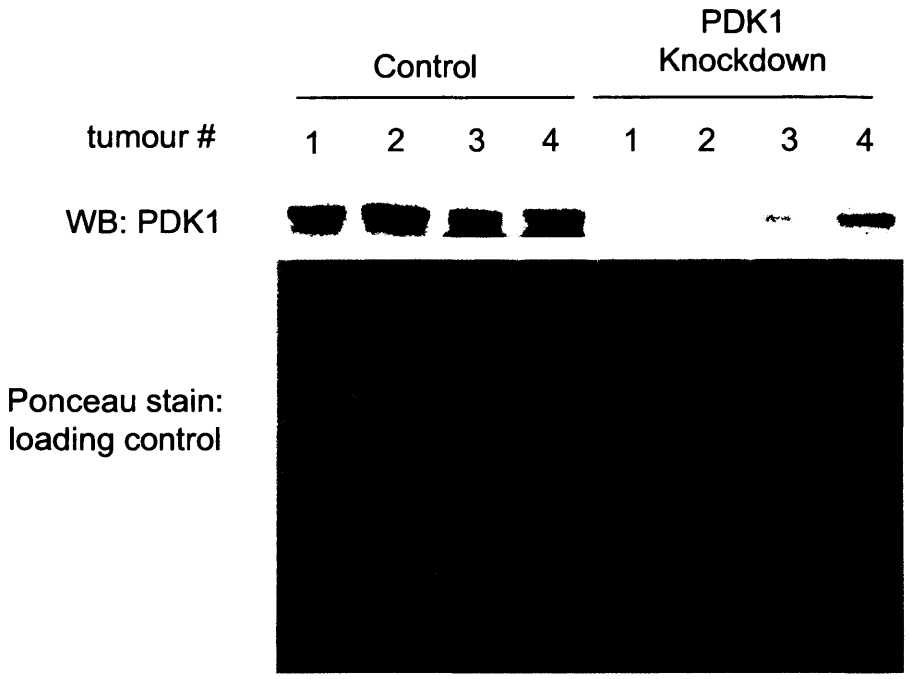

Figure 6.6 Western blot analysis of tumour lysates. A375 cells stably expressing GFP-MLC and also stably expressing pSuper retro shRNA constructs containing either control empty cassettes or PDK1 targeting cassettes were used to generate sub-cutaneous tumours in nude mice. Following imaging tumours were dissected out and homogenized in lysis buffer. Protein content was determined by bradford assay. Tumour lysates were then analysed by western blot to determine that PDK1 levels were stably depleted in vivo.

6.3.2 Depletion of PDK1 is maintained in vivo

Cells within the xenograft tumours were visualised by their expression of GFP-MLC. Tumours of A375 cells depleted of PDK1 grew at similar rates and reached 4-6 mm in diameter in about 3 weeks, similar to the controls (Figure 6.7). This was not unexpected at no differences in proliferation had been seen in vitro. Xenograft tumours were dissected after they had been imaged and stored at –80 °C until the imaging of all the tumours had been completed. Tumour samples were then homogenised in lysis buffer and the protein content was determined by Bradford assay. Equal amounts of tumour derived proteins were then analysed by western blotting to ensure that PDK1 levels remained depleted in tumours at the time of imaging (Figure 6.6). The results showed that PDK1 was depleted in 4 knockdown tumours compared to 4 control tumours, albeit less effectively in tumour number 4. (PDK1 knockdown tumours of clone 3 and clone 8 cells were tested for PDK1 expression). Equal loading was determined by ponceau staining.

6.3.3 Quantification of cell morphology in primary tumours

Cells within PDK1 depleted tumours appeared more elongated than controls, this was similar to what had been observed and quantified in 3D in vitro environments (Figure 6.8). To quantify cell morphology in vivo, still images from the intravital multi-photon microscopy were used and the area and perimeter of these cells were measured manually using Volocity software. Over 400 controls cells were compared to over 400 PDK1 knockdown cells from a variety of different areas from 4 different mice, using the same ratio of area to perimeter as had been used previously. Results showed that PDK1 depleted cells were significantly more elongated/protrusive than control cells ($p<0.001$) (Figure 6.9). This is in agreement with the result from the initial siRNA screen and the subsequent detailed morphological analysis in vitro.

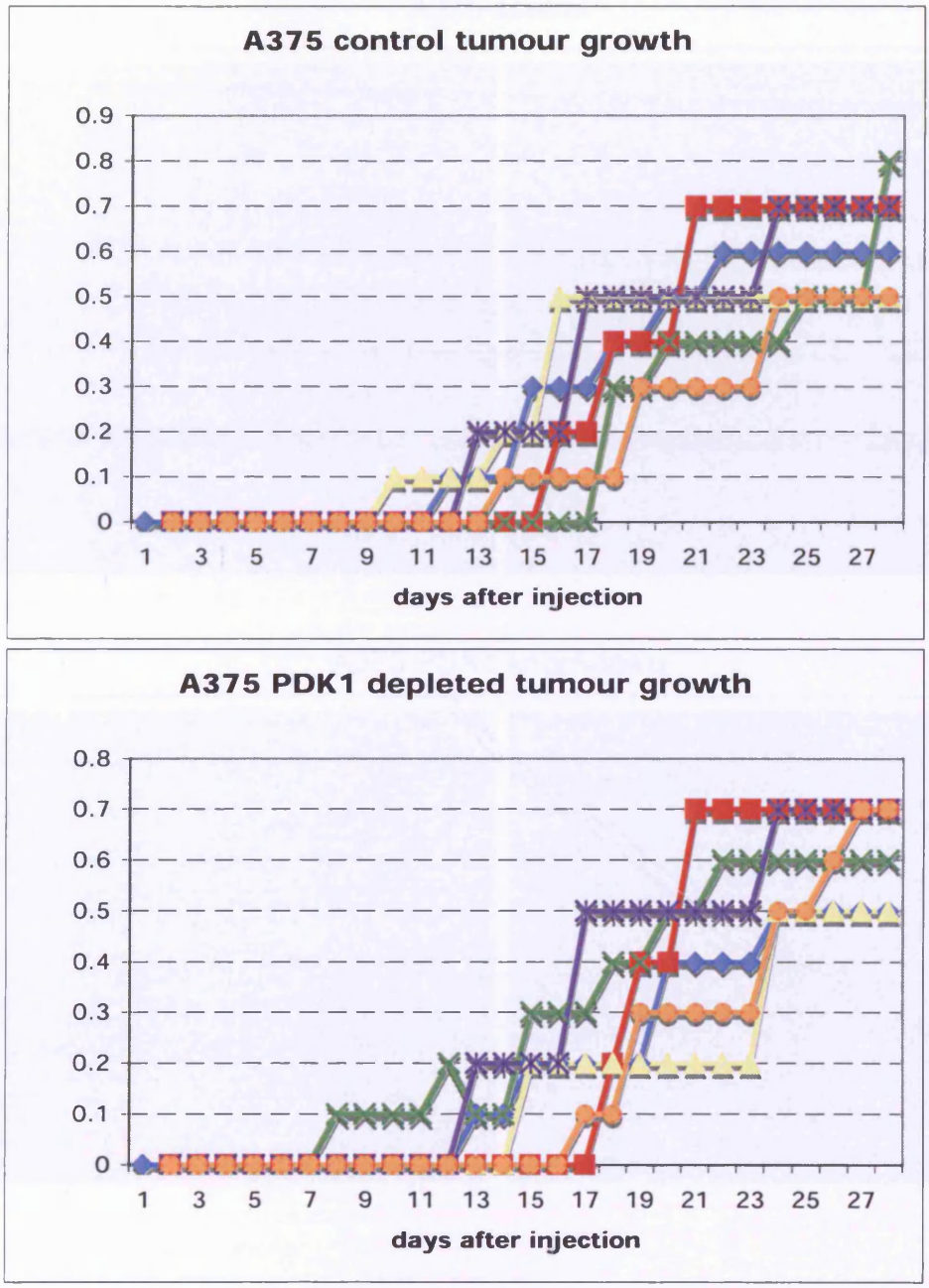

Figure 6.7 Growth of A375 GFP MLC xenograft tumours in nude mice. Shown above are measurements of 5 examples of control tumours and PDK1 depleted tumours. Tumours growth was measured and recorded every 2-4 days by the biological resources unit staff. Graphs show the maximum measured diameter in mm plotted against the number of days after injection.

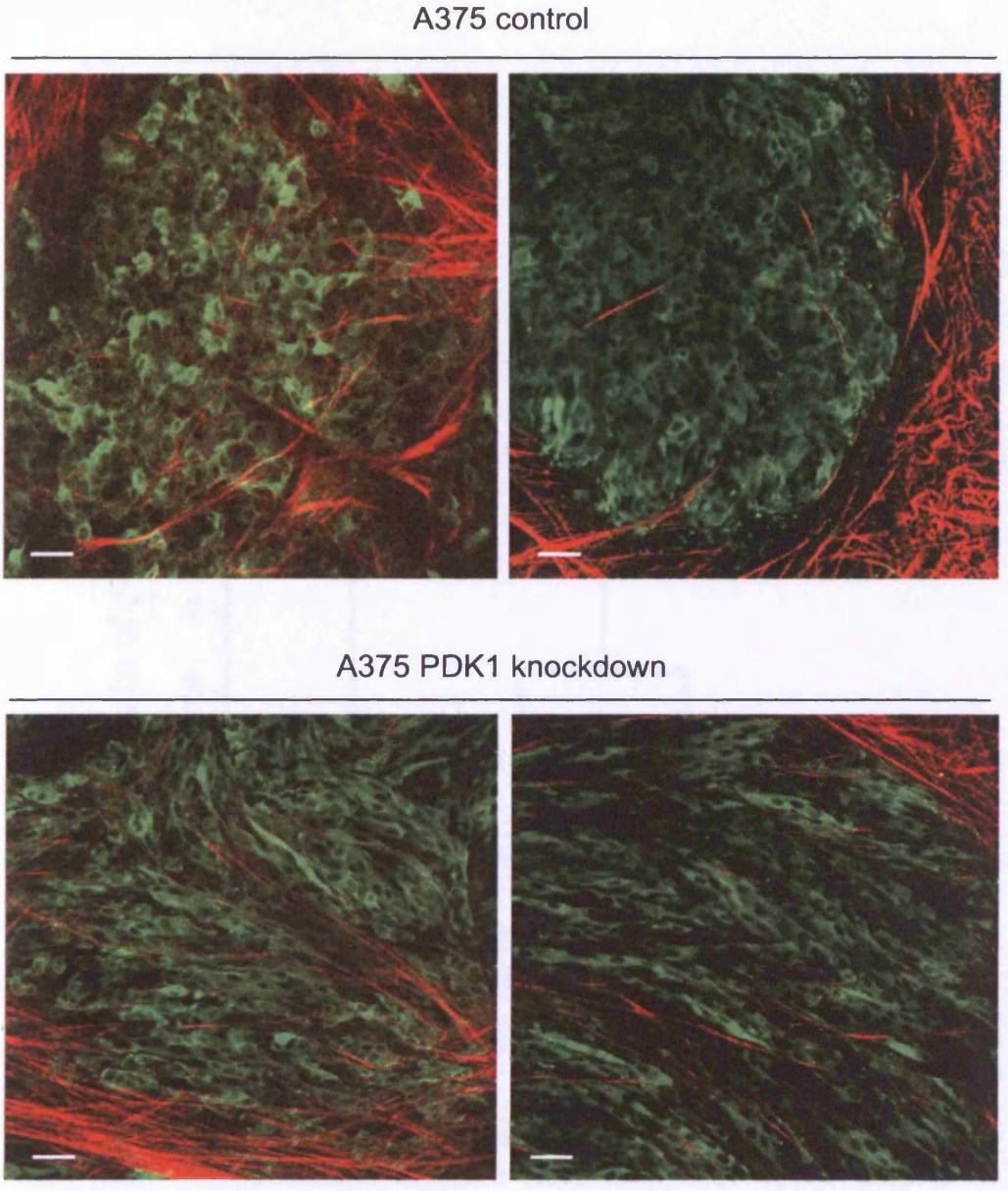

Figure 6.8 Cell morphology of A375 GFP-MLC tumours in vivo. Images of subcutaneous tumours in live nude mice. Tumours are imaged using multi-photon confocal microscopy. Cells expressing GFP-MLC are shown in green. Collagen fibres are shown in red and are imaged using second harmonic signal. Scale bar indicates 50 μm (images are from tumours imaged by Erik Sahai)

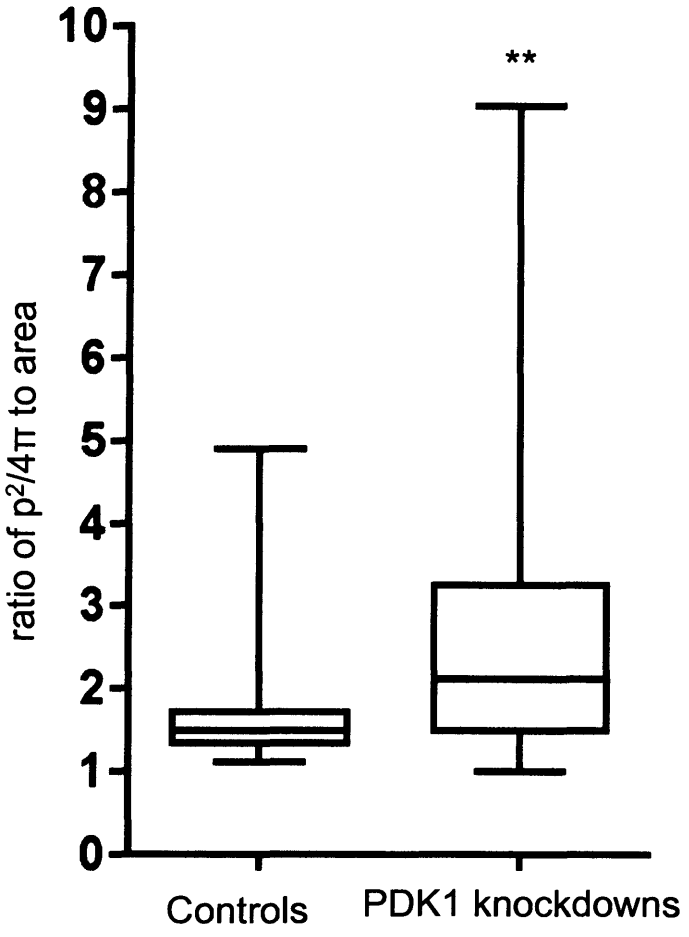

Figure 6.9 Quantification of cell morphology in vivo. A375 GFP-MLC subcutaneous tumours were analysed. Upper graphs shows cell morphology as quantified by the ratio (perimeter)2/(2πarea). Cells were drawn around manually and perimeter and area were calculated using Volocity software. Over 400 cells were analysed for each condition. ** indicates $p<0.001$ (Mann Whitney U test).

6.4 PDK1 depleted tumours show reduced cell motility in vivo

6.4.1 Quantification of cell movement events in primary tumours

A375 cells in xenograft tumours were visualised by their expression of GFP MLC as above. The first observation was that A375 cells within the tumour are mostly non-motile. Only approximately 1% of imaged cells were able to move.

20 different areas from 4 mice growing control tumours and 4 mice containing PDK1 depleted tumours were analysed. The mean number of movement events observed in control tumours was approximately 3 (per mm^2, per hour), which is similar to the control data for the tumours treated with PBS in the previous analysis (Figure 6.1). These data sets are slightly complicated to analyse as they are not normally distributed, and many tumour areas showed no motility at all in the period of imaging. Despite the large variation in cell motility between different areas of control tumours, it was clear that PDK1 depleted tumours showed much less cell motility (Figure 6.10). The average number of movement events in PDK1 deleted tumours was less than 0.5 (per mm^2, per hour), around 6 fold less than in the controls. Many imaged areas of PDK1 depleted tumours showed no movement events at all, and areas with many cells moving within the same area were never observed (please see accompanying supplementary movies for examples of cell motility in vivo).

6.4.2 Analysis of different types of cell movement

In control tumours, over half of all movement events were classified as rapid amoeboid movement, compared to just a quarter of movement events in PDK1 depleted tumours (Figure 6.11). The majority of movement events in PDK1 depleted tumours fell in the elongated/protrusions category, a larger proportion than in the control tumours (~40%). Chaotic/blebbing motility was the least common type of cell motility in both control tumours and PDK1 depleted tumours.

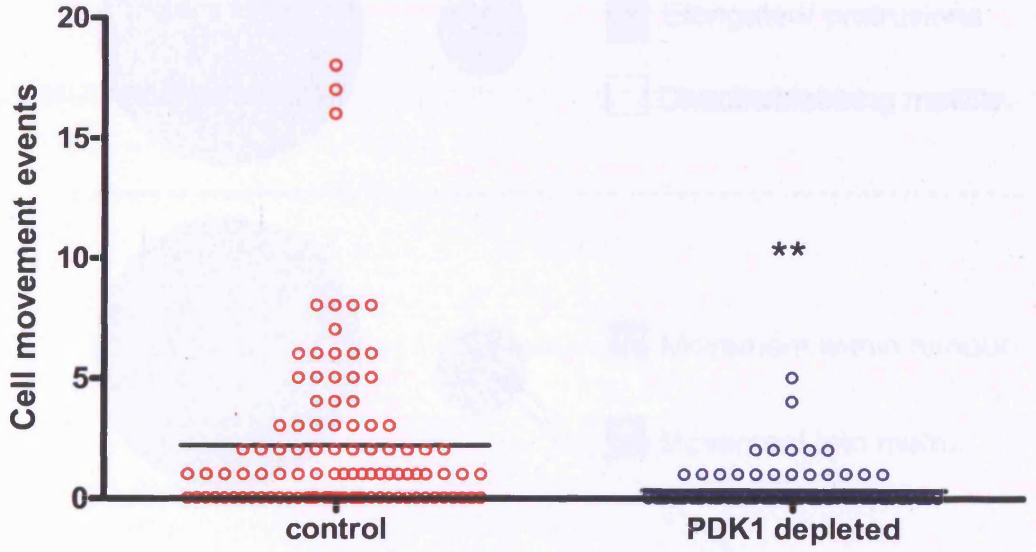

Figure 6.10 Quantification of cell motility in vivo. A375 GFP-MLC subcutaneous tumours were analysed. graph shows quantification of cell movements from over 20 different areas of tumours from 4 control and 4 PDK1 knockdown tumours. Data is normalised to movements events per mm2 per hour. ** indicates $p<0.001$ Mann Whitney U test. Please see supplementary movies for examples of cell motility in vivo.

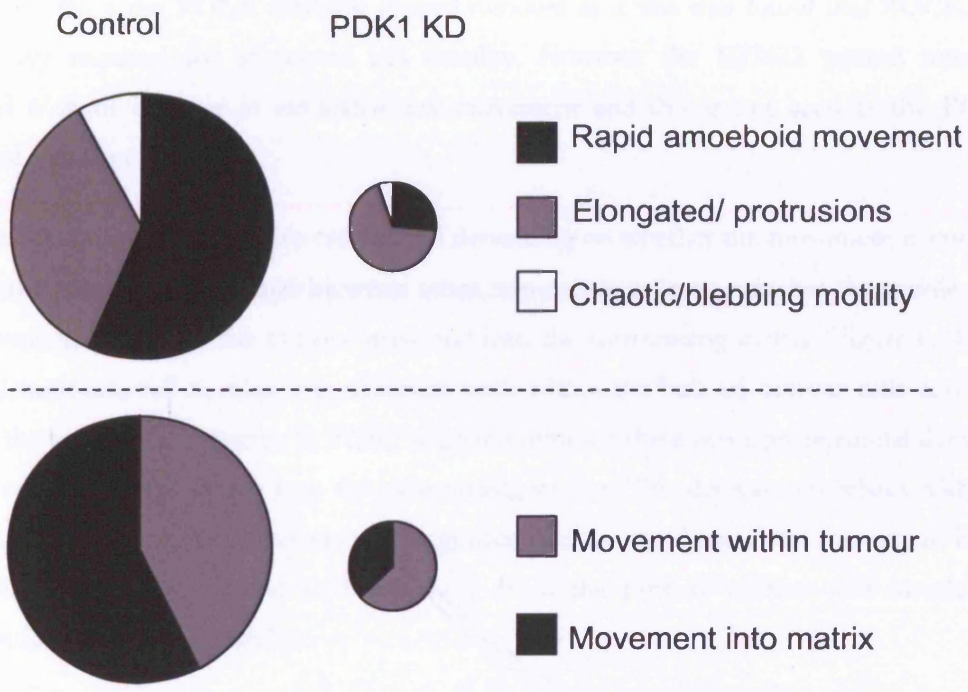

Figure 6.11 Analysis of types of cell motility observed in A375 tumours in vivo. Cell movement events were classified in the categories above depending on the type of cell movement and whether this movement was observed within the tumour or moving away from the tumour into the surrounding matrix.

Even though there was a significant reduction in overall cell motility, there was an even higher proportional difference in the numbers of cells exhibiting rapid amoeboid motility. This further indicates that PDK1 is specifically required for amoeboid cell movement, and that cells lacking PDK1 are still capable of extending protrusions. These data are similar to the results from the ROCK inhibitor treated tumours as it was also found that ROCK was specifically required for amoeboid cell motility. However the Y27632 treated tumours showed a slight increase in elongated cell movement and this is not seen in the PDK1 depleted tumours.

Movement events were also sub-categorised depending on whether the movement event was within the primary tumour and between other non-motile cells, or whether the motile cells were moving outside of the tumour mass and into the surrounding matrix (Figure 6.11). In control tumours, cell motility was observed both within the bulk of tumour cells and also within the surrounding matrix. In PDK1 depleted tumours there was a proportional decrease in the cell movement events into the surrounding matrix. This decrease correlates with the decrease in rapid amoeboid movement, suggesting that the rapid amoeboid movement is the type of cell motility required to break away from the primary tumour and invade the surrounding matrix successfully.

6.5 PDK1 depleted cells are less able to colonise lungs and form metastases

6.5.1 Lung colonisation of A375 cells

To determine whether the reduced cell motility that had been observed in PDK1 depleted cells in vitro and in vivo might also impact the overall metastatic potential of these cells, the ability of A375 cells to colonise the lungs of mice was determined. $1x10^6$ GFP-MLC A375 cells (control or stably PDK1 depleted as previously described) were injected into the tail vein of nude mice in 100 µl PBS. After 4 weeks, the lungs of these mice were removed and the number of metastases was determined by fluorescence imaging. After 4 weeks we found that very few metastases had begun to form, and in most mice, no metastases were found (Figure 6.12). It may be because A375 cells are not able to survive transit in the blood circulation. This was surprising considering that published data had shown that A375 cells should be capable of colonising the lungs [66]. Perhaps the A375 cells we used for these

experiments were altered from the originally described cell lines due to time in cell culture conditions. Although this experiment did not yield statistically significant results, there were no metastases at all in any of the mice injected with PDK1 depleted cells, suggesting that this might be worth investigating further.

The ability of A375 cells to lodge in the lungs and extravasate was compared in a short-term assay. Control and PDK1 depleted A375 cells were labelled with either red or green cell tracking dyes and mixed in equal numbers before injection into the tail vein of nude mice. As an internal control, control cells were dyed both red and green then mixed and injected as above. This would indicate if there were any effects of the different dyes on the ability of cells to extravasate, lodge and survive in the lungs, or whether there was any bias in which colour cells were more visible and therefore counted more often. 4 hours after i.v. injection, the lungs were removed and imaged as above (Figure 6.12). The ratio of PDK1 depleted cells to control cells was counted and calculated for each of 20 20X fields, then averaged and standardised to control vs. control, to account for differences in detecting red or green cells. The actual value for control versus control was 1.12, showing that they are roughly equal as would be expected. Observing cells at a 4 hour time point meant that there were more cells to count and it was therefore possible to determine whether any differences were statistically significant. In mice injected with a mixture of control and PDK1 depleted cells, there was a smaller number of PDK1 cells than control cells per field, although the reduction was only marginal, and the numbers of cells were relatively small, it was statistically significant ($p<0.05$).

6.5.2 Short-term lung metastasis assay MTLn3E cells

To see whether PDK1 could affect the extravasation and lung colonisation in other cell lines, the short-term lung metastasis assay was repeated using MTLn3E cells that are more effective at colonising the lungs than A375 cells. The MTLn3E cells were stably expressing the membrane labels CAG-gap Cherry, or CAG-gap eGFP, and were then transiently transfected with either non-targeting control siRNA oligos or PDK1 targeting siRNA oligo 2. The two different coloured MTLn3E cells were mixed in equal numbers and $1x10^6$ cells were injected into the tail vein of nude mice in 100 µl PBS. To ensure no bias from the different sensitivity of the different fluorescent labels, the experiment was performed both ways around, with the control cells labelled green or red on different occasions. 2 hours after

injection half of the mice were culled and their lungs were imaged (Figure 6.14). At this time point equal numbers of both control and PDK1 depleted cells were observed in the lungs and they appeared to be localised in small capillaries. However after 24 hours, significantly more control cells than PDK1 depleted cells had entered the lung tissue; the ratio of control to PDK1 depleted cells was around 7:3.

The colonisation of the lung assays suggested that PDK1 also played a role in other stages of the metastatic process. It is difficult to determine the exact role as successful colonisation of the lungs might require several factors such as survival in the blood stream, cell motility for extravasation, and also survival in a new host tissue. These mechanistic issues remain unanswered at present.

Cell line injected I.V.	repeat	Number of lung mets.
A375 GFP-MLC parental polyclonal	1 2 3	1 1 0
A375 GFP-MLC pSuper control clone	1 2 3	1 0 0
A375 GFP-MLC pSuper PDK1 shRNA clone 3	1 2 3	0 0 0
A375 GFP-MLC pSuper PDK1 shRNA clone 8	1 2 3	0 0 0

Figure 6.12 Number of lung metastases arising 4 weeks following tail vein injection of A375 cells. 1 x 10^6 A375 cells stably expressing GFP-MLC and pSuper retro containing either an empty control cassette or PDK1 targeting cassette were injected in 100µl PBS into tail veil of nude mice. 3 mice were used for each cell line tested. 4 weeks following injection mice were sacrificed, the lungs were removed and imaged to determine the number of lung metastases arising.

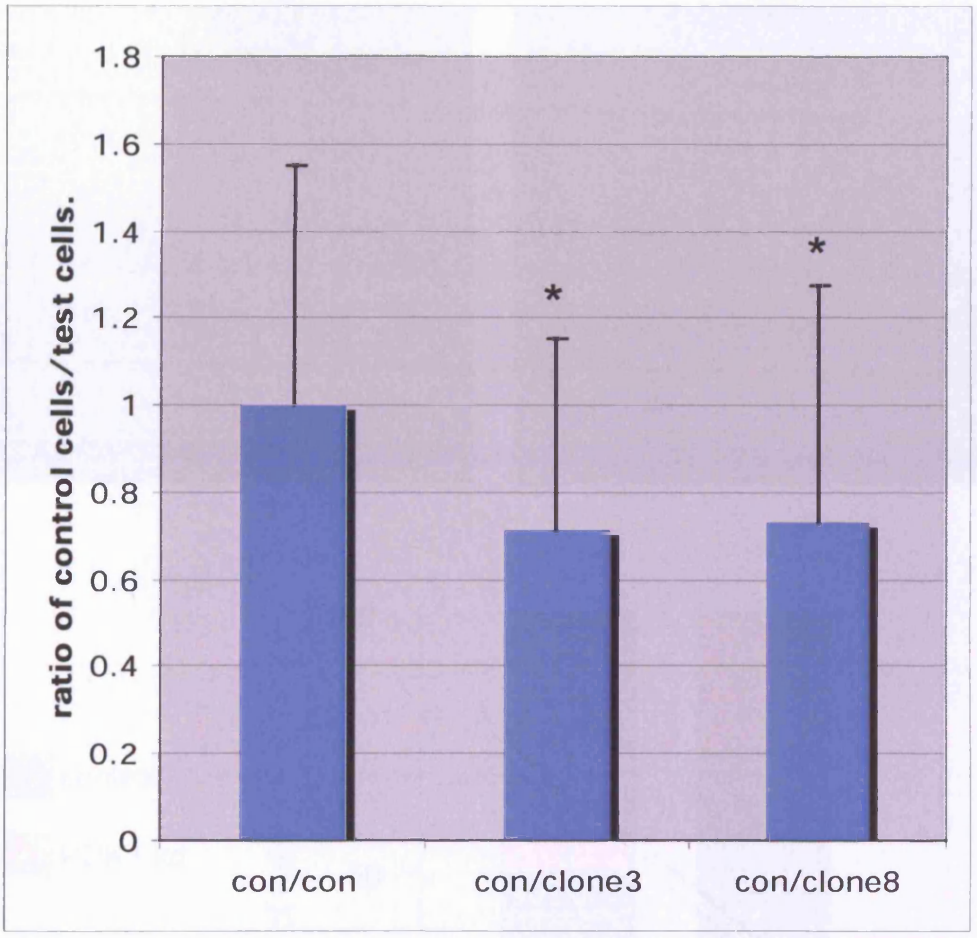

Figure 6.13 Comparison of the ability of A375 cells to lodge and extravasate into lungs in short term assay. A375 cells stably expressing GFP-MLC and pSuper retro containing either an empty control cassette or PDK1 targeting cassette were labeled with either cell trackers dyes SNARF1 or CFSE in suspension in vitro. Equal numbers of control and PDK1 KD cells were mixed and a total of 1 x 10^6 were injected in 100µl PBS into tail veil of nude mice. Control (green) mixed with control (red) was used to standardise differences between the sensitivity of the dyes. The ratio of control cells to test cells is shown in the graph, normalised to control versus control (Actual value for control versus control was 1.12). * indicates $p<0.01$ T Test.

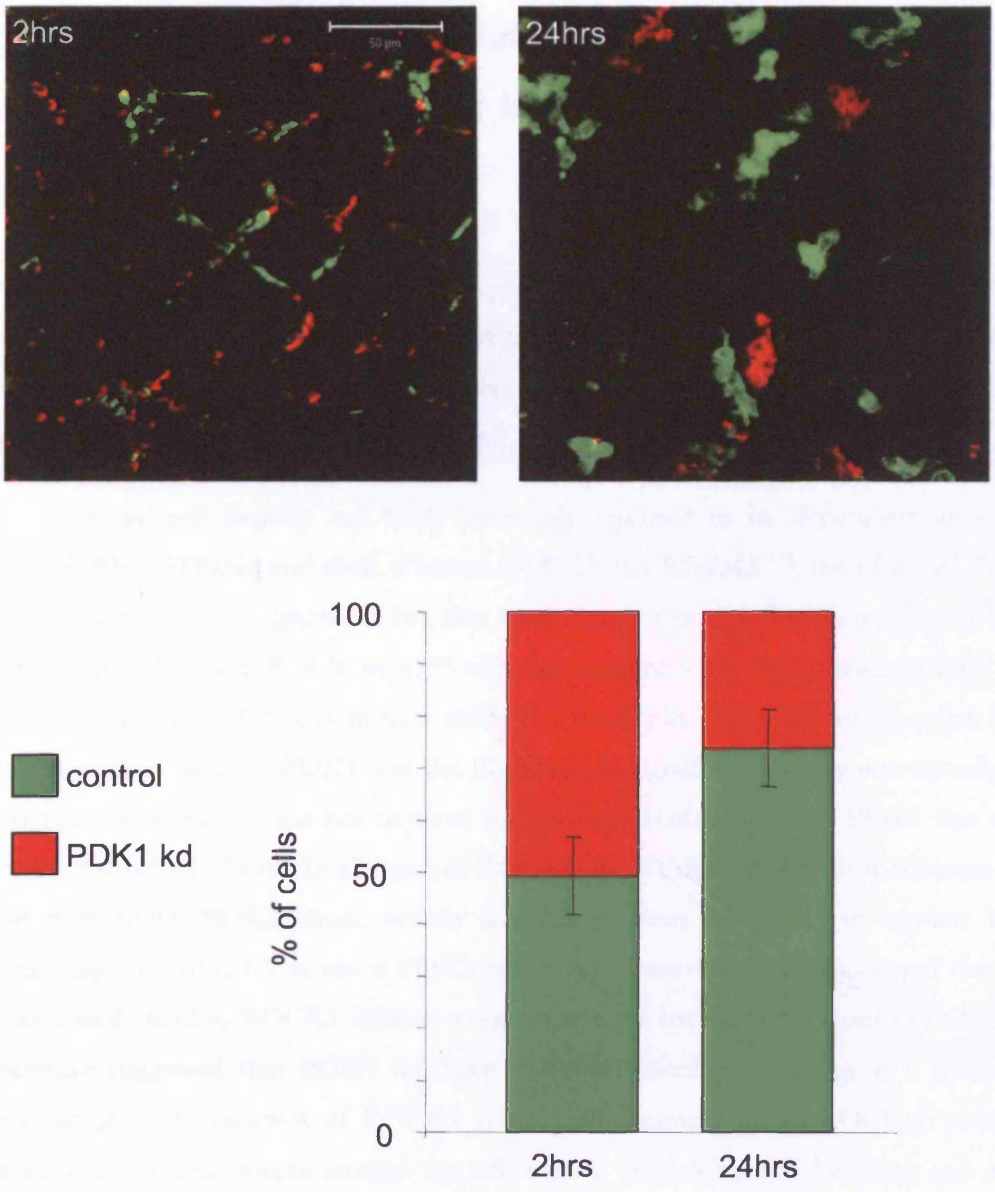

Figure 6.14 Analysis of the ability of MTLn3E cells to colonise the lungs following i.v. injection. MTLn3E cells labeled with either GFP or Cherry were transiently transfected with either control siRNA(GFP) or PDK1 targeting siRNA(Cherry). The two populations were mixed in equal numbers and 500 000 cells were injected into the tail vein of nude mice. The lungs were dissected at 2 and 24 hours and the numbers of GFP and Cherry cells were compared. Scale bar indicates 50 microns.

7 Chapter 7 - PDK1 regulates ROCK1 localisation independently of PDK1 kinase activity

7.1 Chapter Summary

Having determined that PDK1 was required for the regulation of cortical F-actin and rounded cell morphology, and furthermore that PDK1 depletion significantly reduced cancer cell motility both in vitro and in vivo, it was then interesting to continue this investigation to try to elucidate a mechanism through which PDK1 was causing these effects.

As amoeboid cell motility has been previously reported to be dependent on signalling through Rho GTPases and their effectors ROCK1 and ROCK2 [154], the effect of PDK1 on this pathway was investigated. It has also been shown that the phosphorylation of MLC is controlled by Rho and ROCK in A375 cells (see chapter 5 – siRNA screen results) [170]. Cells lacking PDK1 were defective in their ability to correctly localise and phosphorylate MLC so the interaction between PDK1 and the Rho/ROCK signalling pathway was investigated. It was found that PDK1 was not required for RhoA activation, but that PDK1 was required for the correct membrane localisation of ROCK1. PDK1 did not alter ROCK kinase activity and furthermore PDK1 kinase activity was not required for PDK1 to regulate ROCK1 suggesting that ROCK1 is not a PDK1 substrate. However it was discovered that PDK1 does directly bind to ROCK1 utilising a sequence in the hydrophobic motif of ROCK1. It is therefore suggested that PDK1 regulates amoeboid motility by acting as a scaffold and promoting the localisation of ROCK1 at the cell periphery where ROCK is able to co-ordinate contractile forces around the cell cortex, promoting cell blebbing and allowing amoeboid motility.

7.2 PDK1 regulates MLC organisation and phosphorylation in A375 cells

7.2.1 Depletion of PDK1 causes mislocalisation of pMLC

Contractile forces require polymerised actin to incorporate myosin in non-muscle cells. The limiting step in this process is the phosphorylation of the myosin light chain, which

completes the machinery and allows contraction [165]. Having seen that depletion of PDK1 disrupted the cortical actin organisation and the ability of amoeboid cells to contract and form membrane blebs, the effect of PDK1 on the phosphorylation of myosin light chain (MLC) was examined. A375 cells were transfected with either control or PDK1 targeting oligos and then plated on collagen/matrigel gels. The localisation of phosphorylated myosin light chain was determined by I.F. using antibodies against both the single (S19) and double (T18S19) phosphorylated forms (Figure 7.1). In control cells both pMLC and ppMLC are localised around the cell cortex in a similar arrangement to what was observed for actin staining. Both actin and pMLC were seen in the cell cortex but were not present in blebs that appeared to be comprised of mostly membrane and little actin. When PDK1 was knocked down, the cell became more elongated and pMLC/ppMLC was no longer efficiently localised to the cell cortex. pMLC and ppMLC were more diffusely localised in the cytoplasm or in patches at the tips of protrusions (Figure 7.1). The total levels of pMLC/ppMLC also seemed reduced overall compared to the controls. The reduction and mislocalisation of MLC could explain the less contracted cell morphology and reduced blebbing motility observed.

7.2.2 Depletion of PDK1 causes reduction in levels of pMLC in both 2D and 3D culture conditions

The I.F. analysis of MLC suggested that the phosphorylation of MLC was impaired when PDK1 was knocked down. A375 cells plated on collagen/matrigel and depleted of PDK1 were analysed by western blot for levels of pMLC (S19). As seen by I.F., western blot analysis confirmed that pMLC was indeed reduced by 60-70 % in PDK1 depleted cells compared to controls (Figure 7.2). Reduced pMLC could either be a cause or a consequence of changes in cell morphology.

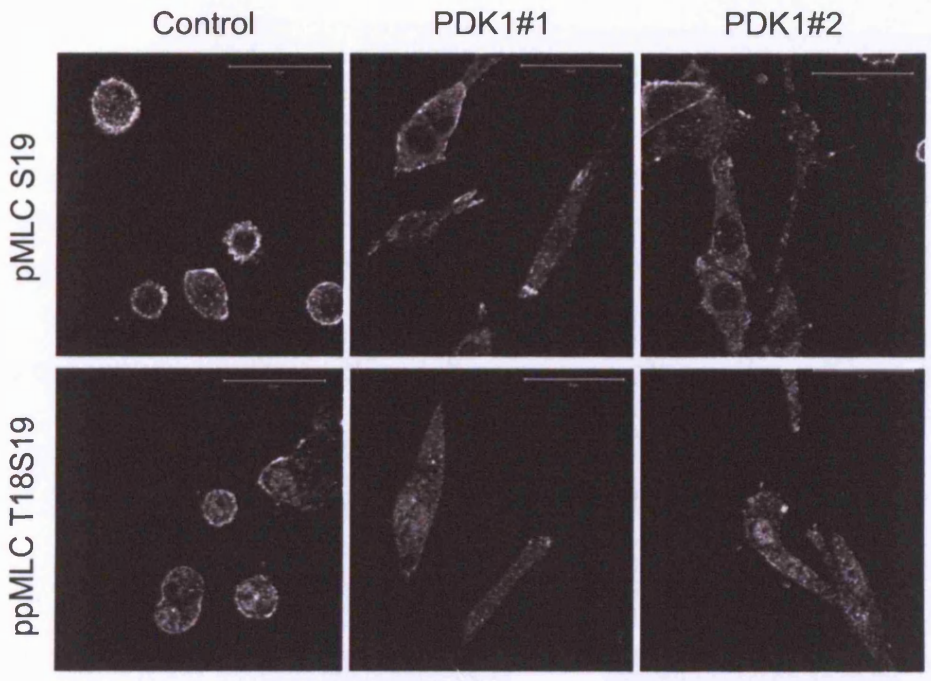

Figure 7.1 Immunofluorescence showing pMLC and ppMLC are mislocalised when PDK1 is depleted. A375 cells were transfected with either control or PDK1 targeting siRNA prior to plating cell on 3D matrix. 24 hours later cells were fixed and stained for pMLC and ppMLC. Scale bar indicates 50 μm.

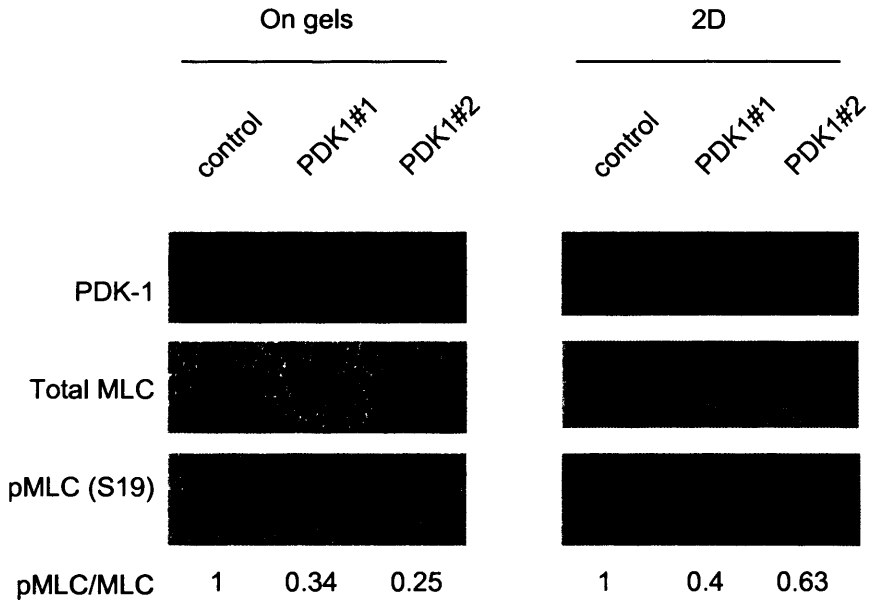

Figure 7.2 MLC phosphorylation is reduced when PDK1 is depleted. Western blot analysis of A375 cell lysates taken from both 2D and 3D culture. For 3D conditions, cells were plated onto a layer of collagen/matrigel matrix similar to that used for the analysis of morphology. Cells lysates were used to determine the levels of pMLC. The ratios of pMLC/total MLC were calculated by measuring densitometry and are shown beneath the blots.

To answer this question, levels of pMLC were analysed in A375 cells plated on a 2D substrate where no change in morphology is observed when PDK1 is depleted. Even in the absence of changes in cell morphology there is a still approximately a 50% reduction (Figure 7.2) in levels of pMLC meaning that reduced phosphorylation of MLC is likely to be an initiating event and the probable cause of the changes in morphology seen when cells are on 3D deformable microenvironments.

7.3 Deletion of PDK1 does not impair activation of RhoA

PDK1 could be signalling to contractile machinery by interfering with the activation of RhoA. To test this the levels of RhoGTP were measured in A375 cells. A375 cells were plated onto cell culture dishes and transfected with either control or PDK1 siRNA oligos. Cells were serum starved for 12 hours then stimulated with 20 % serum for 5 minutes. Cell lysates were taken from these cultures and the lysates were incubated with GST-RBD Rhotekin to pull down the active, GTP-bound RhoA. Under these conditions there was no obvious decrease in the levels of active RhoA. If anything there was a slight increase in active RhoA when PDK1 was depleted (Figure 7.3). This means that insufficient activation of RhoA is not the cause of the elongated morphology and reduced cell motility that is observed when PDK1 is depleted. So that even with high levels of activated RhoA, signalling downstream, leading to contractility, is disturbed when PDK1 is depleted.

7.4 ROCK1 localisation is altered when PDK1 is depleted

7.4.1 Over-expression of ROCK1 and ROCK2 in PDK1 depleted cells

A375 cells when plated on a rigid 2D substrate such as glass appear as spread cells with some stress fibres. When ROCK is over expressed the contractile forces in the cell are increased and are able to overcome the adhesions holding the cell flat. This causes the cell to become rounded and exhibit membrane blebs. The function of ROCK kinases can be tested using this assay (as described in chapter 3). As it had been seen that the activation of RhoA was not inhibited when PDK1 was depleted, the effect of PDK1 depletion on the ability of ROCK to cause cell rounding and blebbing was analysed.

Figure 7.3 RhoA activation in A375 cells depleted for PDK1. A375 cells were transfected with either control, PDK1 targeting siRNA and plated onto 10cm cell culture dishes. 48 hours following transfection cells were serum starved over night then serum stimulated for 5 minutes. Cell lysates were incubated with glutathione agarose beads bound to GST rhotekin RBD to pull down GTP-bound RhoA. Results of pull downs were analysed by western blot and levels of RhoA GTP were compared to levels of total RhoA in the cell lysate.

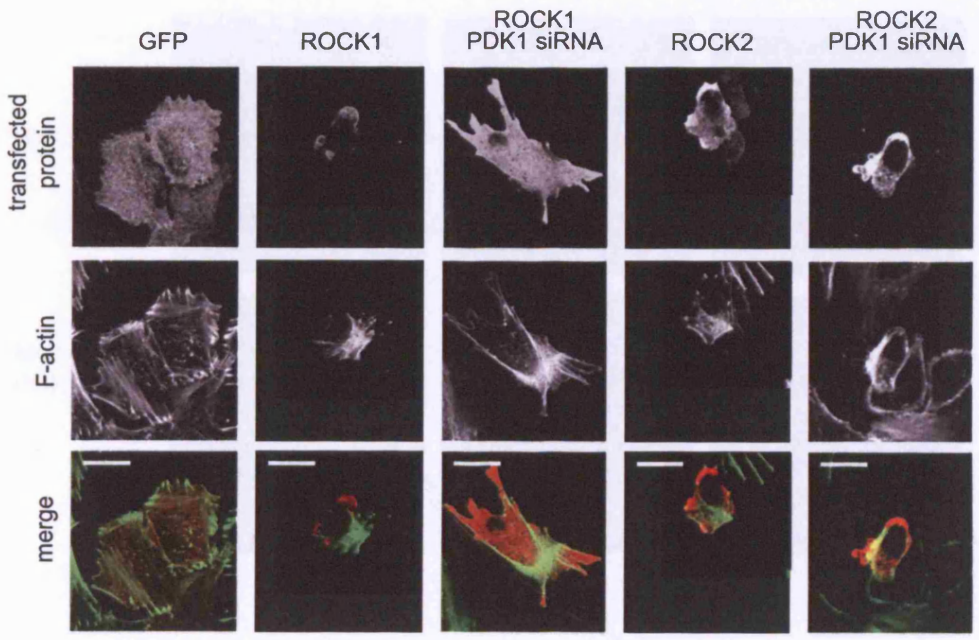

Figure 7.4 PDK1 is required for ROCK1 membrane localisation and ROCK1 driven membrane blebbing in A375 cells. A375 cells were transfected with either control or PDK1 targeting siRNA. 24 hours later cells were transfected with myc-ROCK1 or ROCK2 constructs. 24 hours later cells were fixed and stained with 9E10 and FITC phalloidin. Scale bar indicates 20 μm.

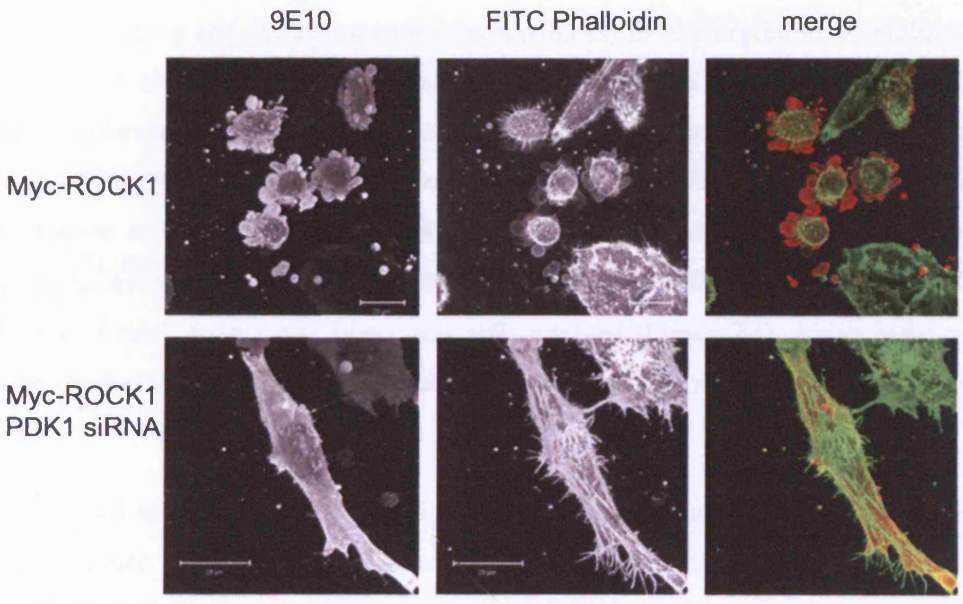

Figure 7.5 PDK1 is required for ROCK1 membrane localisation and ROCK1 driven membrane blebbing in A375 cells. A375 cells were transfected with either control or PDK1 targeting siRNA. 24 hours later cells were transfected with myc-ROCK1 and plated onto 3D collagen/matrigel matrix. 24 hours later cells were fixed and stained with 9E10 and FITC phalloidin. Scale bar indicates 20 μm.

Transfection of either ROCK1 or ROCK2 resulted in membrane blebbing in approximately 60% of A375 cells transfected with control siRNA, compared to around 10% of A375 cells transfected with GFP as a control (Figure 7.4, 7.5, 7.6). However the ability of ROCK1 to cause membrane blebbing was dramatically reduced when A375 cells had previously been transfected with siRNA oligos targeting PDK1. Interestingly, the ability of ROCK2 to cause membrane blebbing and cell contraction was unaffected by the depletion of PDK1 (Figure 7.4, Figure 7.6). In control cells, the over-expressed myc-ROCK1 was mostly localised at the plasma membrane and this localisation correlated with the phenotype of membrane blebbing. When PDK1 was absent, the over-expressed myc-ROCK1 was localised either in the cytoplasm or in unidentified puncta within the cell, which may be a kind of vesicle. Interestingly, even though membrane blebbing was reduced in the absence of PDK1, the generation of thick actin stress fibres was still observed (Figure 7.4), which indicated that although the localisation of ROCK1 is altered in the absence of PDK1, it is retaining some activity.

The same assay was carried out in A375 cells plated on collagen/matrigel gels to determine how the rigidity of the matrix affected the cell morphology of cells over-expressing ROCK1(Figure 7.5). Over-expression of myc-ROCK1 in these conditions causes very dramatic cell blebbing, perhaps because the matrix is deformable, the result of increased contractile forces is more readily converted to cell rounding, whereas on rigid substrates, contraction is mostly seen as increases in tension and thickening of stress fibres. When myc-ROCK1 was over expressed in A375 cells depleted of PDK1 plated on collagen/matrigel matrix, the cells still remained elongated and actin filaments ran from one end to the other, indicating the lack of contractile forces when PDK1 is absent. Numerous actin rich filopodium-like structures were also observed (Figure 7.5).

7.4.2 Localisation of endogenous ROCK1 is altered in the absence of PDK1

To test whether PDK1 also regulated the localisation of endogenous ROCK1, A375 cells transfected with a control siRNA or PDK1#1 siRNA plated on glass coverslips were fixed and stained for endogenous ROCK1 (Figure 7.7). The actin cytoskeleton was visualised with FITC phalloidin.

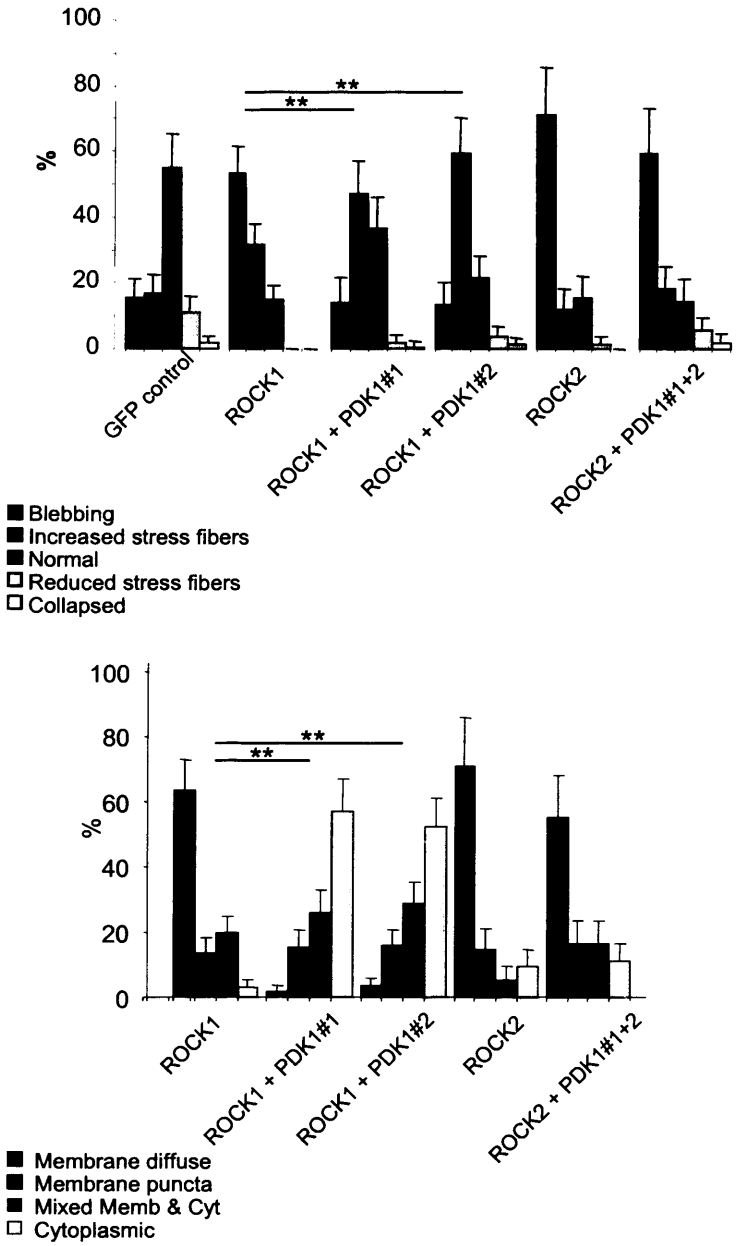

Figure 7.6 Quantification of phenotypes of myc-ROCK1 and myc-ROCK2 over-expressed in A375 cells transfected with either control or PDK1 siRNA oligos. A375 cells were transfected with either control or PDK1 targeting siRNA. 24 hours later cells were transfected with myc-ROCK1 or ROCK2 constructs. 24 hours later cells were fixed and stained with 9E10 and FITC phalloidin. Cells were counted and allocated into categories for f-actin organisation and ROCK construct localisation as described in figure 3.6. ** indicates $p<0.001$ (Chi squared tests).

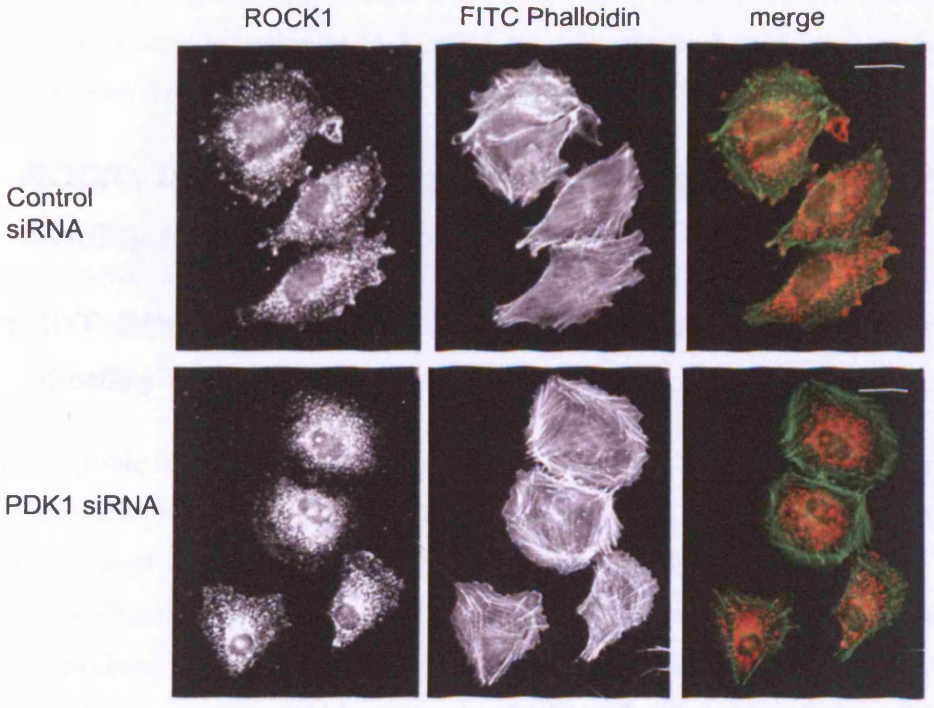

Figure 7.7 PDK1 is required for membrane localisation of endogenous ROCK1. A375 cells were transfected with either control of PDK1 targeting siRNA oligos and plated onto glass cover slips. 48 hours later cells were fixed and stained with an antibody against endogenous ROCK1 and FITC phalloidin. Scale bar indicates 20 μm.

Endogenous ROCK1 localised in the cell periphery in control transfected cells. This peripheral localisation was reduced in A375 cells transfected with PDK1#1 siRNA. As noted previously, knockdown of PDK1 in A375 cells on rigid substrates did not alter cell morphology. Similar analysis of the localisation of endogenous ROCK1 in A375 cells plated on deformable collagen/matrigel matrix was carried out by Erik Sahai and it was shown that under these conditions endogenous ROCK1 was also localised to the cell periphery and colocalised with a membrane marker [233].

7.5 ROCK1 is unable to co-ordinate contractile forces and cell motility in the absence of PDK1

7.5.1 GFP-ROCK1 localises at the rear of blebbing cells to coordinate motility

To gain dynamic insight into how the localisation of ROCK1 co-ordinates contractile forces and membrane blebbing, GFP-ROCK1 was transfected into A375 cells plated on collagen/matrigel matrix, and these cells were then imaged individually by confocal microscopy (Figure 7.8). In control cells where PDK1 expression was not altered, GFP-ROCK1 localised to the plasma membrane and membrane blebbing was observed. The contractile forces cause large blebs to be rapidly formed and as a result the cell body was translocated at speeds of up to 5 microns per minute. Although the cells imaged were rapidly changing direction, during translocation in any direction, GFP-ROCK1 accumulated at the back of the cell as shown in the kymograph in Figure 7.8 (see also supplementary movie 7.8).

When PDK1 was depleted, A375 cells were elongated as had been previously seen. In PDK1 depleted cells, GFP-ROCK1 was distributed in the cytoplasm and sometimes at the cell periphery, however the over-expression of GFP-ROCK1 did not cause the cells to bleb as in control cells (note examples in Figure 7.8 iii and iv and in the accompanying supplementary movies). This corresponds with the results of over-expressing myc-tagged ROCK1 in A375 cells depleted of PDK1.

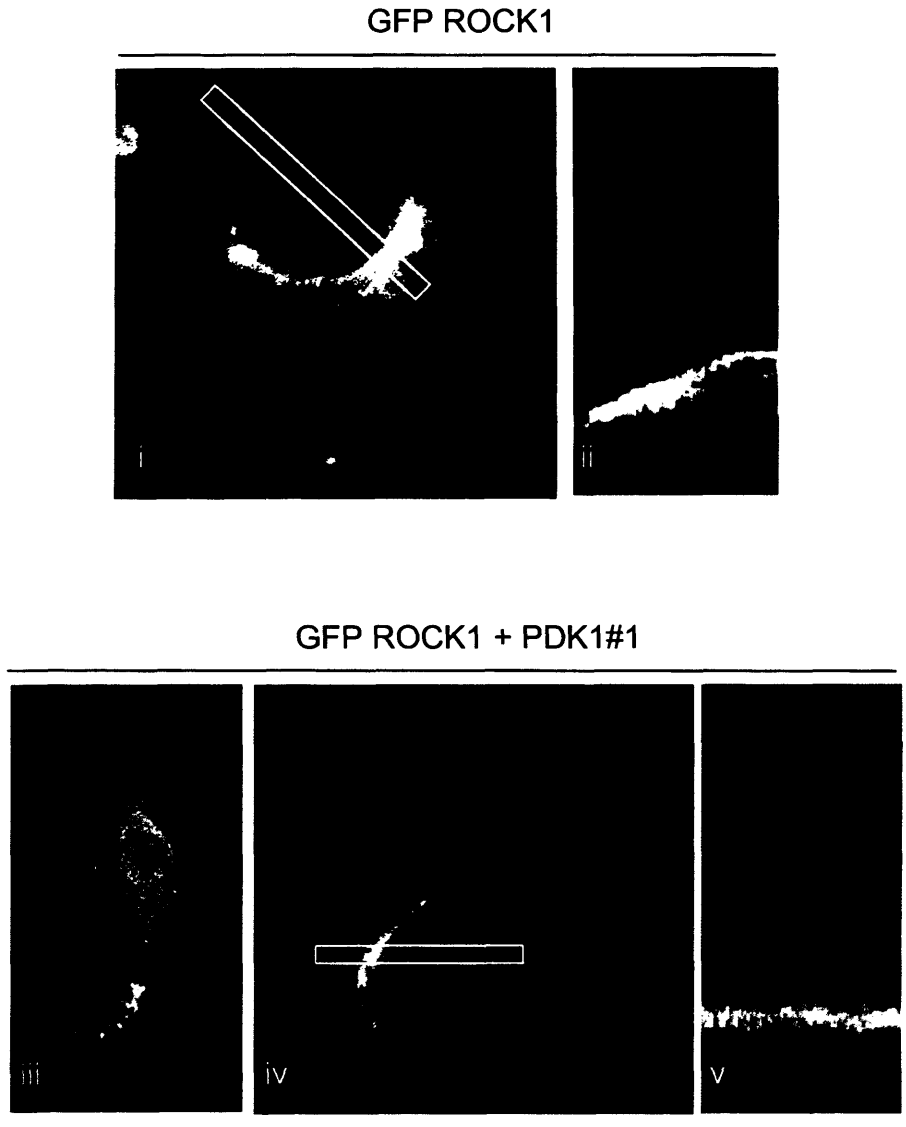

Fig 7.8 Dynamic analysis of GFP-ROCK1 localisation in control or PDK1 depleted cells. A375 cells were transfected with either control of PDK1 targeting siRNA and subsequently transfected with GFP-ROCK1. The cells were then plated in a 3D matrix and imaged by confocal microscopy at a rate of 1 frame every 3 seconds. Highlighted sections indicated slices of the image used to generate kymographs in panels ii and iv. Panels iii and iv show the range of localisation seen when GFP-ROCK1 is expressed in A375 cell depleted of PDK1.

Even in cases where GFP-ROCK1 was localised asymmetrically at the cell periphery, this did not result in translocation of the cell body (shown in kymograph in Figure 7.8). These results confirm that PDK1 is required for the correct localisation of ROCK1 and that when ROCK1 is not correctly localised, it is not able to coordinate contractile forces for amoeboid movement.

7.6 PDK1 does not alter ROCK1 kinase activity

Results have indicated that PDK1 is required for the correct localisation and function of ROCK1. ROCK1 is a member of the AGC family of kinases and other members of this family such as PKB/Akt have been shown to be phosphorylated by PDK1 in the activation loop and/or the hydrophobic motif. One possibility is that PDK1 is required to modify ROCK1 to activate ROCK1 kinase activity. Although results from chapters 3 and 4 show no data to support the hypothesis that ROCK1 is phosphorylated in either the activation loop or the hydrophobic motif, results in this chapter suggested that it was worth testing in an additional assay.

7.6.1 Effect of addition of PDK1 to ROCK1 kinase activity

To confirm that PDK1 did not regulate ROCK1 by activating ROCK1 kinase activity, recombinant ROCK1 was used to phosphorylate recombinant MLC either with or without the addition of exogenous PDK1 (Figure 7.9). If PDK1 was able to modify ROCK1 and increase its kinase activity then this could explain the reduction in cell contraction and blebbing when PDK1 was depleted. However the addition of PDK1 did not alter the kinase activity of ROCK1. Furthermore, we were unable to detect any phosphorylation of ROCK1 by PDK1 in this assay, although PDK1 was able to strongly phosphorylate Akt under these conditions and so was active (Figure 7.10) (see also chapter 4 Figure 4.4).

7.6.2 Endogenous I.P. kinase assay

To confirm the results of the above experiments, it was tested whether the depletion of PDK1 affected the kinase activity of endogenous ROCK1. Endogenous ROCK1 was immunoprecipitated from A375 cells transfected with either control non-targeting oligos, or PDK1 targeting oligos (Figure 7.11). The isolated kinase was then used to phosphorylate recombinant MLC in vitro.

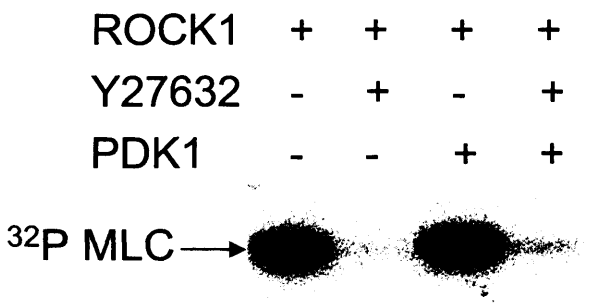

Figure 7.9 Recombinant ROCK1 does not have altered kinase activity in vitro in the presence of exogenous PDK1. Recombinant ROCK1 was used to phosphorylate recombinant MLC in vitro in the presence of ^{32}P-labelled ATP. The addition of recombinant PDK1 to the reaction did not alter the ability of ROCK1 to phosphorylate MLC in this assay

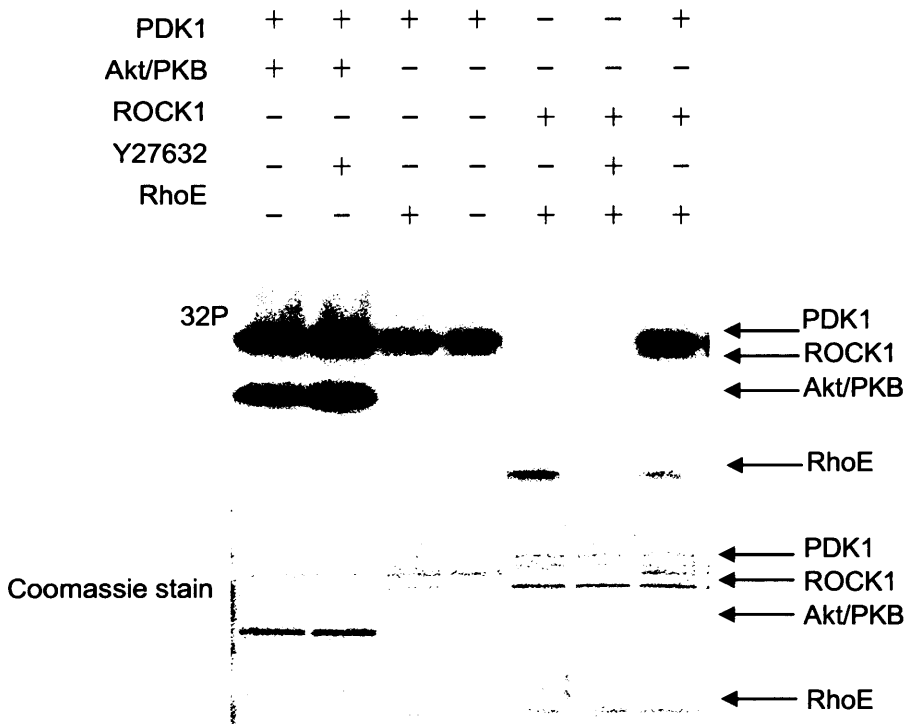

Figure 7.10 In vitro kinase assay showing the effect of addition of PDK1 on ROCK kinase activity. Recombinant PDK1 and ROCK1 were used to phosphorylate recombinant substrates (Akt/PKB, RhoE,). Degree of phosphorylation is shown by the incorporation of ^{32}P ATP. Total protein is shown by coomassie stain.

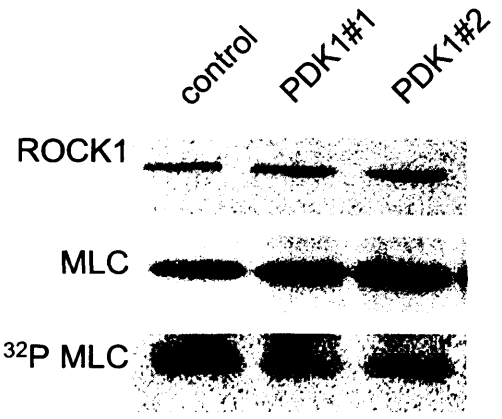

Figure 7.11 Endogenous I.P. kinase assay. ROCK1 phosphorylating recombinant MLC. Endogenous ROCK1 was immune precipitated from A375 cells which had been transfected with either control siRNA or PDK1 targeted siRNA. Endogenous ROCK1 was then used to phosphorylate recombinant MLC in vitro. Degree of phosphorylation was determined by the degree of incorporation of ^{32}P ATP.

There was perhaps a subtle decrease in kinase activity of ROCK1 to phosphorylate the substrate MLC when the kinase had been purified from cells depleted of PDK1, but this was almost undetectable in most repeats of this experiment, and it was unlikely that PDK1 was regulating ROCK kinase activity. This suggested that the loss of the rounded, blebbing phenotype was not caused by loss of ROCK kinase activity, but more likely a loss of membrane localisation, or a loss of activity only at the plasma membrane. ROCK1 can be active within cells and yet not able to co-ordinate blebbing motility. This is also the case when truncated ROCK1 is transfected into cells (see chapter 3). In vitro, truncated ROCK1 (1-727 a.a.) is more active that the wild type, but because it has no Rho-binding domain and cannot localise to the membrane, it remains in the cytoplasm and is only able to induce stress fibres instead of membrane blebbing. The generation of stress fibres and the lack of blebbing is also observed in cells over-expressing ROCK1 in the absence of PDK1.

To this point there is no evidence that PDK1 regulates the kinase activity of ROCK1, and there is also no evidence that ROCK1 is a substrate of PDK1 for modification by phosphorylation.

7.7 PDK1 kinase activity is not required for the regulation of ROCK1

7.7.1 Rescue of ROCK-driven cell blebbing with FLAG-PDK1 mutants

When PDK1 has been depleted from A375 cells, over-expressed ROCK is less able to drive contraction of the acto-myosin cortex and cause membrane blebbing. To rescue this loss of ROCK function, myc-ROCK1 was co-transfected with siRNA resistant FLAG-tagged PDK1 constructs into cells depleted of PDK1. WT, KD, and also PH-deleted PDK1 constructs were compared to gain insight into which properties of PDK1 were required for PDK1 to regulate ROCK1 (Figure 7.12).

Cells depleted for PDK1 and expressing both myc-ROCK1 and either WT or KD FLAG-PDK1 were able to exhibit membrane blebbing similar to that observed when ROCK1 alone was over-expressed in cells still expressing endogenous PDK1. Only the mutant PDK1 in which the PH domain had been deleted was unable to rescue the membrane blebbing when co-expressed with ROCK1 (Figure 7.12).

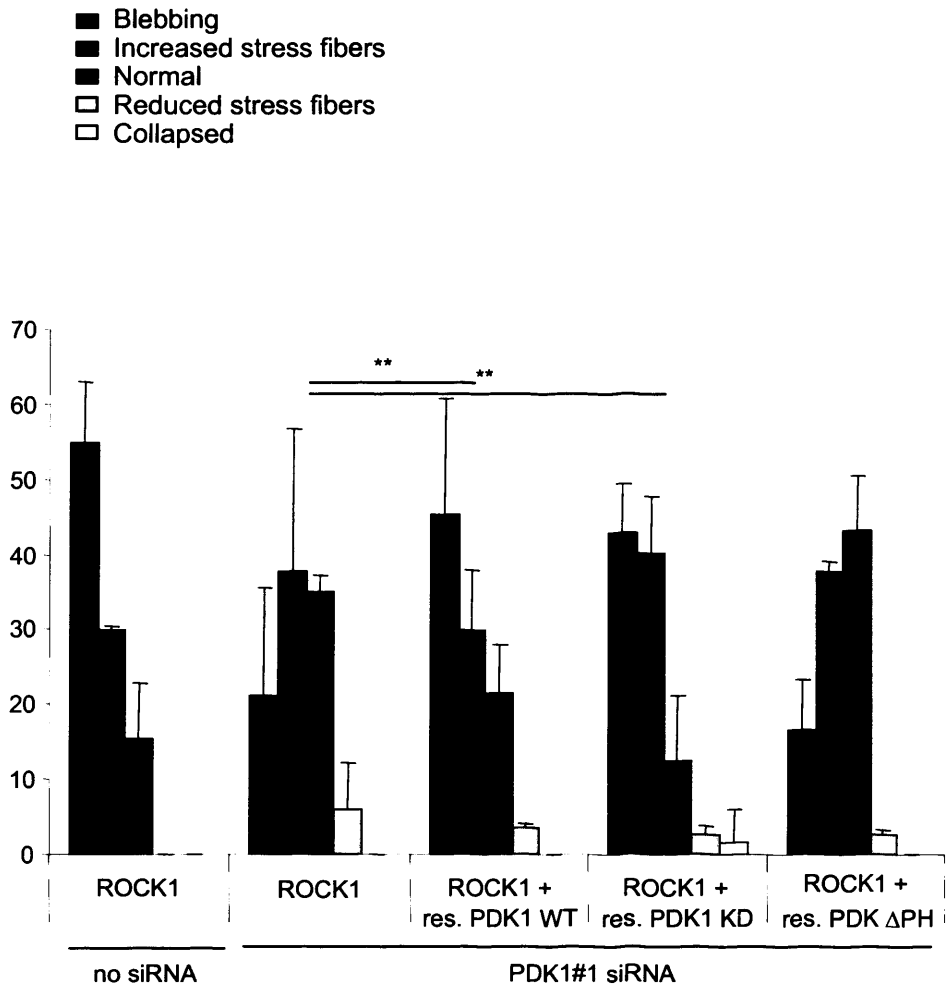

Figure 7.12 The effect of expression of siRNA resistant PDK1 to rescue the blebbing phenotype of ROCK1 expressed in PDK1 depleted A375 cells. A375 cells were transfected with either control or PDK1 targeting siRNA sequences. Subsequently they were then transfected with myc-ROCK1 either alone or in combination with siRNA resistant Flag-PDK1 constructs (WT, KD, PH deleted). 48 hours after DNA transfection, cells were fixed and stained with JAK6 and anti-Flag. The phenotypes of cells expressing both constructs were classified using the f-actin categories described previously. ** indicates $p<0.001$ (Chi-squared test).

7.7.2 Rescue of cell morphology with siRNA resistant FLAG-PDK1 mutants

To test whether siRNA resistant PDK1 could rescue the defects in cortical acto-myosin contraction controlled by endogenous ROCK, siRNA resistant FLAG-tagged PDK1 was transfected into A375 cells 24 hours after they had been transfected with siRNA against PDK1 (Figure 7.13). A375 cells plated on collagen/matrigel and depleted of PDK1 were mostly elongated as had been previously seen. It was found that both WT and KD PDK1 were able to revert A375 cells plated on collagen/matrigel matrix to a rounded morphology with membrane blebs. eGFP was transfected as a control and as expected expression of this construct did not change the cell morphology, and PDK1 depleted cells remained elongated (Figure 7.13, Figure 7.14). This experiment shows that kinase activity of PDK1 is not required for PDK1 to regulate endogenous ROCK1.

7.8 PDK1 and ROCK1 co-localise at the cell periphery

Having found that PDK1 did not regulate the kinase activity of ROCK1 but required its PH domain, and therefore presumably its membrane localisation, to regulate ROCK1 it was next tested whether ROCK1 and PDK1 co-localised. To test the hypothesis that PDK1 could regulate ROCK1 at the plasma membrane, A375 cells plated on 2D and expressing both myc-ROCK1 and FLAG-PDK1 were stained with antibodies against their specific tags and imaged by confocal microscopy (Figure 7.15). Analysis if the immune fluorescence showed that the localisation of ROCK1 and PDK1 overlaps at the cell cortex and around the cell periphery. This was also true for kinase dead PDK1. However PH-deleted PDK1 was localised in the cytoplasm and did not overlap with ROCK1 localisation at the plasma membrane. In this case the over-expressed ROCK1 is at the plasma membrane presumably interacting with endogenous PDK1 that was still present in these cells. The degree of co-localisation was analysed using Zeiss LSM510 image examiner software and pixels with high intensity of both myc and FLAG staining are show in the right hand panel of Figure 7.15.

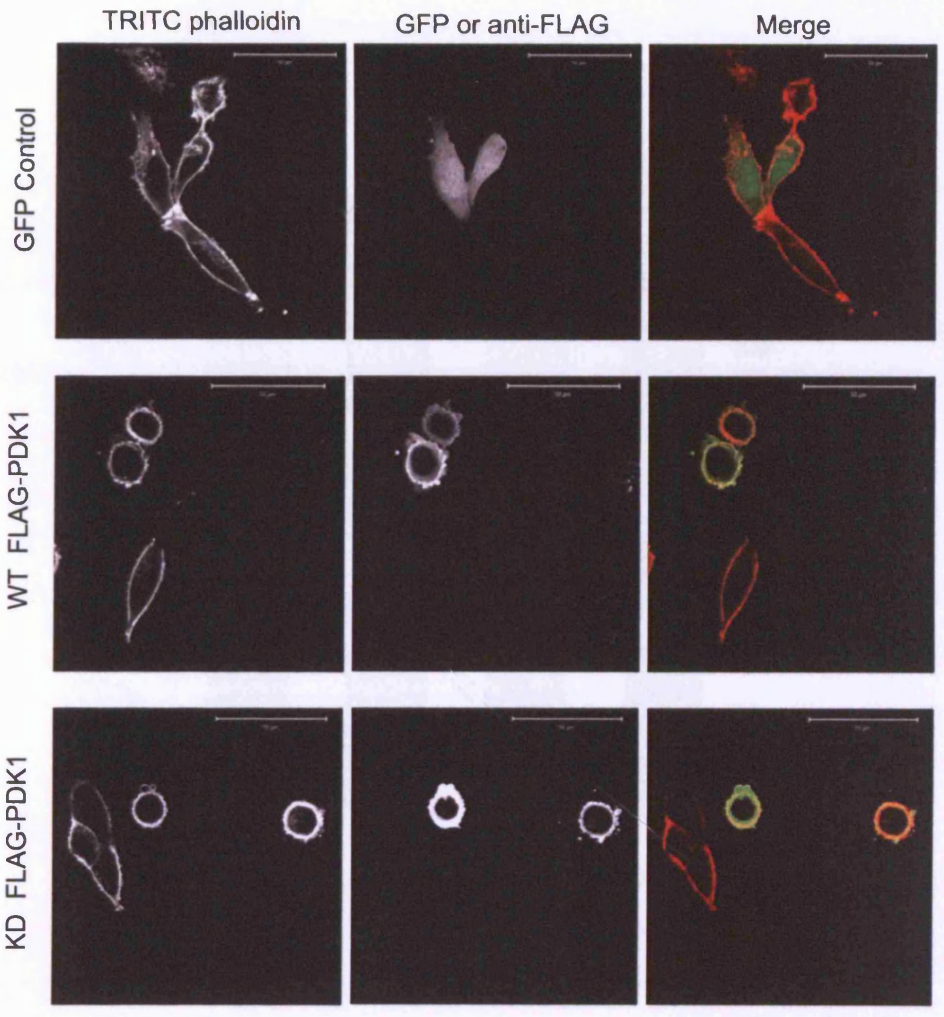

Figure 7.13 Phenotypic rescue by expression of SIRNA resistant FLAG-PDK1 constructs. A375 cells were transfected with PDK1 targeting siRNA oligo sequences and plated on to 3D collagen/matrigel matrix. Subsequently they were then transfected with GFP or Flag-PDK1 constructs resistant to siRNA. 24 hours following DNA transfection cells were fixed and stained with anti-Flag and TRITC phalloidin. Scale bar indicates 50 μm.

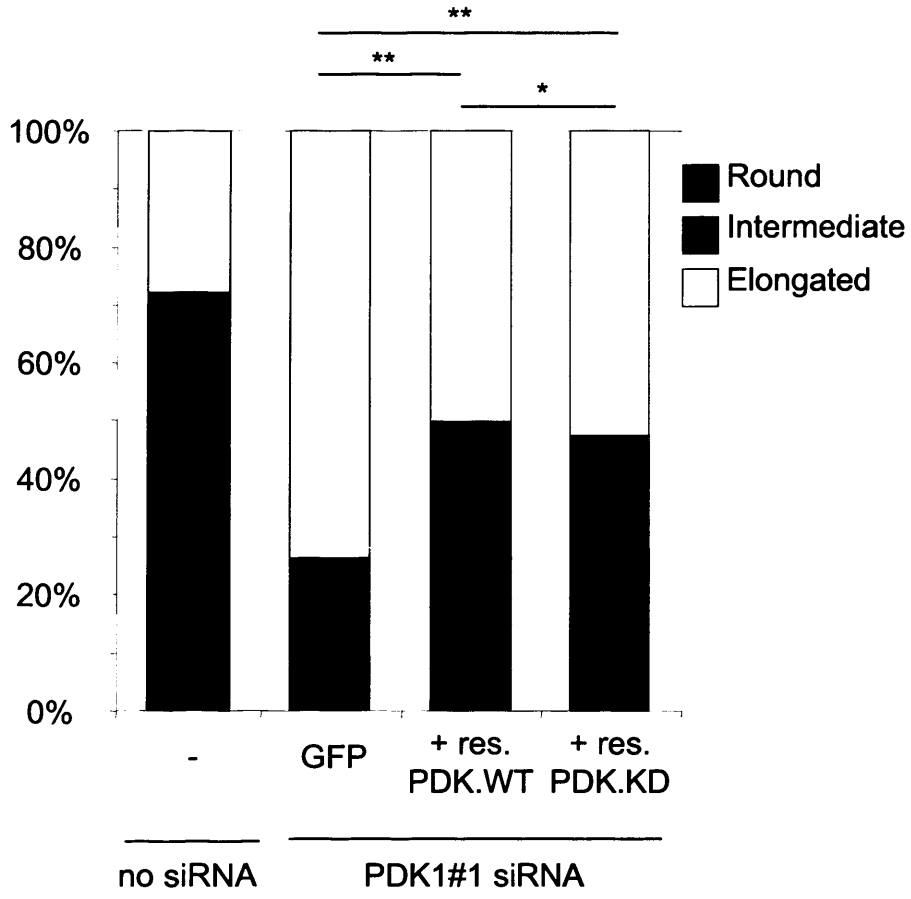

Figure 7.14 Expression of siRNA resistant PDK1 constructs are able to restore rounded cell morphology to A375 cells depleted of PDK1. A375 cells were transfected with PDK1 targeting siRNA oligo sequences and plated on to 3D collagen/matrigel matrix. Subsequently they were then transfected with Flag-PDK1 constructs resistant to siRNA. 24 hours following DNA transfection cells were fixed and stained with anti-Flag and TRITC phalloidin. The phenotype of cells expressing Flag-PDK1 constructs was classified as rounded, intermediate or elongated. Graph shows pooled data from 3 independent experiments, each experiment contains >50 cells. * indicates $p<0.01$ and ** indicates $p<0.001$ (Chi-squared tests).

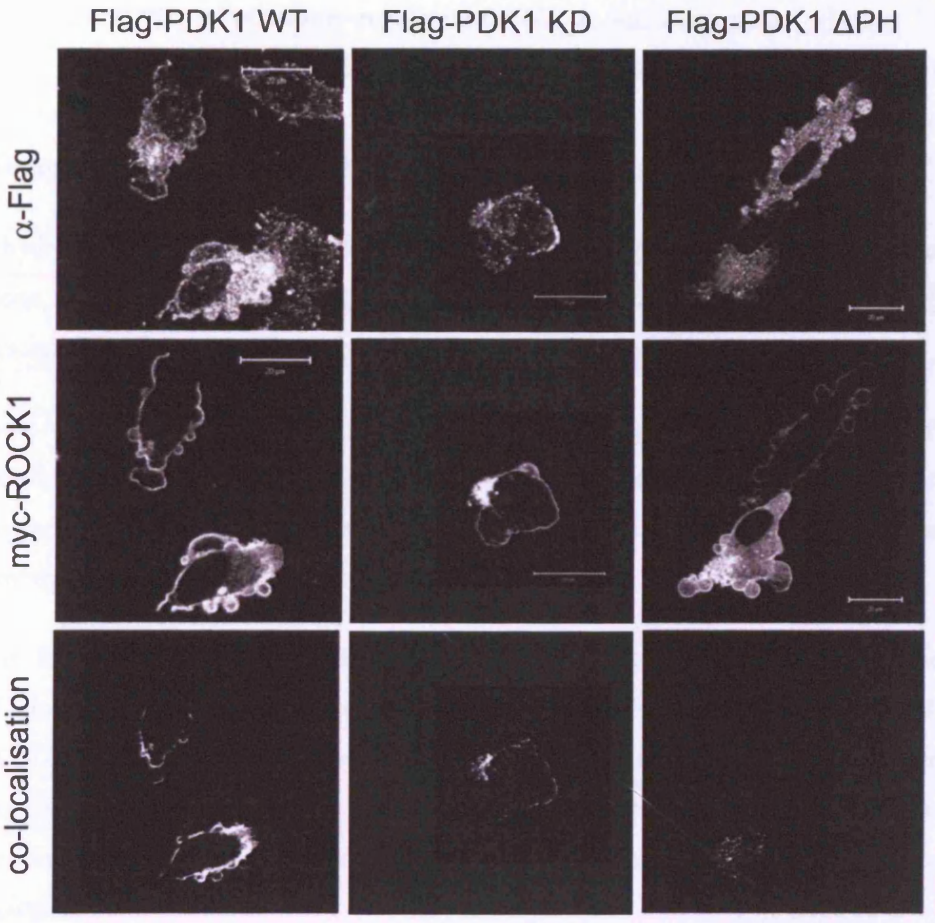

Figure 7.15 Flag-PDK1 and myc-ROCK co-localise at the cell periphery. A375 cells were co-transfected with myc-ROCK1 and Flag-PDK1 constructs. Cells were fixed and stained with JAK6 and anti-FLAG antibodies. Co-localisation was determined by analysis with LSM 510 software. Scale bar indicates 20 μm.

7.9 PDK1 directly binds to ROCK1

Finding that PDK1 and ROCK1 are both required to be localised at the plasma membrane in order for PDK1 to positively regulate ROCK1, it was next tested whether PDK1 and ROCK1 were able to interact and form a complex. Even though there was no evidence that ROCK1 was a PDK1 substrate, PDK1 may still directly or indirectly act to help maintain membrane localisation of ROCK1 by binding and acting as a scaffold.

The hydrophobic region of ROCK1 was tested for binding to PDK1 as sequence analysis on Scansite, had predicted a potential PDK1 binding site centred on T398 of ROCK1 (chapter 3 shows investigations into whether T398 is a regulatory phosphorylation site).

To test whether ROCK1 did bind to PDK1 in this region, short fragments of ROCK1 hydrophobic motif were cloned into GST-protein expression vectors. Recombinant protein was produced and purified from E. coli and used in an in vitro binding assay with recombinant PDK1 (Figure 7.16).

It was found that the region of ROCK1 spanning 338-415 a.a. strongly interacted with PDK1 in vitro (Figure 7.16). Interestingly the corresponding region of ROCK2 did not bind to PDK1 in this assay even though Scansite predicted a similar binding site centred on the hydrophobic motif. This was in agreement to previous data in which it was found that depletion of PDK1 did not affect the ability of over-expressed ROCK2 to cause membrane blebbing.

The binding region of ROCK1 was further narrowed down to 375-415 a.a. A GST-fragment of ROCK1 containing 358-380 a.a. did not bind to PDK1 (Figure 7.16). This raised the question whether PDK1 was able to positively regulate ROCK1 through direct binding at the plasma membrane thereby promoting ROCK1 signalling at this location.

7.9.1 PDK1 binds equally well to ROCK1 mutated at conserved threonine residues in the hydrophobic motif

Having found that PDK1 binds directly to ROCK1 using a region that was previously investigated in chapter 3 for the presence of regulatory phosphorylation sites, it was next tested whether mutation of these sites affected the binding of PDK1 to the ROCK1 hydrophobic motif. The binding assay above was repeated using GST fragments of ROCK1

containing T380A, T398A or both T380A T398A mutations (Figure 7.17). It was found that PDK1 bound equally well to all of the fragments tested and that the mutations introduced did not inhibit the interaction between PDK1 and ROCK1.

The region of ROCK1 required for binding to PDK1 directly overlapped with one of the regions of ROCK1 required for binding to the negative regulator RhoE. RhoE requires both 375-420 a.a. and also a site in the extreme N-terminus (0-50 a.a.). It was also investigated whether PDK1 was able to bind RhoE, and it was found that this was not the case (see lane 3 in Figure 7.16). Therefore, it was unlikely that PDK1, ROCK1 and RhoE were all able to interact in one large complex. As PDK1 and RhoE require the same sequence of amino acids to interact with ROCK1 the next hypothesis to test was whether PDK1 and RhoE compete for binding to this region.

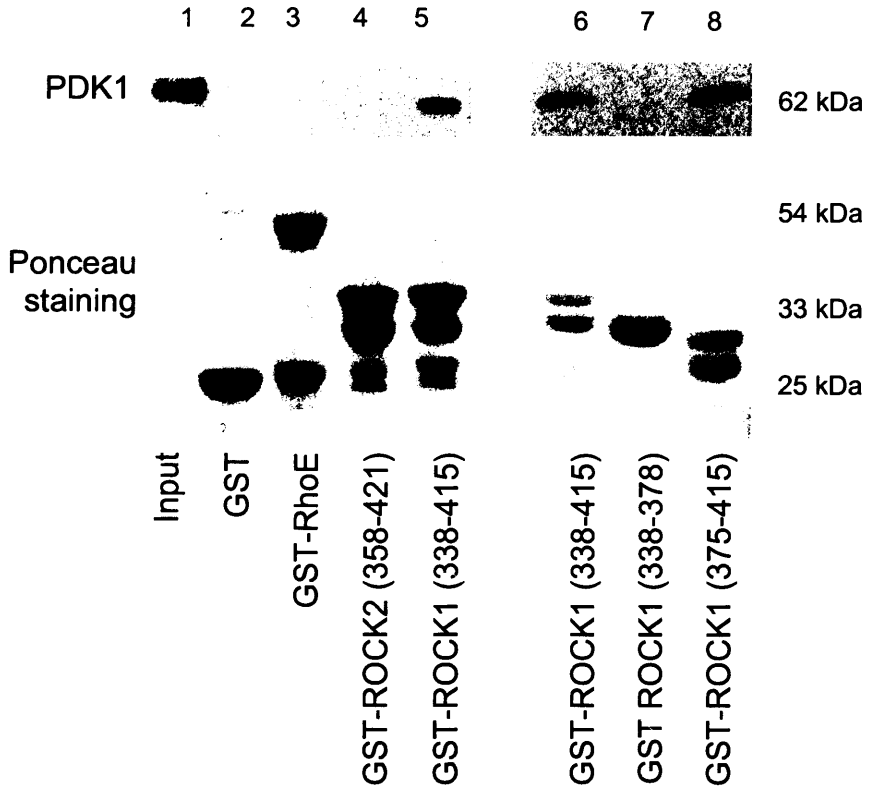

Figure 7.16 GST-tagged fragments of ROCK1 are able to bind recombinant PDK1 in vitro. Recombinant GST fragments of ROCK1 were expressed in E.coli and purified. Glutathione agarose beads bound to ROCK1 fragments were then incubated with recombinant PDK1 in kinase assay buffer without ATP. Beads were washed extensively and binding was determined by western blot. Levels of GST proteins are determined by ponceau staining.

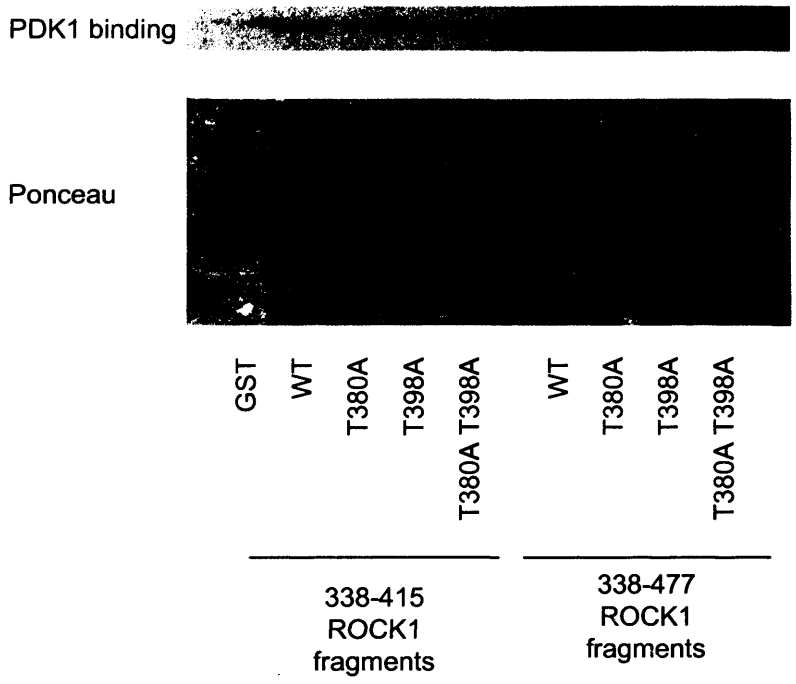

Figure 7.17 GST tagged fragments of ROCK1 containing T/A mutations are able to bind recombinant PDK1 in vitro. Recombinant GST fragments of ROCK1 were expressed in E.coli and purified. Glutathione agarose beads bound to ROCK1 fragments were then incubated with recombinant PDK1 in kinase assay buffer without ATP. Beads were washed extensively and binding was determined by western blot. Levels of GST proteins are determined by ponceau staining.

8 Chapter 8 - PDK1 regulates cancer cell motility in 3D environments by antagonising the inhibition of ROCK1 by RhoE

8.1 Chapter Summary

Previous results had indicated that PDK1 was able to regulate the localisation of ROCK1 at the plasma membrane by directly binding to a region around the hydrophobic motif of ROCK1. The binding domain directly over-lapped with a region of ROCK1 reported to be required for interaction with the negative regulator RhoE. This chapter describes the detailed investigation of the mechanism behind this regulation of ROCK1. It was found that PDK1 and RhoE are able to directly compete for binding to ROCK1 and that their binding was mutually exclusive. Further to this it was also found that exogenous or over-expressed PDK1 was able to disrupt the interaction of ROCK1 and RhoE. The final proof of this mechanism was that in A375 cell lines stably depleted of PDK1, endogenous ROCK1 was found to be bound to endogenous RhoE, and this complex could be isolated by co-immune precipitation.

If the changes in cell morphology and the reduction in cell motility observed when PDK1 is depleted, are due to the inhibition and mislocalisation of ROCK1 by RhoE, then knockdown of RhoE in conjunction with PDK1 should be able to at least partially rescue the phenotype. The final part of this chapter details experiments showing that double knockdown of PDK1 and RhoE is able to restore the ability of over-expressed ROCK1 to localise at the plasma membrane and cause membrane blebbing. Furthermore, double knockdown is able to restore cortical acto-myosin contraction, which was measured by rounded morphology and also the restoration of phosphorylation of MLC in the cell cortex. The final experiment was able to show that double knockdown of both PDK1 and RhoE was able to restore cell motility to MTLn3E cells.

8.2 PDK1 directly competes with RhoE for binding to the same region of ROCK1

8.2.1 In vitro binding competition assay

To test whether PDK1 and RhoE directly competed with each other for the binding to and regulating of ROCK1, GST-tagged RhoE was used in an in vitro binding assay. Recombinant ROCK1 (17-557 a.a.) bound strongly to GST-RhoE, but as increasing concentrations of recombinant PDK1 were included in the binding assay, the interaction between GST-RhoE and ROCK1 was disrupted (Figure 8.1). The molar concentration of RhoE was estimated by coomassie staining compared to known concentrations of other proteins of similar size. However the exact amount of RhoE in the binding assay would vary depending on the efficiency of the pulldown from the bacterial lysate on the day of the assay. The average amount of GST-RhoE used in each individual binding assay was approximately 1 μg. 0.2 μg of recombinant ROCK1 was added, and this interaction was able to be disrupted with PDK1 (between 0.6 and 1.2 μg) (Figure 8.1). This is the equivalent of approximately 10^{-12}mol - 20^{-12}mol PDK1 being able to compete with 2X10 $^{-12}$mol GST RhoE for binding to ROCK1.

8.2.2 RhoE ROCK1 interaction is disrupted by PDK1 in cell lysates

To further test the hypothesis of a direct competition between PDK1 and RhoE, GST-RhoE was used to pull down over-expressed myc-ROCK1 from A375 cell lysates (Figure 8.2). The interaction of GST-RhoE and full-length ROCK1 is poor in this assay; this has also been reported by Ridley A. and colleagues [85]. This result suggests that under normal conditions ROCK1 is not associated with RhoE but is binding to PDK1 instead, at least in the cell lines tested here. The binding of GST-RhoE to myc-ROCK1 can be significantly increased when PDK1 is depleted from the cell lysates by siRNA (compare lanes 1 and 2 Figure 8.2). This can be reversed either by the addition of recombinant PDK1 to the binding assay (lanes 3 and 4), as we had previous seen in the in vitro binding assay (Figure 8.1). We were also able to reverse the binding of myc-ROCK1 to RhoE by over-expressing siRNA resistant FLAG-tagged PDK1 in the A375 cells (lanes 5 and 6).

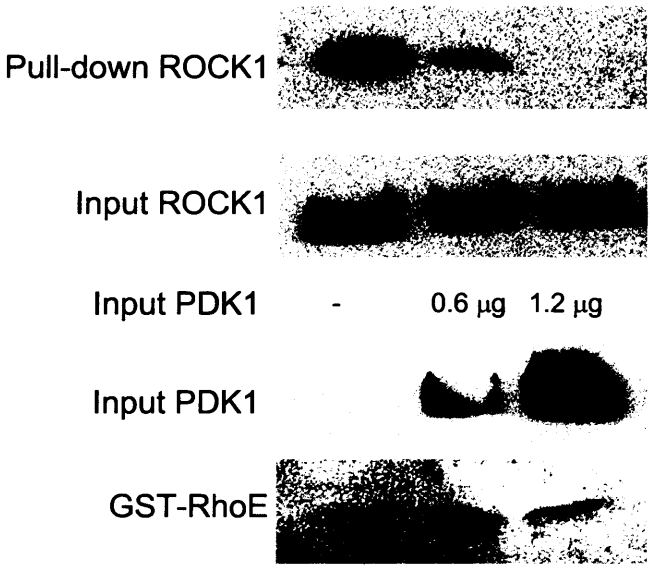

Figure 8.1 GST-RhoE binding to recombinant ROCK in vitro is disrupted by the addition of PDK1. GST-RhoE, bound to glutathione agarose beads was incubated with combinations of ROCK1 and PDK1. Binding of ROCK1 to GST RhoE was determined by western blot. The input of ROCK1 and PDK1 to the binding assay was also determined by western blot. Level of RhoE bound to glutathione agarose was determined by ponceau stain.

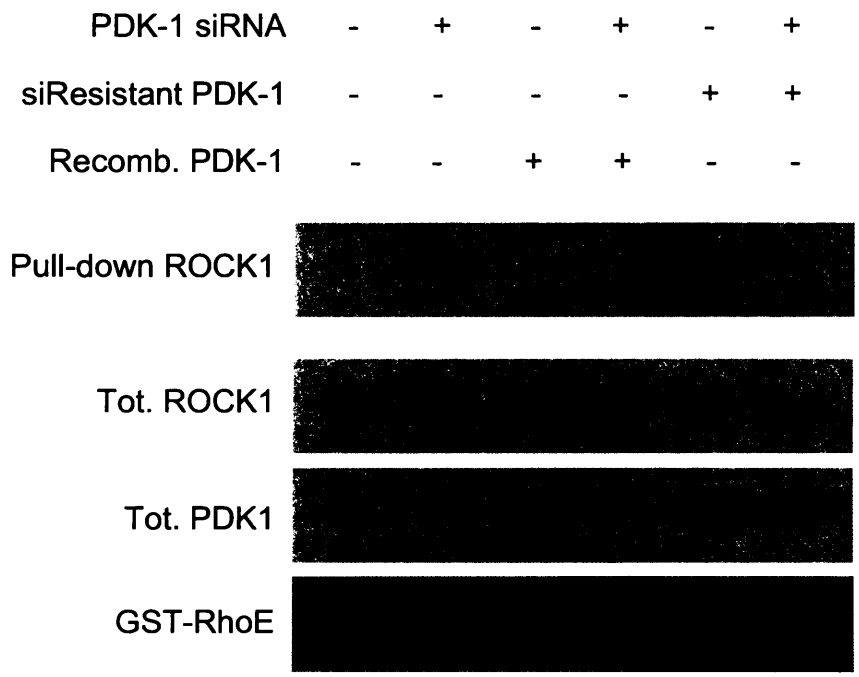

Figure 8.2 GST-RhoE is able to bind myc-ROCK1 in A375 cell lysates depleted of PDK1. GST-RhoE bound to glutathione agarose beads was incubated with cell lysate form A375 cells transfected with PDK1 targeting siRNA and transiently transfected with either myc-ROCK1 alone or in combination with siRNA resistant Flag-PDK1. Lanes 3 and 4 show samples in which recombinant PDK1 was added to the cell lysate during incubation with GST RhoE (note slightly higher band). Levels of myc-ROCK1 and PDK1 in the lysate, and the binding of myc-ROCK1 to GST RhoE were determined by western blotting. Levels of GST RhoE were determined by ponceau stain.

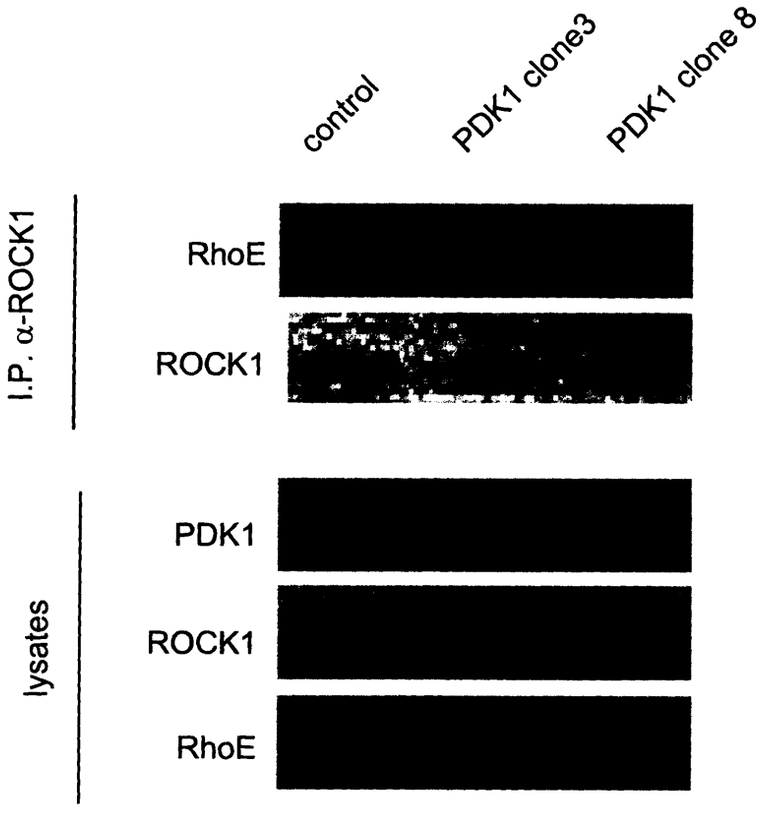

Figure 8.3 Endogenous ROCK1 with co-I.P. with endogenous RhoE in A375 cells stably depleted of PDK1. A375 cell lines stably expressing pSuper constructs encoding shRNA against PDK1, or a control empty cassette were lysed and endogenous ROCK1 was immune precipitated. Cell lysates and i.p.s were analysed by western blot to check for levels of endogenous ROCK1, PDK1 and RhoE.

These results indicate that in A375 cells the competition between PDK1 and RhoE for binding to ROCK1 is able to occur, and that the system can be manipulated to sway the binding in favour of either PDK1 or RhoE by altering the levels of PDK1 available for ROCK1 to interact with.

8.3 In the absence of PDK1 ROCK1 forms a complex with RhoE and is inhibited

8.3.1 Endogenous Co-I.P. of ROCK1 and RhoE in PDK1 depleted cells

The final test of this hypothesis was to be able to show that the competition between PDK1 and RhoE was happening in the case of the endogenous proteins. Using the stably depleted A375 cell lines that had been used for the in vivo experiments, it was possible to show that in cells depleted of PDK1, ROCK1 was complexed and therefore mislocalised and inhibited by RhoE. Endogenous ROCK1 was co-immune precipitated with endogenous RhoE, only from the A375 cells stably depleted of PDK1 (Figure 8.3). The two stably depleted cell lines shown in this assay contain slightly different amounts of PDK1 and as a result the amount of RhoE complexed with RhoE is also altered. This result is evidence that when PDK1 is not available to bind ROCK1 at the plasma membrane, ROCK1 is found in a complex with RhoE.

8.3.2 The localisation of ROCK1/RhoE complexes

GFP-RhoE when over-expressed in A375 cells is located mostly at the plasma membrane but also on some intracellular membranes (Figure 8.4). Myc-ROCK1 over-expressed alone is also localised to the plasma membrane as previously shown in chapter 3, 4, and 5. When GFP-RhoE is over-expressed, this biases the competition between PDK1 and RhoE in favour of ROCK1 binding to RhoE, as there is more RhoE available. Therefore, similar a similar phenotype to depletion of PDK1 should be observed. A375 cells expressing both myc-ROCK1 and GFP RhoE were analysed by immune fluorescence (Figure 8.4). Myc-ROCK1 was no longer membrane localised, and the over-expression of myc-ROCK1 was no longer able to induce membrane blebbing. It was also interesting that GFP-RhoE might be less membrane localised when expressed with ROCK1.

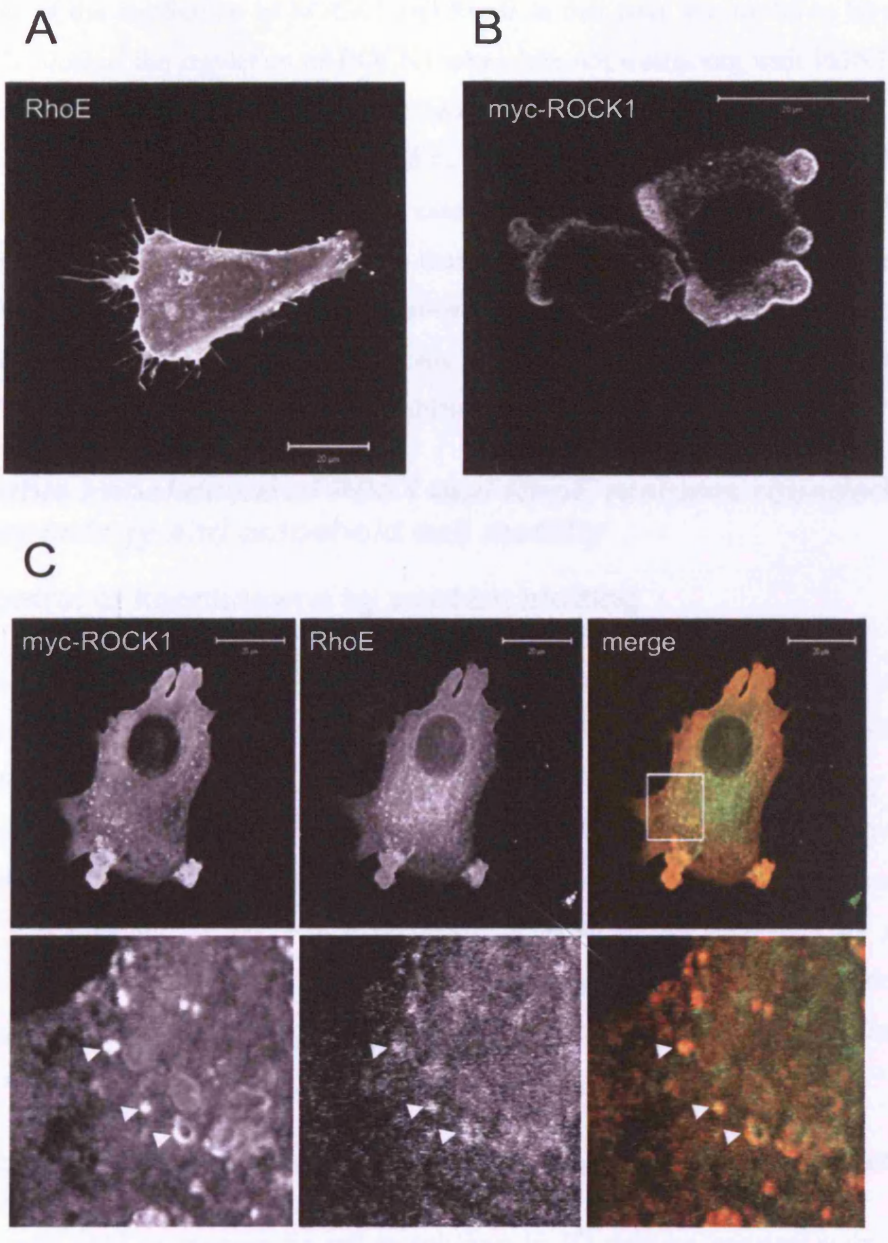

Figure 8.4 Myc-ROCK1 and GFP-RhoE co-localise in membrane puncta/vesicles. A375 cells expressing myc-ROCK1 and/or GFP-RhoE and plated on glass coverslips were fixed and stained with 9E10. A) GFP RhoE expressed alone is membrane localised. B) myc-ROCK1 expressed alone is membrane localised. C) Confocal imaging identified that myc-ROCK1 and GFP-RhoE when expressed together, partially co-localised in punctate structures or vesicles, as shown in the lower panel by the arrow heads. Scale bar indicates 20 μm.

The analysis of the localisation of ROCK1 and RhoE in this assay was useful to be able to give an indication of the regulation of ROCK1 when it is not interacting with PDK1 at the plasma membrane. Analysis of the immune fluorescence showed that ROCK1 and RhoE were partially co-localised in puncta (Figure 8.4). Although the nature of these vesicles was unclear, this analysis was able to show that in cases where the cellular concentration of RhoE is higher than the concentration of PDK1, that ROCK1 and RhoE are co-localised and presumably in a complex as indicated by the above in vitro data. The puncta observed in this assay are similar to those observed when cells over-expressing ROCK1 are treated with LY294002 (see Figure 3.13) or have PDK1 depleted.

8.4 Double knockdown of PDK1 and RhoE restores rounded cell morphology and amoeboid cell motility

8.4.1 Control of knockdowns by western blotting

If the model that PDK1 and RhoE are able to compete for binding to ROCK1 is correct, and that in the absence of PDK1, ROCK1 is inhibited by interacting with RhoE, then knocking down RhoE with siRNA in cells already depleted of PDK1 should partially rescue the defects observed. Throughout this work, 2 different PDK1 siRNA sequences targeting different sites in the PDK1 gene sequence have been used to verify the phenotypes described. It is now shown that 2 different RhoE targeting siRNA sequences are able to successfully knockdown a significant proportion of RhoE both when used in isolation and also in conjunction with siRNA targeting PDK1. The western blot in figure 8.5 confirms the efficient double knockdown.

8.4.2 Rounded cell morphology is restored by double knockdown

A375 cells were used to examine the cell morphology in 3D collagen/matrigel matrix when both PDK1 and RhoE were depleted by siRNA transfection. As had been seen previously, knockdown of PDK1 caused the cells to become more elongated with long protrusions. The ratio of perimeter^2/4πarea was used as previously to measure how round the cell morphology was. The closer this ratio is to 1, the rounder the cell morphology. In some cases the ratio was as high as 8 when PDK1 was depleted (Figure 5.4). When RhoE was knocked down alone, there was not a significant difference in cell morphology compared to controls (Figure 8.6), this is consistent with the results from the siRNA screen (Figure 5.1).

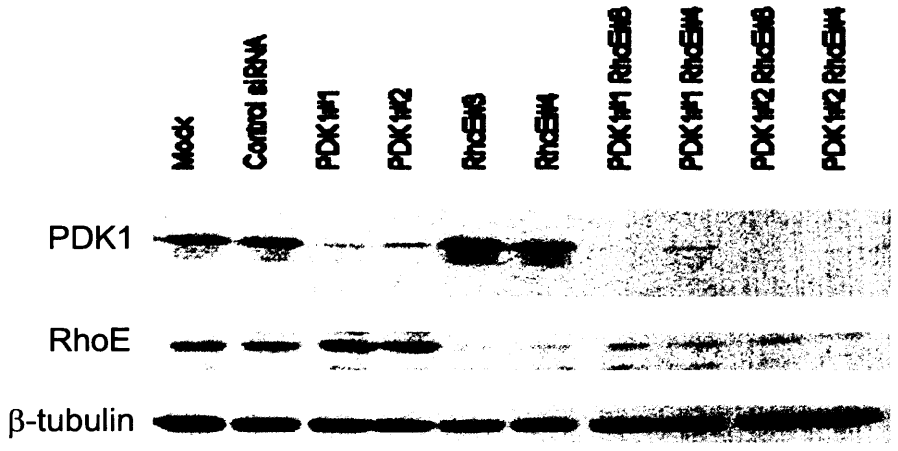

Figure 8.5 Western blot to show the efficient knockdown of PDK1 and RhoE with siRNA oligos. A375 cells were transfected with combinations of PDK1 and RhoE targeting siRNA oligos. Efficient knockdown was checked by western blot of cell lysates 36 hours post transfection.

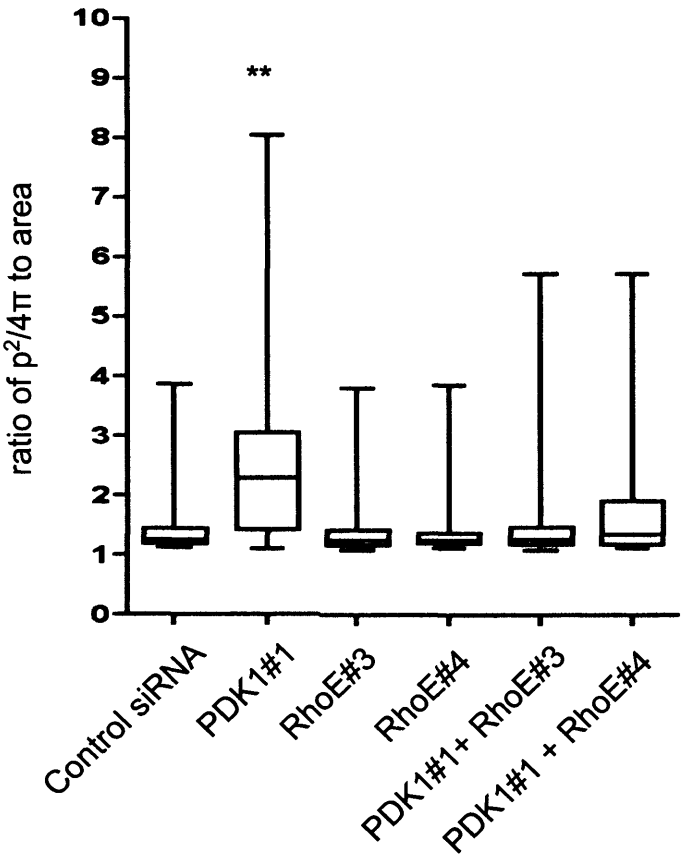

Figure 8.6 Quantification of rescue of cell morphology when cells are depleted of both PDK1 and RhoE. A375 cells were depleted of PDK1 or RhoE or a combination of both. Cells were then plated on a collagen/matrigel matrix. Measurements of area and perimeter were taken from >100 cells. The ratio of 4πarea/perimeter^2 is shown in the form of a box plot, showing min, max, median and 25th and 75th percentiles. * indicates $p<0.001$ (compared to the control) Mann Whitney U test.

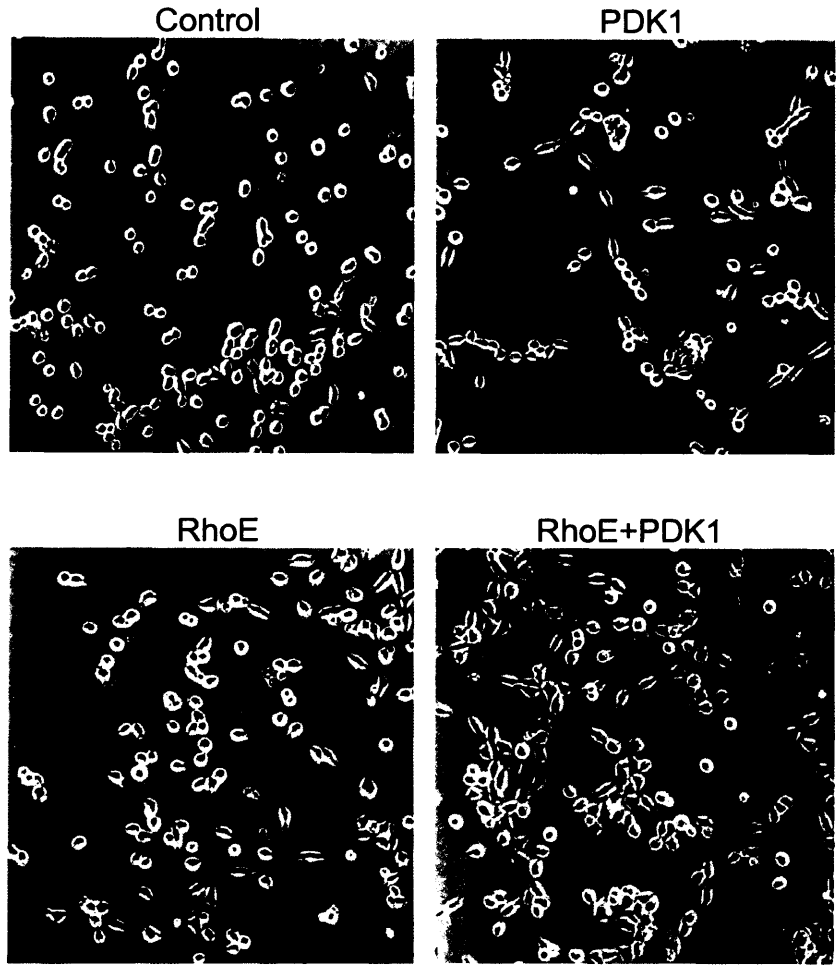

Figure 8.7 Morphology of MTLn3E cells. Similar to A375 cells, depletion of PDK1 causes elongated cell morphology. Double knockdown of PDK1 and RhoE partially restored rounded morphology.

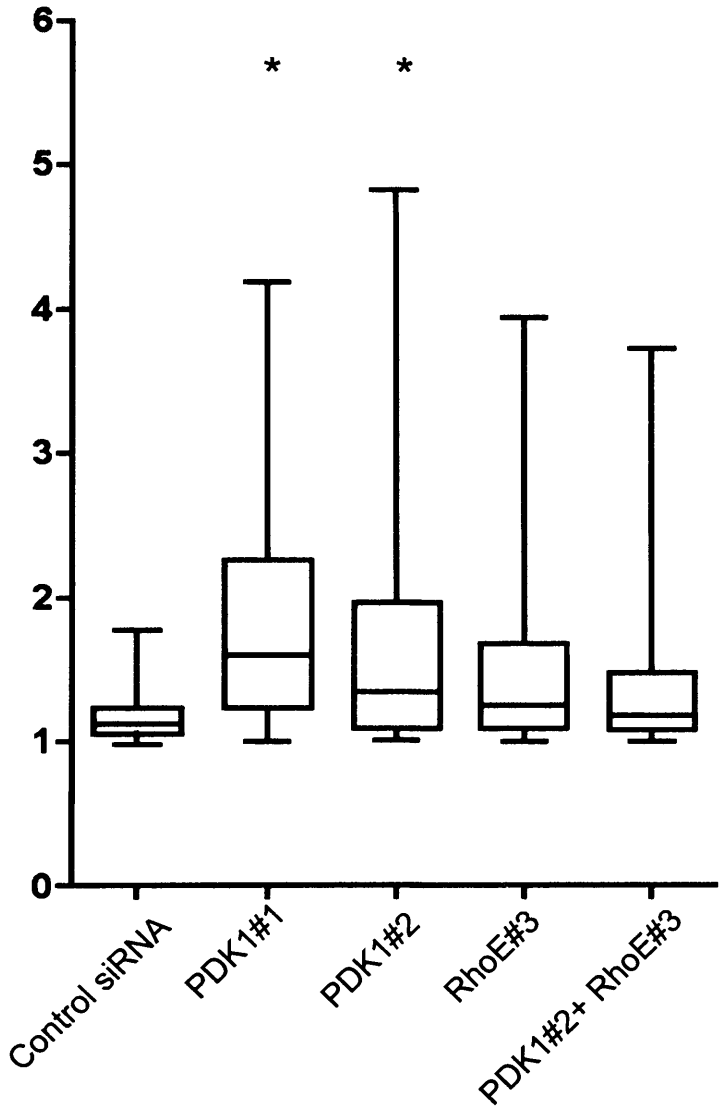

Figure 8.8 Quantification of changes in morphology in MTLn3E cells . Measurements of area and perimeter were taken from >100 cells. The ratio of 4πarea/perimeter2 is shown in the form of a box plot, showing min, max, median and 25th and 75th percentiles. * indicates $p<0.01$ (compared to control) Mann Whitney U test.

As the A375 cells on the 3D matrix are already mostly rounded and have high levels of contractile forces, further reduction of RhoE, a negative regulator of ROCK-driven contraction did not cause any increase in contraction. However when PDK1 and RhoE were knockdown together, the quantification of the cell morphology showed that there was no significant difference from control cells. This means that double knockdown of PDK1 and RhoE was able to reverse the changes in cell morphology caused by knockdown of PDK1 alone. Looking in detail at the spread of values (ratio of perimeter^2/4πarea), there are some cells transfected with siRNA against both PDK1 and RhoE that remain more elongated than the controls. So even though the majority are able to become rounded again, it seems that if there is still an imbalance between PDK1 and RhoE, then the morphology is not completely rescued (Figure 8.6). It seems that a very fine balance between these two proteins and their effects on ROCK1 determines cell morphology. These results were also seen using MTLn3E cells (Figure 8.7, Figure 8.8), and RhoE siRNA was able to make the elongated PDK1 depleted cells rounder. However knockdown of RhoE alone also caused some disruption of rounded cell morphology in MTLn3E cells, which was not expected. It must be concluded that although A375 and MTLn3E cells share many mechanisms to regulate cortical F-actin and amoeboid cell motility, there are still differences that we do not yet understand.

8.4.3 Double knockdown restores cortical actin organisation and MLC phosphorylation

To look at whether the regulation of cortical acto-myosin network was restored, A375 cells transfected with siRNA targeted against PDK1, RhoE or both together were plated onto 3D collagen/matrigel matrix and then fixed and stained for ppMLC (Figure 8.9). It was seen that rounded cell morphology was restored when both PDK1 and RhoE were knocked down, as had been previously seen. In addition to this, level of the phosphorylation of MLC was restored and was located throughout the cell cortex, similar to the localisation seen in control cells. This indicates that when both PDK1 and RhoE are depleted, endogenous ROCK1 is able to localise correctly at the plasma membrane, and is able to co-ordinate contraction of the acto-myosin cortex through the phosphorylation of MLC, similarly to control cells.

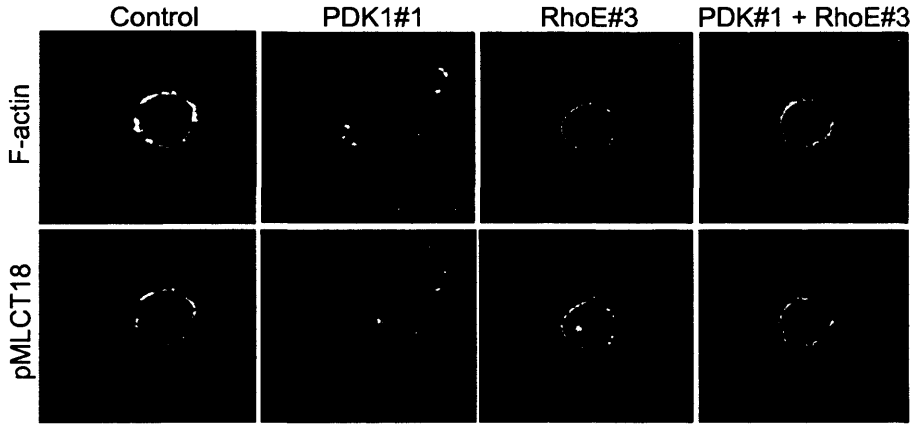

Figure 8.9 Double knockdown of PDK1 and RhoE restores cortical acto-myosin contractility. A375 cells were transfected with either control, PDK1, RhoE or a combination of PDK1 and RhoE siRNA. Cells were then plated on top of collagen matrigel matrix. 48 hours later cells were fixed and stained with TRITC phalloidin, and ppMLC (T18S19).

8.4.4 ROCK driven blebbing is rescued by double knockdown

The double depletion of PDK1 and RhoE was also able restore the ability of over-expressed myc-ROCK1 to cause membrane blebbing (Figure 8.10). In the absence of PDK1, myc-ROCK1 was not membrane localised and was only able to induce stress fibres in the cytoplasm rather than co-ordinating contractile forces around the complete cell cortex to induce blebbing. When RhoE is knocked down in addition to PDK1 then myc-ROCK1 is able to localise at the plasma membrane (Figure 8.10 lower panel) presumably through interaction with RhoA. This seems to be sufficient for ROCK1 to co-ordinate the contraction of the cell cortex, as the number of cells expressing myc-ROCK1 and exhibiting membrane blebbing is similar to that seen in the control (Figure 8.10 upper panel).

8.4.5 Double knockdown restores cell motility in MTLn3E cells

All the experiments in this chapter have so far shown that knockdown of RhoE in addition to depletion of PDK1 is able to restore the ability of both over-expressed and endogenous ROCK1 to drive contraction and rounded blebbing cell morphology. Early results and previously published data had also shown a link between rounded cell morphology and the ability of cell to invade 3D environments in an amoeboid manner. This was the basis for the initial siRNA screen, to identify novel regulators of amoeboid cancer cell invasion using a morphology-based read-out, and the assumption that hits that disrupted rounded cell morphology could also be required for amoeboid cell motility.

To finally test the model that the depletion of PDK1 disrupts cell morphology and reduces cell motility by allowing RhoE to bind to and inhibit ROCK1, it was tested whether double knockdown of both PDK1 and RhoE was able to restore cell motility. MTLn3E cells were used in this assay as their movement in 3D collagen/matrigel matrix is more persistent and easier to measure than the chaotic motility of A375 cells. Measuring the movement of MTLn3E cells on collagen/matrigel gels over 10 hours revealed that this hypothesis held true and that double knockdown of PDK1 and RhoE was able to restore cell motility in this cell line and there was no significant difference from the controls (Figure 8.11). Knockdown of RhoE alone did not alter cell speed (Figure 8.11).

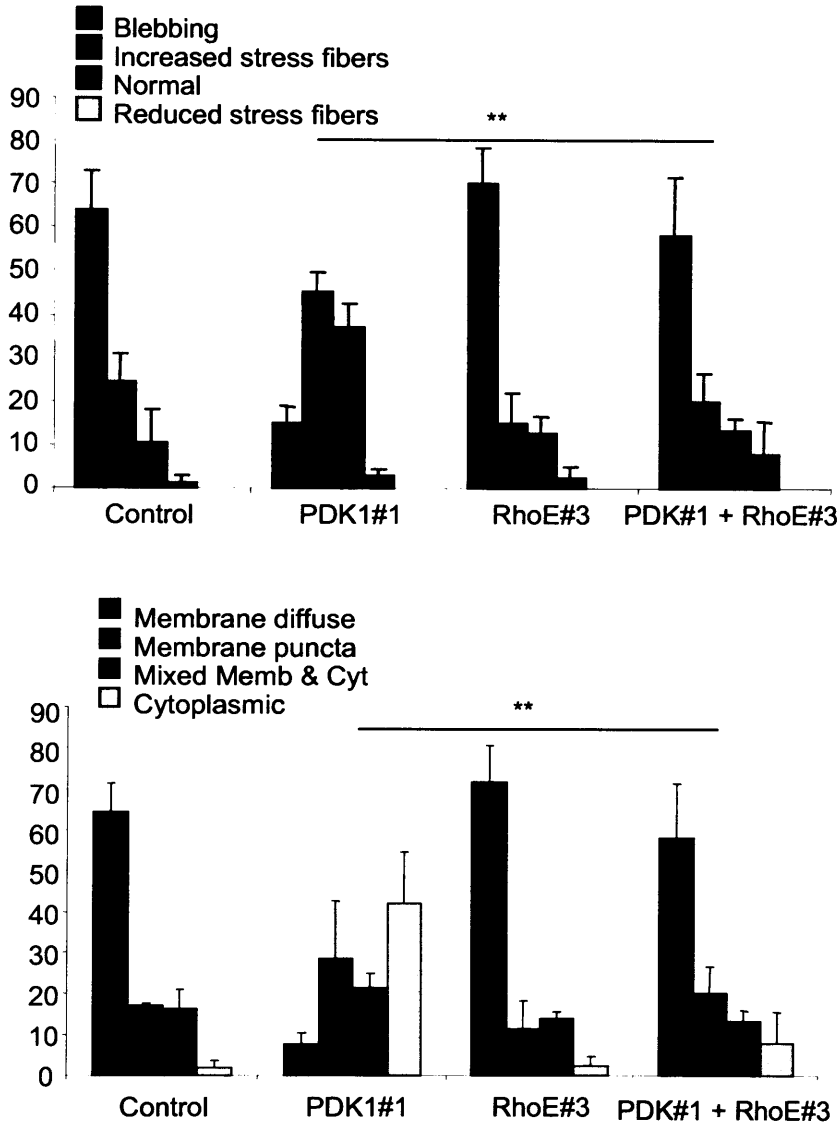

Figure 8.10 Double Knockdown of PDK1 and RhoE restores blebbing phenotype and membrane localisation of over-expressed ROCK1. Graphs to show phenotypes of over-expressed ROCK1 in A375 cells. A375 cells plated on 2D substrate were transfected with either control, PDK1, RhoE or a combination of PDK1 and RhoE siRNA. 24 hours later myc-ROCK1 was transfected. 24 hours later cells were fixed and stained with 9e10 and TRITC phalloidin. Cells expressing myc-ROCK1 were then scored into the above categories based on the actin phenotype and the localisation of the ROCK construct. ** indicates $p<0.001$ (Chi squared test).

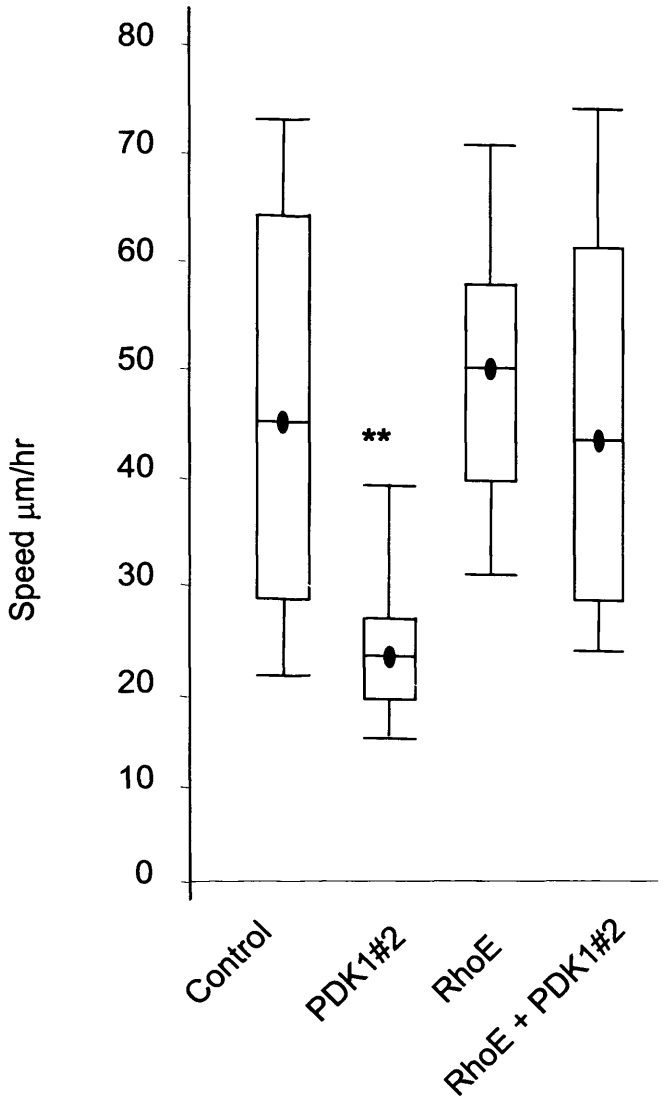

Figure 8.11 Quantification of the rescue of MTLn3E cell motility when both PDK1 and RhoE are depleted. MTLn3 cells were transfected with either PDK1 or RhoE targeting oligos and plated on collagen matrigel. Low resolution phase contrast time-lapse sequences were analysed to determine the effect of PDK1/RhoE depletion on cell motility. ** indicates $p<0.001$ Mann Whitney U test.

9 Chapter 9 – Investigating the relationship between cancer cell motility and pigment production in vivo.

9.1 Chapter Summary

The previous chapters have uncovered a strong correlation between invasive behaviour of cancer cells and rounded contractile cell morphology. The siRNA screening in chapter 5 was carried out based on this hypothesis and it was found that PDK1 controlled both morphology and cell motility in vivo.

Further to this, I was interested to investigate the motile behaviour of melanoma in greater detail. Differentiated melanocytes residing in the skin have a dendritic phenotype, exhibiting multiple protrusions and low contractile forces. Having seen that the A375 cells (human melanoma cell line) do not resemble dendritic melanocytes it was possible that the acquisition of motile invasive behaviour coincided with failure to fully differentiate. To investigate this, the mouse melanoma cell line B16F2 was used. B16F2 cells are able to produce melanin in vitro and respond to melanocyte-stimulation hormone (MSH) by becoming dendritic in morphology. These features made this cell line suitable to determine if there was a correlation with cell motility, cell morphology and pigment production. The A375 cells used in the previous chapters are not able to produce pigment and so they were not suitable for this part of the project.

It was found that it was possible to image vesicles containing pigment by both reflectance and multi-photon microscopy. The fluorescent vesicles were ablated by inhibition of PKA, and increased in number by stimulation of cells with MSH. Multi-photon imaging of B16F2 xenograft tumours in vivo revealed that pigment production throughout the tumour was heterogeneous. Time-lapse movies were captured and it was found that motile cells tended to contain less pigment than non-motile cells in the same field perhaps indicating that the invasive cells were less differentiated.

It was also possible to quantify the pigment content of B16F2 cells by FACS. B16F2 cells stimulated with MSH showed significantly greater emission in the violet range. Based on this, B16F2 cells isolated from xenograft tumours were sorted by FACS into two populations based on their pigment content. Cells expressing high melanin were compared to those expressing low pigment by microarray analysis to identify signalling pathways responsible for a switch to a less differentiated, more motile phenotype. From the microarray it was found

that TGFβ2 amongst other genes was up regulated in the cells containing less pigment. This was tested in vitro and it was confirmed that both TFGβ1 and TFGβ2 inhibited melanogenesis, even in the presence of MSH. These results add to the body of evidence that TGFβ can induce invasive pro-metastatic behaviour of cancer cells in vivo, but in addition, that this signal could also potentially perturb or reverse differentiation.

9.2 Melanin containing vesicles can be imaged by multi-photon microscopy.

9.2.1 Imaging of melanin in vitro

B16F2 cells plated on glass and stimulated with MSH were imaged on an inverted multi-photon confocal microscope. The pigment containing vesicles could be seen by transmitted light passing through the sample without contrast. Imaged this way the cells looked mostly transparent, the only clearly visible feature being the black dots which we assume to be melanosomes. Looking at cells in this way showed that even in the presence of MSH for 48 hours, not all cells respond and produce more pigment, indicating that this cell line is innately heterogeneous in their sensitivity and response to stimuli. The cells that had responded to MSH contained many melanosomes throughout the cytoplasm although melanosomes were more concentrated at the cell periphery, and in cell protrusions. Collecting a reflectance image from the 543 nm single photon laser showed that the cells containing more black vesicles also had a higher reflectance signal. The pattern of reflectance and melanosomes was similar but what was surprising was that signals were also detected following multiphoton excitation. The emission following multiphoton excitation was very broad and was collected in multiple detection channels (410-450 nm, 500-550 nm, 565-615 nm) following excitation at 850 nm (Figure 9.1). Cells containing more melanosomes as determined by transmitted light, also had a higher signal in the reflectance and fluorescent emission channels (Figure 9.1). The broad range of emission was curious and suggested that the signal we were seeing was not the result of conventional fluorescence. For this reason this signal will now be named 'Near Infra-Red stimulated Visible light Emission' (NIRVE), a term invented solely for the purpose of describing the data in this chapter.

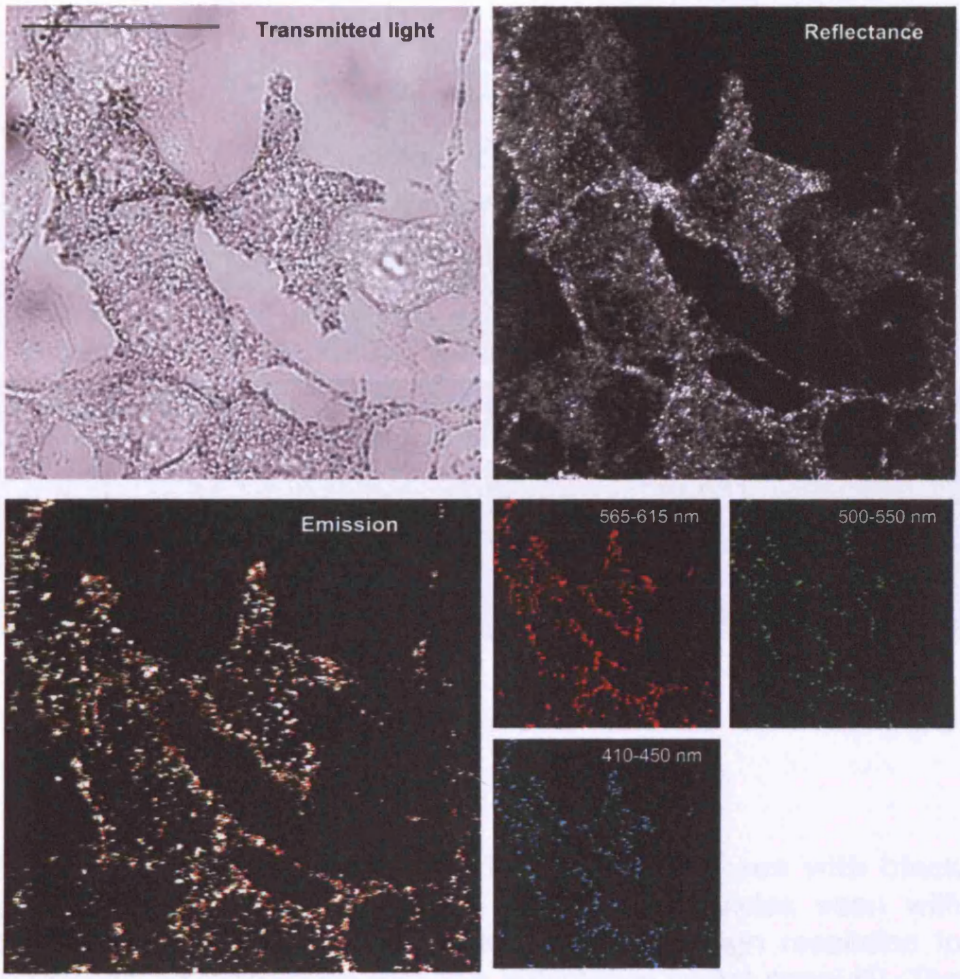

Figure 9.1 Pigment containing vesicles can be visualised by multiphoton microscopy. B16 F2 cells plated on glass-bottomed cell culture dishes were stimulated with α-MSH for 48 hours. Images were taken using a 63X oil immersion lens without contrast. Reflectance was seen using single photon laser (543 nm). Emission was also collected at various wavelengths following 2-photon excitation at 850 nm. Scale bar indicates 50 μm.

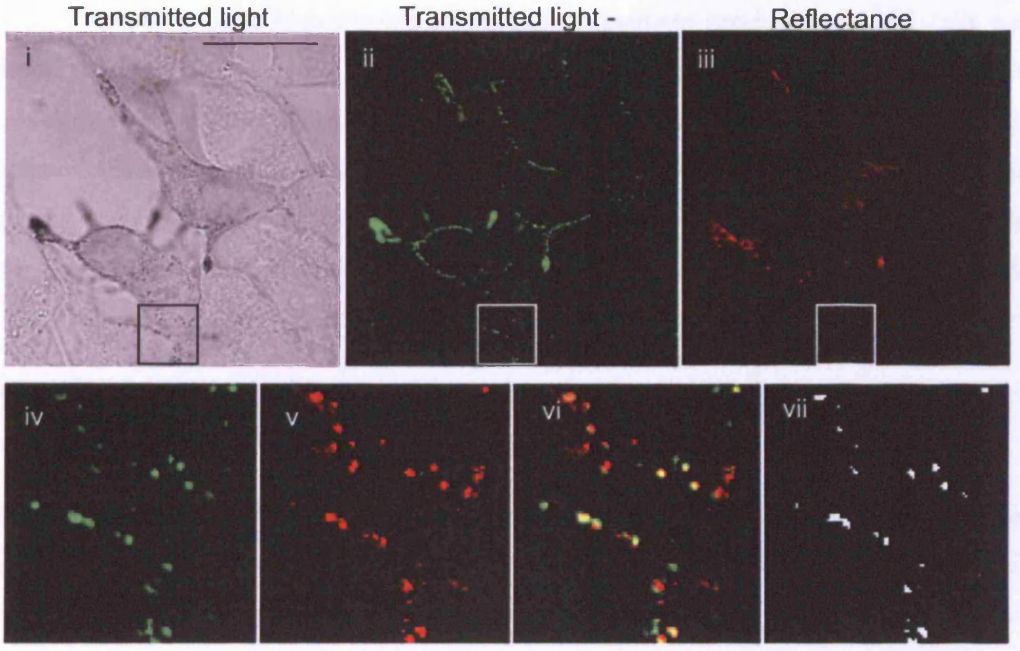

Figure 9.2 Reflectance signal directly co-localises with black pigment containing vesicles. The black vesicles seen with transmitted light in panel i) were analysed at high resolution to determine co-localisation with the reflectance signal panel iii). The transmitted light image was inverted (panel ii). Co-localisation was determined digitally using LSM510 software (panels iv-vi). Pixels of high intensity for both channels are shown in panel vii. Scale bar indicates 50 µm.

9.2.2 Co-localisation of black vesicles and reflectance signals

In more detailed analysis, high-resolution images of pigment-producing B16F2 cells were taken and smaller areas analysed. The high magnification images allowed the co-localisation of the vesicles seen in the transmitted and reflectance images to be determined. To do this, the transmitted light image was inverted using ImageJ software and overlaid with the reflectance image (Figure 9.2). Colocalisation was determined by highlighting pixels of high intensity of both channels (Figure 9.2 vi vii). The result clearly showed that the black vesicles were also the source of the reflectance signal.

9.2.3 Fluorescence signal is induced by MSH and inhibited by inhibition of PKA

To test whether the fluorescent vesicles imaged above were pigment containing melanosomes, it was tested whether their presence was increased by stimulation with MSH and inhibited by inhibition of PKA with the compound H89. The change in pigmentation can be clearly seen by trypsinising the treated populations of cells and centrifuging then into a cell pellet. The colour of these cell pellets is shown in Figure 9.3. The untreated cells appear brown, probably an indication that only some of the population are producing pigment. MSH causes the cell pellet to look much darker as a higher proportion of cells are now producing large quantities of pigment. Treatment of the cells with the PKA inhibitor H89 caused the cell pellet to appear white as melanogenesis was now blocked in these cells.

In addition to making cells darker in the cell pellet, MSH also caused cells to contain more NIRVE vesicles. In contrast H89 treatment caused cells to lose NIRVE vesicles (Figure 9.4). The changes in NIRVE signal were imaged using fixed B16F2 cells plated on cover slips, then stained with DAPI and TRITC phalloidin (Figure 9.4).

Figure 9.3 Pigmentation of B16F2 melanoma cells can be manipulated in vitro. Inhibition of PKA with the compound H89 (10 μM) inhibits melanogenesis. Stimulation of B16F2 cells with α-MSH stimulates melanogenesis. The changes in pigmentation can be seen by trypsinising the cells and spinning them into a cell pellet. The images above were taken with a digital camera.

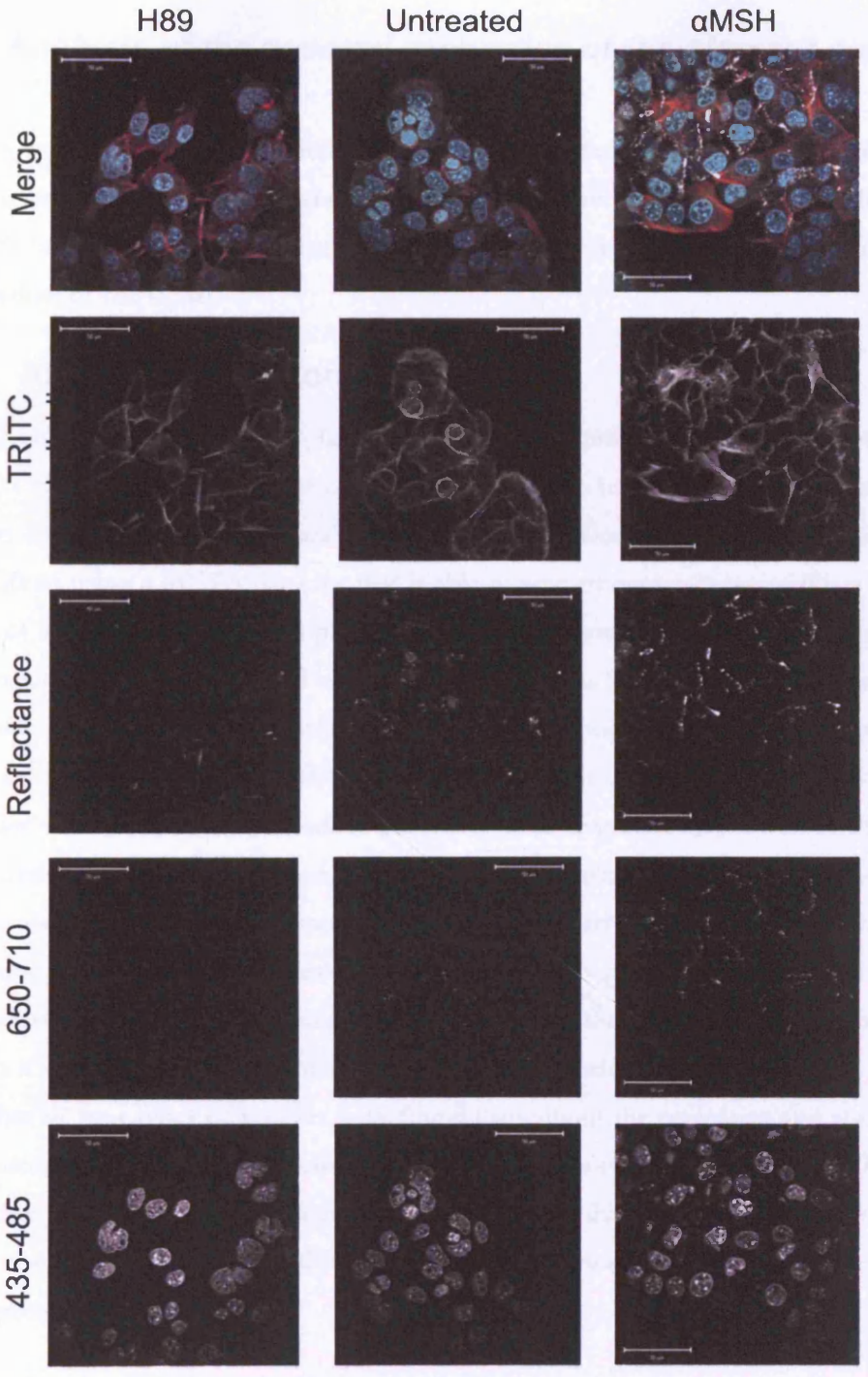

Figure 9.4 Increased pigment production can be measured by multiphoton microscopy. B16F2 cells plated on glass-bottomed cell culture dishes were treated for 48 hours with either 10 μM H89 or α-MSH and imaged using both single and 2-photon confocal microscopy. Excitation wavelengths were 543 and 825 nm. Emission wavelengths are as indicated above. Scale bar indicates 50 μm.

9.3 *Analysis of the spectral properties of the pigment containing vesicles.*

As this type of imaging of pigment production by melanocytes or melanoma cells had not been previously described, it was decided to investigate the spectral properties of these vesicles further. The emission and excitation spectra were determined as well as estimating the lifetime of the signal.

9.3.1 Analysis of emission spectra

B16F2 cells were plated onto glass-bottomed dishes and stimulated with α-MSH for 48 hours. Cells were then fixed but not stained. Cells were imaged by excitation with a multi-photon laser tuned to 800 nm and the emission was collected at wavelengths ranging from 380-750nm using a META detector that is able to scan trhough a range of filters to collect a range of emission from the sample (Figure 9.5). The first striking result was that emission was detected across a very broad range of wavelengths (as had been previously seen in Figure 9.1), the broad range of emission was actually composed of 4 different spectra. This indicated that there were 4 different types of pigment-containing vesicles. The different 'varieties' of vesicles are colour coded according to their spectra and shown in Figure 9.5 A. Some vesicles show only one spectra and some vesicles instead contained a combination of 2 or 3 or even all four separate spectra, indicating that each vesicle does not always contain only one type of NIRVE vesicle. Together the 4 spectra cover wavelengths from approximately 400-680 nm (Figure 9.5B). By separating the signal into each of the 4 distinct spectra it was possible to determine the localisation of each type of signal (Figure 9.6). It was seen that all four types of vesicles were found throughout the cytoplasm and also in the cell protrusions, and it was not possible to say that the localisation of each was different from any other. However analysing larger number of cells in this way may reveal differences that could correlate the spectra to different stages of melanosomes maturation, though this is only speculation at this point.

9.3.2 Analysis of excitation spectra

Similarly to above the excitation spectra for the pigment-containing vesicles was examined. A broad range of emission was collected using a KP 650 filter whilst the multiphoton laser scanned through excitation wavelengths between 690-1030 nm (Figure 9.7 A). The laser power alters with the wavelength, to compensate for these changes an algorithm was written

by the light microscopy department by Daniel Zicha at the CRUK LRI which ensures that the sample is hit with the same laserpower. The KP 650 filter is a special type of dichroic filter used for infra red multiphoton imaging. It allows excitation wavelengths longer than 650 nm to pass onto the specimen and allows emission in the visible range to pass through towards the detectors. The results show that the best excitation of the pigment occurs between 700-850 nm (Figure 9.7 B). It is likely that excitation also occurs at wavelengths shorter than 690 nm but it was not technically possible to test this.

9.3.3 Analysis of the lifetime of the signal

It had sometimes been observed that the signal collected from the pigment resulted in a 'streaking' in the direction of scanning. This was curious and seemed to be dependent on the scan speed. Figure 9.8A shows an example of the same cells imaged at two different scan speeds. The green signal shows horizontal streaking whereas the red signal is more discrete. The pixel time of the two overlaid images is 1.6 μs vs. 106 μs. This result suggested that the lifetime of the signal was extremely long meaning that depending on the scanning conditions the signal was able to 'leak' into the neighbouring pixels as the area was scanned. When the pixel time was low, streaking occurred, as the emission was still present even after the scan had moved to the next position.

To test this theory lifetime imaging was carried out using a FLIM detector that was able to count the photons emitted over a 30 second period (Figure 9.8 B). Analysis of the photons as they were emitted showed that following the initial peak there was a sharp decrease as would be expected for a normal fluorophores. However this initial drop is followed by an area of the curve with a much shallower gradient, indicating that some component of the emission is very prolonged and could potentially explain the streaking effect we had observed. The life time of the signal appears to be very long and beyond the capabilities of the FLIM detector to calculate.

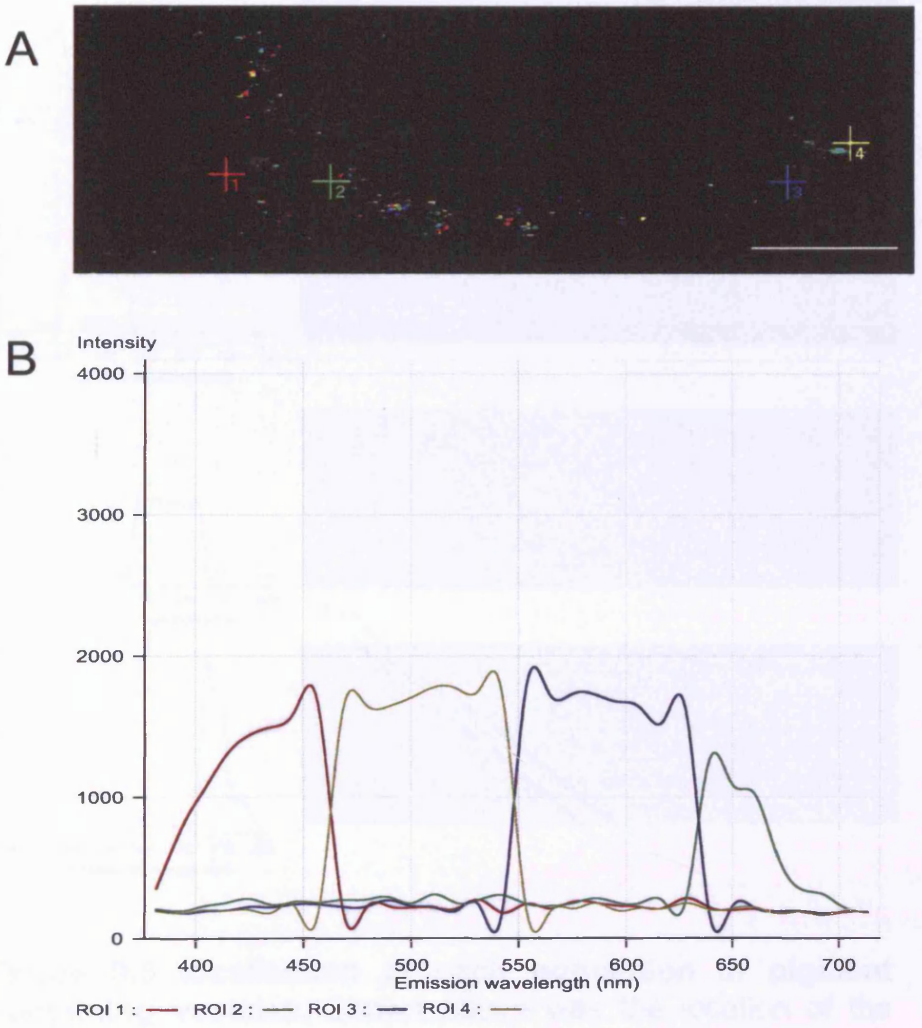

Figure 9.5 detailed analysis of emission spectra reveals 4 distinct spectra. Pigment containing B16 F2 cells were plated onto glass bottomed dishes and imaged using a multiphoton laser. Emission was detected between 380 -750 nm using a meta detector attached to a Zeiss510 confocal microscope. A) each pixel is pseudocoloured according to the emission recorded. Scale bar indicates 10 microns B) Overlay of the intensity of 4 distinct types of emission plotted against the wavelength.

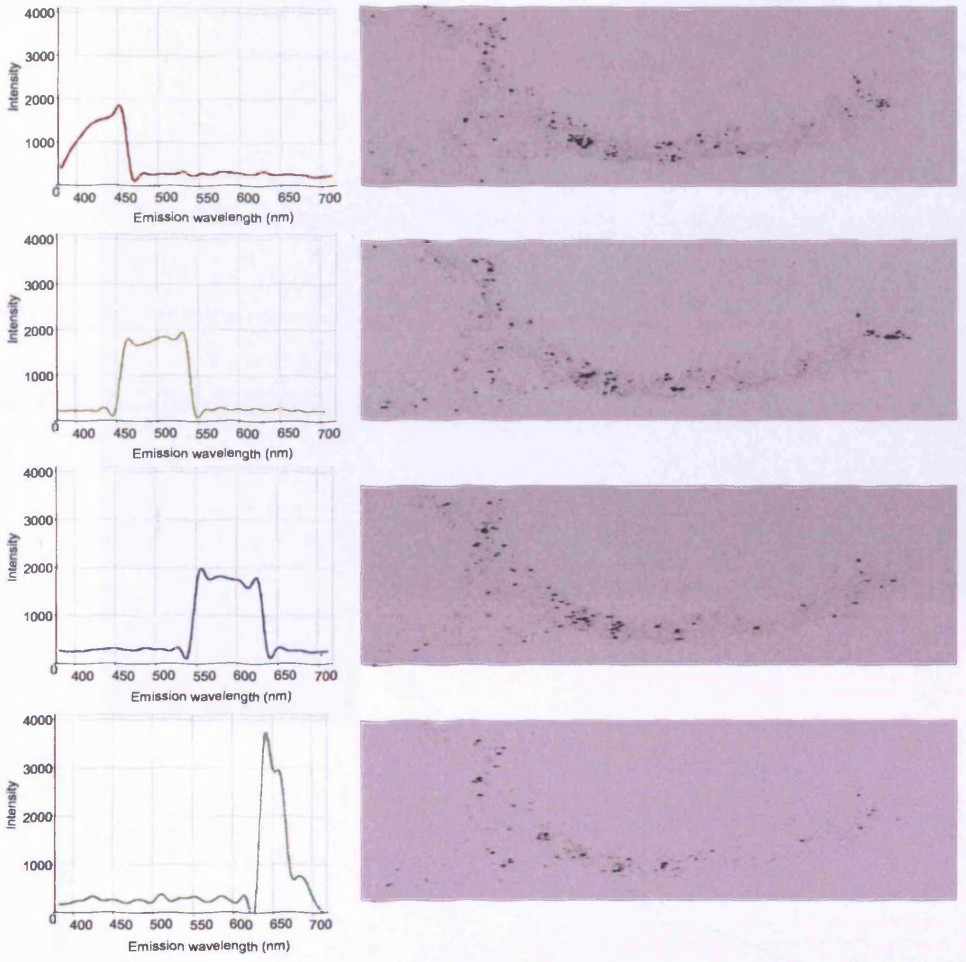

Figure 9.6 localisation of each population of pigment containing vesicles. Shown above was the location of the 'speckles' that correspond to each of the 4 different emission spectra identified.

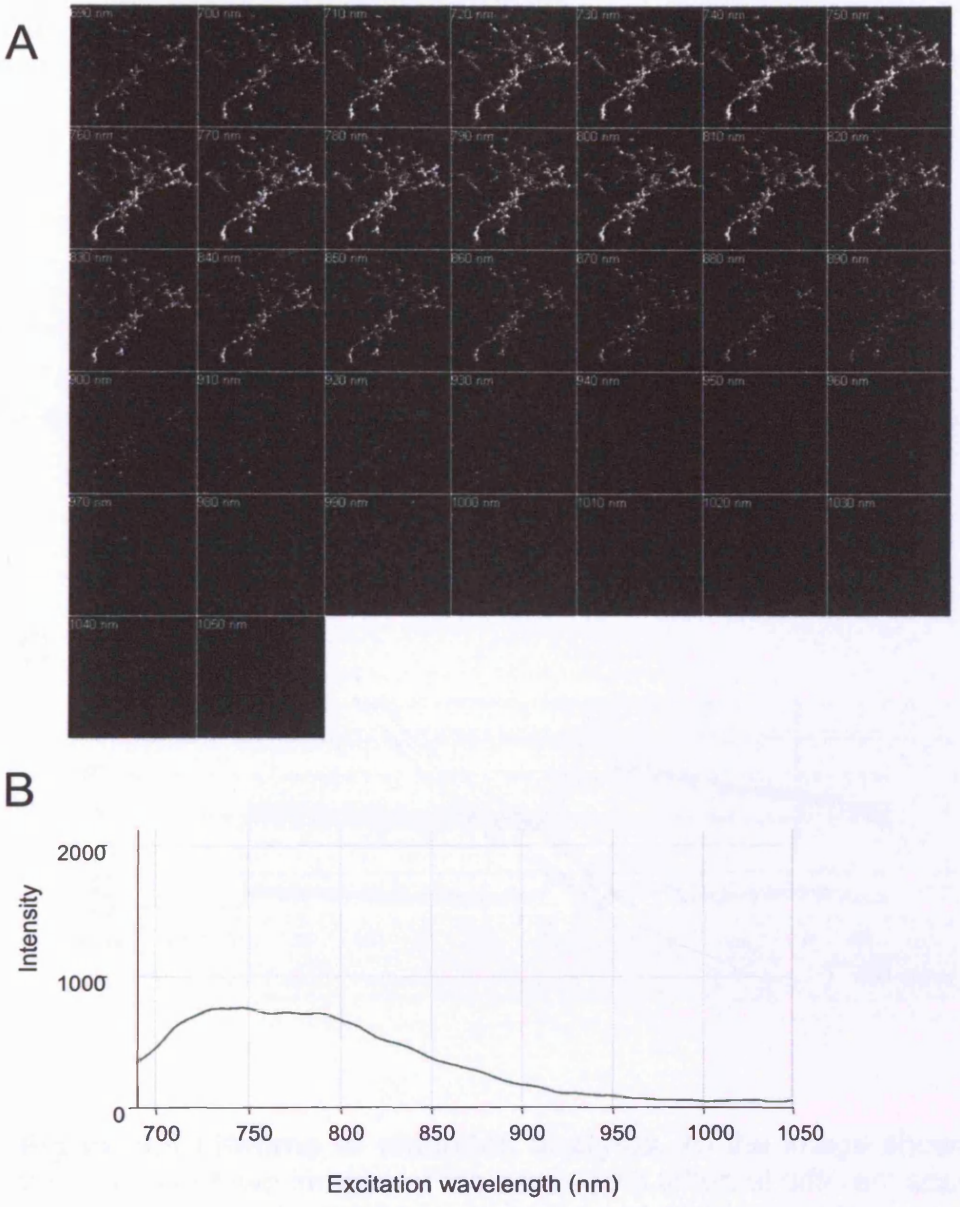

Figure 9.7 Analysis of excitation spectra of pigment containing vesicles. Pigment containing B16 F2 cells plated on glass bottomed dishes were imaged using a multiphoton laser. The excitation wavelength of the laser was tuned to scan between 760-1030 nm and the emission in the visible range was collected. A) gallery view of sequential images corresponding to the increasing excitation wavelengths. B) graph showing the intensity of emission plotted against excitation wavelength.

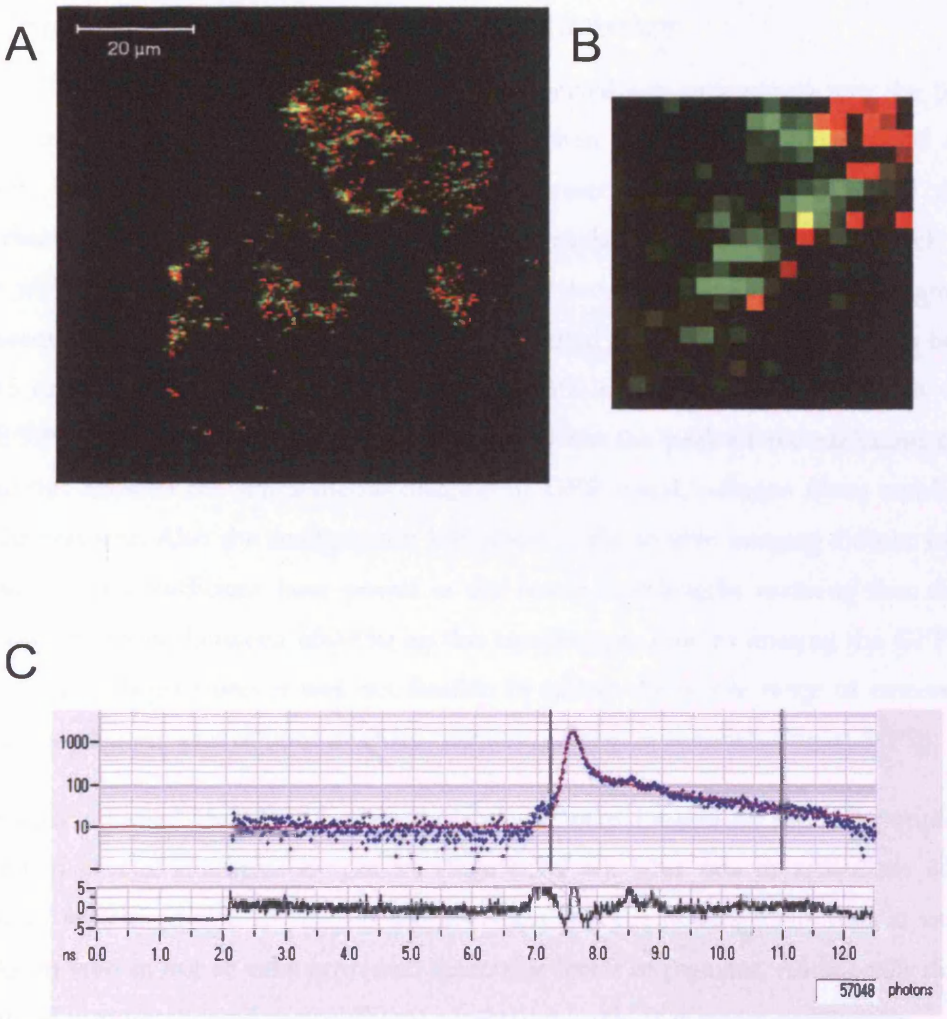

Figure 9.8 Lifetime of emission analysis. A) the image shows the overlay of two images of the same cells taken at different scan speeds. The red image has a pixel time of 106 µs and the green image has a pixel time of 1.6 µs. B) zoomed in image to show streaking of green image compared to red, in the direction of scanning. C) Life time imaging showing graph of photon count against time.

9.4 *Visualisation of melanin in xenograft tumours in vivo.*

9.4.1 High resolution imaging of living tumours

B16F2 cells stably expressing GFP-CAAX were injected sub-cutaneously into the flank of nude mice. The resulting tumours were imaged when they reached between 4-6 mm in diameter. High-resolution imaging using a 63X water immersion lens showed the cell membranes labelled with GFP. Cell nuclei and cytoplasm could be seen as black empty spaces within the GFP signal. It was found that it was possible to image pigment in fluorescent vesicles in the same way as had been carried out in vitro. The emission between 575-615 nm was collected following excitation at 850 nm to identify the melanin vesicles (Figure 9.9 A). 850 nm was chosen although it was not the peak of the excitation spectra, because this allowed the simultaneous imaging of GFP signal, collagen fibres and NIRVE from the pigment. Also the multiphoton laser used to the in vivo imaging did not have the capability to give sufficient laser power at the lower wavelengths meaning that the best excitation was found between 800-850 on this microscope. Due to imaging the GFP signal and also the collagen fibres it was not feasible to collect the whole range of emission and 575-615 was chosen, as it did not over-lap with other imaging channels (Figure 9.9 B).

The images revealed that the fluorescent vesicles were located at the cell periphery as indicated in several examples by arrows (Figure 9.9 A). This was in agreement with the location of vesicles in cells in vitro. It was also clear that the heterogeneity seen in vitro was also seen in vivo as not all cells expressed detectable levels of pigment. Additionally different areas of the tumour showed very different expression levels of pigment production.

9.4.2 Time lapse multi-photon imaging of melanoma tumours

It was not possible to image the B16F2 tumours at high resolution over the time-lapse period as too much photo bleaching and possibly photo damage and tissue damage from the laser would occur. Instead the tumours were imaged using a 20X lens with a lower numerical aperture, and with lower laser power and less averaging, to protect against this (Figure 9.10 A). Images taken at 30 s intervals showed some cells within the tumour moving. Movements were either as single cells or in collective chains between other cells (Figure 9.10 B and accompanying supplementary movies). Some areas of tumour showed no motility whilst other areas contained many cells moving. Motile cells were generally rounded as had been seen in the imaging of the A375 tumours suggesting that B16F2 cells might also use

amoeboid cell motility to invade in vivo. Arrows identify an individual motile cell (Figure 9.10 B). The image in part B is composed of 3 time points of the same area overlaid in red, green and blue. The white areas of the image indicate directly overlapping red, green and blue signal and therefore show non-motile areas, motile cells are shown in red, green and blue, as the 3 time points do not overlay.

9.5 Motile cells in vivo contain less melanin than non motile cells

For each time-lapse movie made, motile cells were identified. The level of pigment contained within these cells was measured by signal intensity and compared with the average pigment intensity in the whole frame. The data is plotted as a relative frequency distribution. The Y-axis shows the proportion of each population (motile cells and non-motile cells). The total population of cells, motile and non-motile, shows a skewed distribution ranging from 0 to 7, centred on 1. The majority of cells contain melanin between the ratios of 0.5 and 1.5. Results showed that the ratio of the melanin content was mostly less than 1 in the motile cells (Figure 9.11). The non-motile cells were a more spread population based of pigment content with a few cells containing large amount of signal, and others containing very little. The motile cells in addition to containing less pigment, also move with a rounded morphology, and are no longer dendritic as a pigment producing melanocytes would be, which may indicate a less differentiated state.

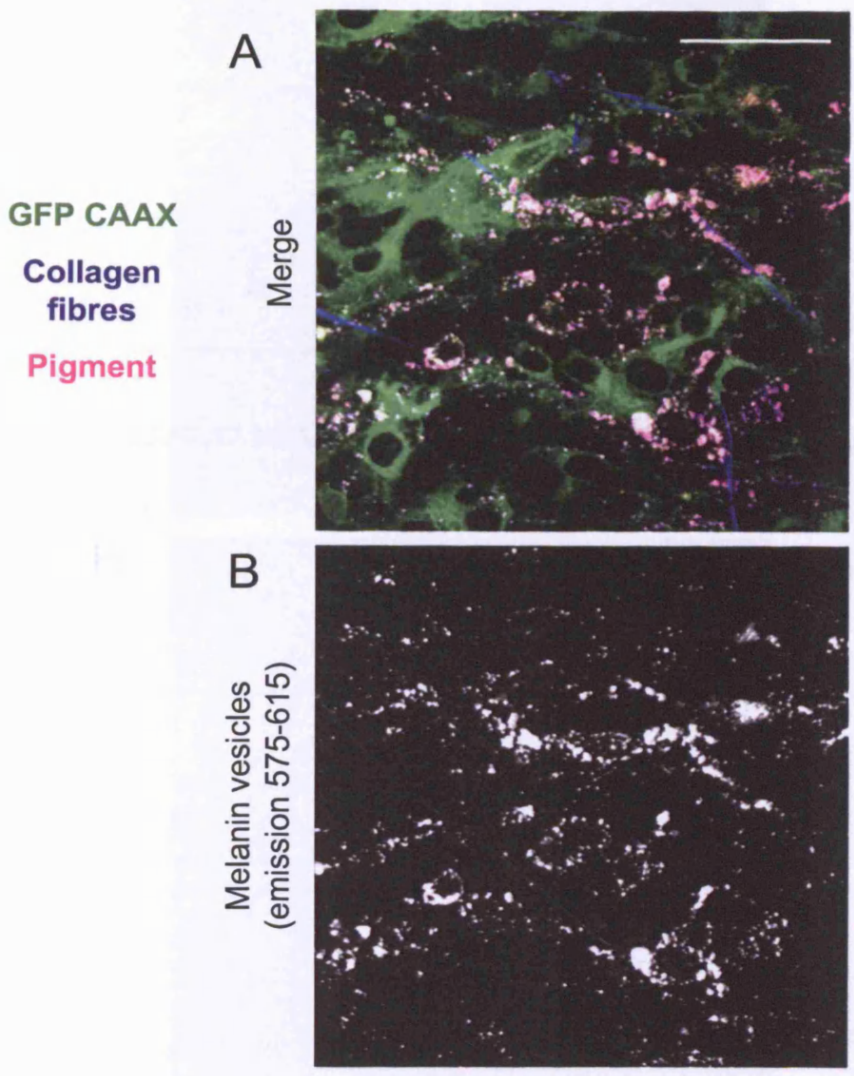

Figure 9.9 High resolution imaging of B16F2 xenograft tumours in vivo. B16F2 GFP CAAX tumours grown subcutaneously in nude mice were imaged using multiphoton confocal microscopy and a 63X water immersion lens. Imaging revealed that the pigment containing vesicles seen in vitro could be imaged using similar parameters as in vitro. The pigment containing vesicles appeared to be mostly around the cell periphery. A) merged image showing GFP CAAX expressing tumour cells, collagen fibres in blue (2nd harmonic signal), and pigment in pink. B) image of separate channel of pigment only. Scale bar indicates 20 μm.

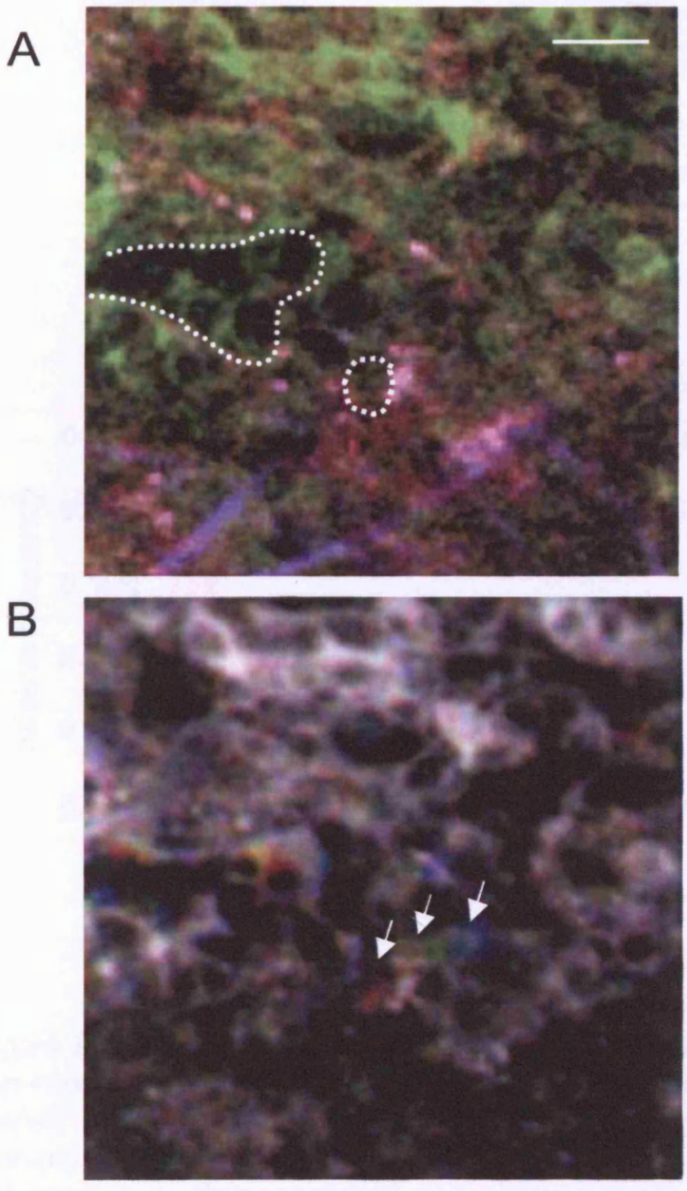

Figure 9.10 Analysis of B16 F2 cell movement in vivo. B16F2 GFP CAAX tumours grown subcutaneously in nude mice were imaged using multiphoton confocal microscopy A) merged image showing GFP CAAX expressing tumour cells, collagen fibres in blue (2nd harmonic signal), and pigment in pink. Dashed outlines indicate single moving cell and group of collectively moving cells. Scale bar indicates 20 microns B) 3 consecutive time points are overlaid in the image above. The first time point (0) in red, the 2nd (90 sec) in green and the 3rd (180 sec) in blue. Cells which are non motile will appear white as the 3 colours are overlaid. Motile cells are shown in red/green/blue and one example is indicated by the arrows above. Please also see the accompanying supplementary movies.

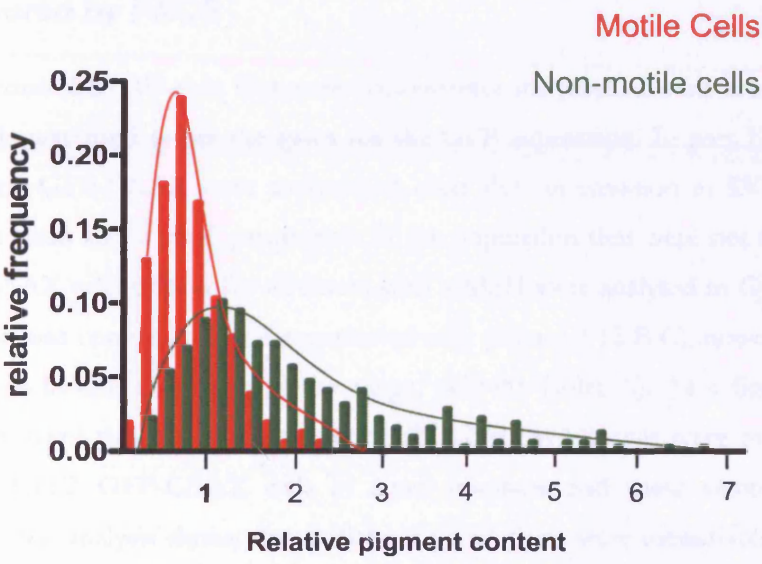

Figure 9.11 Motile B16F2 cells contain less melanin than non-motile cells in vivo. In vivo time-lapse multi-photon movies were analysed using LSM510 software. Average intensity of melanin was measured for each area. Cells within that area were then analysed and given a score for melanin expression relative the average level. The cells were sub-divided into motile (red) and non-motile (green) categories and the frequency distribution of the results is shown above. 155 motile cells and 316 non-motile cells were analysed from 15 different imaged areas from 4 xenograft tumours. Relative melanin content is categorised into bins of width 0.2.

9.6 Melanin expression can be determined by FACS analysis

As the spectral properties of melanin expressing cells had been discovered and utilised in the microscopy assays, it was next investigated whether optical parameters could also be used to examine and sort the B16F2 tumour cells by FACS (Figure 9.12, Figure 9.13) into high and low melanin expressers for further analysis.

9.6.1 MSH stimulation causes measurable shifts in violet emission measured by FACS

As a negative control B16F2 cells that were not fluorescently labelled were used (Figure 9.12 A). This sample was used to set the gates for the GFP expression. In part B) B16F2 cells stably expressing GFP-CAAX were analysed. A clear shift in emission in 530-30 Blue was observed. There was also a small proportion of the population that were not GFP-positive. B16F2 GFP-CAAX cells treated for 48 hours with α-MSH were analysed in C). The level of GFP expression was comparable to the untreated cells (Figure 9.12 B C), however there was a significant shift in emission in the violet range, (450-40 Violet A). As a final test of this change in fluorescent properties, untreated B16F2 GFP-CAAX cells were mixed with the MSH treated B16F2 GFP-CAAX cells in equal numbers and these samples were run together. In D) the analysis shows that 2 distinct populations were identifiable. E) shows a histogram of the violet emission of the mixed sample in D). Separating the two peaks and measuring the proportion of cells in each population showed that there were approximately equal numbers in each population as there should have, as the mix was made with equal numbers of each separate sample. The two populations did still over lap to some degree which was not unexpected as looking at the cells in vitro on cover slips had shown that not all cells in the population respond to α-MSH stimulation to the same degree.

9.6.2 Sorting of B16F2 tumours by FACS

Having shown that it was possible to measure the pigment content of cultured B16F2 cells by FACS, it was now tested whether the same technique could be applied to tumour cells extracted from the B16F2 GFP-CAAX xenograft tumours. If this was feasible then it could be possible to separate the less pigmented (containing the more motile cells) population from the more highly pigmented (less motile) population.

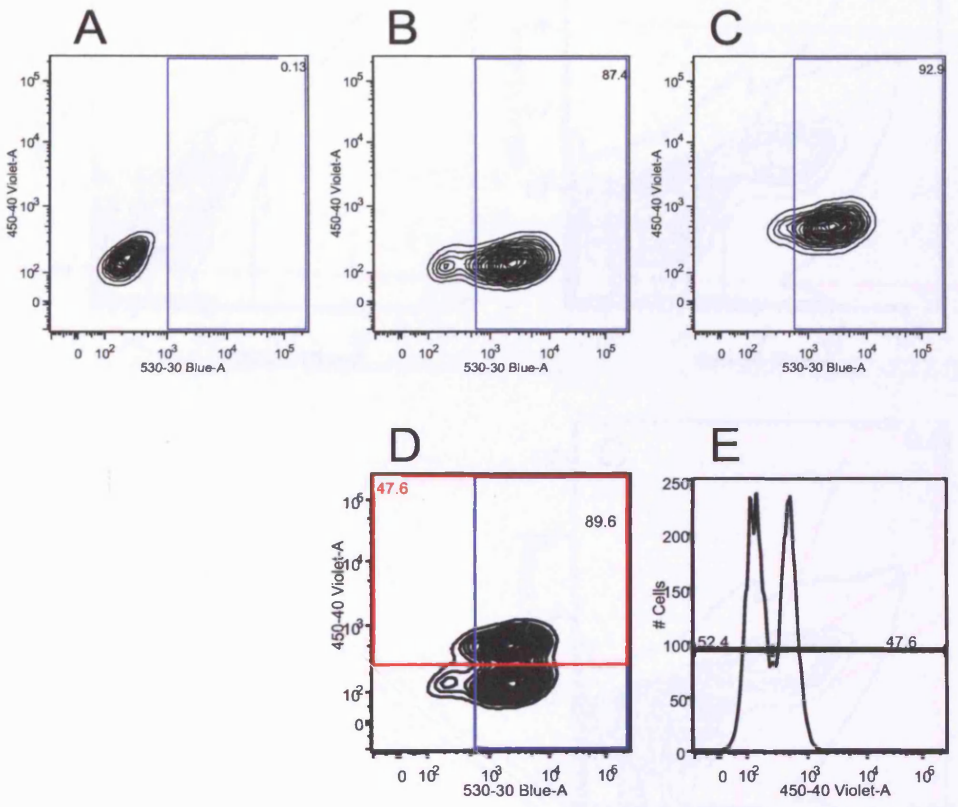

Figure 9.12 FACS analysis of melanin production by B16F2 in vitro. A)Unlabelled B16F2 B)B16F2 stably expressing GFP CAAX C)B16F2 stably expressing GFP CAAX stimulated with α-MSH for 48 hours. D)Mixed population of untreated B16F2 GFP CAAX and α-MSH treated B16F2 GFP CAAX. E) Histogram of violet emission of mixed population in D)

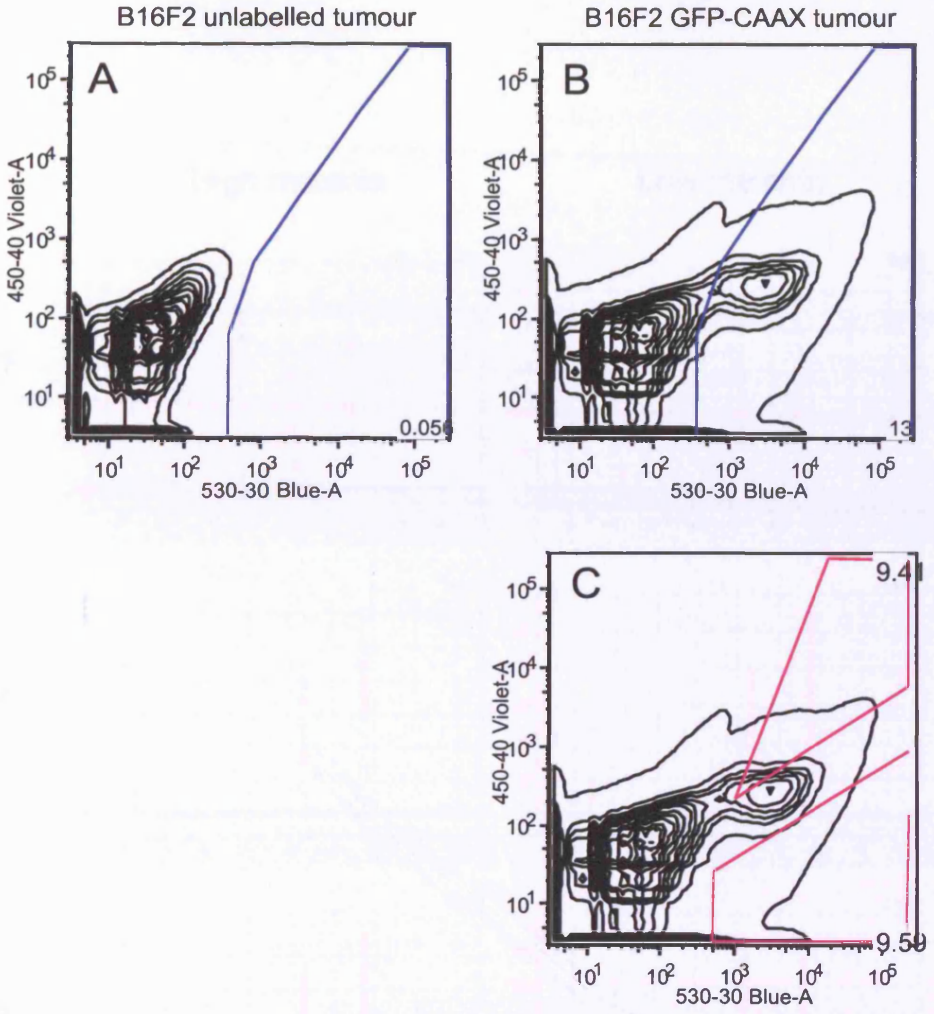

Figure 9.13 FACS sorting of dissected B16F2 GFP CAAX tumour cells. B16F2 GFP CAAX or unlabelled B16F2 cells were injected subcutaneously into nude mice and tumours were allowed to grow to approximately 1 cm in diameter. Tumour cells were extracted and sorted by FACS. Part B shows the GFP positive population, and part C shows the gates used to separate the GFP positive cells into two groups based on their melanin content.

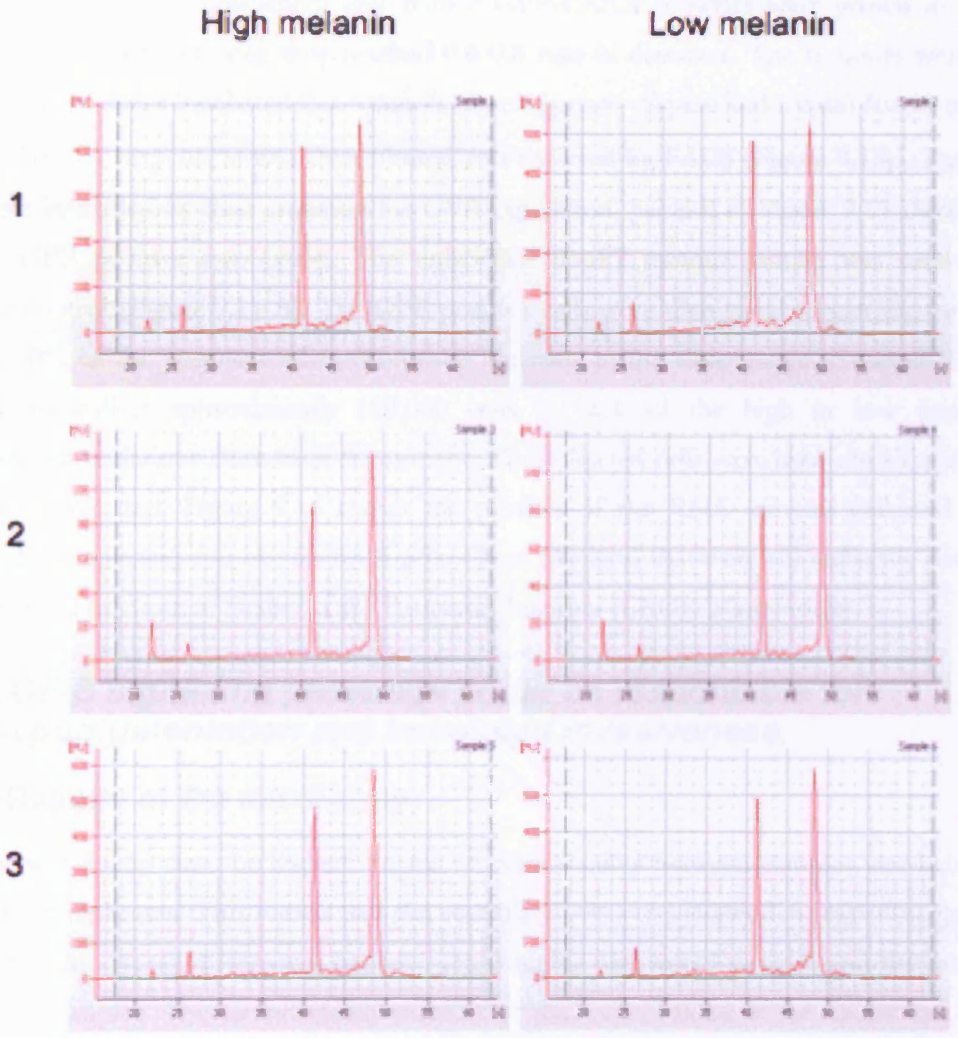

Figure 9.14 RNA profiles of 3 replicates sent for microarray analysis. The 3 pairs of RNA samples were run out on Aglient pico RNA chips. The profiles are shown above.

RNA extracted from these populations would then be analysed by microarray to try to determine signalling pathways altered between the two different populations.

Subcutaneous B16F2 (unlabelled) and B16F2 GFP-CAAX tumours were grown in nude mice and dissected out once they reached 0.6-0.8 mm in diameter. The tumours were cut into small pieces and incubated in a solution of collagenase, dispase and trypsin for 90 min at 37 °C. The cell suspension was then filtered and analysed by FACS (Figure 9.13). Tumour cells were identified by their emission for GFP expression, panel B in Figure 9.13 shows the distinct GFP positive population. The unlabelled B16F2 tumour sample was used as a negative control (Figure 9.13 A). The GFP positive cells were then gated to sort the top and bottom 10% of the population based on their emission in the violet range. Generally it was possible to collect approximately 100,000 cells in each of the high or low (melanin expression) populations from each experiment. The collected cells were then centrifuged and RNA was extracted. Figure 9.14 shows the profiles of the RNA samples collected in 3 independent replicates run out on RNA pico Chips (Agilent) that were subsequently sent for analysis at the microarray facility at the Patterson Institute (CRUK Manchester).

9.7 TGF-β signalling pathways could be responsible for hypopigmentation and increased invasiveness.

9.7.1 Results of the microarray

Firstly it was found that the highest degree of commonality between samples was between each pair of replicates. This means that the variability between independent experiments was higher that the overall differences between the 3 highly pigmented samples and the 3 lower pigmented samples. This unfortunately means that the level of noise in the results was high, although this is not unexpected considering that the RNA was extracted from FACS sorted tumour cells extracted from living tumours. Nonetheless, several interesting candidate genes were identified which were consistently up or down regulated between the cell populations (Figure 9.15). Among the identified genes was TGF-β2, which will be investigated further in this chapter.

mean fold change	Gene name
3.49499981	RIKEN cDNA A130004G11 gene
3.253531426	phosphatidylinositol glycan anchor biosynthesis, class C
3.203391919	macrophage scavenger receptor 1
3.074942594	predicted gene, EG214321
2.803932736	ADP-ribosylation factor-like 15
2.579357596	methyl-CpG binding domain protein 1
2.492769541	ataxin 1
2.435398687	utrophin
2.433645158	CUG triplet repeat, RNA binding protein 2
2.353345464	expressed sequence C78441
2.342984881	mitochondrial carrier homolog 2 (C. elegans)
2.333445831	forkhead box K2
2.29172782	RIKEN cDNA 5830474E16 gene
2.268505136	amyloid beta (A4) precursor protein-binding, family B, member 2
2.253053135	nuclear receptor subfamily 2, group C, member 2
2.236508536	retinitis pigmentosa 9 (human)
2.219804237	Smg-6 homolog, nonsense mediated mRNA decay factor (C. elegans)
2.186186495	like-glycosyltransferase
2.146184519	melanoma antigen, family H, 1
2.142588278	smoothened homolog (Drosophila)
2.122154341	glutamine fructose-6-phosphate transaminase 1
2.077992981	cell growth regulator with ring finger domain 1
2.046118573	DNA segment, Chr 9, Wayne State University 90, expressed
2.016492906	excision repair cross-complementing rodent repair deficiency, complementation group 6
1.991367614	expressed sequence C80258
1.973734804	microtubule associated serine/threonine kinase 2
1.953981121	vasohibin 1
1.943084942	kit ligand
1.924419707	chemokine (C-X-C motif) receptor 4
1.922101198	neural cell adhesion molecule 1
1.882293569	suprabasin
1.859582847	RIKEN cDNA 5730419I09 gene
1.858646074	FCH domain only 2
1.810351726	expressed sequence C76628
1.786922203	phosphatase and tensin homolog
1.749416594	secretion regulating guanine nucleotide exchange factor
-3.97877074	steroid 5 alpha-reductase 2-like
-3.756834213	expressed sequence T25656
-2.870838975	small nuclear ribonucleoprotein D3
-2.862794085	expressed sequence T25656
-2.34866994	RIKEN cDNA 4930414L22 gene
-2.309742409	centromere protein A
-2.225585523	vacuolar protein sorting 13A (yeast)
-2.220773022	transforming growth factor, beta 2
-2.165699485	myeloid leukemia factor 1 interacting protein
-2.107059637	RIKEN cDNA 4933440H19 gene
-2.098114329	transforming growth factor, beta 2
-2.005345288	sorbitol dehydrogenase
-1.941578554	RIKEN cDNA A930005H10 gene
-1.907397033	deltex 3-like (Drosophila)
-1.907104277	zinc finger protein 110
-1.860407267	formin-like 3
-1.855516149	syntaxin 3
-1.792237	zinc finger and BTB domain containing 11
-1.773858522	mesoderm specific transcript
-1.767461621	RAB2B, member RAS oncogene family
-1.75090716	SRY-box containing gene 6
-1.686951396	zinc finger protein 110
-1.669476593	cDNA sequence D10627
-1.628090867	RNA binding motif protein 39
-1.615550228	RNA binding motif protein 39
-1.575011319	RAB2B, member RAS oncogene family

Figure 9.15 Results from microarray. The genes that were consistently up or down regulated in all three replicates are listed above in order of highest to lowest fold change. The top part of the table lists genes that were expressed at higher levels in the cells containing more pigment. The lower part of the table shows genes that were expressed at higher levels in the tumour cells expressing less pigment.

Another very interesting result was that phosphatase and tensin homolog (PTEN) was expressed at higher levels in the high-pigmented cells. This potentially means that in addition to switching off melanin production, the lower pigmented cells are also down regulating a well-documented tumour suppressor gene. Genes encoding proteins involved in pigment production such as MITF or the enzyme tyrosinase did not appear in this list. However there was one melanoma antigen (family H1) that was more highly expressed in the more highly pigmented cells. Two other genes potentially playing a role in cell motility that were expressed more highly in highly pigmented cells were the chemokine receptor CXCR4 and the neural cell adhesion molecule (NCAM), although as this population was found to be less motile their high expression is difficult to explain and it was beyond the scope of this chapter to investigate all genes involved in cell motility.

9.7.2 TGF-β2 is up-regulated by less-pigmented melanoma cells in vivo.

Micro array results showed that TGF-β2 was up regulated in the cell population containing less melanin pigment. Although the level of noise in the results was fairly high due to the nature of the experiment and the way that the RNA samples were collected, TGF-β2 was consistently higher in the lower pigmented samples in all three independent replicates tested. The mean fold change was approximately 2.2 (Figure 9.15). As TGFβ signalling has been known to play a role in cancer and also epithelial to mesenchymal transition (EMT), it was decided to investigate this further.

9.8 Investigating the effect of TGFβ signalling on B16 cells in vitro

To test the results from the microarray a series of in vitro experiments were conducted to see what effect TGFβ signalling had on the pigmentation, cell morphology, and motile behaviour of the B16F2 cells in vitro. The hypothesis from the results of the of the microarray would be that TGFβ may be functionally relevant in one or all of these processes.

9.8.1 TGFβ signalling inhibits pigmentation in B16F2 in vitro

As TGFβ2 had been found to be more highly expressed in cells containing less pigment, it was tested whether TGFβ2 directly influenced melanogenesis in B16F2 cells in vitro (Figure 9.16). It was found that both TGFβ 1 and TGFβ2 reduced the level of pigmentation in vitro within 24 hours of treatment (Figure 9.16A, B). It was also interesting that even when cells

were also stimulated with MSH, TGFβ was able to inhibit the pigmentation production. It was also true that the inhibition of pigment production occurred even at very low doses of TGF beta. Although both TGFβ1 and TGFβ2 had similar effects, the inhibition of pigmentation seems slightly more efficient with TGFβ than with TGFβ2.

9.8.2 TGFβ signalling induces stress fibre formation

B16F2 cells were plated on glass bottomed dishes and stimulated with either α-MSH TGFβ1 or TGFβ2 for 24 hours, then fixed and stained with FITC phalloidin to reveal the actin cytoskeleton. Figure 9.17 shows the untreated cells contain some stress fibres and that treatment of cells with α-MSH, even for just 24 hours causes cells to become more spread and the number of stress fibres appears reduced. Stimulation of cells with either TGFβ1 or TGFβ2 had a different effect and caused cells to induce formation of more stress fibres indicating a higher degree on tension in these cells. It can also be seen that TGFβ1 or TGFβ2 inhibits pigment production in these cells by the lack of NIRVE signal.

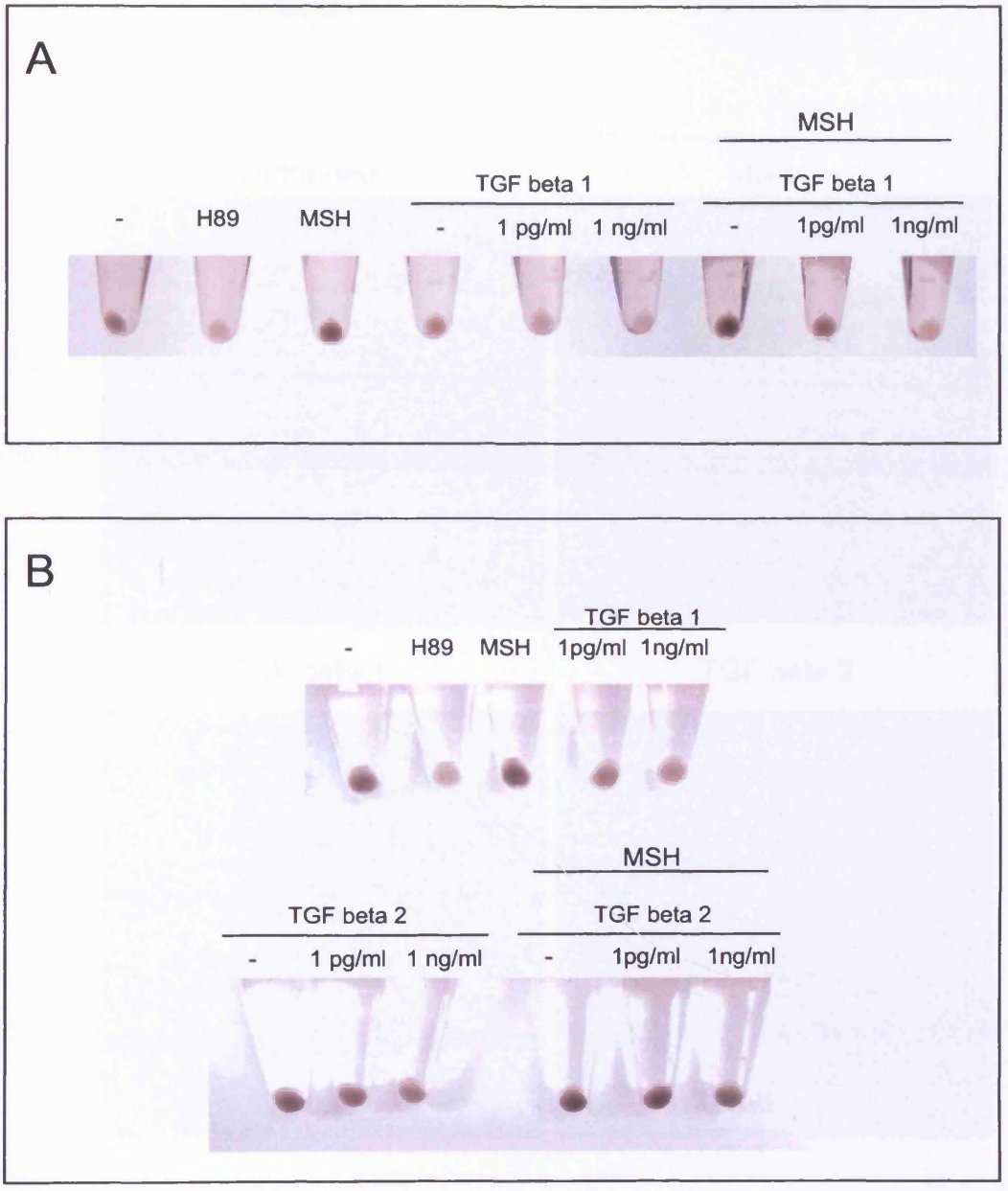

Figure 9.16 TGFβ 1 and TGFβ 2 inhibit pigment production in B16F2 in vitro. B16F2 cells were plated in 6 well cell culture plates and treated with H89, MSH and/or TGF beta 1/TGF beta 2 for 24 hours. Cells were then trypsinised and centrifuged. The colour of the cells pellet was recorded using a digital camera.

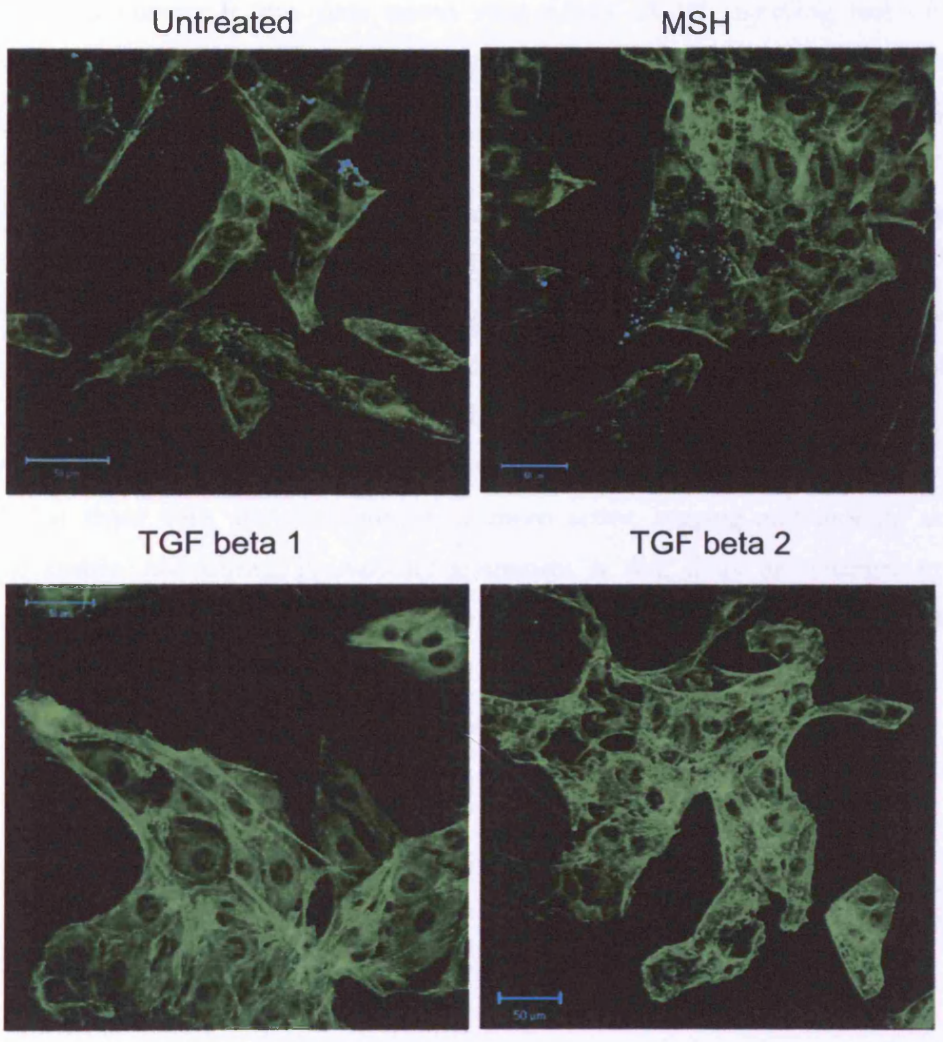

Figure 9.17 TGFβ 1 and TGFβ 2 increase stress fibre formation in B16 F2 cells in vitro. B16F2 cells were plated onto glass bottomed dishes and treated with MSH, TGF beta 1 or TGF beta 2 for 24 hours. Cells were then fixed and stained with FITC phalloidin (green). Pigment was imaged using multiphoton excitation at 820 nm (blue). Scale bar indicates 50 µm.

9.8.3 TGFβ signalling inhibits dendritic cell morphology

When plated on deformable collagen/matrigel matrix, B16F2 cells show a mixture of cell morphologies ranging from dendritic to rounded cells. Stimulation with MSH caused cells to become more dendritic. It was next tested what effect TGFβ signalling had on the morphology of B16F2 cells in this in vitro system. B16F2 cells were plated on deformable collagen/matrigel matrix, and treated with either MSH, TGFβ1 or TGFβ2 for 4 days (Figure 9.18). Cells were then fixed and stained with FITC phalloidin and DAPI. The collagen/matrigel matrix was imaged using reflectance signals. In this long term treatment assay it was found that cells treated with MSH were quite spread with numerous thin dendritic protrusions, this was also seen in a sub-population of the untreated cells. However treatment with either TGFβ1 or TGFβ2 inhibited the formation of these dendritic protrusions and cells were fairly rounded instead. Looking at the matrix it was also seen that there were more holes in the matrix around cells treated with either TGFβ1 or TGFβ2. This suggested that these cells are more motile or more active, tugging and pushing at the deformable matrix and tearing it. Another alternative is that there are changes in the proteolytic activity of these cells and TGFβ1 or TGFβ2 increase the ability of B16 cells to degrade the matrix surrounding them.

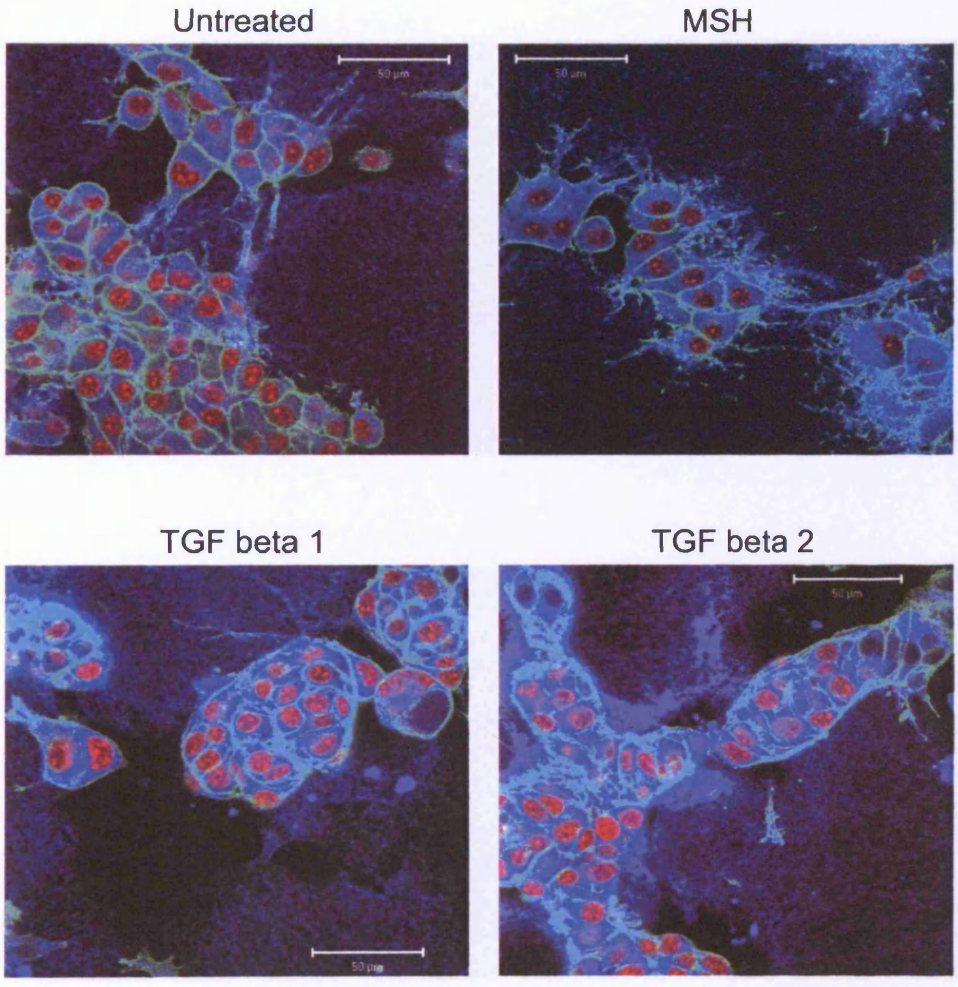

Figure 9.18 TGFβ 1 and TGFβ 2 inhibit dendritic morphology of B16 F2 cells in vitro. B16 F2 cells were plated on deformable collagen/matrigel and treated with MSH, TGF beta 1 (1 ng/ml) or TGF beta 2 (1ng/ml) for 4 days. Cells were then fixed and stained with DAPI (red) and TRITC phalloidin (green). The matrix is imaged by reflectance (blue). Scale bar indicates 50 μm.

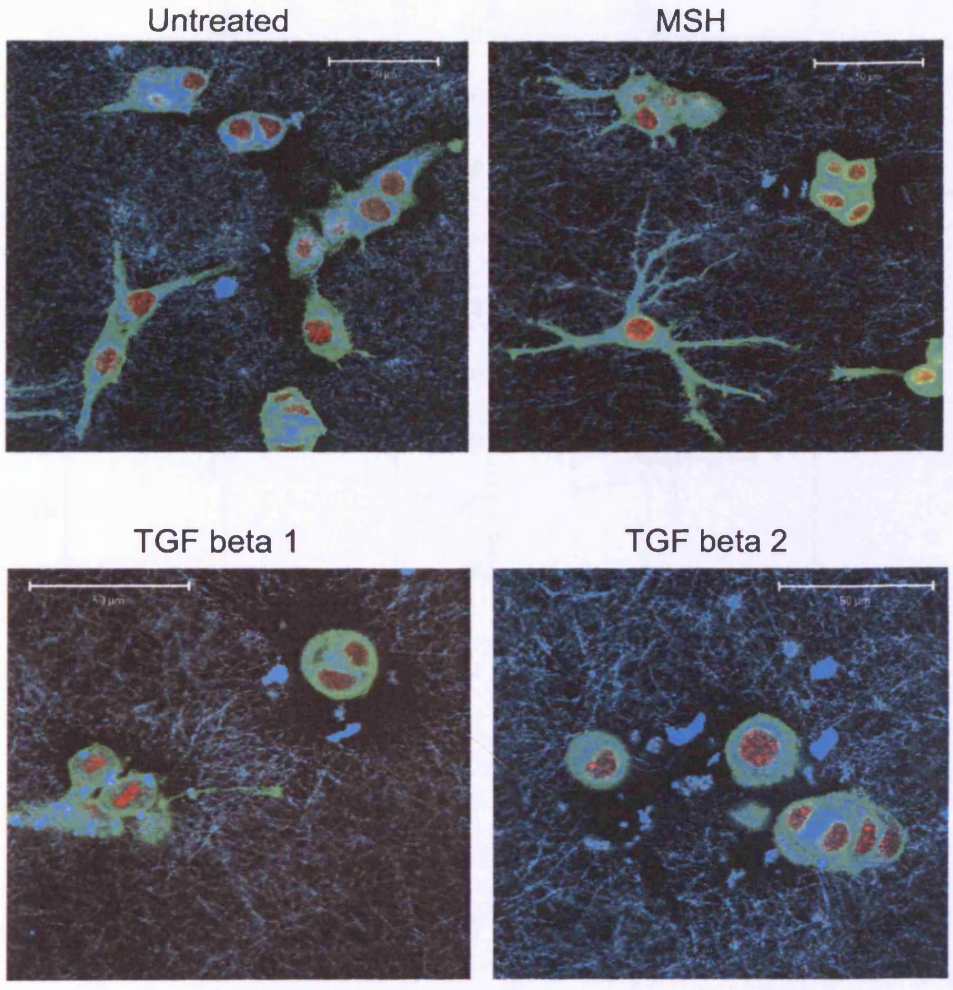

Figure 9.19 TGFβ1 and TGFβ2 inhibit dendritic morphology of B16 F2 cells within 24 hours of stimulation. B16 F2 cells were plated on deformable collagen/matrigel and treated with MSH, TGF beta 1 (1 ng/ml) or TGF beta 2 (1ng/ml) for 24 hours. Cells were then fixed and stain with DAPI (red) and TRITC phalloidin (green). The matrix is imaged by reflectance (blue). Scale bar indicates 50 μm.

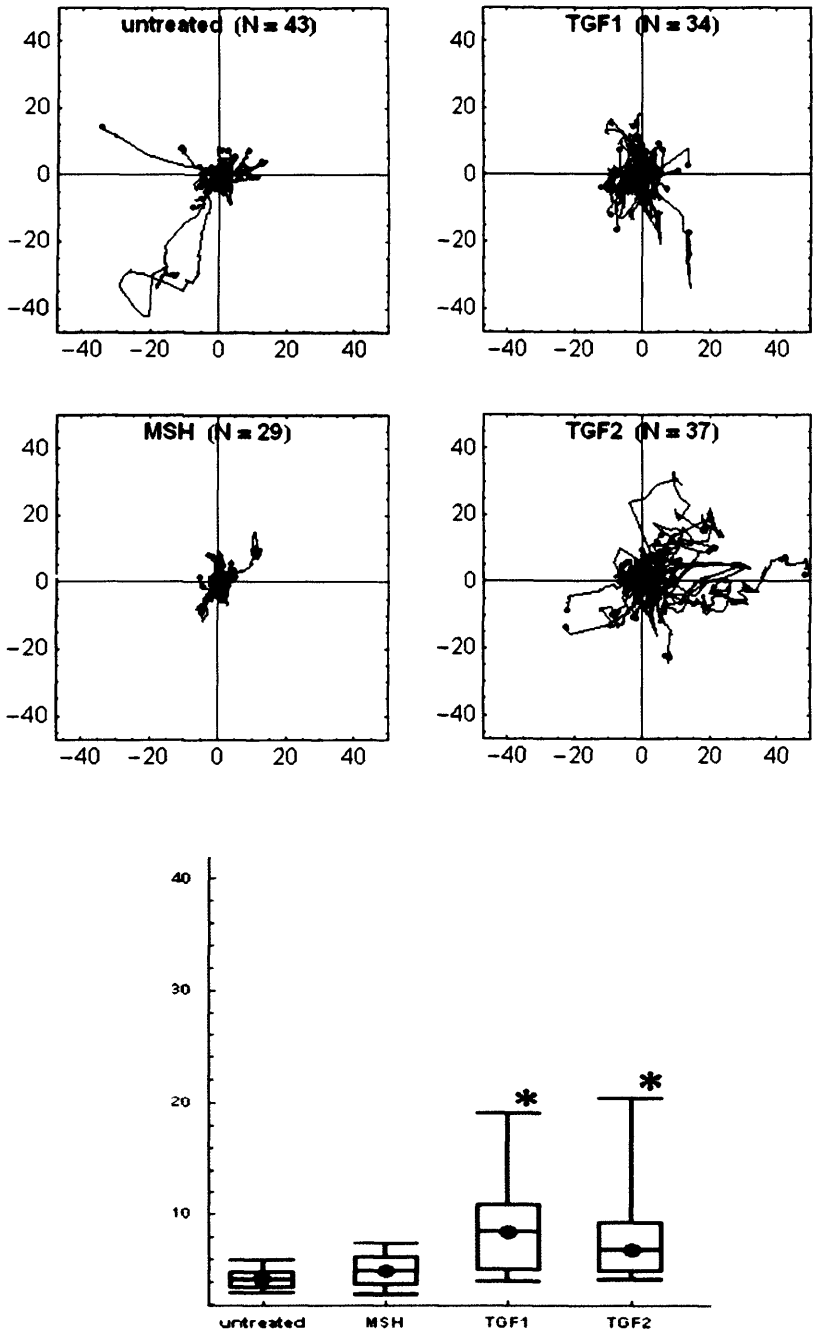

Figure 9.20 TGFβ causes increased cell motility in B16F2 cells plated on deformable collagen/matrigel matrix. A) Graphs showing tracks of each treatment group all centred at zero. B) box plots showing range of cells speeds of each treatment group. * indicated $p<0.01$ Anova test.

It was next tested at what time point the cell rounding induced by TGFβ signalling occurred. The same experiment as above was carried out but cells were fixed after only 24 hours. This time was chosen because the inhibition of pigmentation occurred in this time frame. Figure 9.19 shows that at 24 hours cells treated with TGFβ1 or TGFβ2 were rounded and did not exhibit dendritic protrusions like the untreated cells or the MSH treated cells.

9.8.4 TGFβ signalling increases cell motility

In addition to causing retraction of dendrites and causing cells to become more rounded, TGFβ signalling also increased cell motility. This was measured by plated B16F2 cells on deformable collagen/matrigel matrix and performing phase contract time lapse imaging. Untreated cells and cells treated with αMSH appeared dendritic with multiple long protrusions. The cells treated with either TGFβ1 or TGFβ2 became less dendritic as would be predicted from previous data, but they also became more motile, moving grater distances (Figure 9.20). Movement of the non-treated cells tended to be the extension and retraction of cell protrusions but for this analysis only translocation of the nucleus was tracked (see supplementary movies for examples of cell motility used for this quantification). Not all the cells responded to TGFβ and moved faster, this seemed to occur in a sub population of cells only, and can be seen by the large spread of cell speeds in the box plot.

Although it is unlikely that TGFβ signalling is solely responsible for the differences in pigmentation and motile behaviour that we see in vivo, initial results suggest that TGFβ is capable of causing both hypopigmentation and increased cell motility. TGFβ signalling might be a good potential target in treating melanoma as it would be predicted that this would target the highly motile and potentially more metastatic sub-population of tumour cells.

10 Discussion

The experiments within this thesis have covered 3 main areas: firstly the search for regulatory phosphorylation sites within ROCK1, secondly the discovery that PDK1 is able to regulate amoeboid cell motility in vivo through interacting with ROCK1, and finally, the investigation into the heterogeneity of melanoma cells in vivo and the finding that TGFβ signalling may be responsible for inhibiting pigmentation and stimulating motile behaviour. Although each different starting point was designed to learn more about cancer cell motility, each line of investigation has generated further questions. The results and the further implications are discussed in detail in this chapter.

10.1 Investigating the regulation and function of ROCK1

The first results in chapter 3 showed that ROCK1 was regulated by more inputs than just binding to RhoGTP. Binding of ROCK1 to RhoA was required for the membrane localisation of ROCK1 but not the kinase activity of ROCK1 (Figures 3.1, 3.2). The localisation of ROCK1 affected ROCK1 function, i.e. cytoplasmic distribution led to the generation of stellate stress fibres, and membrane localisation led to cell blebbing; it is possible that ROCK1 is able to carry out different functions in different cellular locations. Different substrates available in the cytoplasm and membrane compartments could account for these differences in phenotypes. Defining whether ROCK1 preferentially phosphorylates different substrates in different locations could be an interesting avenue to explore. The activation of RhoA in specific areas of the cell could be one way in which ROCK activity is permitted in specific locations, for example to the cleavage furrow during cytokinesis [92, 175]. Localised activation of Rho and therefore localised membrane accumulation of ROCK could also model how ROCK activity could be polarised to the rear of blebbing cells as seen in chapter 7 (Figure 7.8). Although data in this thesis confirm the importance of Rho binding to regulate ROCK, it was found that Rho function was more important in the localisation of ROCK and had less input into regulating ROCK kinase activity. The next step was to investigate other mechanisms of regulation such as phosphorylation.

The investigations into potential phosphorylation sites in ROCK1 revealed that ROCK1 does not require phosphorylation at T233 in the activation loop for its activity. This result means that ROCK1 functions differently to other members of the AGC family kinases despite its significant sequence homology with other family members. This finding has been confirmed by structural analysis of the ROCK1 kinase domain and it has been shown that the activation loop of ROCK1, even in the absence of phosphorylation resembles an active conformation [234, 235]. Furthermore, the basic residues in the kinase domain that would normally interact with phosphate of the phosphorylated activation loop residue (Thr233) are not conserved in ROCK1. Instead these residues are hydrophobic (Phe120, Met221, Cys231) [234]. With hindsight it was not unexpected that mutation of T233 and D232 did not significantly alter kinase activity of ROCK1.

Mutation of the hydrophobic motif was also carried out. Mutation of T398 inhibited kinase activity of ROCK1 and caused ROCK1 to become mislocalised, which initially led us to believe that it was a regulatory site. However substitution of an acidic residue at T398 failed to restore a phenotype similar to WT ROCK1. Since the structure of ROCK1 kinase domain is now available, it looks unlikely that T398 is a phosphorylation site in ROCK1. T398 is buried within the structure of the kinase domain and would be unlikely to become accessible to be phosphorylated [235]. The most plausible explanation for the results obtained in chapter 3 is that mutation of T398 causes a mis-folding of the kinase domain, which would explain the loss of kinase activity and mis-localisation.

The investigations into the role of T380 were more revealing. T380 is situated on the outer surface of the kinase structure so is therefore a possible phospho-acceptor site [235]. Results in chapter 3 showed that mutation of T380 caused the kinase to be mislocalised but did not inhibit kinase activity. This could be explained by the result that T380A binds more strongly to the negative regulator RhoE. This would mean that T380A ROCK1 was interacting with endogenous RhoE and inhibited from interacting with its substrates, therefore unable to co-ordinate contraction for cell blebbing. Inhibition of PI3K signalling with the inhibitor LY294002 caused WT-ROCK1 to behave similarly to T380A ROCK1, as it caused the kinase to be mislocalised, but did not inhibit kinase activity. Initially it was hypothesised that T380 could be phosphorylated downstream of PI3K signalling, which may still be the case. However, subsequent work in chapter 7 can explain that this could also be due to the

reduced levels of phospholipids in the plasma membrane and following this, reduced levels of PDK1 at the membrane to bind ROCK1 (see Figure 1.6). Therefore treatment of cells with LY294002 causes the balance of PDK1 and RhoE to be swayed such that there is more RhoE available to bind to ROCK1. This would mimic the phenotype of T380A that binds more strongly to RhoE than the WT ROCK1. The outstanding questions surrounding the role of T380 arise from the behaviour of T380D and T380E mutants. The acidic substitution of T380 was firstly found the render ROCK1 resistant to the mislocalisation and reduced blebbing cause by treatment of cells with LY294002 (Figure 3.10). This would suggest that T380E is less dependent on the availability of phospho-lipids and PDK1 at the plasma membrane to induce cell blebbing. Consistent with this is the failure of T380E ROCK1 to be effectively inhibited by RhoE over-expression (Figure 3.15). However it was also found that T380E ROCK1 bound more strongly to RhoE than WT-ROCK1, which is contradictory to the in vivo result. Results in chapter 8 showed that T380 is contained within the region of ROCK1 required for binding to both PDK1 and RhoE and it could perhaps be hypothesised that mutation of T380 changes the binding affinity of ROCK1 to both PDK1 and RhoE, so that in some assays T380E ROCK1 appears more active than WT-ROCK1 (due to stronger binding to PDK1), but in other assays it appears that it was more inhibited than WT-ROCK1 (due to stronger binding to RhoE). Therefore T380E may be a version of ROCK1 that is more highly sensitive to the balance between PDK1 and RhoE. Mutation of T380 to alanine did not affect the binding of ROCK1 to PDK1 but the binding of T380D or T380E to PDK1 remains to be tested (Figure 7.17). Despite the binding data suggesting that T380E binds more strongly to RhoE, functional data did not support this as co-expression of GFP-RhoE with T380E only had a small inhibitory effect of the induction of cell blebbing.

It is possible that T380 in the hydrophobic motif of ROCK1 is modified to regulate the function of ROCK1. Unfortunately it has not been possible to identify the presence of phosphate on this residue despite attempting to generate phospho-antibodies and also carrying out analysis by analysis by mass spectrometry. The antibodies we generated were not very specific and a better purification method may result in a better antibody to use as a tool to investigate this further. The mass spectrometry analysis was carried out using ROCK1 protein that was autophosphorylated. We now know that T380 is not an autophosphorylation site in ROCK1 as this peptide was seen in the analysis but never appeared to be phosphorylated. However, testing a range of kinases against peptides

containing T380 may reveal that T380 is indeed a substrate for an as yet unidentified kinase. Also the purchased recombinant ROCK1 protein used for the mass spectrometry analysis was isolated from a baculovirus culture and not mammalian cells. So although no constitutive phosphorylation occurs in insect cells it does not rule out regulation of T380 in mammalian cells.

Results in chapter 4 have revealed that ROCK1 will also autophosphorylate itself in at least 2 positions: S479, and T518. A relevant function of these phosphorylation sites is yet to be confirmed. Neither of these sites is contained within regions that have been reported to be required for dimerisation of ROCK1, and neither site is in the hydrophobic motif or the activation loop, which were investigated by mutagenesis in chapter 3. The function of T518 was investigated further in chapter 4 and it was found that although T518A ROCK1 was able to localise to the plasma membrane and had kinase activity similar to WT ROCK1 in vitro, the ability of T518A ROCK1 to cause cell contraction and induce membrane blebbing was reduced compared to WT-ROCK1. This was similar to the phenotype seen when truncated ROCK1 was tagged to the plasma membrane by cloning the CAAX sequence of K-Ras or RhoA onto the C-terminus.

T518 occurs in a region of ROCK1 that has been reported to be part of a Rho-interacting domain with homology to the HR1 domain in PKN [109, 236]. Some initial attempts to test whether mutation of T518 results in altered binding to RhoA has not revealed any obvious differences but this might still be an interesting avenue to explore more thoroughly. Acidic substitution of T518 would also be important to investigate to complete this line of investigation. The role of S479 has not been investigated at this point.

It seems that to effectively drive cortical F-actin contraction and blebbing, ROCK1 requires kinase activity, localisation to the plasma membrane, and also another signal, because tagging truncated ROCK1 to the plasma membrane was not sufficient to induce contraction and rounding of cells to mimic WT ROCK1. Perhaps auto-phosphorylation of T518 or S479 or at other sites such as T380, or perhaps undiscovered sites in the C-terminus, are the remaining inputs required. Truncated-ROCK1 (1-727), which remains cytoplasmic and induces star-like stress fibres, includes the region containing T518. It will be interesting to determine whether T518 is phosphorylated in truncated ROCK1. More investigation will be required to determine if these sites really regulate ROCK1 function, and where and when

these phosphorylations occur. Although these sites are present in truncated ROCK1 (1-727) tagging this construct to the membrane did not induce rounding of the cells. Perhaps the C-terminus is required either for these phosphorylations to take place or for a conformational change to occur downstream of the phosphorylation.

10.2 The identification of PDK1 as a regulator of amoeboid cell motility.

The next approach undertaken to determine novel regulators of rounded/blebbing morphology and amoeboid cell motility was an siRNA screen. Knowing that amoeboid cell motility required signalling through ROCK [153], it was also possible that we would have uncovered pathways feeding directly into the phosphorylation of ROCK that had been the focus of chapters 3 and 4. As it turned out we did not find a signalling pathway that controlled the phosphorylation of ROCK but did discover that PDK1 directly bound to ROCK and regulated its localisation by acting as a scaffold at the plasma membrane.

10.2.1 siRNA screen identifying candidate signalling pathways required for amoeboid cell motility

The siRNA screen was a useful way to identify novel regulators of rounded cell morphology and in the case of PDK1, disruption of rounded cell morphology also led to inhibition of amoeboid cell motility. Plating cells onto thick layers of collagen/matrigel more accurately mimics the range of morphologies seen in vivo, than rigid 2D cell culture. This is due to the deformable nature of the gel, allowing the contractile forces exerted by the cell to remodel the matrix and determine the cell morphology. On rigid substrates, the cells stretch flat and the underlying changes in contractility that alter cell morphology are sometimes masked. This was clearly seen in the case of depleting PDK1 as no discernable change in morphology was seen in 2D culture, but in deformable collagen the disruption of rounded cell morphology was significant.

Contractility in A375 cells has been previously reported to be largely dependent of signalling through Rho and ROCK [170]. This has been validated further by the siRNA screen, as the strongest elongated phenotypes were seen when Rho-ROCK signalling was disrupted: RhoA siRNA, ROCK1 or ROCK2 siRNA, TAT-C3, Y27632, HA1077, H1152. The other positive control was the treatment of cell with blebbistatin, which directly inhibits contraction of

myosin filaments. Depletion of another Rho effector, Citron kinase, which is also able to regulate the phosphorylation of MLC did not disrupt rounded cell morphology. Interestingly depletion of the Cdc42 effectors, MRCKα/β, which can also regulate phosphorylated myosin, also did not affect the contractility of A375 cells, indicating that the effector that is required for contractility is ROCK 1 and 2 in A375 cells, confirming the previously published data [170].

Another interesting result was that depletion of either Dia1 or Dia2, 2 other Rho effectors, also caused A375 to become more flattened and less rounded. Dia1 and Dia2 have been thought to regulate contractility during cytokinesis, but recent research has shown that Dia1 is able to activate Rho signalling by interacting with the Rho-GEF, LARG [232]. In this way Dia1 could function upstream of RhoA and be necessary for contractility effected through ROCK. We found that depletion of Dia2 has similar effects to depletion of Dia1 in our screen so may also function upstream to modify signalling through Rho and ROCK.

It has previously been reported that amoeboid cell motility does not require integrin mediated adhesions [220, 221]. The results from the siRNA screen are consistent with this finding, as knockdown of a range of integrin isoforms did not disrupt rounded cell morphology, indicating that signalling through these integrins was not required to regulate contractility in A375 cells. However it has not been tested whether cell motility is dependent on integrins in this model system. It might also be necessary to deplete multiple integrin molecules simultaneously to investigate this fully. It is thought that amoeboid cell motility uses much more transient contacts with the ECM and may use different adhesion molecules to achieve this, though as yet the alternative adhesion molecules have not been identified. A recent paper showed that leukocytes moving in an amoeboid manner also do not require integrins [164]. It may be true that cancer cells moving in an amoeboid manner use similar mechanisms to move as leukocytes and we may find more commonality as these areas of research are investigated further.

Although integrins are not required for rounded cell morphology, depletion of paxillin or vinculin caused cells to become elongated. Both of these molecules are commonly known as components of focal adhesions, an adhesion complex that we do not observe in A375 cell plated in deformable collagen/matrigel matrix. As A375 cells do not utilise conventional

focal adhesions in 3D culture or in vivo, then why then are paxillin and vinculin required for their contractile phenotype? One possibility is that vinculin and paxillin are required to link the actin cytoskeleton to the plasma membrane. Membrane blebbing can only occur if the actin cortex is attached to the plasma membrane, so that the membrane is pulled and squeezed in concert with contraction of the actin filaments. It will be interesting to investigate this idea further and look in detail how the actin cytoskeleton in organised in cells lacking vinculin or paxillin. A test of this hypothesis will be whether over-expression of ROCK1 is able to cause blebbing in cells lacking vinculin and paxillin. Paxillin and vinculin might function independently of binding to integrins in the cell membrane, as knockdown of integrins did not have the same effect as the depletion of paxillin and vinculin. Vinculin can be recruited to adherens junctions so some of its functions are certainly integrin-independent [237]. It is also possible that there is significant redundancy between integrins meaning that the single knockdowns tested in the screen are not sufficient to disrupt the localisation and function of paxillin and vinculin.

10.2.2 Differences between 2D and 3D cell motility

It was interesting that PDK1 had not previously been identified as a regulator of cell motility. This is probably because most analysis of cell morphology and cell motility has been carried out on rigid 2D substrates. It is clear in chapter 5 that the effect of PDK1 depletion only becomes apparent when cells are plated on a deformable 3D matrix. It seems that the same population of cells are able to adopt different modes of cell motility based on the environment or substrate they are presented with. On glass these cells are able to spread, form large complex focal adhesions and use actin polymerisation to push lamellipodia forward. The contractile machinery in 2D is manifested as actin stress fibres. When faced with a deformable matrix such as they might encounter in vivo, A375 cells adopt a different mechanism of cell motility in which actin is organised around the cell periphery in thick cortical bundles/meshwork, and contractile forces are generated to increase hydrostatic pressure pushing membrane blebs forwards as protrusions.

ROCK activity is required for retraction of the 'tail' of cells moving on 2D substrates but is dispensable for the formation of lamellipodia and for actin polymerisation [63]. In 3D environments, ROCK is absolutely required for amoeboid cell motility and A375 and MTLn3E cells are less able to invade if ROCK is inhibited (see Figure 5.8)[153, 154]. Conversely inhibiting ROCK in 2D systems is able to increase cell speed [238]. This has been shown by

several groups using ROCK inhibitors, and also indirectly by the expression of RhoE [239]. On rigid substrates where cells can form strong attachments, it seem that high levels of contractile forces are not required and slow the cell down, but in 3D deformable matrices higher levels of contractile forces may be required for movement. It is now also clear that PDK1 is also required for co-ordination of acto-myosin contraction in deformable 3D matrices.

Another clear difference is that on 2D substrates, almost all the A375 cells in the population are able to migrate some distance, meaning that this mechanism of cell motility is something that the whole population of cells is capable of. However in vivo, the subcutaneous tumours imaged reveal that in any one imaging period, only around 1 % of cells are motile (Sahai lab – unpublished data, and estimate from in vivo data in chapter 6), and in many areas no cell motility is observed (Figure 6.1). This would suggest that amoeboid cell motility is a mechanism that only a sub-population of the cancer cells is capable of. This could be due to genetic heterogeneity within the population; this could also be due to differences in the tumour microenvironment, providing signals allowing cell motility in specific tumour areas.

One significant difference between the cell motility observed in vivo and cell motility on deformable substrates is the directionality. Although we can monitor blebbing in vitro that causes rapid changes in cell shape and rapid changes in the position of the cell centroid, we are unable to model the directional amoeboid movement we see in living tumours. In tumours we do occasionally see cells blebbing chaotically, changing shape but not changing their position in the tumour significantly, and we also see cells switching from directed amoeboid movement to pausing and moving more chaotically in one position. This would suggest that in vivo, cells are responding to a cue from the microenvironment to indicate the direction they should follow. To date we are unable to reproduce this effect in vitro.

The directional migration in vivo could be chemotaxis/haptotaxis, or it might also be a more passive process, with cells that have escaped the primary tumour moving in the direction of interstitial flow within the tissue, for example towards draining lymph nodes. However this second possibility seems unlikely as it would mean all motile cells were moving in the same direction, but it has also been observed that host cells within the tumour often migrate in opposite directions to tumour cells [198](Pinner & Sahai, unpublished data). If chemotaxis is involved, more investigation is required to determine which signals are responsible.

The ECM also dictates the direction chosen by tumour cells. Imaging matrix components by reflectance imaging has revealed 'tracks' of less dense matrix through which motile tumour cells will migrate in trails, with multiple cells following the predetermined path [198, 240]. It has been shown previously that A375 cells and other cells moving in an amoeboid manner do not require proteases to invade, but having seen tracks in the matrix which amoeboid cells follow, it might also be true that they do not require proteases only because another cell has already carried out that job on their behalf. We have seen that A375 tumours contain cells with both rounded cell morphology and also elongated morphology. Although the majority of cell motility we observe is amoeboid (rounded morphology), elongated motility is also occurring and protease activity by these cells could potentially explain the presence of less dense 'tracks' in the tumour matrix. Alternatively protease activity and remodelling of the matrix could be done by carcinoma-associated fibroblasts [79]. The directional migration of tumour cells in vivo is a complex issue and invasion may occur through the synergistic actions of host and tumour cells, as well as the heterogeneous populations of tumour cells utilising different forms of cell motility [153, 213, 222].

The first in vivo experiment was to test the requirement of ROCK1 and ROCK2 for cancer cell motility in tumours. Treatment of tumours with the inhibitor Y27632 caused a significant reduction in amoeboid cell motility (Figure 6.1). This confirmed previous analysis showing that ROCK activity was required for rounded cell morphology and amoeboid invasion in vitro [153]. Interestingly there was also a slight increase in the numbers of cells invading in an elongated mode (Figure 6.3). This could potentially be because low ROCK activity allows other mechanisms of cell motility to function instead, such as the activation of Rac (Marshall lab unpublished data).

Despite the limitations of the 3D cell culture performed on deformable collagen/matrigel gels described above, the fact that depletion of PDK1 caused the same changes in cell morphology and reduction in cell motility in vivo highlights the similarities between the behaviour of cell in vivo and in the deformable collagen/matrigel gels used to observe cells in vitro. This method of cell culture is certainly a closer approximation to amoeboid cell motility than 2D culture. Intravital imaging of tumours has only been utilised relatively recently and there are many unanswered questions in this area of research. Now that we can collect dynamic information about tumour cell behaviour in vivo we can start to address how the knowledge of cell motility gathered from 2D studies applies to the in vivo situation.

10.2.3 PDK1 is required for amoeboid cell motility

The depletion of PDK1 disrupted rounded cell morphology of A375 cells on collagen/matrigel gels almost to the same degree as treating cells with ROCK inhibitor, Y27632. In MTLn3E cells, depletion of PDK1 also disrupted rounded cell morphology but instead of becoming elongated and protrusive, cells generally appeared flatter. This difference is apparent when the ratios between Figure 5.4 (A375) and Figure 5.6 (MTLn3E) are compared. The ratio of the perimeter and area used for the analysis of morphology can be more useful than just measuring the ratio between the longest and shortest axis of the cell because the perimeter measurement can supply information about either the length of the cell and/or the number of protrusions. Nonetheless, both of these factors are important when measuring the disruption of rounded morphology.

In vivo, depletion of PDK1 caused a significant reduction in the number of cells able to move and invade the surrounding extra-cellular matrix. The loss of PDK1 reduced the numbers of cells moving both in an amoeboid manner and also in an elongated manner. There was a higher proportional reduction in the amoeboid category, further evidence that PDK1 is required for amoeboid cell motility. A375 cells have previously been shown to be able to switch between amoeboid and elongated cell morphology [153], however in the case of PDK1 depletion this switch does not seem to occur and the number of cells moving in an elongated manner is also reduced. This could be because PDK1 is also required to regulate mesenchymal motility by another mechanism, possibly signalling through other members of the GTPase family such as Rac or Cdc42. For example, PDK1 has been shown to be required for motility of endothelial cells through a mechanism involving signalling through Akt/PKB.

10.2.4 The role of PDK1 in other stages of the metastatic process.

It is intriguing that depletion of PDK1 also reduces the ability of tumour cells to colonise the lungs. Although the experimental set up used is not a real mimic of the metastatic process, the lung colonisation assay can give some insights into how cells survive transit in the blood stream, and whether they can lodge, extravasate and survive and proliferate in the lung environment. Of the three different ways this experiment was carried out, the short term assay using MTLn3E cells is the most convincing. The A375 cells are apparently cleared from the lungs much faster than the MTLn3E cells. Both cell lines can be used to grow subcutaneous tumours in nude mice to the same degree of efficiency and grow at similar rates, however in the lung, the MTLn3E cells are more effective at forming tumours in the lungs following i.v. injection. This could be due to the MTLn3E responding better to growth factors availably in the lung tissue, it could also be due to the A375 cells becoming damaged in transit in the blood stream. The differences in the fate of different cell lines in this assay would be interesting to investigate further but is beyond the scope of the experiments presented here.

Despite the differences between the two cell lines, the lung colonisation experiments showed that depleting PDK1 meant that cells were less able to colonise the lungs. Previous studies have suggested that having strong contractile cortical F-actin organisation can help cell to survive transit in the blood stream and reduce physical damage to the cells [198]. Loss of PDK1 certainly disrupted the actin organisation of both A375 and MTLn3E cells, so one explanation for the differences we see in the lung colonisation assays is that PDK1 depleted cells become damaged in transit and soon after they arrive, they die (between 2 and 24 hours post injection). An alternative explanation could be that to survive and proliferate in the lung, arriving cells must extravasate and that amoeboid cell morphology/motility is better suited to this. At 2 hours post-i.v. injection, cells appear to be collected in small vessels between alveoli, but at 24 hours, this appearance is changed and cells appear to be located in small clusters throughout the lung tissue. To judge this definitively, the blood vessels would need to be labelled fluorescently. If PDK1 depleted cells failed to colonise the lungs because they were less able to extravasate then this would also implicate PDK1 in another type of cell motility/invasion, through endothelium. It could also mean that tumour cells traverse

endothelial barriers in an amoeboid manner similar to cells such as neutrophils without the need for proteases and degradation of the basement membrane [201].

10.2.5 ROCK1 is regulated by PDK1 to drive amoeboid cell motility

The first insight into the mechanism behind how PDK1 regulated amoeboid cell motility is seen in Figure 5.8. The intermediate knockdown of PDK1 in MTLn3E cells due to one mis-matched base in the siRNA oligo sequence resulted in an intermediate inhibition of cell motility. The apparent dose-dependent effect of PDK1 availability on cell motility was interesting as it meant that the total amount of PDK1 was probably the most important factor determining cell motility. It is later shown that kinase activity of PDK1 was not required for PDK1 to regulate ROCK1 (Figure 7.13).

One explanation for how PDK1 was able to regulate amoeboid cell motility was through affecting the activation of RhoA. However it was shown that when PDK1 was depleted, RhoA was activated in response to serum, and that this activation was actually at a slightly higher level than in control cells. So depletion of PDK1 did not inhibit the activation of RhoA but signalling downstream of GTP-bound RhoA was inhibited. The reason why GTP-bound RhoA should be higher in response to serum when PDK1 is depleted is unclear. Perhaps RhoA cycles between GTP and GDP bound states is altered in cells lacking PDK1, so the level of RhoA-GTP appears higher overall, although this is only speculation at this point. It was also found that the steady state levels of RhoA-GTP were unchanged when PDK1 was depleted[233].

One other observation from this experiment was that PDK1 ran at a slightly higher position on the SDS-PAGE gel when the cells had been serum starved. This mobility shift might indicate phosphorylation of PDK1. it would be interesting to find out whether phosphorylation of PDK1 is occurring in serum starved conditions and which sites in PDK1 are affected.

It was found that PDK1 regulated amoeboid cell motility by directly affecting ROCK1 and not Rho activation. The depletion of PDK1 dramatically inhibited the ability of over-expressed ROCK1 to cause membrane blebbing. This inhibition of blebbing was even more

striking when A375 cells over-expressing ROCK1 were plated on deformable collagen/matrigel gels. In this environment the contraction required to cause cell rounding and blebbing is presumably less than is required to overcome focal adhesions in the equivalent 2D assay as the matrix is deformable and able to be pulled and pushed by the cells. This means that the blebbing seen in the control cells expressing ROCK1 is very dramatic but it also highlights the complete lack of contractile forces when PDK1 is depleted as over-expressed ROCK1 cannot even contract the cell enough to pull the deformable matrix they are attached to.

Looking at the localisation of endogenous ROCK1 was technically challenging, as the antibodies available were not very suitable for use in immunofluorescence as the signal was not completely specific or very strong. However it was possible to see localisation of endogenous ROCK1 at the cell periphery of A375 cells on 2D substrates. This localisation was lost when PDK1 was depleted. Even though this is not an ideal way to show the membrane localisation of endogenous ROCK1, the fact that the signal at the cell periphery is reduced when PDK1 is depleted suggests that there is less ROCK1 at the plasma membrane when PDK1 is depleted. Better imaging of endogenous ROCK1 in cells on deformable gels has since been carried out by Erik Sahai and this has confirmed that PDK1 does regulate the localisation of endogenous ROCK1 [233].

Dynamic analysis of the localisation of GFP-ROCK1 was able to give better insight into the mechanism behind the contraction co-ordinated by Rho-ROCK signalling. In blebbing control cells, GFP-ROCK1 was located at the cell periphery, and when a cell was not making significant movement in any one direction, GFP-ROCK1 was spread more or less uniformly around the whole cell circumference. However, in cells making significant translocation of the cell body, GFP-ROCK1 was asymmetrically localised at the rear of the cell perhaps acting to cause squeezing and shortening on the actin cortex at the back causing the cytoplasm and nucleus of the cell to be pushed forwards, though this is only speculation at this point. Watching the time-lapse movies the impression is that ROCK1 remains at the plasma membrane but is able to move within the membrane to accumulate in one part on the cell. To test this it would be interesting to use a photo-activatable GFP tagged to ROCK1 to monitor whether membrane localisation was maintained during blebbing.

The localisation of ROCK activity during amoeboid cell motility could provide the polarisation required for directed cell movement. It has been seen in vivo that cells moving in an amoeboid manner are able to change direction rapidly, and from the in vitro time-lapse movies, it can be seen that the localisation of ROCK1 is also able to change rapidly. Asymmetric ROCK1 activation could then drive amoeboid cell motility. ROCK1 localisation requires binding to RhoA or RhoC, so the localised activation and membrane localisation of RhoA could determine the localisation of ROCK1 in the membrane. As the membrane localisation of PDK1 is determined by the interaction of its PH domain with phospholipids, asymmetric PI3K signalling could determine the localisation of PDK1 which would in turn result in prolonged ROCK1 activity in specific parts of the cell membrane. As we have seen that PDK1 co-localises with ROCK1 at the plasma membrane it could actually be asymmetric localisation of PDK1 that regulates the asymmetric localisation of ROCK1. ROCK1 had been observed at the back of blebbing cells in vitro, suggesting that $PI(3,4,5)P_3$ could be at higher concentrations at the back of amoeboid moving cells. This would be controversial as $PI(3,4,5)P_3$ has been reported to be located at the leading edge of cells [182, 186], but these data have resulted from analysis of cells in rigid 2D environments, and as discussed earlier, cell motility in vivo can be co-ordinated differently. It has been shown that A375 cells with a rounded phenotype on deformable matrices have a uniform distribution of $PI(3,4,5)P_3$ [153], suggesting that PI3K signalling is not spatially separated from front to back under these conditions.

If the distribution of $PI(3,4,5)P_3$ is uniform in amoeboid cells then the hypothesis would be that RhoA controls the localisation of ROCK1 activity, but that PDK1/RhoE control the duration and magnitude of ROCK activity at the membrane.

10.2.6 PDK1 binds directly to ROCK1 at the plasma membrane

ROCK1 also required PDK1 for plasma membrane localisation. Interestingly PDK1 was only required for the membrane localisation of ROCK1 and not ROCK2. Over-expression of ROCK2 did cause membrane blebbing but was also able to cause membrane blebbing in the absence of PDK1. It was also found that PDK1 bound directly to ROCK1 but did not interact with ROCK2 (Figure 7.16). To fit with this, ROCK2 is also not inhibited by binding to RhoE [85]. It seems that the competitive mechanism between PDK1 and RhoE discovered here in the regulation of amoeboid cell motility only involves ROCK1 and that ROCK2 is

regulated in a separate manner. It has been reported that Raf-1 is able to regulate the localisation of ROCK2 by physical interaction that is required to maintain ROCK2 in its correct location. In this work it was also found that kinase activity of Raf-1 was not required, and that the interaction was specific to ROCK2 and not ROCK1 [118]. It can be concluded that amoeboid cell motility is driven by Rho signalling through ROCK1, if there was any compensation between ROCK1 and ROCK2 we would not see such dramatic changes in morphology and inhibition of cell motility when PDK1 was depleted. However we do seen a strong disruption of rounded cell morphology when ROCK2 is depleted so perhaps ROCK2 also has a role in amoeboid cell motility but a role that is distinct from ROCK1 and does not require PDK1. Over-expression of ROCK2 is able to drive contractility, but is apparently not sufficient to drive amoeboid cell motility when ROCK1 is inhibited. ROCK1 and ROCK2 have been shown to have independent functions in a variety of contexts as discussed in the introduction. Amoeboid cell motility is now another cell behaviour in which ROCK1 and ROCK2 probably have independent functions.

Much effort was put into the investigation as to whether ROCK1 was a substrate of PDK1. Chapter 3 describes in detail the investigation into potential phosphorylation sites in ROCK1, and the hydrophobic motif surrounding T398 was first identified as a potential PDK1 binding site by Scansite analysis. However despite these efforts, no evidence was found to suggest that ROCK1 is phosphorylated by PDK1. Addition of PDK1 did not increase ROCK1 kinase activity, and furthermore no phosphorylation at T398 was ever detected by mass spectrometry. The final evidence that ROCK1 was very unlikely to be a PDK1 substrate was that a kinase dead mutant of PDK1 could rescue the morphological changes caused by PDK1 depletion.

The finding that the PH domain of PDK1 that is required for the membrane localisation of PDK1, was also required to regulate ROCK1 reinforced the result that ROCK1 regulated amoeboid cell motility by localising to the cell periphery. It was therefore logical that PDK1, which was by this point known to regulate the membrane localisation of ROCK1, would also require membrane localisation to carry out this function. This led to testing whether PDK1 could bind to ROCK1 directly. When it was found that PDK1 bound directly to ROCK1 using a sequence of the ROCK1 hydrophobic motif it was tested one final time whether T398 (the site indicated by Scansite) was implicated in the binding between PDK1 and ROCK1. Figure 7.17 shows that neither mutation of T380 nor T398 to alanine influences the

interaction between ROCK and PDK1. As discussed earlier it would be interesting to investigate whether this is also true for T380D or T380E ROCK1.

10.2.7 The regulation of ROCK1 through the competition between PDK1 and RhoE

Chapter 8 describes experiments leading to the model that the competitive binding of RhoE or PDK1 to ROCK1 at the plasma membrane regulates ROCK1. It was possible to show in vitro that both PDK1 and RhoE interact with ROCK1 directly using a similar, overlapping sequence in the hydrophobic motif in order to do this. It was also possible to manipulate the cell system in order to force ROCK1 into interacting more with one or other binding partner by changing the balance between RhoE and PDK1. As discussed earlier, T380A ROCK1 mutant binds better to RhoE than WT ROCK1, however it is shown that mutation of T380A does not affect binding to PDK1. So even though RhoE and PDK1 utilise the same 40 amino acid sequence (375-415) in the hydrophobic motif to bind to ROCK1, they must still bind to ROCK1 slightly differently. RhoE binding is influenced by the amino acid in position 380, but PDK1 binding is apparently unaffected by mutation to alanine (Figure 7.17).

What this chapter fails to show is that endogenous ROCK1 and PDK1 interact in a cell at the plasma membrane. Numerous attempts to co-immunoprecipitate these binding partners from cells were carried out but all failed. Cross-linking experiments were also carried out to determine what complexes ROCK1 might be involved in. However the cross linking experiments only revealed that ROCK1 was isolated as a single complex of high molecular weight which may be a dimer of ROCK1, or a heterodimer of ROCK1 and ROCK2 (data not shown). The dimerisation of ROCK1 has been previously reported and the regulation of dimerisation is actively being investigated by other laboratories [113]. ROCK1 is known to have many substrates and interacting proteins so it is curious that the only complex of ROCK1 that was isolated is the kinase dimer. There may be something innately interesting about this result, perhaps meaning that interactions of most proteins with ROCK1 are extremely transient. However PDK1 seemed not to associate with any binding partners in this cross-linking experiment suggesting that the approach might be flawed. Another potential reason that it has not been possible to co-immune precipitate ROCK1 with PDK1 is that the lipids of the plasma membrane could play a crucial role in regulating the conformation of the

proteins, or be included in the complex in some way. Therefore to lyse a cell would mean the breakdown of the plasma membrane and also the destruction of the ROCK1/PDK1 complex. Despite this short-coming, it was possible to co-immune precipitate endogenous ROCK1 with endogenous RhoE, and the isolation of that complex was dependent on the level of PDK1 in the cell. Perhaps it was possible to isolate ROCK1 with RhoE because that complex is more stable in the absence of PDK1, and also seems not to require interaction with the plasma membrane. Figure 8.4 shows that ROCK1 and RhoE co-localise in some kind of vesicle when RhoE is over-expressed. Other members of the Sahai lab have tried to identify the nature of these vesicles but no co-localisation with markers for known endocytic or other transport pathways has been identified.

Previous results had given some clue towards building this model of ROCK1 regulation. There was perhaps a slight decrease in the ability of endogenous ROCK1 to phosphorylate MLC in vitro when PDK1 had been depleted from the cells, however this decrease was never very dramatic (Figure 7.11). If this decrease is real, a potential explanation was found in chapter 8 when it was found that in the absence of PDK1, endogenous ROCK1 was found in a complex with RhoE. The ROCK/RhoE complex might be less efficient at phosphorylating MLC, or RhoE co-immune precipitated with the ROCK1 could compete with MLC in the kinase reaction. Figure 7.11 also gives a slight clue to the eventually derived mechanism of competition between PDK1 and RhoE for interaction with ROCK1. Although not hugely obvious, it can be seen that the phosphorylation of RhoE by ROCK1 is slightly decreased when PDK1 is added to the reaction (compare lanes 5 and 7 in Figure 7.11). This is potentially because PDK1 is binding to ROCK1 and preventing ROCK1 from phosphorylating RhoE. This decrease is not observed when ROCK1 is used to phosphorylate MLC (Figure 7.10). Perhaps the interaction of PDK1 with ROCK1 affects the substrates that ROCK1 is able to interact with. Phosphorylation of RhoE by ROCK1 stabilises the ROCK/RhoE interaction so perhaps it is not unreasonable to speculate that interaction with PDK1 favours ROCK activity on substrates such as MLC instead.

Another interesting result is shown in Figure 8.5. Although this western blot was carried out simply to ensure that the proteins had been knocked down efficiently, it could perhaps give some further insight into the mechanism of the competition between PDK1 and RhoE. It was seen that when PDK1 was depleted alone, the levels of RhoE are slightly increased (compare lanes 1 and 2 with lanes 3 and 4). This could mean that the interaction of ROCK

with RhoE when PDK1 is absent might also act to prevent the degradation of RhoE explaining the slight increase in RhoE protein. This slight increase in RhoE protein levels is also seen in the cell lines stable depleted of PDK1, however this small change in protein levels can not explain the greatly increased interaction between ROCK1 and RhoE (Figure 8.3). I would continue to argue that the competition between PDK1 and RhoE for binding to ROCK1 seems the best model for the data. See Figure 10.1 for model of the interplay between PDK1 and RhoE and resulting ROCK activity.

10.2.8 Double knockdown of PDK1 and RhoE rescues cell motility

The final part of chapter 8 describes the testing of the competition model by knocking down both PDK1 and RhoE simultaneously. Results showed that in both A375 cells and MTLn3E cells rounded cell morphology was mostly rescued by the combined knock down of PDK1 and RhoE. In MTLn3E cells knockdown of RhoE alone cause cells to become more elongated/protrusive than in control cells (Figure 8.7). This was strange and unexpected. Although both MTLn3E cells and A375 cells are grouped together as 'amoeboid' by our classification, based on their behaviour in vivo, it is clear that the signalling controlling their morphology is slightly different with respect to the role of RhoE. It is also possible that there might be some off-target effects of the RhoE siRNA sequences when used in the MTLn3E (rat) cells that are not seen in the A375 (human) cells, as they are from different species. Nonetheless, when both PDK1 and RhoE where knocked down, the speed of cell migration of MTLn3E cells on deformable collagen gels was restored to levels similar to the control cells.

If ROCK1 is able to co-ordinate cell motility in the absence of both PDK1 and RhoE then why should this mechanism of regulation exist? ROCK1 requires binding to RhoA for membrane localisation, and in the absence of both PDK1 and RhoE this seems to be sufficient for blebbing cell motility in vitro. It remains to be tested whether amoeboid cells are able to move in vivo without regulation of ROCK1 by PDK1 and RhoE. RhoE could function to limit ROCK activity at the front of the cell. PDK1 could have the opposite function, increasing ROCK1 activity at the rear of blebbing cells. It could be possible that the regulation of ROCK1 by PDK1 and RhoE is not a mechanism that controls total amounts of ROCK1 activity but a mechanism that spatially controls where ROCK1 is

activating F-actin contraction. It might also be that PDK1 and RhoE act to fine tune ROCK activity and provide cells with a 'gain' control mechanism, controlling the magnitude of the response after RhoA has determined the localisation. Therefore the significance of both PDK1 and RhoE depletion might only be apparent in vivo in directed amoeboid movement.

The online database, Oncomine (http://www.oncomine.org/) reveals several cases of metastatic tumours showing altered levels of PDK1 or RhoE. For example some pancreatic cancers have shown to have reduced levels of RhoE, which could potentially mean that these cells have higher levels of ROCK activity and perhaps increased potential for amoeboid cell invasion. RhoE has been reported to be a transcriptional target of p53, an extremely common mutation in a wide range of cancers, meaning that levels of RhoE are likely to mis-regulated in a wide range of tumours [87, 89]. RhoE can also be transcriptionally up regulated by signalling through the MAPK pathway [241], and as discussed in the introduction this pathway is also often over-activated in cancers such as melanomas. Although the work in chapters suggested that low RhoE levels would correlate with increased invasive behaviour, this might only be true for amoeboid invasion, and in elongated/ROCK-independent forms of tumour invasion, high RhoE might be preferable to keep ROCK activity low.

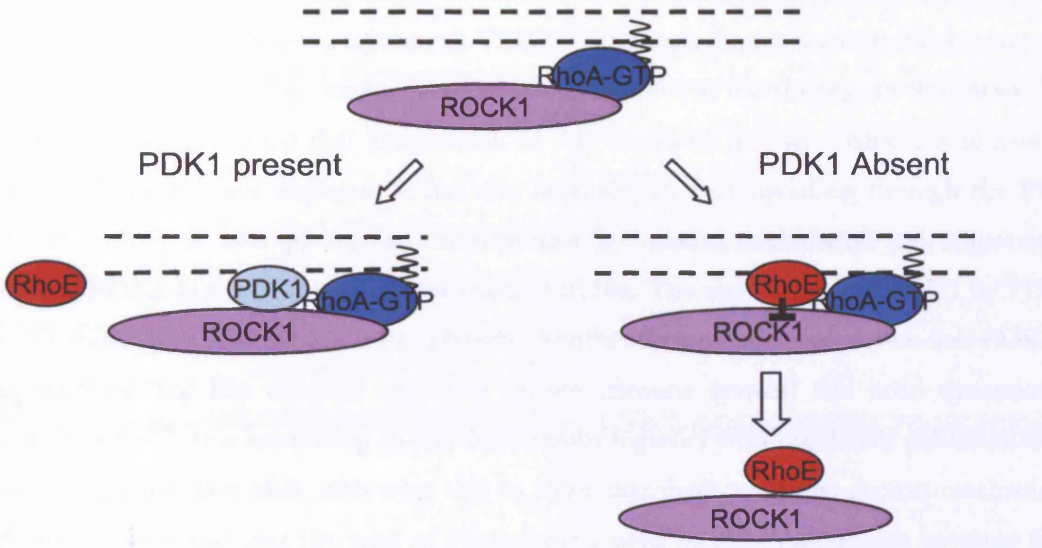

- ROCK1 stays at plasma membrane bound to PDK1
- Contraction of cortex
- Formation of membrane blebs
- Dynamic fast moving cell

- ROCK1 not maintained at PM
- Contraction is not maintained
- Filopodia-like cell protrusions
- Cell remains elongated and less motile

Figure 10.1 Model of the competition between PDK1 and RhoE at the plasma membrane. RhoA binding to ROCK1 is required for translocation of ROCK1 to the plasma membrane. If PDK1 is present, ROCK1 and PDK1 interact allowing sustained ROCK1 activity at the cell periphery. The binding of PDK1 inhibits RhoE from binding to ROCK1. If PDK1 is absent, RhoE binds to and inhibits ROCK1 meaning that contraction is not maintained after RhoA brings ROCK1 to the plasma membrane

Since carrying these experiments, other published work has confirmed that PDK1 is important during other forms of cell motility. It has been found that PDK1 is essential for endothelial cell migration in response to VEGF[120], although the mechanism that is proposed for this involved signalling through Akt, which is different to the findings in this thesis. The siRNA screening showed that knockdown of Akt isoforms did not mimic the phenotype seen when PDK1 was depleted. It has also been shown that signalling through the PI3K isoform p110α is able to regulate angiogenesis by control endothelial cell migration[242], perhaps PDK1 is also involved downstream of p110α. The regulation of ROCK1 by PDK1 is also starting to be shown in other systems. Another recent paper has shown that PDK1 is required for Toll-like receptor signalling (innate immune system) and actin dynamics in dendritic cells[243]. It is interesting to put these results together with previously published work by the group of Alan Hall, who were able to show that there were two distinct mechanisms of phagocytosis and that the type of phagocytosis used by the complement receptor (also innate immune system) was mediated by Rho[244]. These two sets of data potentially implicate PDK1 and ROCK in the actin re-organisation required for phagocytosis during activation of the innate immune system.

10.3 The relationship between pigmentation and cell motility in vivo

Chapter 9 describes a novel imaging method to determine the degree of pigmentation in melanoma cells. To my knowledge this type of imaging has not been previously reported. Although not all differentiated melanocytes will produce pigment, pigment production was a useful indicator along side dendritic cell morphology, to judge how far removed the melanoma cell was from a differentiated melanocyte. Using this imaging technique, it was found that invasive behaviour of melanoma cells in vivo correlated with reduced pigment production. Microarray data from the dissected tumour cells was able to give us some insight into which genes might be differentially regulated and be responsible for reduced pigment production and increased cell motility.

10.3.1 Imaging pigment containing melanosomes

Melanosomes, being full of concentrated dark pigment, were easily identified using transmitted light. It was not initially surprising that these vesicles were also reflective as many

cell and matrix components have some reflective properties. What was unexpected was that the melanosomes would also be seen following multiphoton excitation.

Melanin is thought to have an absorption spectra across a range of UV-visible wavelengths and converts these potentially damaging wavelengths to infrared to protect against DNA damage [7]. This property of the melanin spectra was used in the FACS analysis, and changes emission following excitation with a violet range laser allowed us to distinguish populations of cells based on their pigment production. The spectral properties used for the imaging of cells in vitro and in vivo seem to be the opposite to the above, as the vesicles could be seen when excited with wavelengths in the infrared range and emission was collected in the visible range (Figure 9.1). This has not been previously reported.

The strongest evidence that the spectrum we observed actually corresponded to melanin production was that the signal correlated completely with increases and decreases in pigment production stimulated by α-MSH or inhibition of PKA. The changes in pigment could be seen in the changing colour of the cell pellets, the number of black vesicles seen by transmitted light, and also the multiphoton imaging (Figure 9.3 9.4).

Initially the broad spectrum of emission was also puzzling, as this large range is not normally seen with conventional fluorophores. More detailed analysis showed that there were actually 4 distinct spectra which could explain the large spread, but this then posed the question as to what molecules were responsible for each of the distinct spectra. As melanosomes develop they go through 4 stages of maturation, which can be distinguished by their different appearance by electron microscopy [245]. It could be possible that each stage of maturation causes the vesicles to have different spectra properties. However, during the first 2 stages for maturation melanosomes do not contain any pigment. Pigment production begins in stage III vesicles and only the stage IV vesicles have the black appearance meaning that we can detect them under the microscope by transmitted light [246]. So if the 4 different spectra correspond to the stages of melanosome maturation then it is not the pigment we are seeing but perhaps some other component of developing melanosomes such as the coating of the vesicles or the fibrils inside. Without detailed analysis by electron microscopy alongside the multiphoton imaging we will be unable to answer these questions. Figure 9.6 makes a start into investigating the different nature of the different emission spectra by looking at the cellular localisation of each type of vesicle but the results are not conclusive. If more analysis revealed that one type of vesicle was always closer to the cell periphery than others then this

might indicate that that spectra belonged to the fully mature stage IV melanosome that had been transported to the cell periphery for export out of the cell.

In vivo it was also possible to image the pigment-containing vesicles. It was important to show that the vesicles imaged were actually inside cells and not just pieces of cell debris with strange spectral properties. It was also important to show that the vesicles were contained within tumour cells and were not pieces of phagocytosed cell debris taken up by host cells such as macrophages. To try to show this the B16F2 cells were stably transfected with GFP CAAX to fluorescently label the cell membranes. The high resolution imaging of tumours in Figure 9.9 shows that the pattern of vesicles is not random and is found in shapes following the GFP signal, suggesting that the vesicles are contained within the tumour cells but are located at the cell periphery. Some of the vesicles are not clearly located within the boundaries of GFP signal but they could be vesicles at the end of dendrites. However, due to the close packed nature of the tumour cells in vivo it is not easy to see dendritic protrusions to verify this.

Analysis of the time lapse in vivo movies showed clearly that cells containing pigment tended to be non motile, whilst the motile cells tended to contain very little detectable pigment. The motile cells are also rounded in morphology. Both of these observations suggest that the motile cells are less well differentiated than other cells in the same tumour area. More markers of differentiation would be required to verify this statement, perhaps in vivo imaging of cells expressing a fluorescent reporter construct sensitive to MITF transcriptional activity would be one way to do this, but this was not possible in the time remaining of my PhD.

Assuming that our assumptions are correct and that the motile population of B16 cells is less well differentiated than other non-invasive cells then this could be due to one of two possibilities. Firstly, perhaps the cells were at one stage better 'differentiated' and more similar to melanocytes and producing pigment, but they have received a signal either from surrounding tumour cells, host cells or the local microenvironment causing them to dedifferentiate. Secondly the less 'differentiated' cells could have always been less well 'differentiated', and they might make up, or over-lap with a population of recently termed 'cancer stem cells'[247, 248]. These cells are hypothesised to initiate tumour growth, their progeny being more differentiated and closer to melanocytes. There are theories suggesting that cancer stem cells might also be the cells that are resistant to chemotherapy, causing the tumour to re-grow after seemingly successful treatment [248]. Several markers have been

published that the authors claim can be used to isolate stem cells, one recent marker in melanoma is ABCB5 [26]. Populations of cells expressing ABCB5 are more tumourigenic but whether they are stem cells is still questionable, it is more likely that this marker only isolates a cell population enriched in tumour initiating cells. Other markers are CD133 in pancreatic cancer [249, 250], and nestin in the case of melanoma [251-253].

Although all these data support the theory of a sub population of tumour cells that are more highly tumorigenic than others, it has not yet definitively proven the theory of cancer stem cells. In reference to the data in chapter 9, it is unlikely that all of the motile, poorly pigmented tumour cells are cancer stem cells, as there are so many of them. It is more likely that there is a degree of genetic heterogeneity amongst the cell population and that in addition differences in the local microenvironment cause cells to behave differently from their neighbours.

To find out what changes could be responsible for the differences in pigment production and motile behaviour microarrays comparing the high and low pigmented cells from the tumour was undertaken. The most interesting candidate that came out of this analysis in my opinion was TGFβ2. TGFβ signalling has been extensively studied and has previously been reported to play a role in cell motility in other systems (as discussed in the introduction). It was found that TGFβ signalling inhibited pigmentation of B16 cells (Figure 9.16). This has been previously reported but not much has been done to elucidate the mechanism behind this effect [254]. It has been shown that TGFβ stimulation of cells increases the number of melanosomes in stage III of maturation and prevents their maturation to stage IV. It is thought that TGFβ inhibits tyrosine hydroxylation and prevents melanin synthesis [254]. Results in chapter 9 are consistent with these data but we are not any closer to being able to explain which signalling pathways downstream of TGFβ are responsible for the hypopigmentation.

Additionally it was found that TGFβ signalling inhibited dendritic cell morphology and increased cell motility on deformable matrix in vitro. These results are consistent with the hypothesis that it is TGFβ signalling in vivo that is responsible for the invasive behaviour of the subset of tumour cells we see moving with a rounded morphology and low pigmentation.

10.4 Concluding remarks

This thesis has covered the investigation of cancer cell motility in vivo, covering a range of approaches. The molecular mechanisms regulating the localisation and activity of the kinase ROCK1 were investigated and it was found that unlike other members of the AGC family kinases ROCK1 was not phosphorylated in the activation loop, but that T380 in the hydrophobic extension of the kinase domain is a potential regulatory site, and that other autophosphorylation sites existed that require further investigation. It was also found that ROCK1 is regulated by PDK1 but that this regulation is through a binding interaction and not through phosphorylation. The binding of ROCK1 to PDK1 is hypothesised to allow prolonged ROCK activity at the plasma membrane and prevents ROCK1 from binding to the inhibitory partner RhoE. These findings have been tested in vivo and in 3D in vitro assays. In addition to this it was found that motile melanoma cells had a rounded morphology and did not contain pigment. The mechanism behind this hypopigmentation and increased cell motility in a subset of tumour cells was investigated by microarray analysis and TGFβ signalling was identified as a strong candidate signalling pathway responsible for these changes in cell behaviour.

Although these findings are only small steps towards understanding the larger problem of cancer cell motility in vivo, they have been investigated in detail in order to identify as much mechanistic insight as possible. More work is required to continue to uncover how and why cancer cells become motile in tumours, and this information will be useful in the broader investigation of the process of metastasis.

11 Appendices

11.1 References

1. Gaggioli, C. & Sahai, E. Melanoma invasion - current knowledge and future directions. Pigment Cell Res **20**, 161-172 (2007).
2. Yamaguchi, Y., Brenner, M. & Hearing, V.J. The regulation of skin pigmentation. J Biol Chem **282**, 27557-27561 (2007).
3. Scott, G.A. & Cassidy, L. Rac1 mediates dendrite formation in response to melanocyte stimulating hormone and ultraviolet light in a murine melanoma model. J Invest Dermatol **111**, 243-250 (1998).
4. Scott, G. & Leopardi, S. The cAMP signaling pathway has opposing effects on Rac and Rho in B16F10 cells: implications for dendrite formation in melanocytic cells. Pigment Cell Res **16**, 139-148 (2003).
5. Busca, R. et al. Inhibition of Rho is required for cAMP-induced melanoma cell differentiation. Mol Biol Cell **9**, 1367-1378 (1998).
6. Yamaguchi, Y. et al. Human skin responses to UV radiation: pigment in the upper epidermis protects against DNA damage in the lower epidermis and facilitates apoptosis. Faseb J **20**, 1486-1488 (2006).
7. Meredith, P. & Riesz, J. Radiative relaxation quantum yields for synthetic eumelanin. Photochem Photobiol **79**, 211-216 (2004).
8. Double, K.L. & Halliday, G.M. New face of neuromelanin. J Neural Transm Suppl, 119-123 (2006).
9. Chiaverini, C. et al. Microphthalmia-associated Transcription Factor Regulates RAB27A Gene Expression and Controls Melanosome Transport. J Biol Chem **283**, 12635-12642 (2008).
10. Bronner-Fraser, M. Neural crest cell migration in the developing embryo. Trends Cell Biol **3**, 392-397 (1993).
11. Widlund, H.R. & Fisher, D.E. Microphthalamia-associated transcription factor: a critical regulator of pigment cell development and survival. Oncogene **22**, 3035-3041 (2003).
12. McGill, G.G. et al. Bcl2 regulation by the melanocyte master regulator Mitf modulates lineage survival and melanoma cell viability. Cell **109**, 707-718 (2002).
13. Davies, H. et al. Mutations of the BRAF gene in human cancer. Nature **417**, 949-954 (2002).
14. Gray-Schopfer, V.C., da Rocha Dias, S. & Marais, R. The role of B-RAF in melanoma. Cancer Metastasis Rev **24**, 165-183 (2005).
15. Chudnovsky, Y., Adams, A.E., Robbins, P.B., Lin, Q. & Khavari, P.A. Use of human tissue to assess the oncogenic activity of melanoma-associated mutations. Nat Genet **37**, 745-749 (2005).
16. Rodolfo, M., Daniotti, M. & Vallacchi, V. Genetic progression of metastatic melanoma. Cancer Lett **214**, 133-147 (2004).
17. Gupta, P.B. et al. The melanocyte differentiation program predisposes to metastasis after neoplastic transformation. Nat Genet **37**, 1047-1054 (2005).

18. Carreira, S. et al. Mitf regulation of Dia1 controls melanoma proliferation and invasiveness. Genes Dev **20**, 3426-3439 (2006).
19. Lekmine, F., Chang, C.K., Sethakorn, N., Das Gupta, T.K. & Salti, G.I. Role of microphthalmia transcription factor (Mitf) in melanoma differentiation. Biochem Biophys Res Commun **354**, 830-835 (2007).
20. Adler, M.J. & White, C.R., Jr. Amelanotic malignant melanoma. Semin Cutan Med Surg **16**, 122-130 (1997).
21. Seftor, E.A. et al. Epigenetic transdifferentiation of normal melanocytes by a metastatic melanoma microenvironment. Cancer Res **65**, 10164-10169 (2005).
22. Kulesa, P.M. et al. Reprogramming metastatic melanoma cells to assume a neural crest cell-like phenotype in an embryonic microenvironment. Proc Natl Acad Sci U S A **103**, 3752-3757 (2006).
23. Postovit, L.M. et al. Human embryonic stem cell microenvironment suppresses the tumorigenic phenotype of aggressive cancer cells. Proc Natl Acad Sci U S A **105**, 4329-4334 (2008).
24. Topczewska, J.M. et al. Embryonic and tumorigenic pathways converge via Nodal signaling: role in melanoma aggressiveness. Nat Med **12**, 925-932 (2006).
25. Bittner, M. et al. Molecular classification of cutaneous malignant melanoma by gene expression profiling. Nature **406**, 536-540 (2000).
26. Schatton, T. et al. Identification of cells initiating human melanomas. Nature **451**, 345-349 (2008).
27. Shi, Y. & Massague, J. Mechanisms of TGF-beta signaling from cell membrane to the nucleus. Cell **113**, 685-700 (2003).
28. ten Dijke, P. & Hill, C.S. New insights into TGF-beta-Smad signalling. Trends Biochem Sci **29**, 265-273 (2004).
29. Zhang, S. et al. Smad7 antagonizes transforming growth factor beta signaling in the nucleus by interfering with functional Smad-DNA complex formation. Mol Cell Biol **27**, 4488-4499 (2007).
30. Siegel, P.M. & Massague, J. Cytostatic and apoptotic actions of TGF-beta in homeostasis and cancer. Nat Rev Cancer **3**, 807-821 (2003).
31. Gorelik, L. & Flavell, R.A. Immune-mediated eradication of tumors through the blockade of transforming growth factor-beta signaling in T cells. Nat Med **7**, 1118-1122 (2001).
32. Tuxhorn, J.A., McAlhany, S.J., Yang, F., Dang, T.D. & Rowley, D.R. Inhibition of transforming growth factor-beta activity decreases angiogenesis in a human prostate cancer-reactive stroma xenograft model. Cancer Res **62**, 6021-6025 (2002).
33. Stuelten, C.H. et al. Breast cancer cells induce stromal fibroblasts to express MMP-9 via secretion of TNF-alpha and TGF-beta. J Cell Sci **118**, 2143-2153 (2005).
34. Bolos, V. et al. The transcription factor Slug represses E-cadherin expression and induces epithelial to mesenchymal transitions: a comparison with Snail and E47 repressors. J Cell Sci **116**, 499-511 (2003).
35. Peinado, H., Quintanilla, M. & Cano, A. Transforming growth factor beta-1 induces snail transcription factor in epithelial cell lines: mechanisms for epithelial mesenchymal transitions. J Biol Chem **278**, 21113-21123 (2003).

36. Vardouli, L., Moustakas, A. & Stournaras, C. LIM-kinase 2 and cofilin phosphorylation mediate actin cytoskeleton reorganization induced by transforming growth factor-beta. J Biol Chem **280**, 11448-11457 (2005).
37. Mani, S.A. et al. The epithelial-mesenchymal transition generates cells with properties of stem cells. Cell **133**, 704-715 (2008).
38. Cui, W. et al. Concerted action of TGF-beta 1 and its type II receptor in control of epidermal homeostasis in transgenic mice. Genes Dev **9**, 945-955 (1995).
39. Wang, X.J., Liefer, K.M., Tsai, S., O'Malley, B.W. & Roop, D.R. Development of gene-switch transgenic mice that inducibly express transforming growth factor beta1 in the epidermis. Proc Natl Acad Sci U S A **96**, 8483-8488 (1999).
40. Liu, X. et al. Conditional epidermal expression of TGFbeta 1 blocks neonatal lethality but causes a reversible hyperplasia and alopecia. Proc Natl Acad Sci U S A **98**, 9139-9144 (2001).
41. Rodeck, U. et al. Constitutive expression of multiple growth factor genes by melanoma cells but not normal melanocytes. J Invest Dermatol **97**, 20-26 (1991).
42. Van Belle, P., Rodeck, U., Nuamah, I., Halpern, A.C. & Elder, D.E. Melanoma-associated expression of transforming growth factor-beta isoforms. Am J Pathol **148**, 1887-1894 (1996).
43. Wohlgemuth, S. et al. Recognizing and defining true Ras binding domains I: biochemical analysis. J Mol Biol **348**, 741-758 (2005).
44. Hall, A. Rho GTPases and the actin cytoskeleton. Science **279**, 509-514 (1998).
45. Wei, L. et al. Inhibition of Rho family GTPases by Rho GDP dissociation inhibitor disrupts cardiac morphogenesis and inhibits cardiomyocyte proliferation. Development **129**, 1705-1714 (2002).
46. Michaelson, D. et al. Postprenylation CAAX processing is required for proper localization of Ras but not Rho GTPases. Mol Biol Cell **16**, 1606-1616 (2005).
47. Michaelson, D. et al. Differential localization of Rho GTPases in live cells: regulation by hypervariable regions and RhoGDI binding. J Cell Biol **152**, 111-126 (2001).
48. Ridley, A.J., Paterson, H.F., Johnston, C.L., Diekmann, D. & Hall, A. The small GTP-binding protein rac regulates growth factor-induced membrane ruffling. Cell **70**, 401-410 (1992).
49. Ridley, A.J. & Hall, A. The small GTP-binding protein rho regulates the assembly of focal adhesions and actin stress fibers in response to growth factors. Cell **70**, 389-399 (1992).
50. Posern, G. & Treisman, R. Actin' together: serum response factor, its cofactors and the link to signal transduction. Trends Cell Biol **16**, 588-596 (2006).
51. Minden, A., Lin, A., Claret, F.X., Abo, A. & Karin, M. Selective activation of the JNK signaling cascade and c-Jun transcriptional activity by the small GTPases Rac and Cdc42Hs. Cell **81**, 1147-1157 (1995).
52. Clerk, A. et al. Regulation of mitogen-activated protein kinases in cardiac myocytes through the small G protein Rac1. Mol Cell Biol **21**, 1173-1184 (2001).
53. Frost, J.A. et al. Stimulation of NFkappa B activity by multiple signaling pathways requires PAK1. J Biol Chem **275**, 19693-19699 (2000).
54. Olson, M.F., Ashworth, A. & Hall, A. An essential role for Rho, Rac, and Cdc42 GTPases in cell cycle progression through G1. Science **269**, 1270-1272 (1995).

55. Sahai, E. & Olson, M.F. Purification of TAT-C3 exoenzyme. Methods Enzymol **406**, 128-140 (2006).
56. Coleman, M.L., Marshall, C.J. & Olson, M.F. RAS and RHO GTPases in G1-phase cell-cycle regulation. Nat Rev Mol Cell Biol **5**, 355-366 (2004).
57. Bauerfeld, C.P., Hershenson, M.B. & Page, K. Cdc42, but not RhoA, regulates cyclin D1 expression in bovine tracheal myocytes. Am J Physiol Lung Cell Mol Physiol **280**, L974-982 (2001).
58. Vadlamudi, R.K. & Kumar, R. P21-activated kinases in human cancer. Cancer Metastasis Rev **22**, 385-393 (2003).
59. Wheeler, A.P. & Ridley, A.J. Why three Rho proteins? RhoA, RhoB, RhoC, and cell motility. Exp Cell Res **301**, 43-49 (2004).
60. Dvorsky, R., Blumenstein, L., Vetter, I.R. & Ahmadian, M.R. Structural insights into the interaction of ROCKI with the switch regions of RhoA. J Biol Chem **279**, 7098-7104 (2004).
61. Tominaga, T. et al. Diaphanous-related formins bridge Rho GTPase and Src tyrosine kinase signaling. Mol Cell **5**, 13-25 (2000).
62. Sahai, E. & Marshall, C.J. ROCK and Dia have opposing effects on adherens junctions downstream of Rho. Nat Cell Biol **4**, 408-415 (2002).
63. Worthylake, R.A., Lemoine, S., Watson, J.M. & Burridge, K. RhoA is required for monocyte tail retraction during transendothelial migration. J Cell Biol **154**, 147-160 (2001).
64. Sahai, E., Ishizaki, T., Narumiya, S. & Treisman, R. Transformation mediated by RhoA requires activity of ROCK kinases. Curr Biol **9**, 136-145 (1999).
65. Hakem, A. et al. RhoC is dispensable for embryogenesis and tumor initiation but essential for metastasis. Genes Dev **19**, 1974-1979 (2005).
66. Clark, E.A., Golub, T.R., Lander, E.S. & Hynes, R.O. Genomic analysis of metastasis reveals an essential role for RhoC. Nature **406**, 532-535 (2000).
67. McMullan, R. et al. Keratinocyte differentiation is regulated by the Rho and ROCK signaling pathway. Curr Biol **13**, 2185-2189 (2003).
68. Sordella, R., Jiang, W., Chen, G.C., Curto, M. & Settleman, J. Modulation of Rho GTPase signaling regulates a switch between adipogenesis and myogenesis. Cell **113**, 147-158 (2003).
69. Lang, P. et al. Protein kinase A phosphorylation of RhoA mediates the morphological and functional effects of cyclic AMP in cytotoxic lymphocytes. Embo J **15**, 510-519 (1996).
70. Mellor, H., Flynn, P., Nobes, C.D., Hall, A. & Parker, P.J. PRK1 is targeted to endosomes by the small GTPase, RhoB. J Biol Chem **273**, 4811-4814 (1998).
71. Hajdo-Milasinovic, A., Ellenbroek, S.I., van Es, S., van der Vaart, B. & Collard, J.G. Rac1 and Rac3 have opposing functions in cell adhesion and differentiation of neuronal cells. J Cell Sci **120**, 555-566 (2007).
72. Baugher, P.J., Krishnamoorthy, L., Price, J.E. & Dharmawardhane, S.F. Rac1 and Rac3 isoform activation is involved in the invasive and metastatic phenotype of human breast cancer cells. Breast Cancer Res **7**, R965-974 (2005).
73. Wildenberg, G.A. et al. p120-catenin and p190RhoGAP regulate cell-cell adhesion by coordinating antagonism between Rac and Rho. Cell **127**, 1027-1039 (2006).

74. Ohta, Y., Hartwig, J.H. & Stossel, T.P. FilGAP, a Rho- and ROCK-regulated GAP for Rac binds filamin A to control actin remodelling. Nat Cell Biol **8**, 803-814 (2006).

75. Abe, T., Kato, M., Miki, H., Takenawa, T. & Endo, T. Small GTPase Tc10 and its homologue RhoT induce N-WASP-mediated long process formation and neurite outgrowth. J Cell Sci **116**, 155-168 (2003).

76. Takenawa, T. & Miki, H. WASP and WAVE family proteins: key molecules for rapid rearrangement of cortical actin filaments and cell movement. J Cell Sci **114**, 1801-1809 (2001).

77. Takenawa, T. & Suetsugu, S. The WASP-WAVE protein network: connecting the membrane to the cytoskeleton. Nat Rev Mol Cell Biol **8**, 37-48 (2007).

78. Svitkina, T.M. et al. Mechanism of filopodia initiation by reorganization of a dendritic network. J Cell Biol **160**, 409-421 (2003).

79. Gaggioli, C. et al. Fibroblast-led collective invasion of carcinoma cells with differing roles for RhoGTPases in leading and following cells. Nat Cell Biol **9**, 1392-1400 (2007).

80. Lim, L., Manser, E., Leung, T. & Hall, C. Regulation of phosphorylation pathways by p21 GTPases. The p21 Ras-related Rho subfamily and its role in phosphorylation signalling pathways. Eur J Biochem **242**, 171-185 (1996).

81. Lin, D. et al. A mammalian PAR-3-PAR-6 complex implicated in Cdc42/Rac1 and aPKC signalling and cell polarity. Nat Cell Biol **2**, 540-547 (2000).

82. Aspenstrom, P., Ruusala, A. & Pacholsky, D. Taking Rho GTPases to the next level: the cellular functions of atypical Rho GTPases. Exp Cell Res **313**, 3673-3679 (2007).

83. Wennerberg, K. et al. Rnd proteins function as RhoA antagonists by activating p190 RhoGAP. Curr Biol **13**, 1106-1115 (2003).

84. Foster, R. et al. Identification of a novel human Rho protein with unusual properties: GTPase deficiency and in vivo farnesylation. Mol Cell Biol **16**, 2689-2699 (1996).

85. Riento, K., Guasch, R.M., Garg, R., Jin, B. & Ridley, A.J. RhoE binds to ROCK I and inhibits downstream signaling. Mol Cell Biol **23**, 4219-4229 (2003).

86. Riento, K. et al. RhoE function is regulated by ROCK I-mediated phosphorylation. Embo J **24**, 1170-1180 (2005).

87. Ongusaha, P.P. et al. RhoE is a pro-survival p53 target gene that inhibits ROCK I-mediated apoptosis in response to genotoxic stress. Curr Biol **16**, 2466-2472 (2006).

88. Boswell, S.A., Ongusaha, P.P., Nghiem, P. & Lee, S.W. The Protective Role of a Small GTPase RhoE against UVB-induced DNA Damage in Keratinocytes. J Biol Chem **282**, 4850-4858 (2007).

89. Gadea, G., de Toledo, M., Anguille, C. & Roux, P. Loss of p53 promotes RhoA-ROCK-dependent cell migration and invasion in 3D matrices. J Cell Biol **178**, 23-30 (2007).

90. Walsh, S.V. et al. Rho kinase regulates tight junction function and is necessary for tight junction assembly in polarized intestinal epithelia. Gastroenterology **121**, 566-579 (2001).

91. Fujita, H. et al. Molecular decipherment of Rho effector pathways regulating tight-junction permeability. Biochem J **346 Pt 3**, 617-622 (2000).

92. Yokoyama, T., Goto, H., Izawa, I., Mizutani, H. & Inagaki, M. Aurora-B and Rho-kinase/ROCK, the two cleavage furrow kinases, independently regulate the

progression of cytokinesis: possible existence of a novel cleavage furrow kinase phosphorylates ezrin/radixin/moesin (ERM). Genes Cells **10**, 127-137 (2005).

93. Chevrier, V. et al. The Rho-associated protein kinase p160ROCK is required for centrosome positioning. J Cell Biol **157**, 807-817 (2002).
94. Liao, J.K., Seto, M. & Noma, K. Rho kinase (ROCK) inhibitors. J Cardiovasc Pharmacol **50**, 17-24 (2007).
95. Shimizu, Y. et al. ROCK-I regulates closure of the eyelids and ventral body wall by inducing assembly of actomyosin bundles. J Cell Biol **168**, 941-953 (2005).
96. Thumkeo, D., Shimizu, Y., Sakamoto, S., Yamada, S. & Narumiya, S. ROCK-I and ROCK-II cooperatively regulate closure of eyelid and ventral body wall in mouse embryo. Genes Cells **10**, 825-834 (2005).
97. Kawano, Y. et al. Phosphorylation of myosin-binding subunit (MBS) of myosin phosphatase by Rho-kinase in vivo. J Cell Biol **147**, 1023-1038 (1999).
98. Ishizaki, T. et al. p160ROCK, a Rho-associated coiled-coil forming protein kinase, works downstream of Rho and induces focal adhesions. FEBS Lett **404**, 118-124 (1997).
99. Amano, M. et al. Phosphorylation and activation of myosin by Rho-associated kinase (Rho-kinase). J Biol Chem **271**, 20246-20249 (1996).
100. Bernard, O. Lim kinases, regulators of actin dynamics. Int J Biochem Cell Biol **39**, 1071-1076 (2007).
101. Matsui, T. et al. Rho-kinase phosphorylates COOH-terminal threonines of ezrin/radixin/moesin (ERM) proteins and regulates their head-to-tail association. J Cell Biol **140**, 647-657 (1998).
102. Riento, K. & Ridley, A.J. Rocks: multifunctional kinases in cell behaviour. Nat Rev Mol Cell Biol **4**, 446-456 (2003).
103. Chen, X.Q. et al. Characterization of RhoA-binding kinase ROKalpha implication of the pleckstrin homology domain in ROKalpha function using region-specific antibodies. J Biol Chem **277**, 12680-12688 (2002).
104. Ishizaki, T. et al. The small GTP-binding protein Rho binds to and activates a 160 kDa Ser/Thr protein kinase homologous to myotonic dystrophy kinase. Embo J **15**, 1885-1893 (1996).
105. Matsui, T. et al. Rho-associated kinase, a novel serine/threonine kinase, as a putative target for small GTP binding protein Rho. Embo J **15**, 2208-2216 (1996).
106. Feng, J. et al. Rho-associated kinase of chicken gizzard smooth muscle. J Biol Chem **274**, 3744-3752 (1999).
107. Shimizu, T. et al. Parallel coiled-coil association of the RhoA-binding domain in Rho-kinase. J Biol Chem **278**, 46046-46051 (2003).
108. Zhao, Z.S. & Manser, E. PAK and other Rho-associated kinases--effectors with surprisingly diverse mechanisms of regulation. Biochem J **386**, 201-214 (2005).
109. Blumenstein, L. & Ahmadian, M.R. Models of the cooperative mechanism for Rho effector recognition: implications for RhoA-mediated effector activation. J Biol Chem **279**, 53419-53426 (2004).
110. Gao, T., Toker, A. & Newton, A.C. The carboxyl terminus of protein kinase c provides a switch to regulate its interaction with the phosphoinositide-dependent kinase, PDK-1. J Biol Chem **276**, 19588-19596 (2001).

111. Frodin, M. et al. A phosphoserine/threonine-binding pocket in AGC kinases and PDK1 mediates activation by hydrophobic motif phosphorylation. Embo J **21**, 5396-5407 (2002).

112. Leung, T., Chen, X.Q., Manser, E. & Lim, L. The p160 RhoA-binding kinase ROK alpha is a member of a kinase family and is involved in the reorganization of the cytoskeleton. Mol Cell Biol **16**, 5313-5327 (1996).

113. Garg, R., Riento, K., Keep, N., Morris, J.D. & Ridley, A.J. N-terminus-mediated dimerization of ROCK-I is required for RhoE binding and actin reorganization. Biochem J **411**, 407-414 (2008).

114. Yoneda, A., Multhaupt, H.A. & Couchman, J.R. The Rho kinases I and II regulate different aspects of myosin II activity. J Cell Biol **170**, 443-453 (2005).

115. Yoneda, A., Ushakov, D., Multhaupt, H.A. & Couchman, J.R. Fibronectin matrix assembly requires distinct contributions from Rho kinases I and -II. Mol Biol Cell **18**, 66-75 (2007).

116. Ward, Y. et al. The GTP binding proteins Gem and Rad are negative regulators of the Rho-Rho kinase pathway. J Cell Biol **157**, 291-302 (2002).

117. Thumkeo, D. et al. Targeted disruption of the mouse rho-associated kinase 2 gene results in intrauterine growth retardation and fetal death. Mol Cell Biol **23**, 5043-5055 (2003).

118. Ehrenreiter, K. et al. Raf-1 regulates Rho signaling and cell migration. J Cell Biol **168**, 955-964 (2005).

119. Vanhaesebroeck, B. & Alessi, D.R. The PI3K-PDK1 connection: more than just a road to PKB. Biochem J **346 Pt 3**, 561-576 (2000).

120. Primo, L. et al. Essential role of PDK1 in regulating endothelial cell migration. J Cell Biol **176**, 1035-1047 (2007).

121. Lim, M.A. et al. Roles of PDK-1 and PKN in regulating cell migration and cortical actin formation of PTEN-knockout cells. Oncogene **23**, 9348-9358 (2004).

122. Currie, R.A. et al. Role of phosphatidylinositol 3,4,5-trisphosphate in regulating the activity and localization of 3-phosphoinositide-dependent protein kinase-1. Biochem J **337 (Pt 3)**, 575-583 (1999).

123. Wick, M.J., Dong, L.Q., Riojas, R.A., Ramos, F.J. & Liu, F. Mechanism of phosphorylation of protein kinase B/Akt by a constitutively active 3-phosphoinositide-dependent protein kinase-1. J Biol Chem **275**, 40400-40406 (2000).

124. Balendran, A. et al. PDK1 acquires PDK2 activity in the presence of a synthetic peptide derived from the carboxyl terminus of PRK2. Curr Biol **9**, 393-404 (1999).

125. Biondi, R.M. Phosphoinositide-dependent protein kinase 1, a sensor of protein conformation. Trends Biochem Sci **29**, 136-142 (2004).

126. Sonnenburg, E.D., Gao, T. & Newton, A.C. The phosphoinositide-dependent kinase, PDK-1, phosphorylates conventional protein kinase C isozymes by a mechanism that is independent of phosphoinositide 3-kinase. J Biol Chem **276**, 45289-45297 (2001).

127. Biondi, R.M. et al. High resolution crystal structure of the human PDK1 catalytic domain defines the regulatory phosphopeptide docking site. Embo J **21**, 4219-4228 (2002).

128. Collins, B.J., Deak, M., Arthur, J.S., Armit, L.J. & Alessi, D.R. In vivo role of the PIF-binding docking site of PDK1 defined by knock-in mutation. Embo J **22**, 4202-4211 (2003).

129. Cudmore, S., Cossart, P., Griffiths, G. & Way, M. Actin-based motility of vaccinia virus. Nature **378**, 636-638 (1995).

130. Carlsson, F. & Brown, E.J. Actin-based motility of intracellular bacteria, and polarized surface distribution of the bacterial effector molecules. J Cell Physiol **209**, 288-296 (2006).

131. Xu, X. et al. Cell autonomous requirement for Tgfbr2 in the disappearance of medial edge epithelium during palatal fusion. Dev Biol **297**, 238-248 (2006).

132. Folkman, J. Angiogenesis. Annu Rev Med **57**, 1-18 (2006).

133. Yen, T.H. & Wright, N.A. The gastrointestinal tract stem cell niche. Stem Cell Rev **2**, 203-212 (2006).

134. Russo, J.M. et al. Distinct temporal-spatial roles for rho kinase and myosin light chain kinase in epithelial purse-string wound closure. Gastroenterology **128**, 987-1001 (2005).

135. Campbell, J.J. & Butcher, E.C. Chemokines in tissue-specific and microenvironment-specific lymphocyte homing. Curr Opin Immunol **12**, 336-341 (2000).

136. Wurbel, M.A., Malissen, M., Guy-Grand, D., Malissen, B. & Campbell, J.J. Impaired accumulation of antigen-specific CD8 lymphocytes in chemokine CCL25-deficient intestinal epithelium and lamina propria. J Immunol **178**, 7598-7606 (2007).

137. Zwahlen, R., Walz, A. & Rot, A. In vitro and in vivo activity and pathophysiology of human interleukin-8 and related peptides. Int Rev Exp Pathol **34 Pt B**, 27-42 (1993).

138. Gupton, S.L. & Waterman-Storer, C.M. Spatiotemporal feedback between actomyosin and focal-adhesion systems optimizes rapid cell migration. Cell **125**, 1361-1374 (2006).

139. Pantaloni, D., Le Clainche, C. & Carlier, M.F. Mechanism of actin-based motility. Science **292**, 1502-1506 (2001).

140. Stradal, T.E. et al. Regulation of actin dynamics by WASP and WAVE family proteins. Trends Cell Biol **14**, 303-311 (2004).

141. Goley, E.D. & Welch, M.D. The ARP2/3 complex: an actin nucleator comes of age. Nat Rev Mol Cell Biol **7**, 713-726 (2006).

142. Carlier, M.F., Wiesner, S., Le Clainche, C. & Pantaloni, D. Actin-based motility as a self-organized system: mechanism and reconstitution in vitro. C R Biol **326**, 161-170 (2003).

143. Ponti, A., Machacek, M., Gupton, S.L., Waterman-Storer, C.M. & Danuser, G. Two distinct actin networks drive the protrusion of migrating cells. Science **305**, 1782-1786 (2004).

144. Schirenbeck, A., Arasada, R., Bretschneider, T., Schleicher, M. & Faix, J. Formins and VASPs may co-operate in the formation of filopodia. Biochem Soc Trans **33**, 1256-1259 (2005).

145. Gerhardt, H. et al. VEGF guides angiogenic sprouting utilizing endothelial tip cell filopodia. J Cell Biol **161**, 1163-1177 (2003).

146. Snapper, S.B. et al. N-WASP deficiency reveals distinct pathways for cell surface projections and microbial actin-based motility. Nat Cell Biol **3**, 897-904 (2001).

147. Berdeaux, R.L., Diaz, B., Kim, L. & Martin, G.S. Active Rho is localized to podosomes induced by oncogenic Src and is required for their assembly and function. J Cell Biol **166**, 317-323 (2004).
148. Yamaguchi, H., Pixley, F. & Condeelis, J. Invadopodia and podosomes in tumor invasion. Eur J Cell Biol **85**, 213-218 (2006).
149. Charras, G.T., Yarrow, J.C., Horton, M.A., Mahadevan, L. & Mitchison, T.J. Non-equilibration of hydrostatic pressure in blebbing cells. Nature **435**, 365-369 (2005).
150. Charras, G.T., Hu, C.K., Coughlin, M. & Mitchison, T.J. Reassembly of contractile actin cortex in cell blebs. J Cell Biol **175**, 477-490 (2006).
151. Langridge, P.D. & Kay, R.R. Blebbing of Dictyostelium cells in response to chemoattractant. Exp Cell Res **312**, 2009-2017 (2006).
152. Blaser, H. et al. Migration of zebrafish primordial germ cells: a role for myosin contraction and cytoplasmic flow. Dev Cell **11**, 613-627 (2006).
153. Sahai, E. & Marshall, C.J. Differing modes of tumour cell invasion have distinct requirements for Rho/ROCK signalling and extracellular proteolysis. Nat Cell Biol **5**, 711-719 (2003).
154. Wyckoff, J.B., Pinner, S.E., Gschmeissner, S., Condeelis, J.S. & Sahai, E. ROCK- and myosin-dependent matrix deformation enables protease-independent tumor-cell invasion in vivo. Curr Biol **16**, 1515-1523 (2006).
155. Yoshida, K. & Soldati, T. Dissection of amoeboid movement into two mechanically distinct modes. J Cell Sci **119**, 3833-3844 (2006).
156. Coleman, M.L. et al. Membrane blebbing during apoptosis results from caspase-mediated activation of ROCK I. Nat Cell Biol **3**, 339-345 (2001).
157. Frisch, S.M. & Screaton, R.A. Anoikis mechanisms. Curr Opin Cell Biol **13**, 555-562 (2001).
158. Lele, T.P., Thodeti, C.K. & Ingber, D.E. Force meets chemistry: analysis of mechanochemical conversion in focal adhesions using fluorescence recovery after photobleaching. J Cell Biochem **97**, 1175-1183 (2006).
159. Lele, T.P. et al. Mechanical forces alter zyxin unbinding kinetics within focal adhesions of living cells. J Cell Physiol **207**, 187-194 (2006).
160. Zhou, H. & Kramer, R.H. Integrin engagement differentially modulates epithelial cell motility by RhoA/ROCK and PAK1. J Biol Chem **280**, 10624-10635 (2005).
161. Webb, D.J. et al. FAK-Src signalling through paxillin, ERK and MLCK regulates adhesion disassembly. Nat Cell Biol **6**, 154-161 (2004).
162. Gabarra-Niecko, V., Schaller, M.D. & Dunty, J.M. FAK regulates biological processes important for the pathogenesis of cancer. Cancer Metastasis Rev **22**, 359-374 (2003).
163. Cukierman, E., Pankov, R., Stevens, D.R. & Yamada, K.M. Taking cell-matrix adhesions to the third dimension. Science **294**, 1708-1712 (2001).
164. Lammermann, T. et al. Rapid leukocyte migration by integrin-independent flowing and squeezing. Nature **453**, 51-55 (2008).
165. Pellegrin, S. & Mellor, H. Actin stress fibres. J Cell Sci **120**, 3491-3499 (2007).
166. Watanabe, T., Hosoya, H. & Yonemura, S. Regulation of Myosin II Dynamics by Phosphorylation and Dephosphorylation of Its Light Chain in Epithelial Cells. Mol Biol Cell **18**, 605-616 (2007).

167. Fukata, Y., Amano, M. & Kaibuchi, K. Rho-Rho-kinase pathway in smooth muscle contraction and cytoskeletal reorganization of non-muscle cells. Trends Pharmacol Sci **22**, 32-39 (2001).

168. Murata-Hori, M., Fukuta, Y., Ueda, K., Iwasaki, T. & Hosoya, H. HeLa ZIP kinase induces diphosphorylation of myosin II regulatory light chain and reorganization of actin filaments in nonmuscle cells. Oncogene **20**, 8175-8183 (2001).

169. Watanabe, N., Kato, T., Fujita, A., Ishizaki, T. & Narumiya, S. Cooperation between mDia1 and ROCK in Rho-induced actin reorganization. Nat Cell Biol **1**, 136-143 (1999).

170. Wilkinson, S., Paterson, H.F. & Marshall, C.J. Cdc42-MRCK and Rho-ROCK signalling cooperate in myosin phosphorylation and cell invasion. Nat Cell Biol **7**, 255-261 (2005).

171. Thiery, J.P. Epithelial-mesenchymal transitions in development and pathologies. Curr Opin Cell Biol **15**, 740-746 (2003).

172. Etienne-Manneville, S. & Hall, A. Integrin-mediated activation of Cdc42 controls cell polarity in migrating astrocytes through PKCzeta. Cell **106**, 489-498 (2001).

173. Sahai, E., Garcia-Medina, R., Pouyssegur, J. & Vial, E. Smurf1 regulates tumor cell plasticity and motility through degradation of RhoA leading to localized inhibition of contractility. J Cell Biol **176**, 35-42 (2007).

174. Wang, H.R. et al. Regulation of cell polarity and protrusion formation by targeting RhoA for degradation. Science **302**, 1775-1779 (2003).

175. Pertz, O., Hodgson, L., Klemke, R.L. & Hahn, K.M. Spatiotemporal dynamics of RhoA activity in migrating cells. Nature **440**, 1069-1072 (2006).

176. Pertz, O. & Hahn, K.M. Designing biosensors for Rho family proteins--deciphering the dynamics of Rho family GTPase activation in living cells. J Cell Sci **117**, 1313-1318 (2004).

177. Magdalena, J., Millard, T.H. & Machesky, L.M. Microtubule involvement in NIH 3T3 Golgi and MTOC polarity establishment. J Cell Sci **116**, 743-756 (2003).

178. Schaloske, R.H., Blaesius, D., Schlatterer, C. & Lusche, D.F. Arachidonic acid is a chemoattractant for Dictyostelium discoideum cells. J Biosci **32**, 1281-1289 (2007).

179. Schaloske, R. & Malchow, D. Mechanism of cAMP-induced Ca2+ influx in Dictyostelium: role of phospholipase A2. Biochem J **327 (Pt 1)**, 233-238 (1997).

180. Perumpanani, A.J. & Byrne, H.M. Extracellular matrix concentration exerts selection pressure on invasive cells. Eur J Cancer **35**, 1274-1280 (1999).

181. Erickson, C.A. Control of pathfinding by the avian trunk neural crest. Development **103 Suppl**, 63-80 (1988).

182. Ridley, A.J. et al. Cell migration: integrating signals from front to back. Science **302**, 1704-1709 (2003).

183. Devreotes, P. & Janetopoulos, C. Eukaryotic chemotaxis: distinctions between directional sensing and polarization. J Biol Chem **278**, 20445-20448 (2003).

184. Iijima, M. & Devreotes, P. Tumor suppressor PTEN mediates sensing of chemoattractant gradients. Cell **109**, 599-610 (2002).

185. Andrew, N. & Insall, R.H. Chemotaxis in shallow gradients is mediated independently of PtdIns 3-kinase by biased choices between random protrusions. Nat Cell Biol **9**, 193-200 (2007).

186. Heit, B., Liu, L., Colarusso, P., Puri, K.D. & Kubes, P. PI3K accelerates, but is not required for, neutrophil chemotaxis to fMLP. J Cell Sci **121**, 205-214 (2008).
187. Balkwill, F. Chemokine biology in cancer. Semin Immunol **15**, 49-55 (2003).
188. Castellani, M.L. et al. Anti-chemokine therapy for inflammatory diseases. Int J Immunopathol Pharmacol **20**, 447-453 (2007).
189. Zicha, D., Dunn, G.A. & Brown, A.F. A new direct-viewing chemotaxis chamber. J Cell Sci **99 (Pt 4)**, 769-775 (1991).
190. Shields, J.D. et al. Autologous chemotaxis as a mechanism of tumor cell homing to lymphatics via interstitial flow and autocrine CCR7 signaling. Cancer Cell **11**, 526-538 (2007).
191. Haas, P. & Gilmour, D. Chemokine signaling mediates self-organizing tissue migration in the zebrafish lateral line. Dev Cell **10**, 673-680 (2006).
192. Valentin, G., Haas, P. & Gilmour, D. The chemokine SDF1a coordinates tissue migration through the spatially restricted activation of Cxcr7 and Cxcr4b. Curr Biol **17**, 1026-1031 (2007).
193. Wood, S., Jr. Pathogenesis of metastasis formation observed in vivo in the rabbit ear chamber. AMA Arch Pathol **66**, 550-568 (1958).
194. Klein, C.A. et al. Genetic heterogeneity of single disseminated tumour cells in minimal residual cancer. Lancet **360**, 683-689 (2002).
195. Margulis, A. et al. Loss of intercellular adhesion activates a transition from low- to high-grade human squamous cell carcinoma. Int J Cancer **118**, 821-831 (2006).
196. Li, C.Y. et al. Initial stages of tumor cell-induced angiogenesis: evaluation via skin window chambers in rodent models. J Natl Cancer Inst **92**, 143-147 (2000).
197. Wyckoff, J.B. et al. Direct visualization of macrophage-assisted tumor cell intravasation in mammary tumors. Cancer Res **67**, 2649-2656 (2007).
198. Sahai, E. Illuminating the metastatic process. Nat Rev Cancer **7**, 737-749 (2007).
199. Hendrix, M.J. et al. Expression and functional significance of VE-cadherin in aggressive human melanoma cells: role in vasculogenic mimicry. Proc Natl Acad Sci U S A **98**, 8018-8023 (2001).
200. Chang, Y.S. et al. Mosaic blood vessels in tumors: frequency of cancer cells in contact with flowing blood. Proc Natl Acad Sci U S A **97**, 14608-14613 (2000).
201. Rabodzey, A., Alcaide, P., Luscinskas, F.W. & Ladoux, B. Mechanical forces induced by the transendothelial migration of human neutrophils. Biophys J (2008).
202. Wyckoff, J.B., Jones, J.G., Condeelis, J.S. & Segall, J.E. A critical step in metastasis: in vivo analysis of intravasation at the primary tumor. Cancer Res **60**, 2504-2511 (2000).
203. Im, J.H. et al. Coagulation facilitates tumor cell spreading in the pulmonary vasculature during early metastatic colony formation. Cancer Res **64**, 8613-8619 (2004).
204. van der Pluijm, G. et al. Interference with the microenvironmental support impairs the de novo formation of bone metastases in vivo. Cancer Res **65**, 7682-7690 (2005).
205. Paget, S. The distribution of secondary growths in cancer
of the breast. Lancet **1**, 571-573 (1889).
206. Muller, A. et al. Involvement of chemokine receptors in breast cancer metastasis. Nature **410**, 50-56 (2001).

207. Zipfel, W.R. et al. Live tissue intrinsic emission microscopy using multiphoton-excited native fluorescence and second harmonic generation. Proc Natl Acad Sci U S A **100**, 7075-7080 (2003).

208. Flesken-Nikitin, A., Williams, R.M., Zipfel, W.R., Webb, W.W. & Nikitin, A.Y. Use of multiphoton imaging for studying cell migration in the mouse. Methods Mol Biol **294**, 335-345 (2005).

209. Hooper, S., Marshall, J.F. & Sahai, E. Tumor cell migration in three dimensions. Methods Enzymol **406**, 625-643 (2006).

210. Paszek, M.J. et al. Tensional homeostasis and the malignant phenotype. Cancer Cell **8**, 241-254 (2005).

211. Friedl, P. Prespecification and plasticity: shifting mechanisms of cell migration. Curr Opin Cell Biol **16**, 14-23 (2004).

212. Friedl, P. et al. Migration of coordinated cell clusters in mesenchymal and epithelial cancer explants in vitro. Cancer Res **55**, 4557-4560 (1995).

213. Wolf, K. et al. Compensation mechanism in tumor cell migration: mesenchymal-amoeboid transition after blocking of pericellular proteolysis. J Cell Biol **160**, 267-277 (2003).

214. Keely, P.J., Westwick, J.K., Whitehead, I.P., Der, C.J. & Parise, L.V. Cdc42 and Rac1 induce integrin-mediated cell motility and invasiveness through PI(3)K. Nature **390**, 632-636 (1997).

215. Ivanova, L., Butt, M.J. & Matsell, D.G. Mesenchymal transition in kidney collecting duct epithelial cells. Am J Physiol Renal Physiol **294**, F1238-1248 (2008).

216. Yang, J. et al. Twist, a master regulator of morphogenesis, plays an essential role in tumor metastasis. Cell **117**, 927-939 (2004).

217. Zavadil, J. & Bottinger, E.P. TGF-beta and epithelial-to-mesenchymal transitions. Oncogene **24**, 5764-5774 (2005).

218. Rees, J.R., Onwuegbusi, B.A., Save, V.E., Alderson, D. & Fitzgerald, R.C. In vivo and in vitro evidence for transforming growth factor-beta1-mediated epithelial to mesenchymal transition in esophageal adenocarcinoma. Cancer Res **66**, 9583-9590 (2006).

219. Friedl, P., Borgmann, S. & Brocker, E.B. Amoeboid leukocyte crawling through extracellular matrix: lessons from the Dictyostelium paradigm of cell movement. J Leukoc Biol **70**, 491-509 (2001).

220. Hegerfeldt, Y., Tusch, M., Brocker, E.B. & Friedl, P. Collective cell movement in primary melanoma explants: plasticity of cell-cell interaction, beta1-integrin function, and migration strategies. Cancer Res **62**, 2125-2130 (2002).

221. Friedl, P. & Wolf, K. Proteolytic and non-proteolytic migration of tumour cells and leucocytes. Biochem Soc Symp, 277-285 (2003).

222. Wolf, K. & Friedl, P. Molecular mechanisms of cancer cell invasion and plasticity. Br J Dermatol **154 Suppl 1**, 11-15 (2006).

223. Lah, T.T., Duran Alonso, M.B. & Van Noorden, C.J. Antiprotease therapy in cancer: hot or not? Expert Opin Biol Ther **6**, 257-279 (2006).

224. Hidalgo, M. & Eckhardt, S.G. Development of matrix metalloproteinase inhibitors in cancer therapy. J Natl Cancer Inst **93**, 178-193 (2001).

225. Bremer, C., Tung, C.H. & Weissleder, R. In vivo molecular target assessment of matrix metalloproteinase inhibition. Nat Med **7**, 743-748 (2001).

226. Goswami, S. et al. Macrophages promote the invasion of breast carcinoma cells via a colony-stimulating factor-1/epidermal growth factor paracrine loop. Cancer Res **65**, 5278-5283 (2005).

227. Sahai, E., Olson, M.F. & Marshall, C.J. Cross-talk between Ras and Rho signalling pathways in transformation favours proliferation and increased motility. Embo J **20**, 755-766 (2001).

228. Flynn, P., Mellor, H., Casamassima, A. & Parker, P.J. Rho GTPase control of protein kinase C-related protein kinase activation by 3-phosphoinositide-dependent protein kinase. J Biol Chem **275**, 11064-11070 (2000).

229. Bayascas, J.R. & Alessi, D.R. Regulation of Akt/PKB Ser473 phosphorylation. Mol Cell **18**, 143-145 (2005).

230. Chuang, Y.Y., Valster, A., Coniglio, S.J., Backer, J.M. & Symons, M. The atypical Rho family GTPase Wrch-1 regulates focal adhesion formation and cell migration. J Cell Sci **120**, 1927-1934 (2007).

231. Saras, J., Wollberg, P. & Aspenstrom, P. Wrch1 is a GTPase-deficient Cdc42-like protein with unusual binding characteristics and cellular effects. Exp Cell Res **299**, 356-369 (2004).

232. Kitzing, T.M. et al. Positive feedback between Dia1, LARG, and RhoA regulates cell morphology and invasion. Genes Dev **21**, 1478-1483 (2007).

233. Pinner, S. & Sahai, E. PDK1 regulates cancer cell motility by antagonising inhibition of ROCK1 by RhoE. Nat Cell Biol **10**, 127-137 (2008).

234. Jacobs, M. et al. The structure of dimeric ROCK I reveals the mechanism for ligand selectivity. J Biol Chem **281**, 260-268 (2006).

235. Doran, J.D., Liu, X., Taslimi, P., Saadat, A. & Fox, T. New insights into the structure-function relationships of Rho-associated kinase: a thermodynamic and hydrodynamic study of the dimer-to-monomer transition and its kinetic implications. Biochem J **384**, 255-262 (2004).

236. Flynn, P., Mellor, H., Palmer, R., Panayotou, G. & Parker, P.J. Multiple interactions of PRK1 with RhoA. Functional assignment of the Hr1 repeat motif. J Biol Chem **273**, 2698-2705 (1998).

237. Ziegler, W.H., Liddington, R.C. & Critchley, D.R. The structure and regulation of vinculin. Trends Cell Biol **16**, 453-460 (2006).

238. Wozniak, M.A., Kwong, L., Chodniewicz, D., Klemke, R.L. & Keely, P.J. R-Ras controls membrane protrusion and cell migration through the spatial regulation of Rac and Rho. Mol Biol Cell **16**, 84-96 (2005).

239. Riento, K. & Ridley, A.J. Inhibition of ROCK by RhoE. Methods Enzymol **406**, 533-541 (2006).

240. Pinner, S.E. & Sahai, E. Imaging amoeboid cancer cell motility in vivo. Journal of Microscopy **in press** (2008).

241. Hansen, S.H. et al. Induced expression of Rnd3 is associated with transformation of polarized epithelial cells by the Raf-MEK-extracellular signal-regulated kinase pathway. Mol Cell Biol **20**, 9364-9375 (2000).

242. Graupera, M. et al. Angiogenesis selectively requires the p110alpha isoform of PI3K to control endothelial cell migration. Nature (2008).

243. Zaru, R., Mollahan, P. & Watts, C. 3-phosphoinositide-dependent kinase 1 deficiency perturbs Toll-like receptor signaling events and actin cytoskeleton dynamics in dendritic cells. J Biol Chem **283**, 929-939 (2008).

244. Caron, E. & Hall, A. Identification of two distinct mechanisms of phagocytosis controlled by different Rho GTPases. Science **282**, 1717-1721 (1998).

245. Raposo, G. & Marks, M.S. Melanosomes--dark organelles enlighten endosomal membrane transport. Nat Rev Mol Cell Biol **8**, 786-797 (2007).

246. Marks, M.S. & Seabra, M.C. The melanosome: membrane dynamics in black and white. Nat Rev Mol Cell Biol **2**, 738-748 (2001).

247. Ben-Porath, I. et al. An embryonic stem cell-like gene expression signature in poorly differentiated aggressive human tumors. Nat Genet **40**, 499-507 (2008).

248. Bjerkvig, R., Tysnes, B.B., Aboody, K.S., Najbauer, J. & Terzis, A.J. Opinion: the origin of the cancer stem cell: current controversies and new insights. Nat Rev Cancer **5**, 899-904 (2005).

249. Hermann, P.C. et al. Distinct populations of cancer stem cells determine tumor growth and metastatic activity in human pancreatic cancer. Cell Stem Cell **1**, 313-323 (2007).

250. Immervoll, H., Hoem, D., Sakariassen, P.O., Steffensen, O.J. & Molven, A. Expression of the "stem cell marker" CD133 in pancreas and pancreatic ductal adenocarcinomas. BMC Cancer **8**, 48 (2008).

251. Yang, X.H. et al. Nestin expression in different tumours and its relevance to malignant grade. J Clin Pathol **61**, 467-473 (2008).

252. Klein, W.M. et al. Increased expression of stem cell markers in malignant melanoma. Mod Pathol **20**, 102-107 (2007).

253. Ehrmann, J., Kolar, Z. & Mokry, J. Nestin as a diagnostic and prognostic marker: immunohistochemical analysis of its expression in different tumours. J Clin Pathol **58**, 222-223 (2005).

254. Martinez-Esparza, M., Ferrer, C., Castells, M.T., Garcia-Borron, J.C. & Zuasti, A. Transforming growth factor beta1 mediates hypopigmentation of B16 mouse melanoma cells by inhibition of melanin formation and melanosome maturation. Int J Biochem Cell Biol **33**, 971-983 (2001).

11.2 Publications

Pinner, S. & Sahai, E. PDK1 regulates cancer cell motility by antagonising inhibition of ROCK1 by RhoE. *Nat Cell Biol* **10**, 127-137 (2008).

Pinner, S., & Sahai, E. Imaging amoeboid cell cell motility in vivo. *Journal of Microscopy,* In press 2008

Pinner, S., Sahai, E., Tumour heterogeneity controlled by TGFβ determines pigmentation and motile behaviour of melanoma cells in vivo. *(Manuscript in preparation)*

Wyckoff, J.B., **Pinner, S.E.**, Gschmeissner, S., Condeelis, J.S. & Sahai, E. ROCK- and myosin-dependent matrix deformation enables protease-independent tumor-cell invasion in vivo. *Curr Biol* **16**, 1515-1523 (2006).

Sanz-Moreno, V., Gadea, G., Ahn, J., Paterson, H., **Pinner, S.,** Sahai, E., Marshall, C.J., Rac activation and inactivation control plasticity of tumout cell movement. *Under revision at Cell.*

nature
cell biology

nature
cell biology

Supplementary Material

Methods

Screen of cytoskeletal regulators

A375 cells were transfected using smart pools of 4 oligos targeted against each gene (Dharmacon, catalogue numbers are listed below) 56 hours prior to assay end point. CTTN M-010508-00, WASL M-006444-01, ZYX M-016734-00, PXN M-005163-00, VCL M-009288-00, TLN1 M-012949-00, GRB2 M-019220-00, NCK1 M-006354-01, RAC2 M-007741-00, RAC3 M-008836-01, CDC42 M-005057-00, RHOA M-003860-00, RHOB M-008395-01, RHOC M-008555-00, RHOD M-008940-00, ARHE M-007794-01, RND1 M-008929-00, ARHN M-009727-00, RHOF M-008316-00, RHOG M-008995-00, RHOH M-008804-00, RHOJ M-010367-00, RHOQ M-009943-00, RHOU M-009882-00, RHOV M-006374-00, RHOBTB1 M-009389-00, RHOBTB2 M-009252-00, RHOBTB3 M-020480-01, RHOT1 M-010365-00, RHOT2 M-008340-00, DIAPH1 M-010347-01, DIAPH2 M-012029-00, DIAPH3 M-018997-00, WASF1 M-011557-00, WASF2 M-012141-00, CFL1 M-012707-00, PTK2B M-003165-03, PTK2 M-003164-02, LIMK1 M-007730-01, FMNL1 M-019176-00, FMNL3 M-019007-00, PAK1 M-003521-03, PAK2 M-003597-02, FMNL2 M-031993-00, RAC1 M-003560-02, ITGA1 M-008516-00, ITGA2 M-004566-01, ITGA3 M-004571-01, ITGAV M-004565-03, ITGA5 M-00803-01, ITGA6 M-007214-00, ITGB1 M-004506-00, ITGB3, M-004124-02, ITGB4 M-008011-01, CIT M-004613-01, AKT1 M-003000-02, AKT2 M-003001-01, AKT3 M-003002-02.

For ROCK1, ROCK2, MRCKα MRCKβ specific sequences were used as previously published [25]. Approximately 32 hours after transfection cells were trypsinized and plated on top of Collagen/matrigel matrix 24 hours prior to fixation with 4 % PFA and permabilisation with 0.3 % Triton X100. Cells were then stained using TRITC phalloidin, propidium iodide, and DAPI and imaged using a Zeiss LSM 510 confocal microscope. A375 cells were plated onto collagen/matrigel matrix for 18 hours then treated with inhibitors for 6 hours before fixation and staining as above. Concentrations and major targets are as follows: DMSO 0.05 %, Blebbistatin 5μM (non-muscle myosin), TAT-C3 500nM[1] (Rho), Y2763210 μM (ROCK), HA1077 10μM(ROCK,PKA), H1152 5μM(ROCK), U0126 10μM(MEK1/2), SB203580 10μM(p38 MAPK's), SP600125 10μM(JNK's), AG1478 10μM (EGFR's), SB431542 10 μM(TGFbetaRII), LY294002 20μM(PI-3K's), BIM 0.5μM(PKC's), ML-7 25μM(MLCK), PP2 10μM(src family kinases), Go6983 10 μM(PKC's).

RhoGTP pulldown assays

A375 cells transfected with either control siRNA duplexes or duplexes targeted against PDK1. 24 hours after transfection cells were plated on collagen/matrigel gels. A further 24-30 hours later GTP-RhoA was pulled down using the Rho-binding domain of Rhotekin, as previously described[2]. Levels of RhoA were visualised by western blot using RhoA (sc-418 Santa Cruz)

Adhesion assays

Cells were non-ezymatically removed (using Gibco-BRL #13150-016) before replating in 12 well plates that were coated with 1.8mg/ml matrigel, 3.2 mg/ml Collagen type 1 in DMEM + 1% FCS. After 30 minutes non-adherent cells were removed by tipping the media out and washing twice with PBS. Adherent cells were then fixed using 4% PFA and the number of cells in three 20x fields was counted.

Supplementary references

1. Sahai, E. & Olson, M.F. Purification of TAT-C3 exoenzyme. *Methods Enzymol* **406**, 128-40 (2006).
2. Sahai, E., Olson, M.F. & Marshall, C.J. Cross-talk between Ras and Rho signalling pathways in transformation favours proliferation and increased motility. *Embo J* **20**, 755-66 (2001).

Journal of Microscopy, Vol. 231, Pt 3 2008, pp. 441–445
Received 15 October 2007; accepted 21 November 2007

Imaging amoeboid cancer cell motility *in vivo*

S. PINNER & E. SAHAI

Current Biology *16*, 1515–1523, August 8, 2006 DOI 10.1016/j.cub.2006.05.065

Report

ROCK- and Myosin-Dependent Matrix Deformation Enables Protease-Independent Tumor-Cell Invasion In Vivo

Jeffrey B. Wyckoff,[1] Sophie E. Pinner,[2] Steve Gschmeissner,[2] John S. Condeelis,[1] and Erik Sahai[2,*]

Cell

Rac Activation and Inactivation Control Plasticity of Tumor Cell Movement

Victoria Sanz-Moreno,[1] Gilles Gadea,[1] Jessica Ahn,[1] Hugh Paterson,[1] Pierfrancesco Marra,[1] Sophie Pinner,[2] Erik Sahai,[2] and Christopher J. Marshall[1,*]

Cell

Cell